THE EROSION BEHAVIOR OF REVETMENT USING GEOTEXTILE

Chia Chun Ho

THESIS

Présentée par

HO, Chia-Chun

Pour obtenir le titre de Docteur de

L'UNIVERSITE JOSEPH FOURIER – GRENOBLE I

et

NATIONAL TAIWAN UNIVERSITY – TAIWAN

THE EROSION BEHAVIOR OF REVETMENT USING GEOTEXTILE

Date de soutenance: 22 Novembre 2007

Composition du jury:

M.	Jean-Pierre, GOURC	Président
M.	Gwo-Fong, LIN	Rapporteur
M.	Philippe, DELMAS	Rapporteur
M.	Jean Jacques, FRY	Examinateur
M.	Yves-Henri, FAURE	Directeur de thèse
M.	Rong-Her, CHEN	Directeur de thèse

Thèse préparée au sein du Laboratoire d'étude des Transferts en Hydrologie et Environnement.

Acknowledgments

I would like to thank my first advisor, Prof. Rong-her Chen, who gave me the opportunity to work on such an innovative and interesting project. In fact, Prof. Chen has been encouraging me all the time since I am a master student at National Taiwan University (NTU). There are no words to express the full measure of my gratitude. I should also like to acknowledge my indebtedness and gratitude to my second advisor, Dr. Yves-Henri Faure, for the guidance and assistance he provided during my study at LTHE in Grenoble. He gives a profound effect on my research and makes me deeply realized “enjoy study”. Furthermore, the loneliness of letting me forgets to study abroad because of his care in daily lives. I owe him more than I can convey in words.

I am also grateful to Prof. Jean-Pierre Gourc for welcoming me into LIRIGM and their invaluable contributions. He indicated a turning point that I study for double degree program between Taiwan and France. Sincere appreciation is also extended to my committee members, Prof. Philippe DELMAS, Prof. Kwo-Fong Lin, and Dr. Jean-Jacques FRY for their suggestions during this research and for review of the dissertation.

I am also thankful to National Science Council in Taiwan and French Institute in Taipei for funding my study in France. In financial support because of them, I work for this study without economic burden.

I would like to thank En-Tzu Hsieh, Chih-Yu Hsu, and Wen-Bin Chung, graduate students in the Civil Engineering Department of NTU under Prof. Chen, for the assistance and identifying by the experiment of long-term bi-directional flow. Special thanks go to Fan-Wei Kung and Kuo-Lung Wang, whose solved problems in English and informatics. Additionally, I would like to thank the technician in the Civil Engineering Department of NTU, Ying-Hao Chou, who helped me mainly for technical questions and the technician in LTHE, Henry Mora, who installed all set-ups. Without their help this thesis would not have been possible. I am also grateful to my fellow graduate students in NTU, Ya-Yun Yeh, Tai-Lin Ou, and Po-Chuan Chi, have been invaluable resources that I hope I can one day help as much as they have helped me. I take this opportunity of acknowledging the numerous kindnesses I have received at their hands and companionship since I studied in France, Timo Krass, Jean Fourmont, and Cyril Guidoux.

Finally, I especially want to thank my grandmother, my parents, my daughters Hsin-Yu and Hsin-Yeh, for their encouragement, support and understanding during my

graduate years. I have to express my utmost gratitude to my wonderful wife, Chun-Ping . She has been supportive and understanding of everything it has taken to put this together and the career decisions I have made.

Abstract

Unfavorable erosion on revetments may affect the slope stability of riverbanks and jeopardize the safety of adjacent buildings, and debris can be triggered by the soils and rocks eroded from the riverbanks and accumulate on the riverbed. Improvement works are needed to increase the stability of revetments as well as to reduce the possibility of failure. Current practices usually involve building tall concrete revetments, causing negative environmental impacts and instability of riverbanks under long-term erosion. Therefore, it is crucial to find materials suitable for building revetments which are safe and environmentally friendly as well.

Geotextiles used as a riverbank protection material is not only more environmentally-friendly but also more stable in long-term compared to concrete. However, improper design of geotextile revetments can cause considerable loss of riverbank soil, which might result in failure. Today numerous studies on erosion behavior of geotextile revetments have been completed, but most of them focused on only one directional flow behavior. The actual flow behavior in geotextile revetments is rather complicated and can be categorized into uni-directional flow zone, cyclic flow zone, and tangential flow zone.

In this study, the erosion behavior of non-cohesive or low-cohesive soil under the aforementioned three flow conditions was studied by tests using the equipments developed separately. The test result reveals that ground water seepage in the uni-directional flow zone may cause internal erosion of soil, and part of soil particles may be lost through the openings of the geotextile. The rest may be clogged inside the fibers of the geotextile or accumulated behind the geotextile, forming a natural filter layer, thereby causes the decrease of seepage velocity. Once the seepage velocity is lower than the critical velocity, the internal erosion of soil will cease.

Bi-directional cyclic flow zone can be categorized into the short term and the long-term cyclic flow conditions, depending on the flow period, which may induce different soil erosion behaviors. Thus, two test instruments were developed respectively. The result of the large-scale tank test for the short term cyclic flow condition reveals that the soil in the upper layer of the bi-directional cyclic flow zone subjected to cyclic wave loadings may trigger higher excess pore water pressure and result in collapse, while the soil in the middle layer may be eroded by the tangential flow along the riverbank and accumulated downstream. In additional to the opening size of the geotextile, the coverage area of rocks on the geotextile is also a key factor affeeting soil erosion.

The test results using cyclic flow instrument show that under the long-term cyclic flow action, with long cyclic flow period (600 sec/cycle), the seepage velocity in the soil layer is too slow to move soil particles, therefore no erosion is observed. However, as the seepage velocity increases, the effective stress in the soil will decrease due to the rising seepage pressure, thereby causing boiling and triggering considerable loss of soil and settlement. Besides, the influence depth in this flow condition is greater than that of short-term cyclic flow condition. Furthermore, through the hydraulic gradient ratios between the two piezometers installed above and underneath the geotextile, as well as from electron microscopy images of fibers inside the geotextile, it can be found that clogging of soil particles is not so serious as that in uni-directional flows.

Erosion behavior in the tangential flow zone was studied with a parallel erosion test instrument. The result reveals that tangential erosion behavior on the soil surface can be categorized by flow velocity. If the flow velocity is lower than the critical velocity (v_c), no erosion will occur. If the flow velocity is between the critical velocity and failure velocity (v_f), steady erosion will occur on the slope face. If the flow velocity is higher than the failure velocity, intense erosion will occur on the slope face and erosion failure of the revetment may thus be triggered. Moreover, the existence of geotextile on the surface of revetment has less influence on soil erosion. Revetments without geotextile on the slope surface are subjected to continuous erosion and may finally collapse due to cave-in at the toe of slope. A suitable geotextile covered on the surface of the revetment can not only avoid erosion but also form a natural filter layer underneath the geotextile, which prevents the soil from being continuously eroded. Once a natural filter layer is completely formed, the revetment will become stable.

Keywords：Geotextile, Soil erosion, Filtration, Cyclic flow, Tangential flow, Bank protection.

摘要

河川堤岸之不當沖蝕往往會影響河岸邊坡之穩定性並危及鄰近建築物的安全，而且被沖蝕崩落並堆積於河道中之土石材料也可能誘發土石流，因此須施以人工整治，以提高其穩定性，降低災害的發生。目前對於河川的治理大都採行構築高水堤防，並且採用混凝土為築堤材料，對生態環境之衝擊甚大，且對於河川長期沖蝕下之穩定性勘慮，因此尋求其他更合適的材料來替代混凝土築堤，且能同時兼具安全性及生態考量，是一個刻不容緩的問題。

採行地工合成材保護河岸除了具有生態環境營造上的優點之外，若與混凝土堤防護岸相比，其長期穩定性亦較優越，但是如果設計不良則可能造成河岸土壤大量流失進而破壞，目前對於地工合成材護岸之沖蝕行為的研究眾多，且亦已發展出相關之設計準則，然均只針對單向水流行為進行研究，而實際情況下之地工合成材護岸的水流行為複雜，本研究將其區分為單向水流作用區、雙向循環水流作用區及切向水流作用區等三區。

在本計畫中主要以試驗的方式，針對三區不同之水流條件而發展出相應之試驗設備以分別探討無凝聚性或低凝聚性土壤之沖蝕行為。經研究結果顯示，位於單向水流作用區之地下水滲流會引起土壤內部沖蝕，其中一部份的土壤顆粒會穿過地工合成材而流失，另一部份則可能堵塞於地工合成材內部纖維或堆積於地工合成材後方形成自然土壤過濾層並造成滲流速度下降，一旦滲流速度低於臨界流速(v_c)，土壤內部沖蝕便會停止。

循環水流作用區可依水流循環週期而區分為短週期及長週期循環水流，二種水流情況作用下之土壤沖蝕行為各異。因此，本研究各自發展出不同之試驗設備。採用大型水槽試驗針對短週期循環水流情況進行研究後得知，位於循環水流作用區之上部區域的土壤容易受水流反覆的作用而誘發較高的超額孔隙水壓力並引致崩潰破壞，中間區域則因水流沿著河岸邊坡產生切向流動而沖刷土壤表面，並帶至下部區域堆積，研究結果亦顯示除了地工合成材之開孔徑外，覆蓋於地工合成材上方之塊石覆蓋面積亦是控制土壤沖蝕的關鍵因素之一。在長週期循環水流作用下，經由雙向循環水流試驗儀之試驗結果得知，若循環水流的週期甚長(600 sec/cycle)，則土壤內部之滲流流速緩慢，不足以使土壤顆粒產生移動，因此並無土壤沖蝕之虞；然一旦流速加快，則土壤因滲流水壓力的提高而造成有效應力下降，並可能產生土壤砂湧而誘發大量的土壤流失及沉陷，且影響護岸土壤的深度較短週期循環水流者為深。再者，分析位於地工合成材上下二水壓計之水力梯度比，及以電子顯微鏡觀察地工合成材內部纖維構造可以發現，土壤顆粒堵塞的情形並不如單向水流之作用嚴重。

切向水流作用區之土壤沖蝕行為研究則採用平行沖蝕試驗儀進行，研究結果

顯示，土壤表面之切向沖蝕行為可以依水流流速加以區分，若流速低於臨界流速(v_c)，則土壤無沖蝕之虞；介於臨界流速與破壞流速(v_f)之間，土壤產生穩定沖蝕；一旦流速大於臨界流速，土壤便會產生劇烈沖蝕，並可能引起護岸沖蝕破壞，再者，於護岸表面有無鋪設地工合成材所產生之土壤沖蝕行為亦不盡相同，無鋪設地工合成材之護岸可能產生無止盡的土壤沖蝕，直到護岸因坡趾淘空而破壞，若鋪設合宜之地工合成材則可以避免此一現象，並可能在地工合成材下方形成一自然過濾層，進而防止土壤繼續遭受沖蝕，一旦自然過濾層完全形成，護岸便可趨於穩定。

關鍵詞： 地工合成材、沖蝕、過濾、循環水流、切向水流、河岸保護

Résumé

L'érosion des revêtements des digues de rivière peut affecter la stabilité des talus des rives et mettre en danger la sécurité des constructions voisines, et des écoulements de débris peuvent être déclenchés par le sol et les roches érodées de la rive et accumulées dans le lit de rivière. Des travaux d'amélioration sont nécessaires pour augmenter la stabilité des revêtements aussi bien que réduire la possibilité de rupture. Les pratiques actuelles impliquent habituellement la construction d'un épais revêtement en béton, causant des impacts négatifs sur l'environnement et une instabilité des rives sous l'effet de l'érosion à long terme. Afin de remplacer le béton, il est donc crucial de trouver des matériaux de construction respectueux de l'environnement et appropriés à la construction de revêtements sûrs.

Les géotextiles, en tant que matériau de protection de rive sont non seulement plus respectueux de l'environnement, mais aussi plus stables à long terme, comparés au béton. Cependant, une mauvaise conception d'un revêtement géotextile peut entraîner une perte considérable du sol de la rive, ce qui peut conduire à la rupture. Aujourd'hui de nombreuses études sur le comportement de revêtements géotextiles soumis à l'érosion ont été réalisées, mais chacune d'entre elles s'est intéressée uniquement à un type d'écoulement. Le comportement réel d'un revêtement géotextile soumis à écoulement est assez compliqué, et suivant le type d'écoulement on définit dans cette étude trois zones : la zone de flux unidirectionnel, la zone de flux cyclique bidirectionnel, et la zone de flux tangentiel.

Dans ce projet, le comportement sous érosion de sols non cohésifs ou peu cohésifs avec les trois conditions de flux mentionnées ci-dessus a été étudié avec des essais utilisant un équipement développé pour chaque condition de flux. Les résultats d'essais révèlent qu'un écoulement souterrain dans la zone de flux unidirectionnel peut provoquer l'érosion interne du sol et qu'une partie des particules de sol entraînées peut passer à travers les ouvertures du géotextile. Le reste de ses particules peut se colmater à l'intérieur des fibres du géotextile ou s'accumuler derrière le géotextile, formant une couche filtrante naturelle et réduisant la vitesse de l'écoulement. Une fois que la vitesse d'écoulement est plus basse que la vitesse critique, l'érosion interne du sol cesse.

La zone de flux cyclique bidirectionnel peut être identifiée en fonction des conditions de flux de : « flux cylique à court terme » et de cycliques à long terme », selon la période du cycle du flux, pour laquelle le comportement du revêtement géotextile diffère lors de l'érosion. Ainsi, deux instruments d'essais ont été développés. Les résultats d'essais dans un canal à vague grandeur nature avec des conditions de flux

cycliques à court terme révèlent que le sol de la couche supérieure de la zone de flux cyclique bidirectionnel est soumis à la charge cyclique des vagues, ce qui peut entraîner un excès de pression interstitielle et aboutir à l'écroulement, tandis que le sol dans la couche moyenne peut être érodé par le flux tangentiel le long de la rive et accumulé en aval. En outre, en plus de l'ouverture du géotextile, le taux de couverture des roches sur le géotextile est aussi un facteur clef qui contrôle le ravinement du sol. Les résultats d'essai utilisant l'instrument de flux cyclique bidirectionnel à long terme, pour une période de flux cyclique particulièrement longue (600 secondes/cycle), montrent que la vitesse d'écoulement dans la couche de sol est trop faible pour déplacer les particules de sol, et on ne s'attend donc à aucune érosion. Cependant, quand la vitesse d'infiltration augmente, la contrainte effective dans le sol diminue en raison de l'augmentation de pression de l'écoulement, causant ainsi un phénomène de boulance **(boiling)** et un entraînement considérable de sol ainsi que le tassement de celui-ci. En plus, la profondeur d'influence avec cette condition de flux est plus grande qu'avec la condition de flux cyclique à court terme. En outre, d'après les valeurs de gradient hydraulique déduites des mesures réalisées avec deux piézomètres installés au-dessus et au-dessous du géotextile, aussi bien que d'après les images de microscopie électronique de fibres du géotextile, on peut constater que l'extension de la zone de colmatage par les particules de sol n'est pas aussi importante que pour des flux unidirectionnels.

Le comportement en érosion dans la zone de flux tangentiel a été étudié avec l'instrument d'essai d'érosion parallèle. Le résultat révèle que le comportement en érosion tangentiel sur la surface de sol peut être défini par la vitesse de flux. Si la vitesse de flux est inférieure que la vitesse critique (v_c), aucune érosion n'apparaît. Si la vitesse de flux est entre la vitesse critique et la vitesse de rupture (v_f), une érosion permanente se produira à la surface de sol. Si la vitesse d'écoulement est plus grande que la vitesse de rupture, une érosion intense se produira dans le sol et entraînera la rupture du revêtement. De plus, la présence d'un géotextile sur la surface du revêtement a une influence non négligeable sur le comportement en érosion. Les revêtements sans géotextile sur la surface sont soumis à une érosion continue et peuvent finalement s'effondrer en raison d'éboulements en pied de pente. Une couverture géotextile appropriée sur la surface du revêtement peut non seulement éviter l'érosion, mais aussi former une couche filtrante naturelle au-dessous du géotextile qui empêche que l'érosion du sol continue. Une fois que la couche de filtre naturelle est complètement formée, le revêtement est stabilisé.

Mots-clés : Géotextile, Comportement en érosion, Filtration, Ecoulement perpendiculaire, Ecoulement tangentiel, protection de berges.

Table of contents

Chapter 4 Long-term bi-directional flow test 93

List of tables

List of figures

List of symbols and abbreviations

Symbols

A	Flow sectional area (L^2)
A_e	Area of soil erosion surface (L^2)
C	Concentration of soil particle in water (W / L^3)
Cu	Uniformity coefficient of soil (Dimensionless)
Cu'	Linear uniformity coefficient of soil (Dimensionless)
C_ε	Coefficient of soil erosion (Dimensionless)
c'	Effective cohesion of soil (M / L^2)
d_f	Diameter of the fiber of geotextile (L)
d_w	Effective of grain size of soil (L)
d_x	The soil's particle size corresponding to x % passing (L)
F_p	Perpendicular flow (Dimensionless)
Fr_{crit}	Froude number (Dimensionless)
FS	Factor of safety (Dimensionless)
F_t	Tangential flow (Dimensionless)
Gs	Specific gravity of soil (Dimensionless)
g	Acceleration of gravity (L / T^2)
h	Water column height (L)
I	Cyclic flow gradient index (Dimensionless)
I_p	Plasticity index of soil (%)
i	Hydraulic gradient (Dimensionless)
$i_{F,crit}$	Critical hydraulic gradient (Dimensionless)

$i_{p(n)}$ Hydraulic gradient at peak pore pressure between two piezometers, P01 and P02, at the n^{th} cycles (Dimensionless)

I_{HET} Erosion rate index of Hole Erosion Test (Dimensionless)

k_g Permeability of the virgin geotextiles (L/T)

k'_g Permeability of the used geotextiles (L/T)

k_{gs} Permeability of the virgin geotextiles-soil filter system (L/T)

k_s Permeability of soil (L/T)

L The distance between piezometers P01 and P02 (L)

LL Liquid limit of soil (%)

m Number of constrictions (Dimensionless)

m Mass of soil erosion (W / L^2)

m' Soil erosion rate ($W / L^2 / T$)

N Cycle number of cyclic flow test (Dimensionless)

n Porosity of geotextile (Dimensionless)

n_F Porosity of gravel filter (Dimensionless)

O_f The geotextile opening size based on hydrodynamic sieving (L)

O_x Geotextile opening size corresponding to particle size x (L)

q Flow rate (L^3 / T)

S Settlement (L)

T Tortuosity of the pore channels ($\approx 2/\pi \approx 0.65$) (Dimensionless)

t Time (T)

t_{GT} Thickness of geotextile (L)

t_{GT+25} The thickness of geotextile plus 25 mm thick soil (L)

t_{50} The thickness of adjacent 50 mm soil (L)

u Pore water pressure (M / L^2)

u_{P1} Peak pore water pressure at the piezometers P01 (M / L^2)

u_{P2} Peak pore water pressure at the piezometers P02 (M / L^2)

v Flow velocity (L/T)

v_c Critical flow velocity (L/T)

v_F Failure flow velocity (L/T)

$v_{F,crit}$ Scherzinger's critical erosion flow velocity (L/T)

Greek alphabets

Δh_g Water head loss (L)

Δh_{GT+25s} The water head difference in the bottom 25 mm thick soil and geotextile(L)

Δh_{50s} The water head difference in the adjacent 50 mm thick soil and geotextile (L)

α Coefficient of soil erosion (Dimensionless)

β The retention constant (Dimensionless)

β_1 Coefficient of granulometric (Dimensionless)

β_2 Coefficient of soil density (Dimensionless)

β_3 Coefficient of hydraulic gradient (Dimensionless)

β_4 Coefficient of geotextile function (Dimensionless)

$\dot{\varepsilon}$ Estimated rate of mass removal per unit area ($M / T / L^2$)

ϕ' Effective internal friction angle (°)

γ_d Unit weight of dry soil (M / L^3)

γ'_{sB} Effective unit weight of subsoil (M / L^3)

γ_{sat} Saturated unit weight of soil (M / L^3)

γ_w Unit weight of water (M / L^3)

η Dynamic viscosity of water ($M / L \cdot T$)

κ Coefficient of soil erosion (Dimensionless)

λ	Heerten's reduction factor (Dimensionless)
λ_v	Middle loss factor($\approx$4) (Dimensionless)
θ	The slop angle (°)
ρ_w	Density of water (M / L^3)
τ	Estimated shear stress (M / L^2)
τ_c	Critical shear stress (M / L^2)
ψ_g	Normal hydraulic conductivity of virgin geotextile (1/T)
ψ_{GS}	Hydraulic conductivity of soil-geotextile system (1/T)
ψ_S	Hydraulic conductivity of soil (1/T)

Abbreviations

BAW	The Federal Institute for waterway, German
CFGG	The French committee of the geotextiles and geomembrances
DGEG	The German committee of soil mechanics and foundations engineering
FHWA	Federal highway administration
FIH	Franzius-institute for hydraulic, waterways and coastal engineering in Hanover, German
FOS	Filtration opening size
FTU	Formazine turbidity unit
GR	Gradient ratio
HCR	Hydraulic conductivity ratio test
HET	Hole erosion test
LTF	Long-term flow test
MIP	Mercury instrusion porosimetry
NP	Non-plastic

PET	Parallel erosion test
POA	Percent opening area of geotextile
PSD	Pore size distribution of geotextiles
RLGT	Revetment laying geotextile test
RRGT	Reinforced revetment using geotextile test
SET	Slot erosion test
USCS	Unified soil classification system

Chapter 1 Introduction

In order to prevent scouring of riverbanks, concrete structures such as RC (concrete revetment) walls are commonly used. From aesthetic and ecological point of view, however, concrete structures have adverse impacts on the environment. The smooth surface of RC wall makes it difficult for creatures to survive and breed. In addition, they are apt to suffer from long-term scouring problems. Figure 1.1 shows a collapse failure of concrete revetment. The failure took place after several typhoons which brought huge amount of precipitation. In Taiwan, rainstorms often happen in summer and cause water level to go up. After the rainstorm, water level of the river drops rapidly and induces groundwater flow toward the river. Thus, the pore water pressure will be accumulated in the back of impermeable concrete structure and thus decrease the stability of revetment. Figure 1.2(a) is another revetment failure case, caused by the periodic draw-down of irrigation water. The revetment is composed of a layer of concrete cover laid on the top of the soil slope. The constituent of the soil is mainly sands with about 10% silt and clay. The filter used was made of gravel wrapped by geotextile and placed at the drainage holes. The failure, extended more than 1.6 km out of 2.3 km-long revetment, occurred only several months after the revetment was completed. According to the investigations, the failure is due to the periodic drawdown of water level, about 2 m high, per week. In Figure 1.2(b), it can be seen that the soil was eroded so seriously that a large hole was seen underneath the revetment.

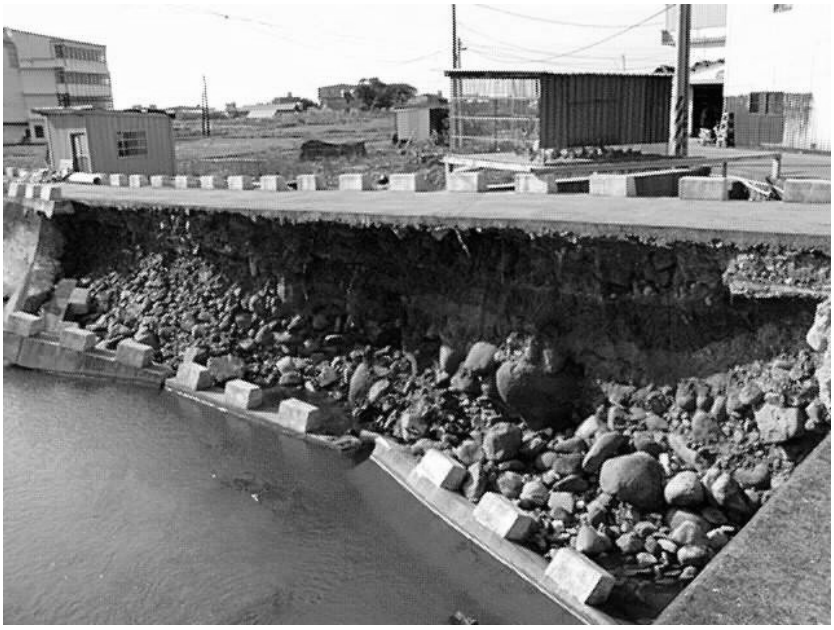

Figure 1.1 The collapsed failure of concrete revetment.

(a)

(b)

Figure 1.2 The slide failure of concrete revetment: (a) the failed revetment after water drawn out; (b) large holes due to soil erosion by water (Chen et al., 2003).

Therefore, it would be beneficial to seek alternative structures that are safe, economic, and more environmentally friendly. Currently, the more popular and state-of-the-art approach is using bioengineering or biotechnical engineering technology to renovate ecology. The purpose is for mankind to coexist with the nature and maintain the environment in a sustainable manner.

One solution to the above issue is to build revetments or embankments using geotextiles. Some examples are vegetated geogrid reinforced slopes or structures consisting of a geotextile layer placed on the soil slope, covered with armor stones (see Figure 1.3). The main function of geotextile is filtration. The revetment using geotextiles has relatively low impact on the environment and good permeability, but there may be the concerns of erosion. In this research, a series of laboratory experiments were performed with different equipments that are able to simulate the erosion behavior of revetment using geotextiles under different water flow directions.

Figure 1.3 Application of geotextiles in revetments (Isére River, France).

Figure 1.4 is the typical cross-section of revetment using geotextile. According to the water flow direction, it can be divided into three zones. Above the high water level is zone 1, where the groundwater always flows into the river and result in the uni-directional flow condition.

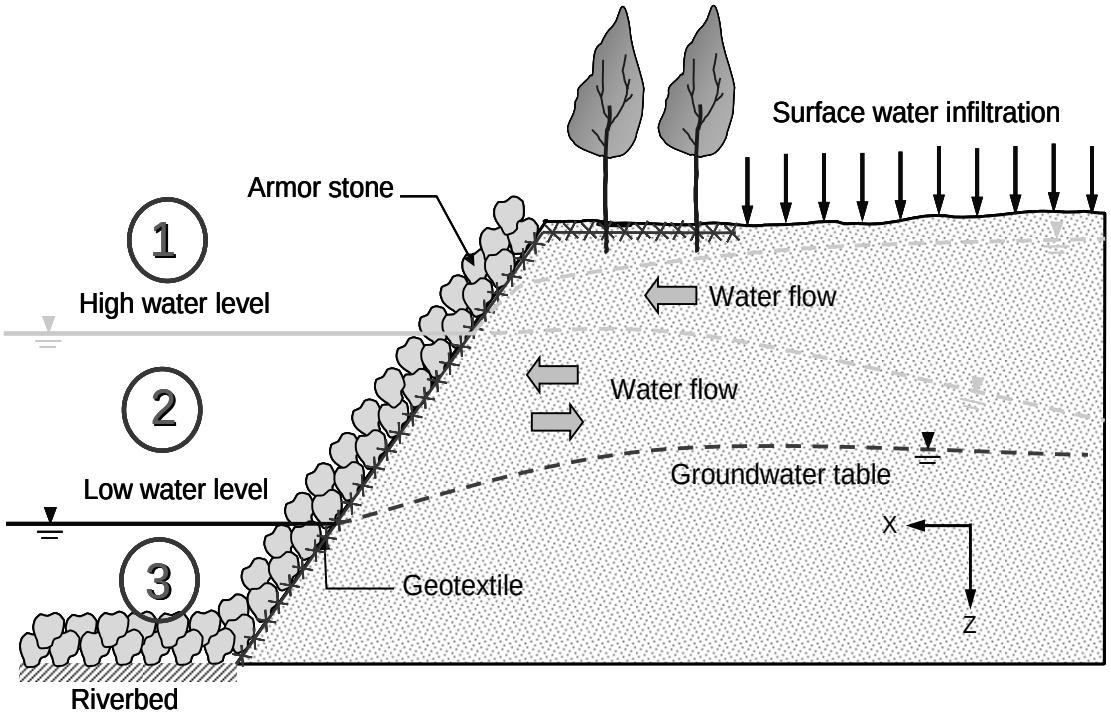

Figure 1.4 A typical cross-section of revetments using geotextiles.

Figure 1.5(a) shows the detail of the soil-geotextile interface of this zone. In a rainstorm, the groundwater flows to the river and causes seepage pressure. According to the hydraulic flow condition groundwater flow can be divided into two components, the flow is perpendicular to the geotextiles (F_p), and the flow is tangential to the geotextiles (F_t). For uni-directional perpendicular flow, so far a great amount of prior research work has been completed and design criteria have been proposed (summarized in Chapter 2). Yet design criteria for revetment using geotextile subject to uni-directional tangential flow have not been studied. Most of the research was focused on the relationship between soil particle size and opening size of geotextiles.

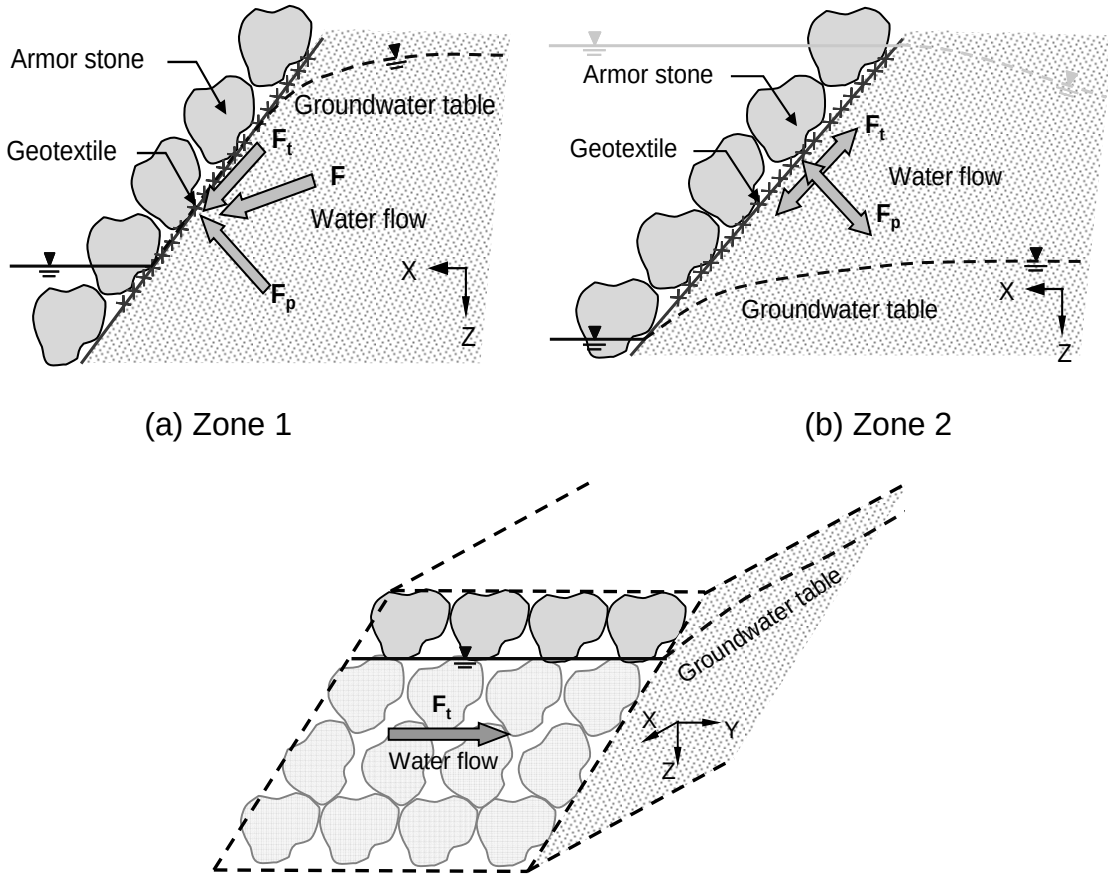

Figure 1.5 A detailed view of soil-geotextile interface.

Between high water level and low water level is zone 2, where the soil-geotextile interface is subject to bi-directional flow. When the groundwater table within the revetment is higher than the river water level, water will flow out from the revetment. On the contrary, water may flow into the revetment when the river water level is higher. The percolation rate of water through a soil-geotextile system is a function of the hydraulic gradient. The hydraulic gradient caused by fluctuation of the water table may be due to sea waves or boats; the wave activity is more violent and rapid with a shorter period. As shown in Figure 1.5(b), this zone also have two hydraulic flow components like zone 1. However, the two components are short-term bi-directional cyclic flow. The erosion behavior induced by the interaction of bi-directional cyclic perpendicular flow and tangential flow is complicated. Therefore, the full-scale flume test was performed as shown in Chapter 3.

If the fluctuation of the water table is caused by tide or the aforementioned periodic drawdown of irrigation water, long-term bi-directional cyclic flow is generated, and the erosion behavior is different from short-term flow. In addition, there

are many industrial parks and thermal power plants built in the tidal lands of Taiwan. These reclamation lands are built by constructing a rubble mound groin in the ocean, as shown in Figure 1.6. The tide causes variation in the groundwater level which may lead to soil loss or ground settlement and jeopardize the structures on the land side. A stable soil-geotextile filter system must be formed under these circumstances. In the situation of long-term bi-directional cyclic flow, as water level changes very slowly, tangential flow is insignificant. This study has developed a bi-directional cyclic perpendicular flow apparatus as described in Chapter 4.

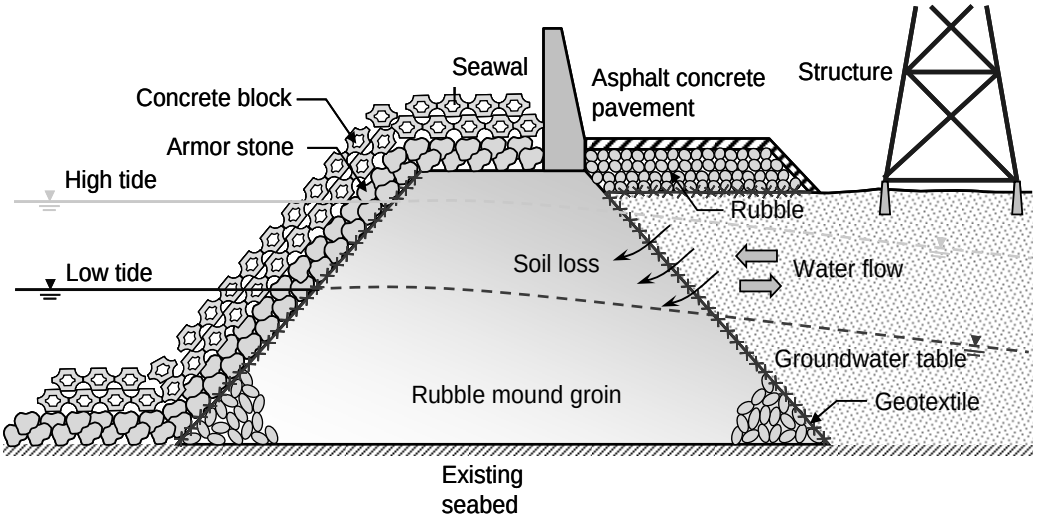

Figure 1.6 A typical cross-section of rubble-mound groin.

As mentioned, no matter in zone 1 or zone 2, the influence of water flow on the soil-geotextile interface only locates in X-Z plane. Zone 3 is under the low water level, and the percolation rate of water through a soil-geotextile system is insignificant due to the small hydraulic gradient between water side and bank side. The soil erosion behavior in X-Z plane is unobvious. However, the water flow along the revetment (Y-Z plane) may cause parallel erosion. Consequently, the main erosion problem in zone 3 is caused by the uni-directional tangential flow in Y-Z plane (see Figure 1.5 (c)). In order to understand the erosion behavior under this condition, the parallel erosion test was developed as described in Chapter 5.

Conclusions and suggestions of this study are summarized in Chapter 6.

Research was carried out at two research institutions, the “National Taiwan University (Taipei, Taiwan)” for long-term bi-directional cyclic flow, and the “LTHE - Laboratoire d'études des Transferts en Hydrologie et Environnement, Université Joseph Fourier (Grenoble, France)” for short-term bi-directional cyclic and tangential erosion test.

Chapter 2 Literature review

Geotextiles are pervious textiles, a subset of geosynthetics, manufactured polymeric materials (geogrids, geomembranes, geocomposites, etc.) used in subsurface projects. The use of geosynthetics in infrastructure construction and repair is increasing as an alternative to natural materials due to controlled fabrication quality, rapid installation, and volumetric economy (Koerner and Soong, 1995). They generally serve at last one primary function such as layer or strata separation, reinforcement, filtration or drainages as a component of the total design (Koerner, 1998). Geotextiles were first used for filters as alternatives to granular soil filters (Barrett, 1966). The earliest application was draining retaining wall backfill. This use reflects the usual focus in designing a geotextile filter as managing a trade off between assuring permeability, also expressed in terms of permittivity, and soil retention.

2.1 Filtration functions

The use of geotextiles is so varied that it is necessary to focus the discussion to their use relevant to this study: soil filter that is allowing water passage while preventing solid transport. Filtration is a process where suspended or dissolved solids are separated from a fluid as it flows through a porous media. The intention is not a set level of solid removal, but also minimal energy (head) loss. Filter design is based on parameters such as its channel morphology, the size and shape distribution and concentration of suspended solids or dissolved solids characteristics, and fluid properties such as viscosity and density. Another important factor when designing a filter is the source of the driving force, which may be hydrodynamic flow, gravity, suction or positive seepage pressure.

A geotextile used as a filter must be permeable enough to allow water to flow freely through the fabric in order not to produce excess pore water pressure in the soil, whilst it is also able to retain soil particles in place, thereby ensuring the stability of the structure. To achieve the optimum performance, according to Caroll (1983), a fabric filter should meet two requirements:

1. Permeability: the pore-channels in the filter should be large enough to enable water to flow away freely from the protected soils, thus preventing build-up of excess hydrostatic pressure.

2. Retention: the pore-channels of a filter should be small enough to retain the erodible soils and prevent piping.

In this chapter, the literature related to this research on topics of filtration mechanism, criterion, the internal erosion model tests and behavior will be reviewed.

2.2 Filtration mechanisms

Under the condition of perpendicular flow that was proposed on the before chapter, the water infiltration rate through a soil-geotextiles system is a function of the hydraulic gradient between the existing water table level and the interface location in the soil and the resistances offered by the soil mass and the geotextiles. Upon these conditions, soil particles can migrate from the soil into the textile to form an interface layer of properties different from those of the soil. The relationship between this layer formation and the soil properties is essential to understand the filtration mechanisms.

The water that infiltrates through the pores of the soil-geotextiles system may change the soil structure and will affect intrinsic permeability. As the soil particles migrate into this system, the permeability decreases. To prevent this phenomenon, a suitable geotextiles should be selected to impede sufficiently the movement of soil particles and to build a natural filter layer. In turn, this layer will stop the smaller particles migrate until stabilization is established. The faster a natural filter established, the smaller amount of soil particles will migrate (Mlynarek et al., 1991).

Rollin et al. (1988) have proposed two mechanisms of natural filter formation based on perpendicular flow condition: the bridging network and the vault formation respectively. The bridging network, as shown schematically in Figure 2.1, usually occurs in non-cohesive soil. At first, the larger size particles are stopped at the geotextile structure. These particles in turn stop smaller particles and this process continues until the soil stabilizes. The vault formation occurs in non-cohesive soils with appreciable clay content or in cohesive soils. Vaults are initiated by the geotextiles fibers as shown in a photographic cross section of a geotextiles sample collected in situ and presented schematically in Figure 2.2.

Schedegger (1957) divided filtration into three classes: medium, cake, and depth filtration. In medium filtration, particles that are larger than the filter entry pores are retained, generally at surface openings or shortly inside the upstream face. This type of filter thus behaves like a sieve, and its plane is normal to the streamlines of the flow. Failure is usually defined as an excessive head loss being required to drive the desired

discharge. It tends to occur as a result of surface blinding or blockage. In depth filtration, particles smaller than the filter pores and dissolved materials are intercepted and retained within the filter section due to impact on or attraction to the walls of the pore channels. In cake filtration, the solids do not enter the filter itself to a great extent, but accumulate on or in front of the surface of the filter, “piling up” on one another. Soil filters are intended to be a variation of cake filtration. Localized particle movements first form the filter cake layer, which thus restrains upgradient particles. The filter is specified to be much more permeable than the native soil to minimize the net head loss in the series flow across the composite filter cake-geotextile filter.

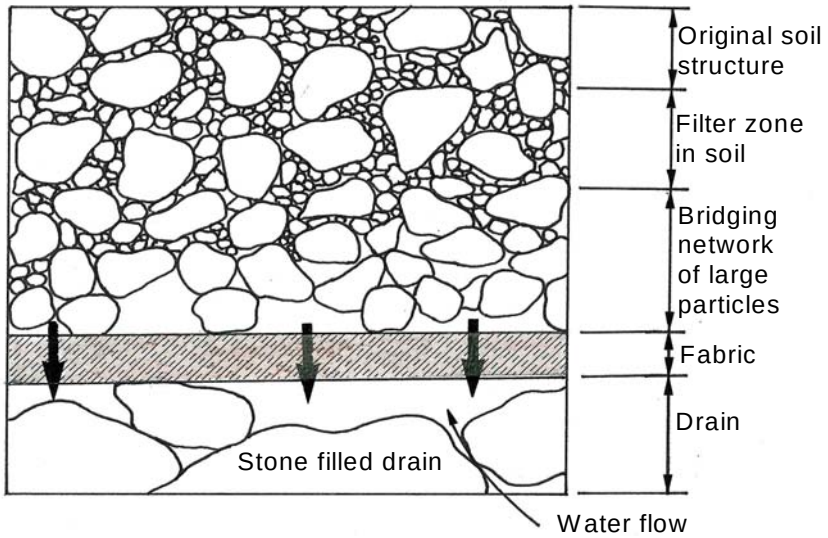

Figure 2.1 Bridging network formations (Rollin et al., 1988).

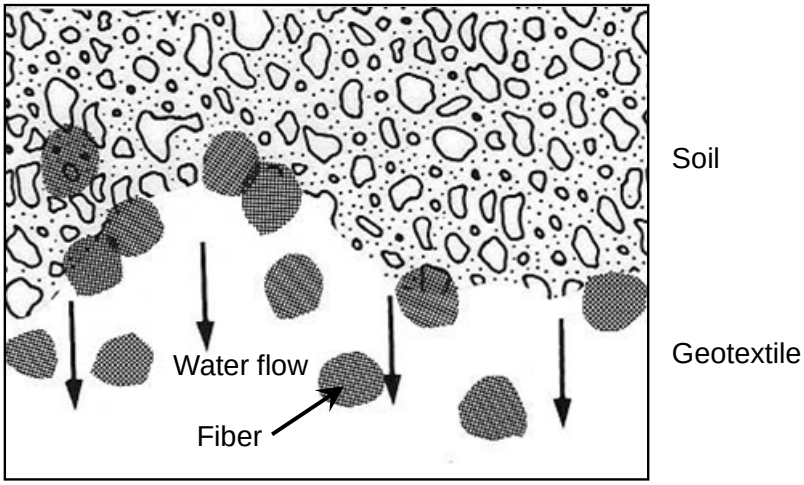

Figure 2.2 Vault network formations (Rollin et al., 1988).

The forming process of filter cake in the soil-geotextiles systems is quite complicated. Mlynarek et al. (1991) summarized by the occurrence of 5 following mechanisms as schematically presented in Figure 2.3:

1. Migration of particles.
2. Loss of fine particles.
3. Filter cake build-up.
4. Trapping of particles inside the geotextiles.
5. Soil stabilization.

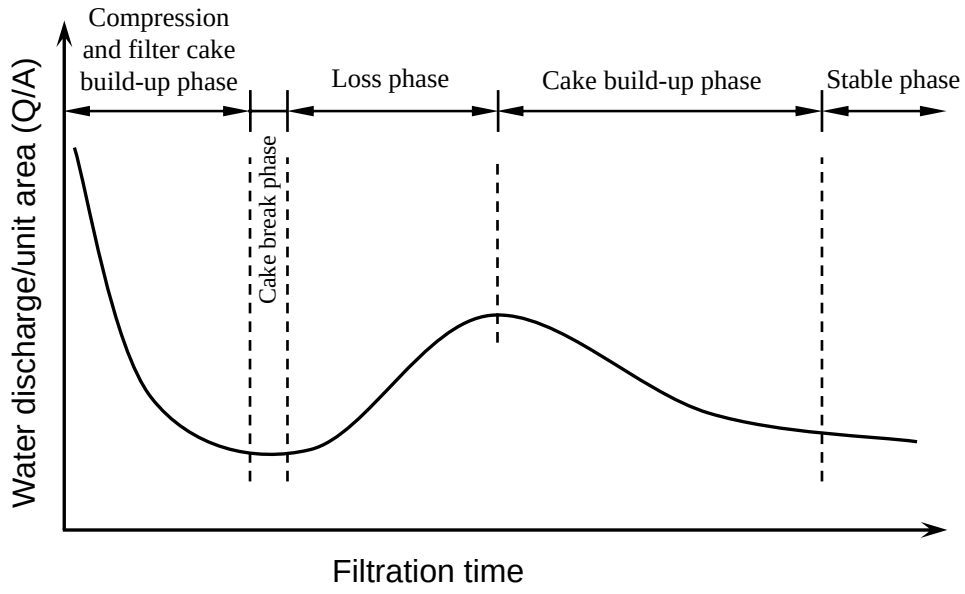

Figure 2.3 Typical mechanisms of flux decay of a system (Mlynarek et al.,1991).

A distinction is made between uni-directional flow and bi-directional flow in filtration design using geotextiles. It is believed that a natural bridge network is induced in the soil adjacent to the geotextile during uni-directional flow. For long-term bi-directional cyclic flow may forms an unstable bridge network. But this network may not develop under impacting water flow (short-term bi-directional cyclic flow), where the influence of changing direction of flow and associated seepage forces acts to destabilize such a network (Giroud, 1982; Kohler, 1993). For uni-directional water flow, Hoare (1984) proposed to adopt thin heat-bonded geotextiles, and for the bi-directional water flow conditions he proposed to adopt thick needle-punched geotextiles.

A geotextile installed in the hydraulic engineering to perform a filter system can be altered in time by many phenomena such as clogging, blocking, blinding and piping.

1. Clogging: A geotextile structure can be modified during or after its installation in a drainage system by particles, sediments and organic matters migrating between its fibers. Its hydraulic properties can also be altered by salt deposition, mineral precipitation and bacterial growth. All these actions can result in the clogging of the geotextile (See Figure 2.4(a)).
2. Blocking: Blocking of openings in a textile structure results when coarse particles migrate at the upstream face of the filter and locate themselves permanently at the entrance of the pores as shown schematically in Figure 2.4(b). It is a physical mechanism located at the geotextile soil interface and usually occurs when particles of a size equal to or larger than the pores of a geotextile have the opportunity to reach the filter freely under a relatively high water flow. Blocking can be expected when a geotextile is selected to retain particles contained in very low concentrated suspensions or whenever a lack of contact between the soil and geotextile exists.
3. Blinding: Blinding is used to describe the mechanism occurring when coarse particles retained by the geotextile intercept fines migrating from the soil in such a way that an impervious layer is established very quickly upstream of these coarse particles as shown schematically in Figure 2.4(c). This phenomenon of the establishment of a multi-layer natural filter interacts with the normal behavior of filtration where it is necessary that fines located close to a filter be carried through the drainage system during the initial period of work to allow the formation of a permeable natural filter between the soil and the geotextile.
4. Piping: Piping must be differentiated from other phenomena since it is related to the upward flow action and alters only a small and local area of a geotextile. Upon hydraulic distribution on a geotextile installed as a separation medium between a granular material and a soft soil, fines from the bottom soil will migrate upward through the geotextile at specific locations producing a flow of suspended particles.

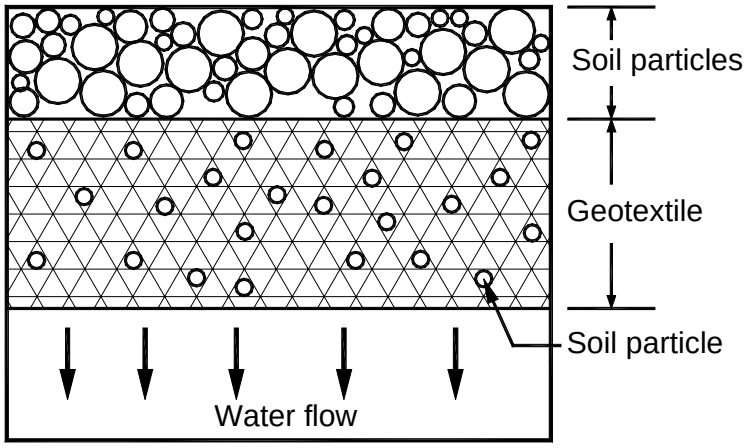

(a) Clogging

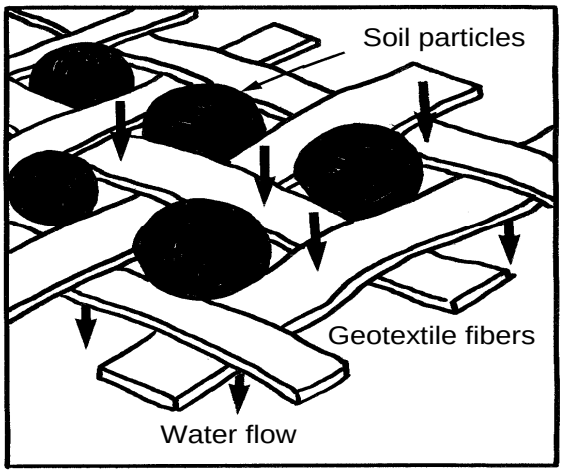

(b) Blocking

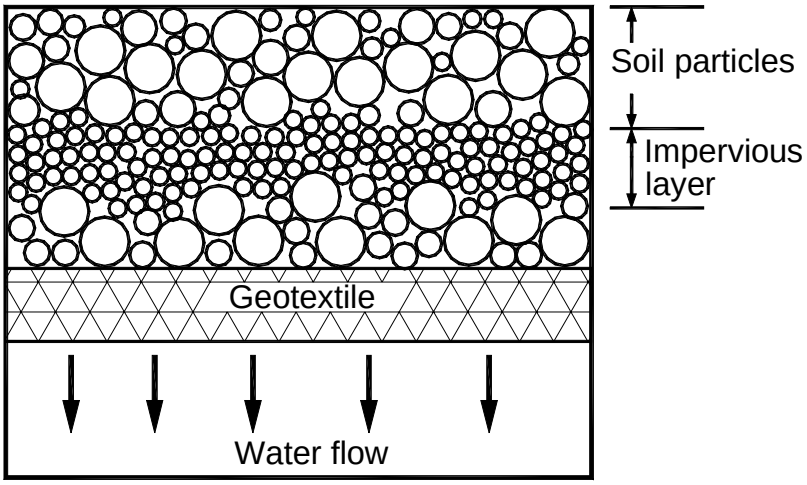

(c) Blinding

Figure 2.4 The filter system altered in time (Mlynarek et al., 1990).

Clogging essentially occurs within a geotextile structure and should not be used to describe in general terms the fouling behavior of a filter. The particles and sediments being stopped upstream of a filter can form a layer affecting the filtration and drainage functions of a geotextile. The phenomena involved must be defined as blocking and blinding mechanisms. The migration of fine soil particles in localized soil paths is referred to as piping (Rollin et al., 1988). Clogging by migration of particles from the soil into the filter represents a failure in both criteria, as both soil loss and water pressure buildup destabilize the soil mass. Marks (1975) showed that nonwoven geotextile clogging depends on mass per unit area. Gourc (1990) showed that clogging would occur when the geotextile void and the soil particles size are similar.

A stable soil-geotextile filter system must be formed under these circumstances. Otherwise, problems associated with the improper system may cause the following consequences:

1. The too large opening size of geotextile may cause the large amount of soil particle loss in certain range of particle size and may induce the internal soil erosion. Consequentially, the turbulence flows within the soil may cause the soil structure collapse and settlement occurs. This phenomenon is especially obvious to the uniform graded or gap-graded soil (John, 1987).

2. The geotextile opening size is too small and then causes clogging within the geotextile or blocking on the geotextile surface and produce excess pore water pressure in the soil.

Moreover, there are a lot of factors that may influence the performance of geotextile filters. Williams et al. (1989) has summed up the following factors:

1. Geotextile properties: permeability, thickness, porosity, primary bonding method, secondary bonding method, compressibility, pore size distribution, flexural rigidity, etc.

2. Soils properties: soil type, particle size, particle size distribution, hydraulic conductivity, soil structure, soil fabric, void ratio, plasticity index, degree of saturation, etc.

3. Boundary conditions: hydraulic gradient, flow velocity, direction of flow, state of stress, stress history, type of support media, etc.

In the following, this study will try to show the influence of some of them, such as the opening and thickness of geotextile, soil particle size distribution, direction of flow, and so on.

2.3 Filtration criteria

The performance of geotextiles is really not to prevent the soil loss directly, but to form a soil-geotextiles filter layer. A steady filter layer should make water pass freely besides should avoid the soil loss. One of the main issues in using geotextiles is their performance once in contact with soil. Opening size, hydraulic conductivity, and soil diameter are very important criteria in selection of geotextiles. Geotextiles with very fine openings may clog the geotextile openings or active soil pores causing cake formation. Research shows that upward flow is more critical than the downward flow (Dierickx and Yuncuoglu, 1982, 1993). Hence, the design of a geotextile filter addresses three requirements: adequate permeability, proper soil retention and long-term performance over the service lifetime. Most of the design criteria of soil/geotextile filtration aim at the well-graded soil. However, the following issues need to be considered if these criteria are adapted to gap-graded soil (John, 1987):

1. As the content of silt or clay exceeds 30%, the coarse particle surface will be covered by silt and the interlock action will lose. Once the silt is eroded, a large amount of fine particle loss and causes the soil structure to collapse. Therefore, it is necessary to consider fine grain retention in the choosing of geotextile.

2. As the content of fine particle is lower than 30%, the fine particle can moves easily within the void between the coarse particle. If the geotextile is chose base on the coarse particle distribution may cause the large amount of fine particle loss. On the other hand, to choose geotextile base on the fine particle distribution may cause the fine particle clogging. Such as this soil condition, to choose a suitable geotextile is difficult.

Giroud(1982) points out that to be using geotextile for filter function (as it is worldwide recognized) must accord with the permeability criteria and retention criteria.

2.3.1 Permeability criteria

Afterward the geotextile is installed, the fine particle will be blocked or accumulated behind the geotextile will reduce the permeability of the filter layer and increase the pore water pressure. The permeability of soil-geotextile filter system must prevent producing excess pore water pressure to avoid revetment failure. Therefore, the pore size of the geotextile should not be too small and maintain the proper flow.

1. Uni-directional flow:

A rigorous permeability criterion of geotextile must take into account the operating conditions in situ: the influence of compression, the possible clogging, and the acceptable hydraulic pressure loss, water flow velocity and gradient in soil. The French Committee of the Geotextiles and Geomembrances (CFGG, 1986) proposed that, for risky conditions (earth dam), the permittivity of geotextile used in situ could be reduce by 300 times because of compressed and clogged or polluted. Then, assuming that hydraulic gradient (i) is less than 10 and water head loss (Δh_g) through geotextile is less than 0.10m, and take into a account a safety factor of 3.3, CFGG suggests that the relationship between the permittivity of virgin geotextile and the permeability of soil are

For critical condition: $\psi_g \geq 10^5 k_s$ (2-1a)

For waterway or slope: $\psi_g \geq 10^4 k_s$ (2-1b)

For clean sand ($d_{12} > 80\mu m$): $\psi_g \geq 10^3 k_s$ (2-1c)

where: ψ_g = Normal hydraulic conductivity of virgin geotextile, s^{-1}.

k_s = Permeability of soil, m/s.

d_{12} = The soil's particle size corresponding to 12% passing.

According to the result that pure sand/geotextile filter system in the different hydraulic head loss, and adopted the safety factor of 10. Giroud (1982) proposes the permeability of geotextile (k_g) can be expressed in the follow equation.

$$k_g \geq 0.1 k_s \quad (2\text{-}2)$$

Gourc (1982) also compared the efficiency of permeability using gravel filter and geotextile filter. The relation is:

$$k_g \geq 0.32 k_s \quad (2\text{-}3)$$

The German Committee of Soil Mechanic and Foundations Engineering (DGEG) based on the suggested of Heerten (1981) and adopted as:

$$k_g \geq k_s \quad (2\text{-}4)$$

FHWA (Federal Highway Administration) adopted the recommend of Christopher and Holtz (1985) and suggested that the geotextile filter is applied in the non-critical applications and non-severe soil condition under the steady state flow, the permeability of geotextiles must be bigger than soil ($k_g \geq k_s$). The relation proposed is the same as DGEG (Eq. (2-4)). However, for the important constructions or under the conditions of high hydraulic flow, weak soil, or a long-term operation, Christopher and Holtz (1985) suggests that

$$k_g \geq 10k_s \tag{2-5}$$

In addition, there are some reports that proposed the permeability criteria according to the relationship between the geotextile opening size and soil particle size. Those are:

Chen et al. (1981): $O_f \geq 2d_{15}$ (2-6)

Lawson (1982): $O_f \geq d_{15}$ (2-7)

Basvary and Mac Lean (1981): $O_f \geq d_{30}$ (2-8)

Where: O_f = The filtration opening size (FOS) based on hydrodynamic sieving.
$d_{15}(d_{30})$ = The soil's particle size corresponding to 15% (30%) passing.

2. Bi-directional flow:

Schober and Teindl(1979) suggest that, in the bi-directional flow condition, the permeability of the geotextile must greater than soil. Hence, the equation is the same as Eq. (2-4). In specific, the Federal Institute for Waterway, Germany (BAW, Bundesanstalt für Wasserbau) recommends that:

$$\begin{aligned} k_g &\geq 10k_s \quad \text{(sand)} \\ k_g &\geq 100k_s \quad \text{(clay)} \end{aligned} \tag{2-9}$$

Generally, the revetment covers with armor stones above the geotextile that will reduce the drainage area and decrease the permeability in situ. In order to avoid over-evaluating the infiltration ability of the geotextile and evaluate the reduce factor, Heerten (1981) took several used samples of geotextile from the site of revetment under bi-directional flow. He has investigated the variation in permeability between the

virgin geotextile (k_g) and the used geotextile (k'_g). And further, the reduction factor (λ) was proposed in Figure 2.5. It will be noted that the factor varies between 1 and 0.01 for non-woven geotextile, whereas it varies between 1 and 5×10^{-4} for woven.

$$k'_g = \lambda k_g \tag{2-10}$$

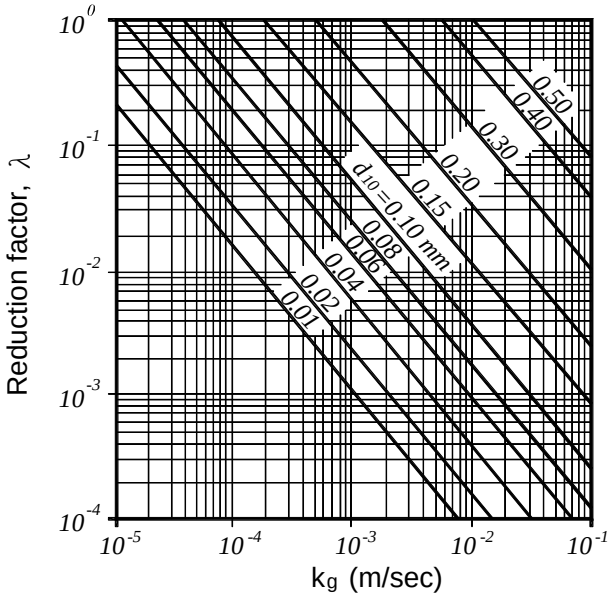

(a) Woven geotextile

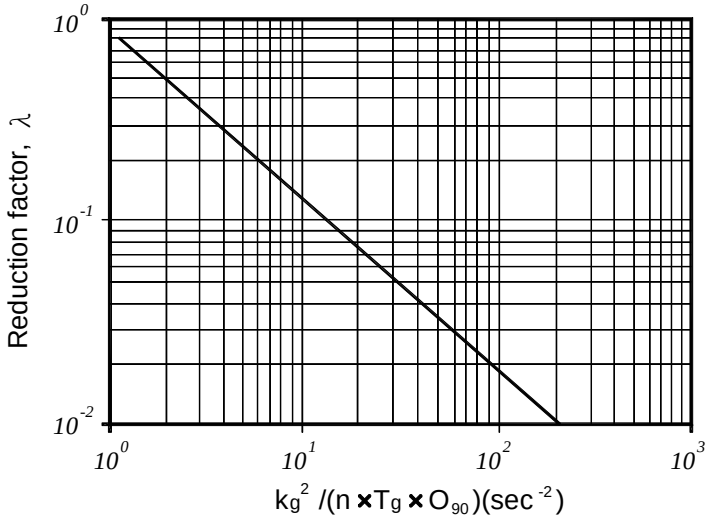

n = Porosity of geotextile $\quad$ t_{GT} = Thickness of geotextile (mm)

O_{90} = Apparent opening size (mm)

(b) Non-woven geotextile

Figure 2.5 Heerten's (1981) reduction factor for bi-directional flow.

Franzius-Institute for Hydraulic, Waterways and Coastal Engineering in Hanover, Germany (FIH, 1987) adopted Heerten's result and suggested considering that the reduction factor while using geotextile for revetment. Machizaud (1982) and Gourc (1982) expressed the difficulty of the permeability measured for samples taken in situ. It is essential to measure the permeability under very low hydraulic gradient, in order not to wash the sample. And it is not easy to restore the porosity as in situ during the experiment.

2.3.2 Retention criteria

A good soil-geotextile filter system needs to satisfy the retention criteria. It is generally selected to retain enough larger soil particles to develop a soil bridge network, leading to develop a stable soil structure which is able to prevent further migration.

As following, several retention criteria are extracted from previous studies to present the different and are adopted to examine the geotextile that used in this study.

1. Uni-directional flow:

For the most part, retention design for geotextiles has been developed from existing soil filter criteria. Like soil filters, the geotextile filter is generally selected such that enough larger soil particles are retained to develop a soil bridge leading to the development of a stable soil structure which is able to prevent further migration. Therefore,

$$O_x \leq \beta d_y \tag{2-11}$$

Where, O_x is geotextile opening size corresponding to x particle size (O_{95}, O_{90}, O_{50}), d_y is soil's particle size corresponding to y percent passing (d_{90}, d_{85}, d_{50}, d_{15}), and β is retention constant.

Giroud (1982) proposed the following relationship between O_{95} and d_{50}, and β is relating with the uniformity coefficient of soil (Cu') and density (see Figure2.6).

$$O_{95} \leq \beta d_{50} \tag{2-12}$$

Heerten (1992) suggested that the suitable opening size and thickness of geotextile is

Opening size (O_{90}): $d_{50} < O_{90} < d_{90}$ (2-13)

and

Thickness (t_{GT}): $30 \times O_{90} < t_{GT} < 50 \times O_{90}$ (2-14)

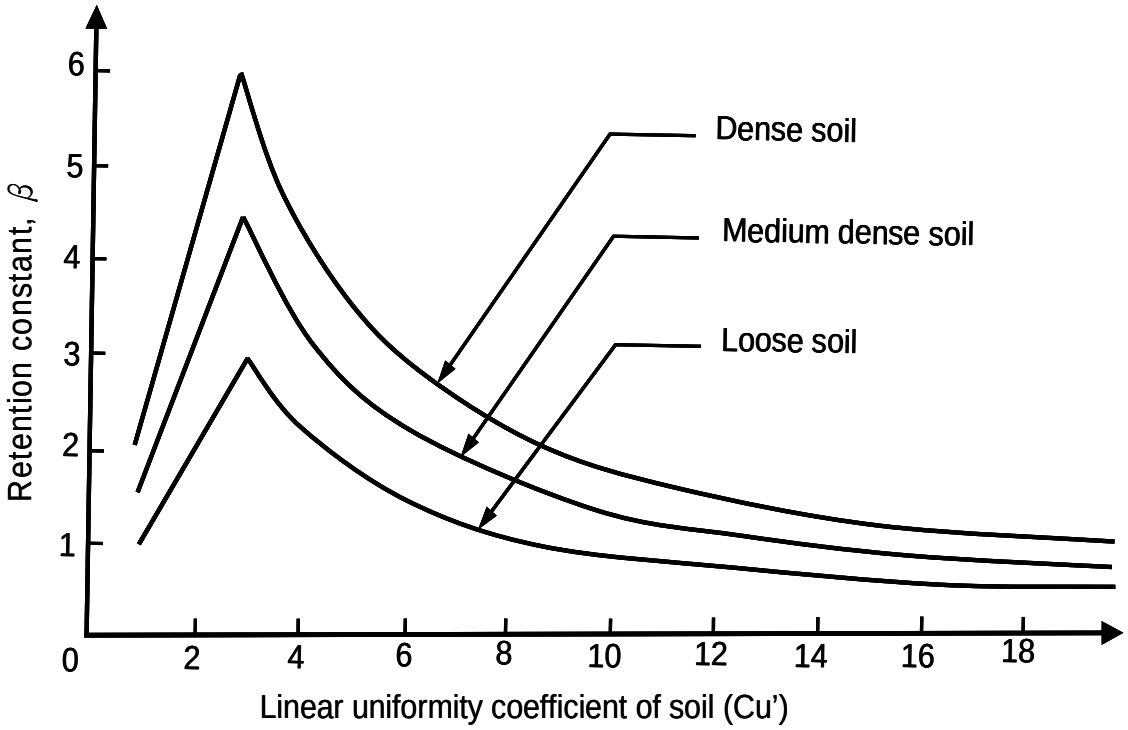

Figure 2.6 The retention criteria of Giroud (1982).

The French Committee of the Geotextiles and Geomembrances (CFGG, 1986) recommended that the retention constant (β) is calculated with:

$$\beta = \beta_1 \times \beta_2 \times \beta_3 \times \beta_4 \quad (2\text{-}15)$$

where

β_1 is the coefficient of granulometric: $\beta_1 = 1.0$ for well graded
$\beta_1 = 0.8$ for uniform graded

β_2 is the coefficient of soil density: $\beta_2 = 0.8$ for loss soil or unconfined
$\beta_2 = 1.25$ for dense soil and confined

β_3 is the coefficient of hydraulic gradient (i): $\beta_3 = 1.0$ for $i < 5$
$\beta_3 = 0.8$ for $5 < i < 20$
$\beta_3 = 0.6$ for $20 < i < 40$

β_4 is the coefficient of geotextile function: $\beta_4 = 1.0$ for pure filter
$\beta_4 = 0.8$ for filter/drainage

In addition, there are many studies based on the relationship of geotextile opening size and soil particle size, and then proposed the retention criteria are listed in Table 2-1.

Table 2.1 The retention criteria under uni-directional flow (Rearrange from Bertacchi and Cazzuffi (1985), and Fischer et al. (1990)).

References	Geotextile type	Base soil type	Retention criterion
Calhoum (1972)	woven	granular soil	$O_{95} \le d_{85}$
		cohesive soil	$O_{95} \le 210\mu m$
Ragutzki (1973) Zitscher (1975)	woven	sand ($C_u \le 2$ and $d_{50} = 0.1 \sim 0.2mm$)	$O_{50} \le (1.7 \sim 2.7) \times d_{50}$
	non-woven	cohesive soil	$O_{50} \le (2.5 \sim 3.7) \times d_{50}$
Ogink (1975)	woven	sand	$O_{90} \le d_{90}$
	non-woven	sand	$O_{90} \le 1.8 \times d_{90}$
Sweetland (1977)	non-woven	sand ($Cu = 1.5$)	$O_{50} \le d_{85}$
		sand ($Cu = 4.0$)	$O_{50} \le d_{15}$
Rankilor (1981)	non-woven	$0.02mm < d_{85} < 0.25mm$	$O_{50} \le d_{85}$
		$d_{85} \ge 0.25mm$	$O_{50} \le d_{15}$
Schober and Teindl (1979)	woven and thin non-woven	sand	$O_{90} \le (2.5 \sim 4.5) \times d_{50}$
	thick non-woven	sand	$O_{90} \le (4.5 \sim 7.5) \times d_{50}$
Millar, Ho and Turenbull (1980)	woven and non-woven	not described	$O_{50} \le d_{85}$
Giroud (1982)	needle-punched non-woven	loose soil ($1 < Cu' < 3$)	$O_{95} \le Cu' \times d_{50}$
		loose soil ($Cu' > 3$)	$O_{95} \le (9 / Cu') \times d_{50}$
		medium dense soil ($1 < Cu' < 3$)	$O_{95} \le 1.5 \times Cu' \times d_{50}$
		medium dense soil ($Cu' > 3$)	$O_{95} \le (13.5 / Cu') \times d_{50}$
		dense soil ($1 < Cu' < 3$)	$O_{95} \le 2 \times Cu' \times d_{50}$
		dense soil ($Cu' > 3$)	$O_{95} \le (18 / Cu') \times d_{50}$
	woven and heat bonded non-woven	soil ($1 < Cu' < 3$)	$O_{95} \le Cu' \times d_{50}$
		soil ($Cu' > 3$)	$O_{95} \le (9 / Cu') \times d_{50}$
Carrol (1983)	woven and non-woven	not described	$O_{95} \le (2 \sim 3) \times d_{85}$

Table 2.1 (continued) The retention criteria under uni-directional flow (Rearrange from Bertacchi and Cazzuffi (1985), and Fischer et al. (1990)).

Reference	Geotextile type	Base soil type	Retention criterion
Heerten (1981) Heerten (1982)	woven and non-woven	granular soil ($Cu \geq 5$)	$O_{90} < 10 \times d_{50}$ $O_{90} \leq d_{90}$
		granular soil ($Cu < 5$)	$O_{90} < 2.5 \times d_{50}$ $O_{90} \leq d_{90}$
		cohesive soil	$O_{90} < 10 \times d_{50}$ $O_{90} \leq d_{90}$ $O_{90} \leq 100\mu m$
Loudière et al. (1982) Loudière et al. (1983)	woven and non-woven	granular soil ($Cu \geq 4$)	$O_{90} < d_{95}$
		granular soil ($Cu < 4$)	$O_{90} < 0.8 \times d_{50}$
		cohesive soil ($Cu \geq 4$)	$O_{90} < d_{85}$ $O_{90} \geq 50\mu m$
		cohesive soil ($Cu < 4$)	$O_{90} < 0.8 \times d_{50}$ $O_{90} \geq 50\mu m$
DGEC (1986)	woven and non-woven	$d_{40} < 60\mu m$	$O_{90} < 10 \times d_{50}$ $O_{90} < 2 \times d_{90}$
		$d_{15} > 60\mu m$	$O_{90} < 5 \times d_{10} \times \sqrt{Cu}$ $O_{90} < d_{90}$
		$Cu < 15$, PI<15%, or $d_{50} = 20 \sim 100\mu m$	$O_{90} < d_{90}$
Christopher and Holtz (1985)	Depend on the geotextile type, base soil type and flow condition		$O_{95} < (1 \sim 2) \times d_{85}$
Fischer, Christopher and Holtz(1990)	Depend on the geotextile type and Cu of base soil type and hydraulic gradient		$O_{50} \leq 0.8 \times d_{50}$ $O_{50} \leq (1.8 \sim 7) \times d_{15}$ $O_{50} \leq (0.8 \sim 2) \times d_{50}$

O_x = geotextile opening size corresponding x particle size (O_{95}, O_{90}, O_{50})

d_x = soil's particle size corresponding to y percent passing (d_{90}, d_{85}, d_{50}, d_{15})

Cu = uniformity coefficient of soil (d_{60} / d_{10})

Cu' = linear uniformity coefficient of soil

2. Bi-directional flow:

For the bi-directional flow condition, the bridge structure is difficult to form, so the opening size of geotextile must be smaller than uni-directional flow condition. Such as Heerten (1982) suggested, for sand, the geotextile's opening size should be smaller than d_{90} or $(2.5\sim10)d_{50}$ under uni-directional flow but smaller than d_{50} under bi-directional flow. A summary of many literatures that proposed the retention criteria of bi-directional flow condition are listed in Table 2.2.

In addition to soil particle size distribution, Ragutzki (1973) and CFGG (1986) point out the influence of soil density. Teindl and Schober (1979) and Ingold (1982) considered the influence of hydraulic gradient. Besides, those criteria showed in Table 2.2 are quite different. That is because the tolerated total mass of soil pass through geotextile is different from each author.

Ingold (1985) used hydrodynamic sieving test after 18 hours, obtains less than 2.3 kg/m^2 of mass of soil pass and proposes that $O_f < 0.23d_{90}$ for Cu = 5 and $O_f < 0.09d_{90}$ for Cu = 50. Moreover, Heerten and Wittman (1985) considered that the retention is ensured for $O_f < d_{85}$ whereas they obtained 11.8 kg/m^2 in 5 hours after a turbulent test (Test BAW) where the propeller turns to 260 turns per minute.

Mlynarek (2000) proposed a flow chart to express retention criteria (Figure 2.7).

In order to accelerate formation of the soil-geotextile filter system, four geotextile properties must be selected properly (Rollin et al., 1988):

(1) A low permeability to decrease the dynamic forces on the particles: the geotextile permeability must not be lower than the soil permeability but should not be very large because the water cannot be evacuated in a drainage system at a rate faster than the one being permitted by the soil.

(2) A low porosity to avoid loss of an excessive quantity of soil particles.

(3) A large enough thickness to increase the water inlet area resulting in a decrease of the dynamic forces on the soil particles.

(4) Surface characteristics offering many free fibers contact with the soil.

Table 2.2 The retention criteria under bi-directional flow (Rearrange from John (1987) and Faure (1988)).

Reference	Geotextile type	Base soil type	Retention criterion
Lawson (1982)	not described	$Cu < 5$	$O_{90} < d_{50}$
Heerten (1982)	woven and non-woven	non-cohesive soil	$O_{90} < d_{50}$
		cohesive soil	$O_{90} < 10 \times d_{50}$ $O_{90} \le d_{90}$ $O_{90} \le 100\mu m$
DGEC (1986)	woven and non-woven	$d_{40} > 60\mu m$	$O_{90} < d_{90}$
		$d_{40} \le 60\mu m$	$O_{90} < 1.5 \times d_{10} \times \sqrt{Cu}$ $O_{90} < d_{50}$ $O_{90} < 500\mu m$
Ragutzki (1973)	woven and non-woven	not confined	$O_{90} \le (0.5 \sim 0.7) \times d_{50}$
	woven	confined	$O_{90} \le (0.5 \sim 1.3) \times d_{50}$
	non-woven	confined	$O_{90} \le (0.5 \sim 1.5) \times d_{50}$
PIANC (1987)	woven and non-woven	$Cu < 5$	$0.05mm < O_{90} < 0.7 \times d_{90}$
		$Cu > 5$	$0.05mm < O_{90} < d_{90}$
Schober and Teindl (1979)	woven and non-woven	not described	$O_{90} \le d_5 \sim d_{85}$ (follow gradient, i)
Ingold (1982)	woven and non-woven	not described	$O_{90} = \alpha d_{50} Cu(1-\sqrt{2/Cu})$ as $\alpha = (i-0.5) \times \sqrt{Cu/4}$
ASPG (Tonus, 1985)	woven and non-woven	$d_{40} > 60\mu m$	$O_{90} \le 1.5 \times d_{10} \times \sqrt{Cu}$ $O_{90} \le d_{60}$
CFGG (1986)	woven and non-woven	dense soil ($Cu > 4$)	$O_{90} < 0.75 \times d_{85}$
		loose soil ($Cu > 4$)	$O_{90} < 0.60 \times d_{85}$
		dense soil ($Cu \le 4$)	$O_{90} < 0.60 \times d_{85}$
		loose soil ($Cu \le 4$)	$O_{90} < 0.48 \times d_{85}$
Holtz (1998)	woven and non-woven	$d_{50} < 74\mu m$	$O_{50} \le 0.5 \times d_{85}$
		$d_{50} \ge 74\mu m$	$O_{95} \le d_{15}$

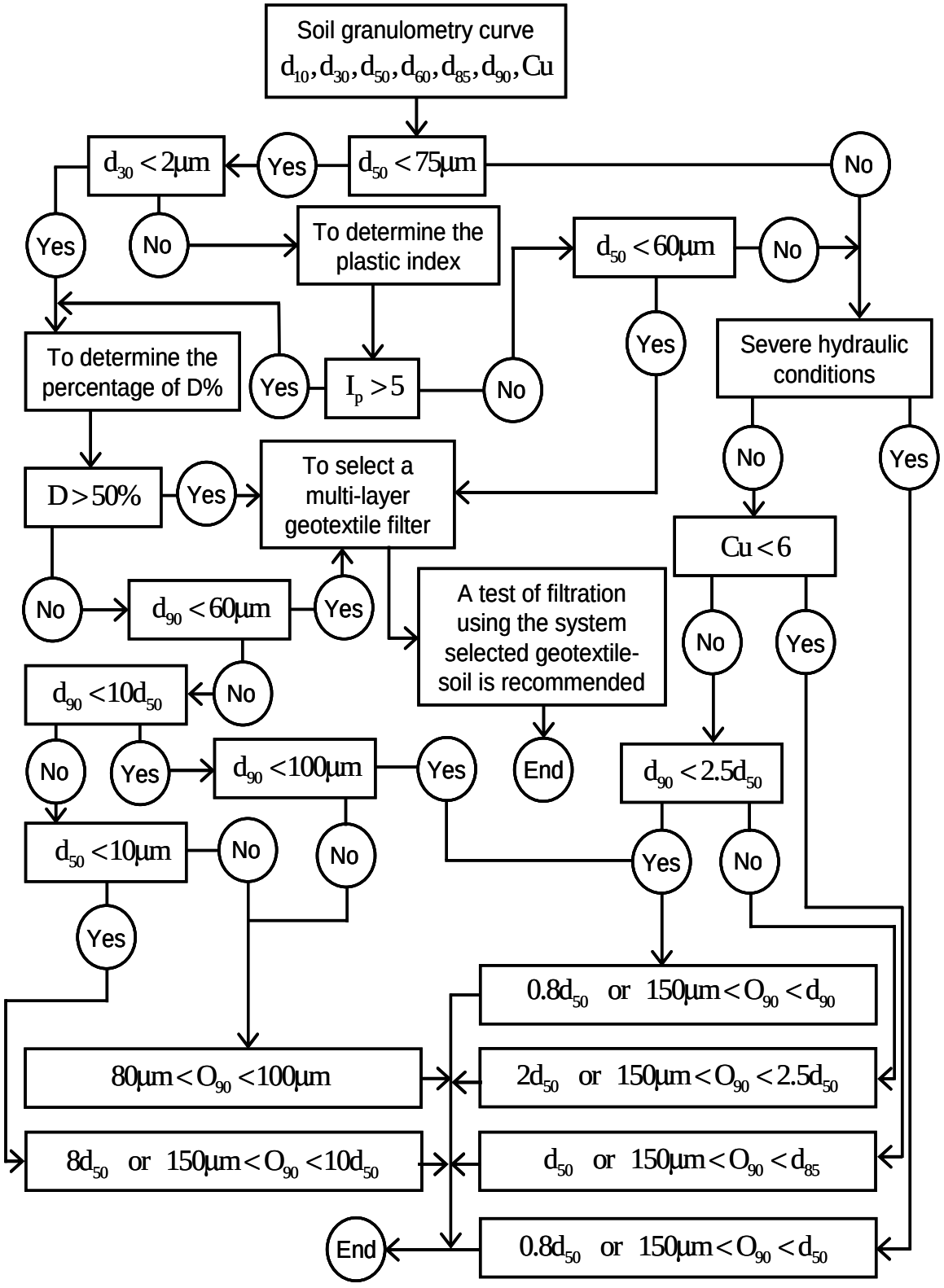

Figure 2.7 The retention criteria under bi-directional flow (Mlynarek, 2000).

2.3.3 Criteria of pore size distribution of geotextile

To compare two different geotextiles with same opening size, each often displays different hydraulic behavior. Bhatia et al. (1991) found that geotextile with similar filtration opening size (FOS) may show different degrees of clogging and soil piping. Lafleur et al. (1996) show that the different textiles structure may have obviously different filtration behaviors even if they have the same FOS. This indicates a need for a more refined description of a filter. To determine the smaller pore sizes of a geotextile, the complete pore size distribution (PSD) must be measured. Pore size determination methods include: dry sieving with soil (Belgium and UK) or glass beads (USA, ASTM D 4751), wet sieving (Swiss and German standards), hydrodynamic sieving (France, Canada and Italy), a suction method (Dennis and Davies, 1984), mercury instrusion porosimetry (MIP) (Elsharief, 1992, and Prapaharan et al., 1989, and Chen, 1986), capillary liquid extrusion porosimetry (Miller and Tyomkin, 1994), the bubble point method (Bhatia and Smith et al., 1994, and Fisher, 1994), the minimum bubble pressure technique (Miller et al., 1986), and image analysis (Wates, 1980, Rollin et al., 1982, and Elsharief,1992). Many designers consider the PSD of a geotextile as being an equally important design property as the soil grain size distribution (Bhatia, 1991). Similar to the practice with graded soil filters that geotextiles have replaced the grain size distribution, and thus, the pore size distribution of both the soil being filtered and the filter should be parallel.

Giroud (1996) propose that the pore size distribution or the textiles structure can be defined by “number of constrictions, m”. As following

$$m = \sqrt{1-n} \times \frac{t_{GT}}{d_f} \tag{2-16}$$

where n is the porosity of geotextile, t_{GT} is the thickness of geotextile and d_f is the diameter of fiber of geotextile. This parameter can be regarded as the average ratio of fiber that the particle will be met while passing through the geotextile. According to the Equation 2-15, the number of constrictions increases as the thickness of geotextile increases, the porosity of geotextile or the diameter of fiber decreases.

In order to know the relationship between the soil-geotextile filtration system behavior with the number of constriction, Bouthot et al. (2002) adopted several geotextiles those with the similar FOS but different in number of constriction to carry out the GR (Gradient Ratio) test. The test result shows in Figure 2.8. Despite

geotextiles with similar FOS, it can be seen that higher soil erosion is systematically associated to high values of m. Considering that piping occurs when the eroded soil mass exceeds 2.5 kg/m^2 (Lafleur et al. 1989), it could be state that a m value of around 55 surely represents a critical limit. A m value of 45 would apparently be a reasonable upper limit.

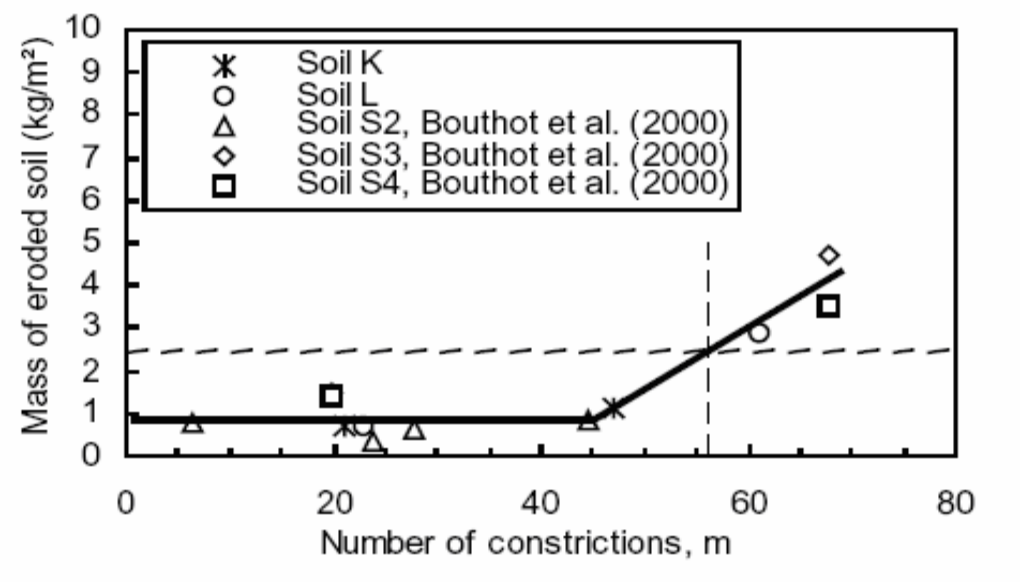

Figure 2.8 Determination of the upper limit of the number of constrictions (Bouthot et al. 2002).

2.4 Filtration tests

The foregoing criteria have a large different and have not consider a differentiation of the geotextile structure. Unfortunately, the geotextiles produced are woven, non-woven, needlepunched or head-bonded whereas their filter behavior is surely very different. The Geotextile Design and Construction Guidelines, FHWA (1989) and Christopher and Fischer (1992) suggested that, the design criteria should be decided by experiments for geotextiles to be used in important construction or with critical conditions. The following will describe the details of the filtration experiments.

2.4.1 Gradient ratio test (GR test)

The gradient ratio test has been developed by the US Army Corps of Engineers to evaluate the potential fouling of the geotextile. Hydraulic head at various locations in a

soil placed in a vertical cylinder is measured after a 24h filtration period. The ratio of two differential hydraulic gradients measured close and far away from the geotextile is defined as the gradient ratio GR.

Following the work of Calhoun (1972), GR is defined as the hydraulic gradient through the lower 25mm (1.0in) of the soil plus geotextile divided by the hydraulic gradient through the adjacent 50mm (2.0in) of the soil. Gradient ratio values exceeding 3.0 where believed to signify excessive geotextile clogging. Thus, a limiting value of 3.0 was established for testing with soil, geotextile, and hydraulic conditions of interest. ASTM D5101 defined the GR value is:

$$GR = \frac{\Delta h_{GT+25s} / t_{GT+25}}{\Delta h_{50s} / t_{50}} \tag{2-17}$$

Where: Δh_{GT+25s} = The water head difference across bottom 25mm soil and geotextile.

t_{GT+25} = The thickness between bottom 25mm soil and geotextile.

Δh_{50s} = The water head difference across adjacent 50mm soil and geotextile.

t_{50} = The thickness of adjacent 50mm soil.

ASTM (1995) redefines the critical GR value according to the GR tests:

$GR = 1.0$, the soil-geotextile filter system is stable;

$GR < 1.0$ expresses that the possible of soil loss, and

$GR > 1.0$ will probably clog or block.

2.4.2 Long-term flow test (LTF test)

For GR test, the test of 24 hours duration is insufficient to obtain the stable soil-geotextile filter system. To increase the test duration until several hundred hours is necessary especially for fine particle soil. Scott (1980) and Marks (1975) studied the time of stable soil-geotextile filter system forms according to the GR test. They proposed that the test duration over 24 hours would be enough for non-cohesive soils but the test duration of several days is necessary for cohesive soil.

Koerner and Ko (1982) took the soil samples from site and placed on a geotextile specimen installed at the bottom of a cylinder and a filtration test is performed at a content water head for a long period of time. It named long-term flow test (LTF test). About 100~150 hours after testing, the stable filter system appeared for silty soil. But for clay, the stable system is observed after one month. Therefore, standard GR test is suitable for sand to investigate the filter behavior. For silts and clays, because the influence of soil weight and low seepage force may cause the soil-geotextile filter system compression. To extend GR test duration or to adopt LTF test is more effective to response this phenomenon.

2.4.3 Hydraulic conductivity ratio test (HCR test)

The hydraulic conductivity ratio (HCR) analysis is a soil-geotextile interaction test which is performed under conditions which simulate the field conditions. The soil sample is prepared using standard laboratory or field sampling techniques which are designed to simulate field placement conditions. The state of stress, stress history and void ratio of the soil and geotextile are carefully controlled throughout the test. Since the soil sample may be fully saturated and the triaxial permeability device used in the HCR analysis provides control of the flow direction and hydraulic gradient, all of the primary variables which affect the filtration characteristics and flow properties of geotextile/soil composites are either controlled or measures during the HCR analysis.

The hydraulic conductivity ratio is defined as the hydraulic conductivity of the soil, ψ_s, divided by the equilibrium hydraulic conductivity of a soil-geotextile composite, ψ_{GS}. Since the hydraulic conductivity of both the soil and the soil-geotextile composite are measured directly, the HCR analysis provides data which are appropriate for the design.

$$HCR = \frac{\psi_{GS}}{\psi_S} \tag{2-18}$$

2.4.4 Cyclic flow test

An overview of the whole system is illustrated in Figure 2.9. The system consists essentially of the flow device, the tank for the collection of soil passing through the filter and the test specimen cylinder. The test specimen cylinder (internal diameter of

300 mm) is composed of the supporting grid, of the outside layer, of the geotextile filter clamped between two rings and of the base soil (laid on the geotextile until it reaches the upper pushing disk connected to the effective stress device).

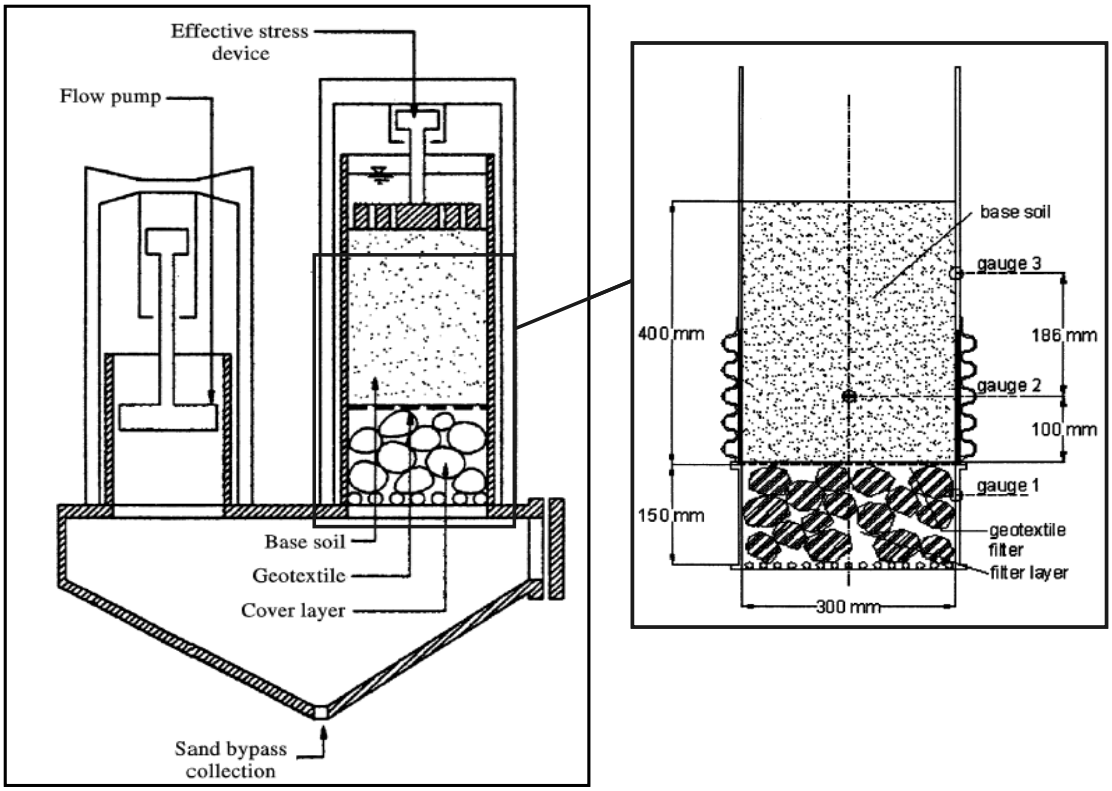

Figure 2.9 The set-up of perpendicular flow equipment and test specimen (Cazzuffi et al., 1999).

The problem to apply a uniform effective stress of known value to the interface was solved by using a deformable cylinder. The desired load is applied to the upper part of the test specimen cylinder. Since the wall close to the base soil-geotextile interface is not rigid, it is the base soil that transfers the stress to the interface. In fact, since the wall moves together with the soil, there are very little relative displacement between the soil and the wall, and hence very little shear stress.

Both gradients and passing soil mass can be measured. Three pressure gauges are inserted into the test specimen; the first one is situated in the outside material close to the geotextile (gauge 1: pressure readings are performed close to the cylinder wall) and the other two in the base soil at different levels (pressure reading close to the geotextile – gauge 2 – are performed in an axial position, while upper readings – gauge 3 – are performed close to the wall), so that the evolution of the filtering system can be

evaluated both near the geotextile and in the base soil (if a significant movement of particles in the base soil could be expected).

Typical pressure gauges response versus time is given Figure 2.10. The figure shows a phase lag and an amplitude damping: both these values were depending on the stress conditions and hydraulic loading cycle characteristics.

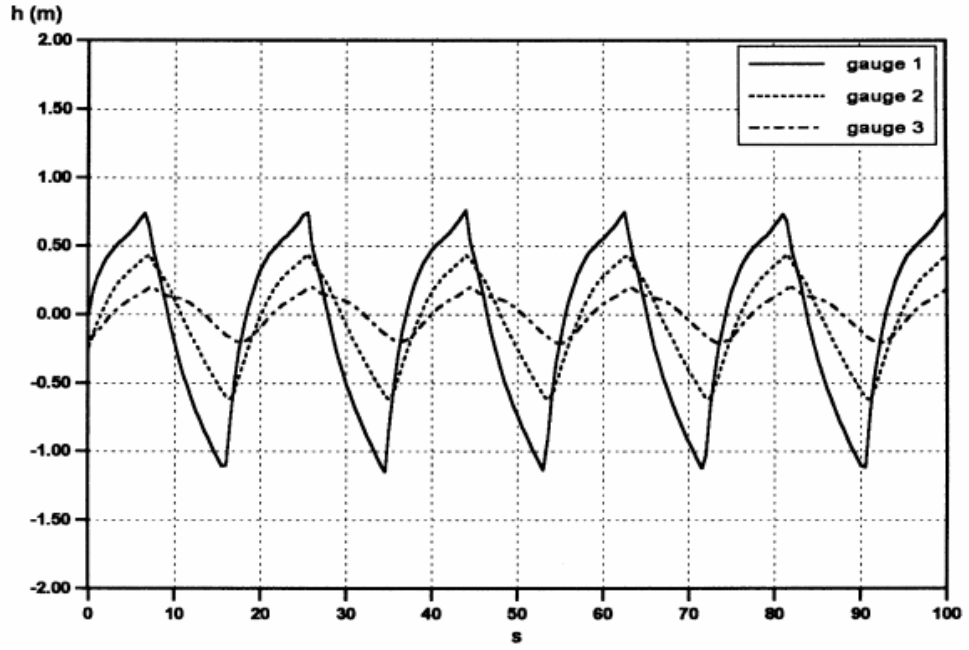

Figure 2.10 Water column height (h) versus time (s) (Cazzuffi et al., 1999).

In order to understand the influence of the punctured holes on the geotextile filter caused by installation damage, Chew et al. (2003) adopted the perpendicular flow equipment to carry out a series test. Three types of geotextiles were used and pre-cut L-shaped holes of different size, various overburden pressure and different periods of wave were employed in this test series. Figure 2.11 illustrates the typical variation of pore pressure of a cyclic waves load. In these figures, it can be seen that the trends of pore pressure is the same for all the cases of the different wave period. When the wave front enters the sand sample, the pore pressure increases rapidly, reaches its peak value. It is then followed by pore pressure reduction when wave front is retracing in the sand mass, and reaches the negative peak value. The peak value of pore pressure decreases as the wave period increases. Therefore the peak pore pressure for 2s period case is the largest; while the peak pore pressure for 10s period case is the smallest. Moreover, Figure 2.11 also shows that the peak value of pore pressure decreases from the bottom of the sample (PPT1) to the top of the sample (PPT3) and illustrates the energy dissipation in the sand mass from PPT1 to PPT3 locations. It was observed that the

peak value of pore pressure decreases from the soil-geotextile interface (PPT1) to the deeper position in subsoil (PPT3). The difference of pore pressure at the different positions will affect sand particles movement and particles rearrangement significantly.

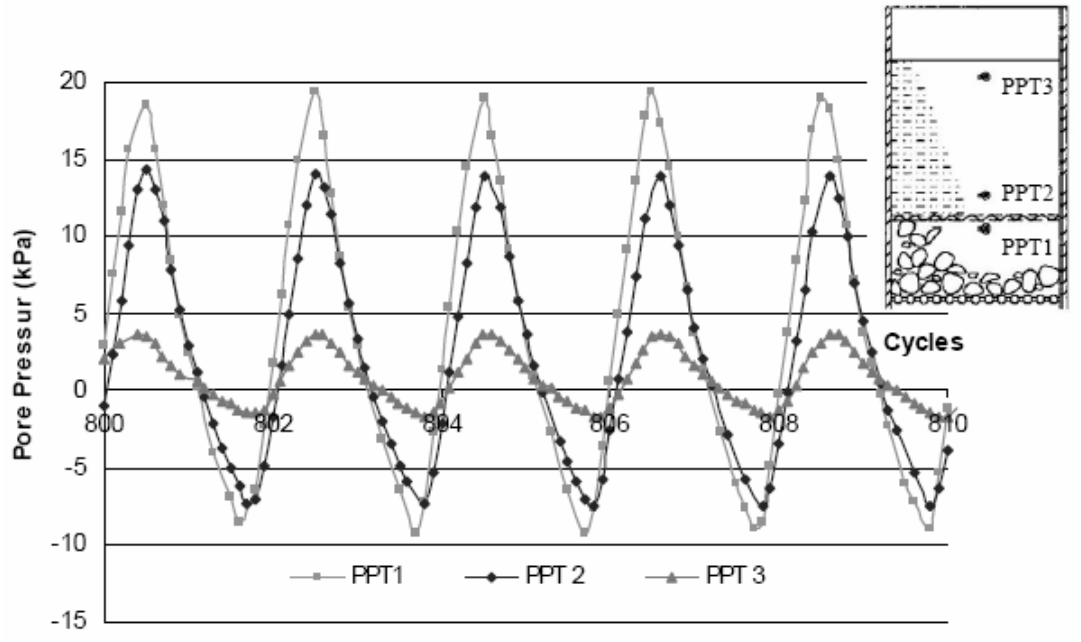

(a) Pore water pressure of 2s wave period

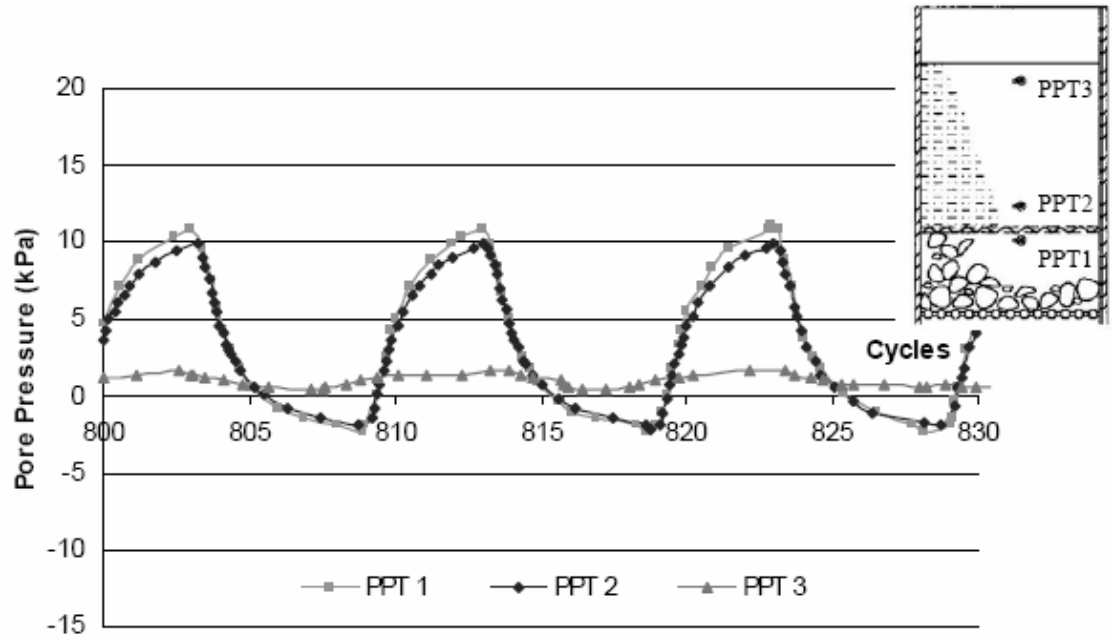

(b) Pore water pressure of 10s wave period

Figure 2.11 Water pressure versus time (Chew et al., 2003).

2.5 Parallel erosion mechanisms and tests

As stated in Chapter 1, the revetment using geotextile may suffer tangential flow as well as the perpendicular flow. Parallel erosion experiments were developed to investigate the soil geotextile behavior subjected to tangential flow, in addition to the internal erosion of soil under the groundwater flow.

2.5.1 Gravel filter-subsoil interface horizontal erosion test

For most of water retaining structures, such as the embankment dams or the riverbanks, groundwater seepage prevails under subsoil. If the subsoil is layered, the seepage might cause the parallel layer erosion between two layers. Scherzinger (1984) proposed that the critical erosion flow velocity ($v_{F,crit}$) of the gravel filter-subsoil interface is related to the critical Froude number (Fr_{crit}).

$$v_{F,crit} = Fr_{crit} \times n_F \times \sqrt{\frac{\gamma'_{sB} \times d_{50B}}{\rho_w}} \tag{2-19}$$

where: n_F = The porosity of gravel filter.
γ'_{sB} = The unit weight of subsoil.
d_{50B} = The subsoil's particle size corresponding to 50% passing.
ρ_w = The density of water.

Wittmann (1980) used the feedback investigations and addressed the critical hydraulic gradient ($i_{F,crit}$) of the rougher situations with the laminated soil is

$$i_{F,crit} = a \times v_{F,crit} + b \times v_{F,crit}^{\ 2} \tag{2-19}$$

$$a = \frac{270 \times (1 - n_F)^2 \times \eta}{n_F^{\ 3} \times \gamma_w \times d_w^{\ 2}} \tag{2-20}$$

$$b = \frac{\lambda_v}{2 \times n_F^{\ 2} \times T^2 \times g \times d_w} \tag{2-21}$$

where: η = Dynamic viscosity of the water.

γ_w = Density of water.

d_w = Effective of grain size.

λ_v = Middle loss factor ($\cong 4$).

T = Tortuosity of the pore channels ($\cong 2/\pi \cong 0.65$).

g = Acceleration of gravity.

In order to understand the effect of the subsoil particles size and the porosity of gravel filter on the interface erosion behavior, Brauns (1985) adopted a gravel filter-subsoil interface horizontal erosion equipment (Figure 2.12) and carried out a series test in laboratory. In this test, three different compositions of very uniform soil and four kinds of gravel filters are used but the porosity are almost the same ($n_F \cong 0.39$). There are fourteen of components with gravel filter and subsoil in this study.

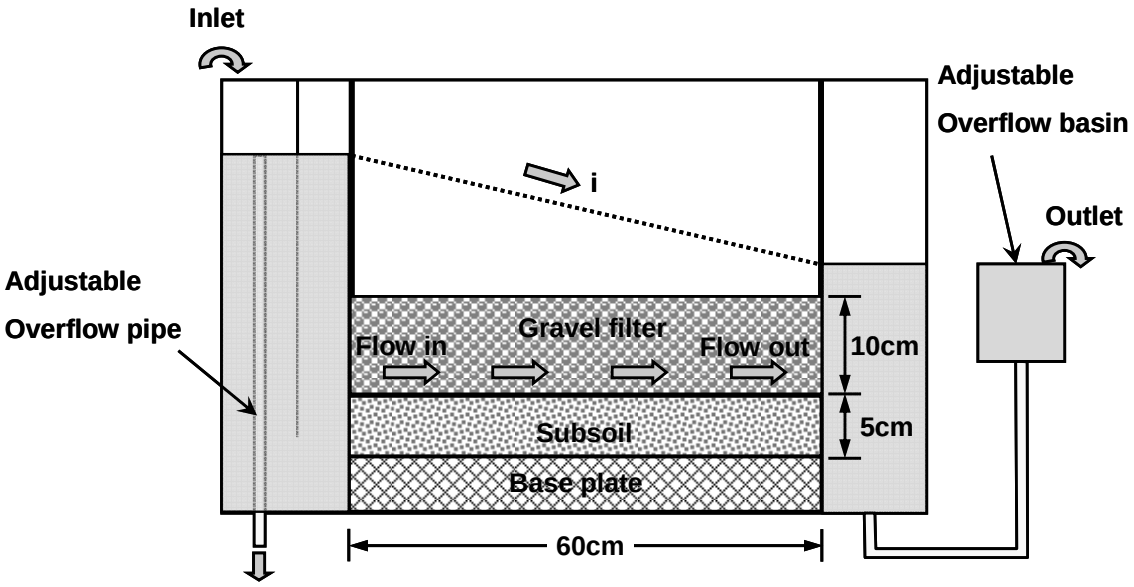

Figure 2.12 Illustration of the gravel filter-subsoil interface horizontal erosion test (Brauns, 1985).

According to the test result, Brauns opined out that the critical Froude number (Fr_{crit}) is 0.65 to 0.70 and the variation is insignificant with gravel filter and subsoil particle size distribution. Hence, he suggested that $Fr_{crit} = 0.65$.

Combining Eq. (2-18) to Eq. (2-21) and using $Fr_{crit} = 0.65$, $n_F = 0.39$, Figure 2.13 is obtained.

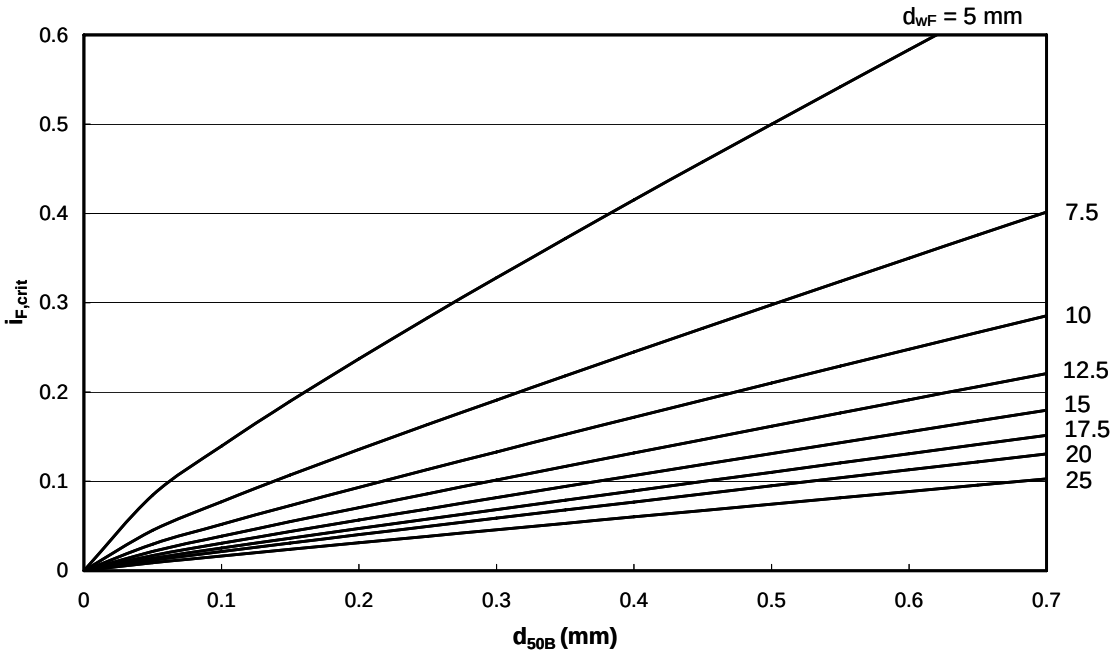

Figure 2.13 Hydraulic criteria for gravel filter-subsoil interface horizontal erosion (Brauns, 1985).

2.5.2 Slot erosion test (SET)

This test is developed by Wan and Fell (2003) and used to characterize the phenomenon of piping. The sample of soil is filling in a rectangular aluminum chamber of 1 m length and 0.15 m height. It is about 30kg weight for one test. This chamber is equipped with a transparent plate (plexiglass) allowing to well observe the phenomenon of erosion. On the transparent side of the sample where was created a slot of 2.2 mm depth and 10mm height. Water circulates infused by the adjustable overflow container and the evolution of the slot can be observed. Figure 2.14 diagram the layout of slot erosion test equipment.

In order to describe the characteristic of the soil erosion clearly, Wan and Fell made the four following assumptions for slot erosion test:

1. The section of the slot is uniform.
2. Only consider the flow resistance on the soil surface of the slot and neglects the resistance on the side of plexiglass.
3. The cross section of the slot evolves into an elliptic section.
4. The width of the slot is proportional to experimental time square (t^2).

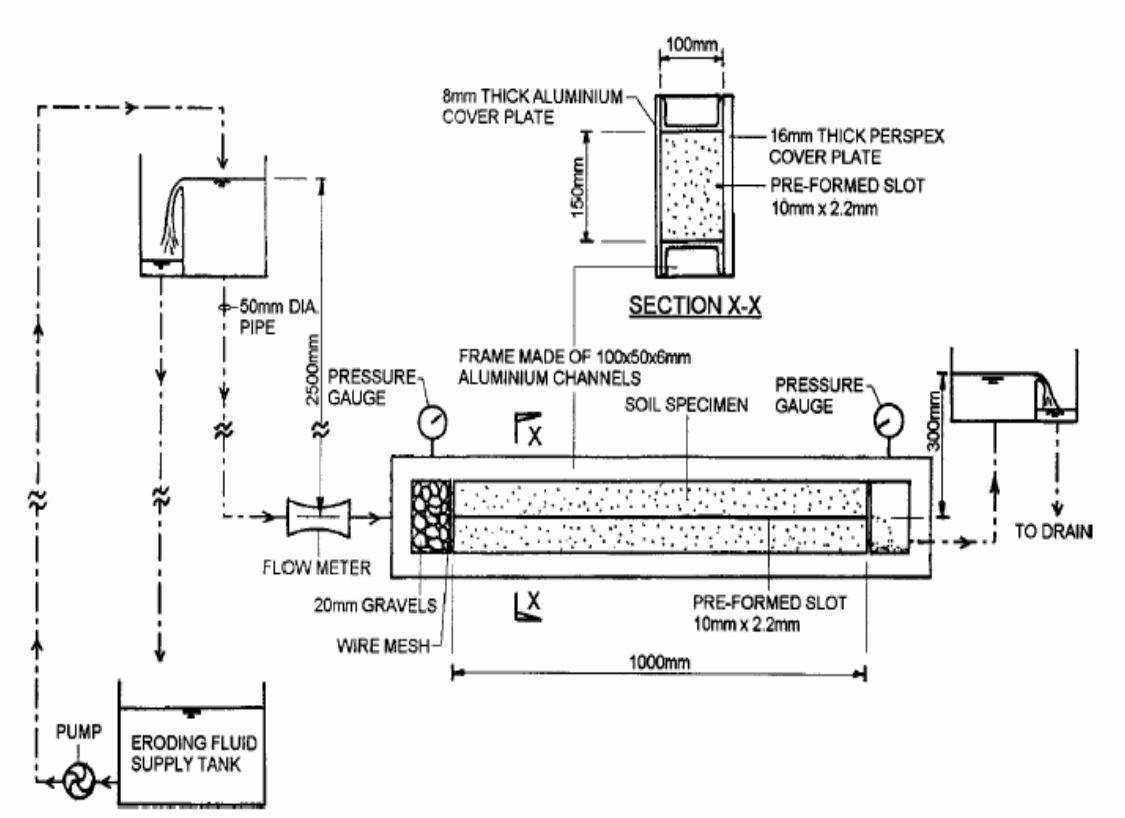

Figure 2.14 Schematic diagram of the slot erosion test (SET) layout (Wan and Fell, 2004).

2.5.3 Hole erosion test (HET)

This test is developed by Wan and Fell (2003) also. The sample of soil is filling in a standard cylindrical steel mould that approximately 100 mm diameter and 115 mm length. The soil sample is compacted and then bored a hole of 6 mm in diameter. As same with SET, to infuse into water circulates within soil sample by the adjustable overflow container (see Figure 2.15). This test was developed because it is faster and economic then the SET.

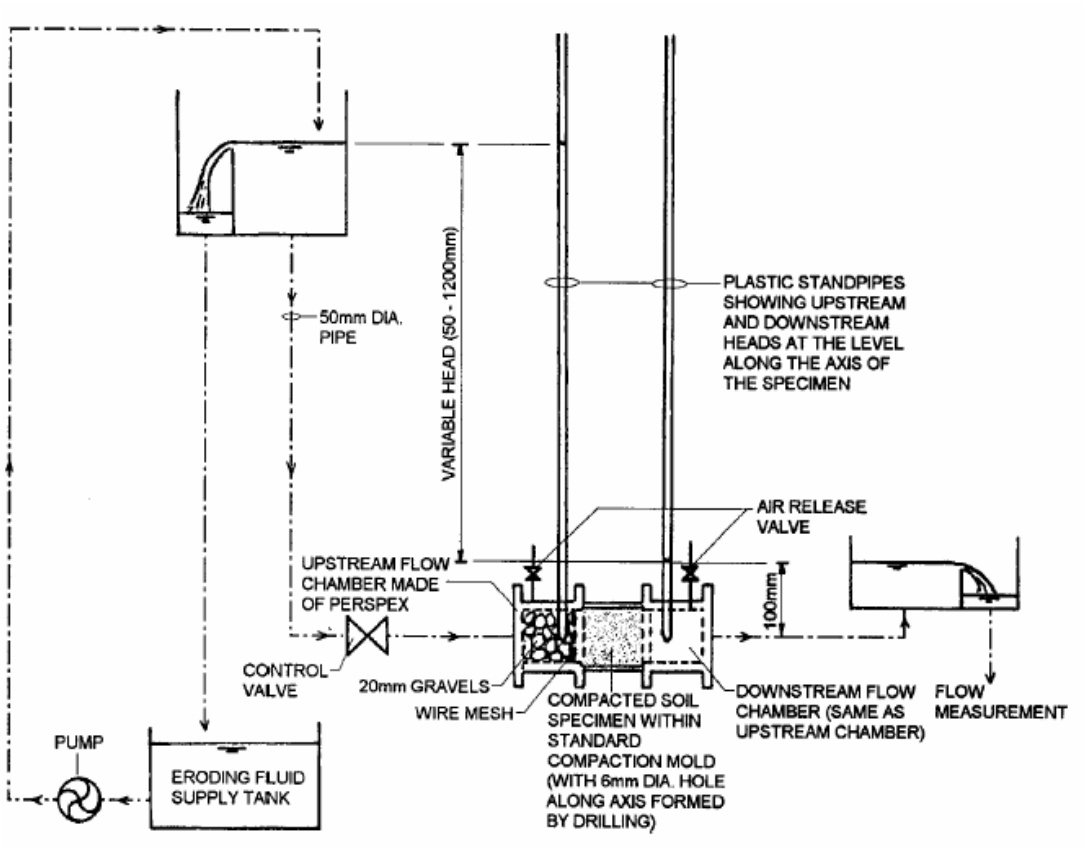

Figure 2.15 Schematic diagram of the hole erosion test (HET) layout (Wan and Fell, 2004).

For HET, Wan and Fell (2003) made three following assumptions in order to understand the appearance of internal erosion:

1. The section of the hole is uniform.
2. The friction coefficients that relate with shear stress and velocity are linearly with time.
3. The influence of flow through soil is neglected compared to the flow which passes through the hole.

According to the 225 sets of HET results, Wan and Fell (2002) proposed the relationship of the estimated rate of mass removal per unit area ($\dot{\varepsilon}$) and the estimated shear stress (τ). It is showed in Figure 2-16.

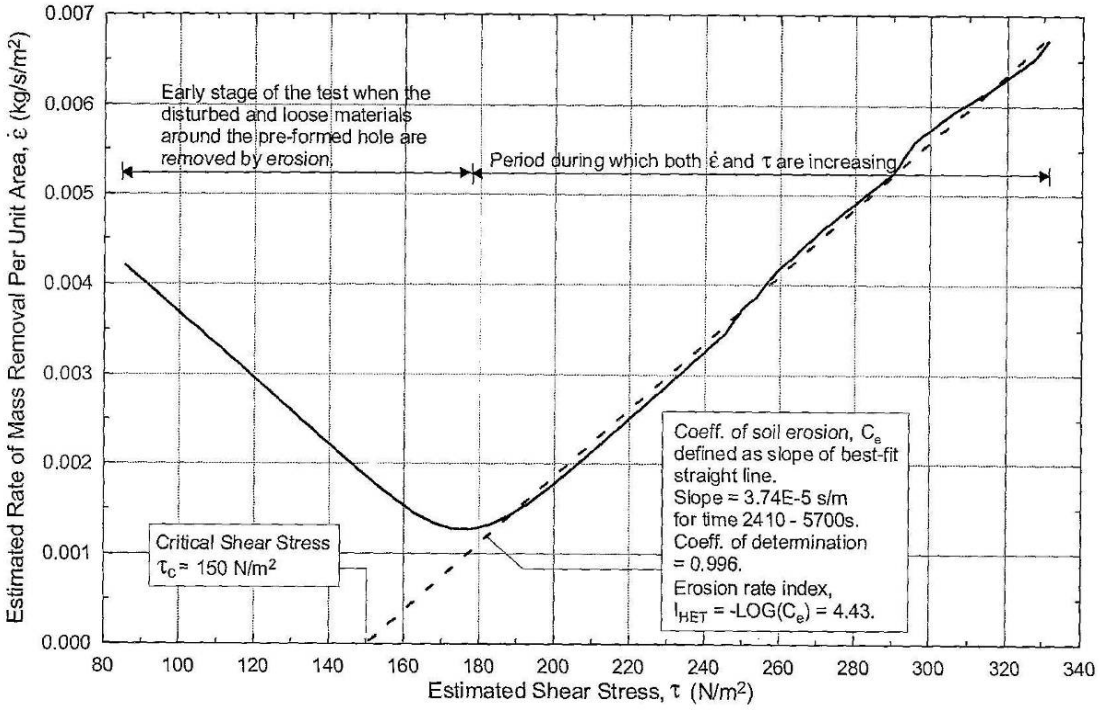

Figure 2.16 The relationship of the estimated rate of mass removal per unit area and the estimated shear stress by HET (Wan and Fell, 2002).

2.6 Summary

To develop continuously experiments, to establish the analytical models, and to accumulate in situ inspections are necessary to understand the mechanisms of soil-geotextile filter system.

In following chapters, the full-scale flume test and bi-directional cyclic flow test were developed to study the soil erosion mechanism and to examine the suitability of current design criteria, and furthermore to put forward more suitable design criteria under the bi-directional cyclic flow condition.

Moreover, the existing experiments to investigate tangential soil erosion are not allowed to observe accurately and to ascertain when the soil erosion occurs. The SET and HET could not provide precise measurements of soil erosion ratio and critical shear stress. These tests are only simple indicators of the erosion behavior of several types of soil without any influence of a filter (geotextile or soil filter). Besides, the two tests assume that the section of the hole is uniform while testing. This assumption is queried on filter/subsoil system. Because of soil erosion behavior relates to area that the filter covers, and the erode area is not uniform.

In this research, a new parallel erosion equipment based on Brauns (1985) was developed and several apparatus were set up to monitor the variation during the testing, in order to more accurately study soil erosion behavior. The equipment and test result are described in Chapter 5.

Chapter 3 Study of short-term bi-directional flow by full-scale flume test

Nowadays, the trend in using geotextile filters under armor stone for protects riverbanks or seacoasts have become popular. When the waves produced by winds or boats pounded on the revetment, it would generate the short period of hydrodynamic pressures in the vicinity of revetment surface. As a result, continued wave action can be very effective in eroding soil and decreasing the stability of the revetment. Furthermore, the short-term waves hinder the formation of a stable soil-geotextile filter system. PIANC (1992) described that the flows in the vicinity of the filter system can be very complex if the waves tend to break, a process further complicated by the presence of the armor stone layer. Hence, the hydraulic conditions in the base soil are very difficult to reproduce accurately in a laboratory test. This is why a full-scale test using a water flume is necessary to study the different mechanisms taking place. It is possible to correctly reproduce the hydrodynamic loading on the revetments. This chapter is to highlight the different mechanisms of short-term bi-directional cyclic flow, and to compare the existing design guidance with experimental results.

3.1 Test equipment

The equipments for large flume experiment including water flume, wave generator, deformation measurement systems, turbidity measurement apparatus, water pressure monitor, and soil particle size investigation.

1. Water flume:

The primary device of this experiment is a large-size steel water flume of 8m long, 1m wide, and 1.3m high (see Figure 3.1). On end of the flume is a wave generator and the other end is the deformation measurement.

2. Wave generator:

The wave generator (see Figure 3.2) consists of a metal panel driven by an electric motor, via a connecting rod and a rotating flywheel. The speed of rotation can be controlled to generate waves of different energies and frequencies to simulate the condition of actual in situ.

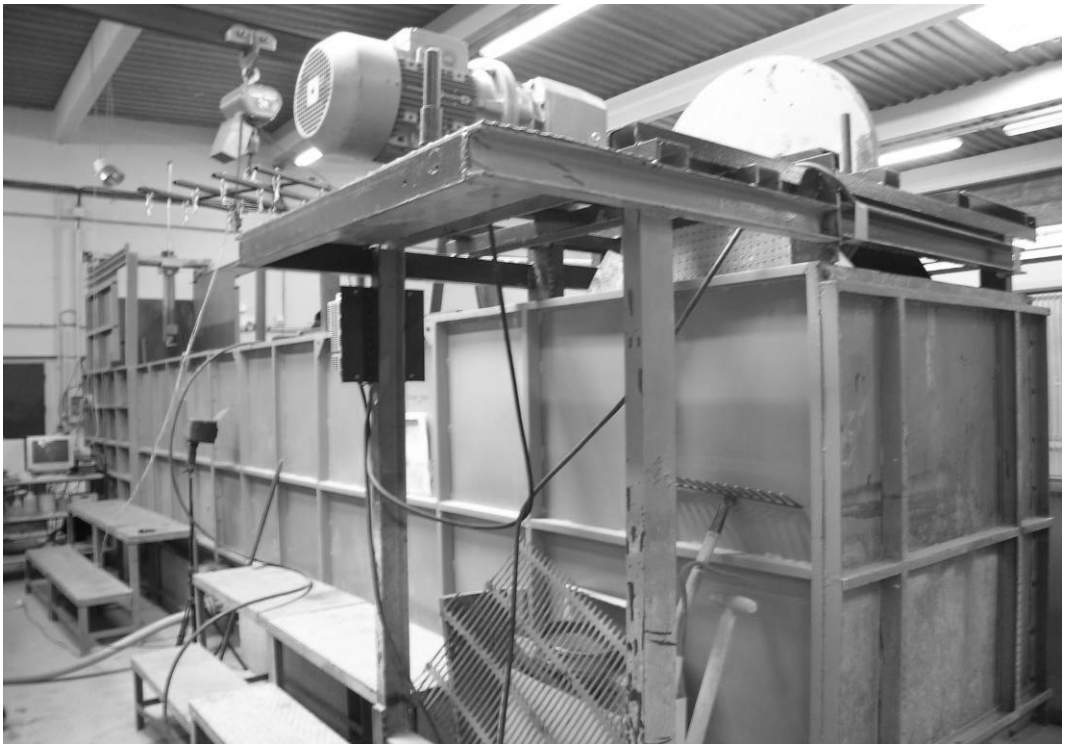

Figure 3.1 General views of the water flume.

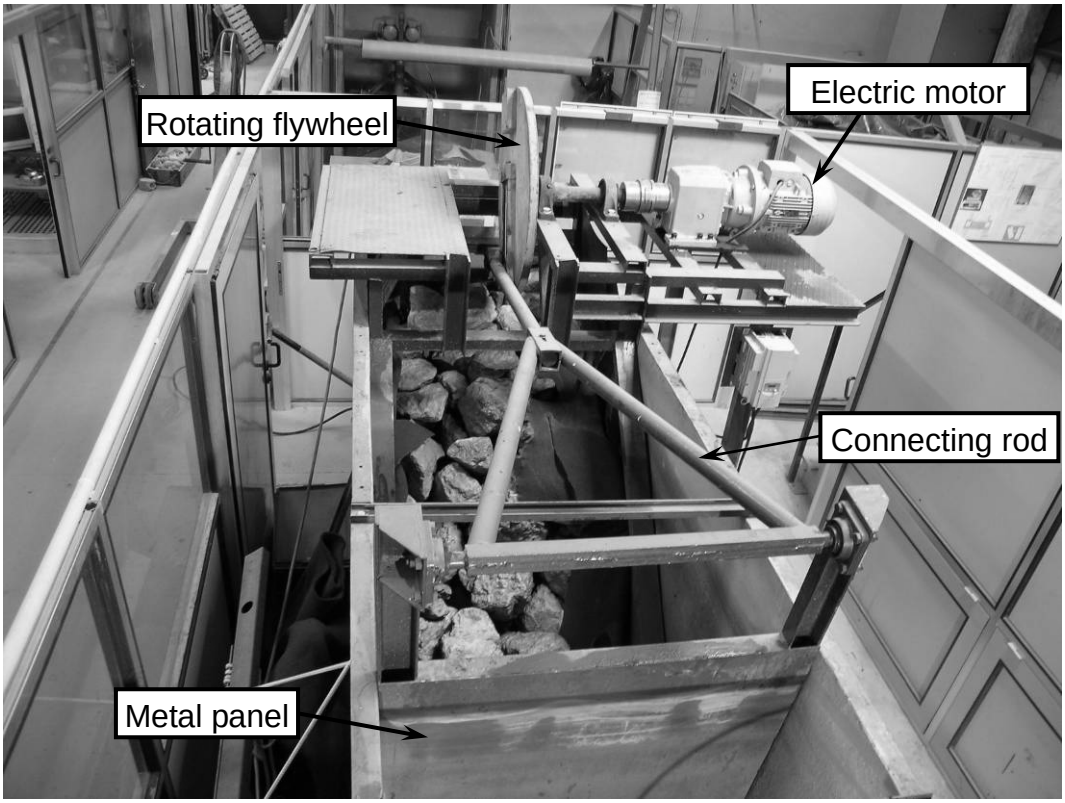

Figure 3.2 General views of the wave generator.

3. Deformation measurement systems:

The deformation of the geotextile revetment surface is measured during the test at regular times. The deformation measurement systems incorporates 3 wire rollers connected severally with a winding reel that slides in all directions, as well as a longitudinally flexible measurement bar (see Figure 3.3 for detail). During the experiment, the end of the measurement bar is placed behind the measurement point (in physical contact). Once the automatic reading system is turned on, the extended length of the steel wire in 3 directions can be recorded. This way the coordinates of the measurement point can be determined. During the experiment, multiple measurements are taken for the same measurement points for recording of the deformation.

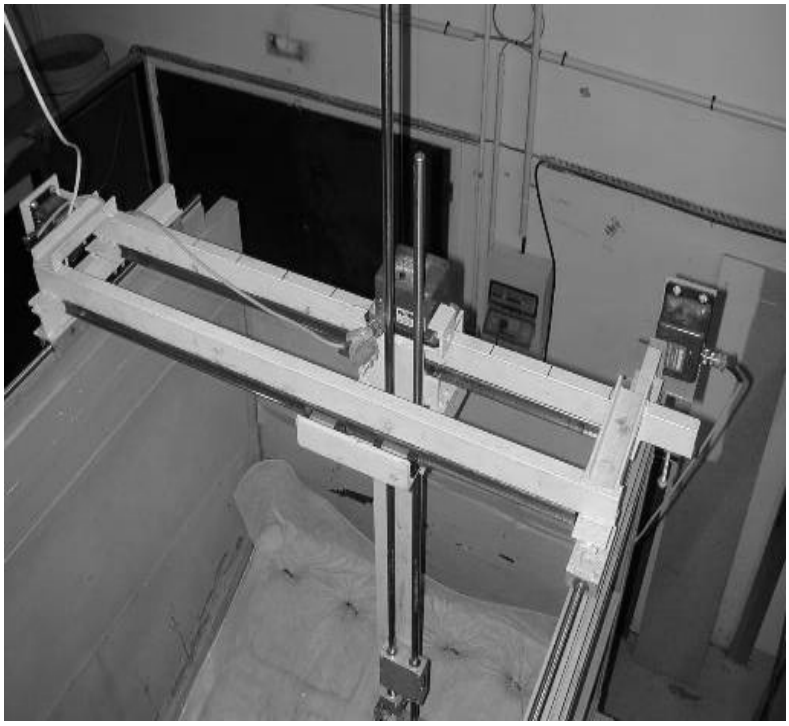

Figure 3.3 Deformation measurement systems.

4. Turbidity measurement apparatus:

In order to determine whether the base soil of the geotextile revetment is filtered out due to erosion during the experiment, it is necessary to measure the turbidity periodically until the turbidity is constant for determining the mechanism and process through which the soil is filtered out. A beam of an infrared light passes through a vial containing a sample of water from the flume. A sensor detects the amount of light scattered by the non-dissolved particles present in the sample. Such reading is converts in to FTU values (Formazine Turbidity Unit, ISO 7072) (see Figure 3.4).

Figure 3.4 Turbidity measurement apparatus.

5. Water pressure monitor:

In order to understand the variation of pore water pressure under bi-directional cyclic flow during the test, 2 piezometers are installed respectively under the geotextile (see Figure 3.5). In addition, a water level observation well is established at the rearward of revetment close to the flume's wall and the water level indicator is used to measure changes in water levels (see Figure 3.6).

Figure 3.5 Water pressure monitor - piezometers.

Figure 3.6 Water level observation well and indicator.

6. Soil particle size investigation:

The granulometric analysis of the soil in various places can provide interesting information for this study. After the test, several soil samples are taken to investigate the particle distribution and are compared with the original soil. It is possible to understand the behavior of soil eroded and to check the suitable of geotextile used. these analyses were carried out by granulometric laser (MALVERN Instruments - Mastersizer X) (Figure 3.7).

Figure 3.7 The laser granulometer.

3.2 Test materials properties

This experiment used one type of soil material and two types of geotextiles. The material characteristics used is described following.

3.2.1 Soil material

The soil used in this experiment comes from non-cohesive fine silty sand, a sedimentary deposit of the river Isère. This is one of the principal geological materials found in the Grenoble area and it is common to find it constituting the old dikes built along the Isère valley. It contains some rounded gravel and pebbles but 90% of its grain size is lower than 400 microns. Figure 3.8 shows the granulometric curve of the fraction lower than 400 microns. It is a low plasticity soil ($I_P = 8$) and its average dry unit weight after compaction in the flume is $\gamma_d = 16 kN/m^3$. According to the consolidated undrained triaxial test (Blaza, 2002), the effective internal friction angle (ϕ') is 35.4° , the effective cohesion (c') is 8.5 kN/m^2, and the Darcy's permeability (k_s) is 1.0×10^{-5}cm/s.

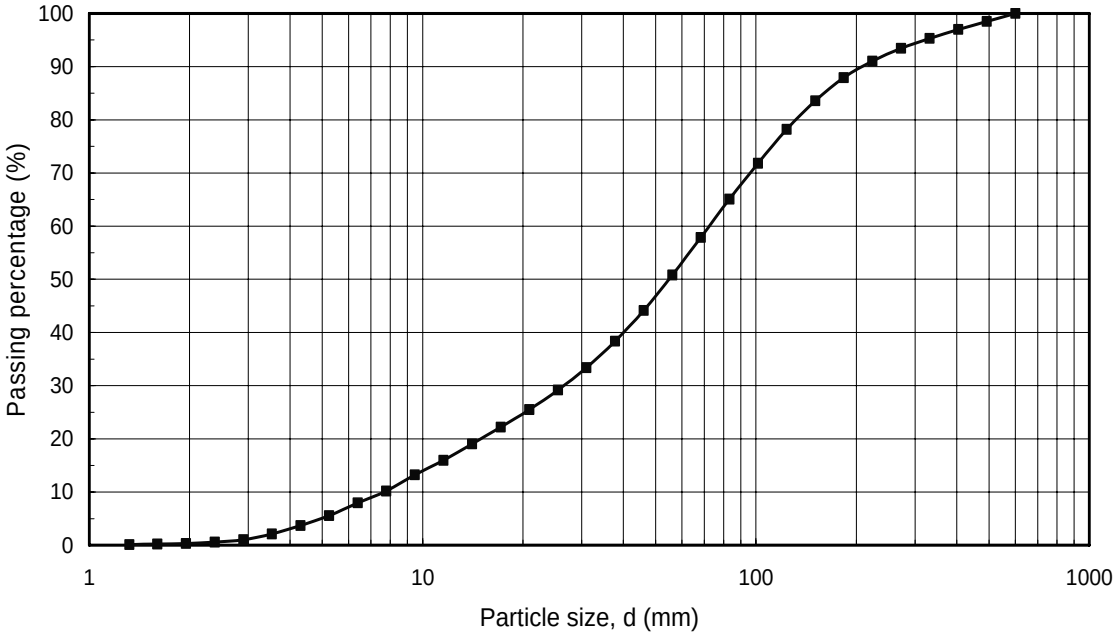

Figure 3.8 Grain size distribution of the soil.

3.2.2 Geotextile material

There are two types of geotextile used in this experiment, BF400 and SF1100 both non-woven but with different structures. Table 3.1 gives their characteristics.

1. BF400

This geotextile is a thin needle-punched non-woven material with double-layer, each with a different fibre diameter that is produced by the Bidim Company. It is an especially product designed to prevent soil erosion. The sub-layer functions as the filter, which is placed in contact with the fine base soil, while the other layer is for reinforcement and is in contact with the armour stone.

2. SF1100

SF1100 is a thick needle-punched non-woven geotextile (Depotex) in one layer that produced by the Naue Fasertechnik GmbH & Co. Its Opening Size (O_f) is equal to that of BF400. However, according to Giroud's theory (Giroud 1996), the number of constrictions needed to obtain the same O_f as BF400 is larger because the fibers of SF1100 are coarser. The test results presented will therefore enable a comparison to be made between two geotextiles with the same O_f but with a different number of constrictions.

Table 3.1 Geotextiles characteristics

Name	Mass Specific Filter layer (g/m^2)	Thickness of Filter layer (mm)	O_f (microns)	Number of Constrictions	Permeability (m/s)
BF400	170	1.7	80	25	2.5×10^{-3}
SF1100	1120	7.8	80	50	3.8×10^{-3}

3.2.3 Examination of the materials used with the current design guidance

In order to understand whether the experiment materials selected are suitable, the current design guidance that introduced in Chapter 2 is used to examine the relationship of soil-geotextile filter system.

1. Permeability criteria

The permeability of BF400 is $k_g = 2.5\times10^{-3}$ m/s and SF1100 is 3.8×10^{-2} m/s that are both larger than the permeability of soil used ($k_s = 1.0\times10^{-5}$ m/s), and therefore is conform to Schober and Teindi (1979) suggested. Besides, k_g is more than ten times larger than k_s that also in accordance with the recommended from BAW (Eq. (2-9)) under bi-directional cyclic flow.

2. Retention criteria

Before examining, some parameters of soil particle size must be decided from Figure 3.8. According to the criteria of Table 2.2 and Figure 2.7 to examine whether the experiment materials selected are suitable. The results are shown in Table 3.2.

Table 3.2 The examined results of the retention criteria of test materials (Under cyclic flow).

References	Base soil type	Retention criteria	Examining Result
Heerten (1982)	non-cohesive soil	$O_{90} < d_{50}$	NG
DGEC (1986)	$d_{40} \le 60\mu m$	$O_{90} < 1.5\times d_{10}\times\sqrt{Cu}$ $O_{90} < d_{50}$ $O_{90} < 500\mu m$	NG
Ragutzki(1973)	not confined	$O_{90} \le (0.5 \sim 0.7)\times d_{50}$	NG
PIANC (1987)	$Cu > 5$	$50\mu m < O_{90} < d_{90}$	OK
CFGG (1986)	loose sand ($Cu>4$)	$O_{90} < 0.6\times d_{85}$	OK
Holtz(1998)	$d_{50} < 74\mu m$	$O_{90} \le 0.5\times d_{85}$	OK
Mlynarek (2000)	See Fig. 2.7	$80\mu m < O_{90} < 100\mu m$	OK

Note: $O_{90} = 80\mu m$

$d_{10} = 7.5\mu m$ $d_{30} = 25\mu m$ $d_{40} = 40\mu m$

$d_{50} = 55\mu m$ $d_{60} = 71\mu m$ $d_{85} = 175\mu m$

$d_{90} = 205\mu m$

$Cu = d_{60} / d_{10} = 9.5$ $I_p = 8$

3.3 Test performed

There are two objects of the large flume test in this study. For the steady riverbank of no sliding potential, geotextile is placed on the bank directly and then covered by armor stones. The main function of geotextile is to prevent the fine soil on the surface of bank eroded. Hence, the first object of the large flume test is to investigate the erosion behavior under this condition. It denominated the revetment laying geotextile test (RLGT). The experiment is arranged as Section 3.3.1. In addition, for the steep riverbank or having important structure adjacent to the riverbank that often adopts geotextile to build a reinforced revetment (see Figure 3.9). In this condition, geotextile not only has the function of filter but also reinforce the riverbank. Therefore, the deformation of reinforced revetment, the stress variation of geotextile, the variation of pore water pressure, and the erosion influence range under bi-directional cyclic flow are interesting. This research carried out the second object of the large flume test to study the behavior of reinforced revetment using geotextile as described in Section 3.3.2. It named the reinforced revetment using geotextile test (RRGT).

Figure 3.9 The reinforced revetment using geotextile.

3.3.1 The test arrangement of RLGT

This test is carried out by Faure and Le Lay (2002), Le Lay (2001), Blaza (2002), and Toralba (2003). The equipment layout is shown in Figure 3.10.

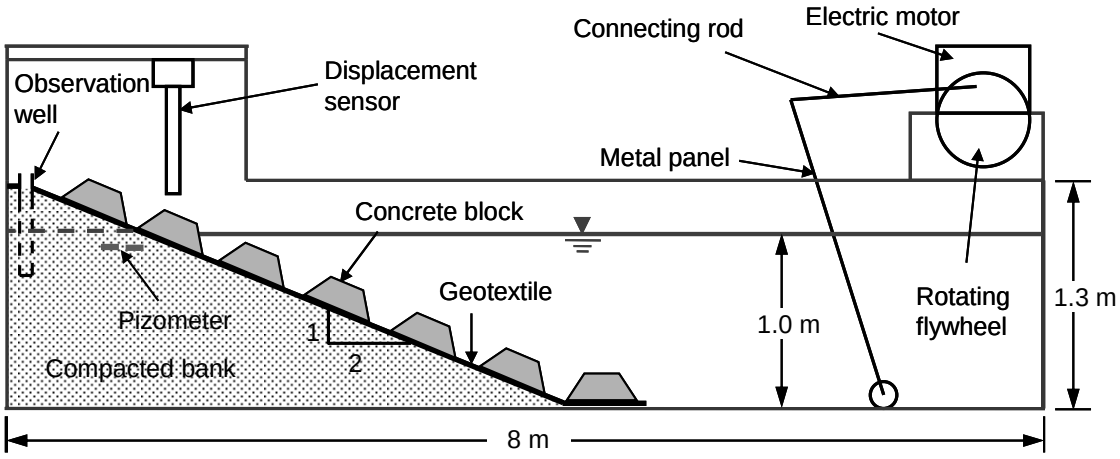

Figure 3.10 The equipment layout of RLGT.

The test procedure includes following six steps (see Figure 3.11):

1. To fill and to compact the soil by layer to construct the bank with a slope of 2H in 1V or 2.5H in 1V. The slop angle 26.6° or 21.8° is less than the soil effective internal friction angle (ϕ'=35.4°).
2. Two piezometers and one groundwater observation well are placed in different positions under the bank surface.
3. A geotextile is laid on the soil slope and covered by the concrete blocks. In order to reduce the boundary effects, geotextile geotubes (100 mm diameter) filled with coarse sand are installed at the both sides of flume wall. This geotube is itself then overlaid by the riprap rock.
4. To pour water into the flume of 1m depth and to wait more than 48 hours to make the soil saturated.
5. To start the waves generator in different amplitudes and to measure the pore water pressure automatically during the experiment. At regular times, to survey the deformation of concrete blocks and the turbidity of water.
6. After the experiment, the geotextile is lifted and the erosion behavior of slope surface is observed. Moreover, soil samples were taken in different situations to investigate the variation of granulometric.

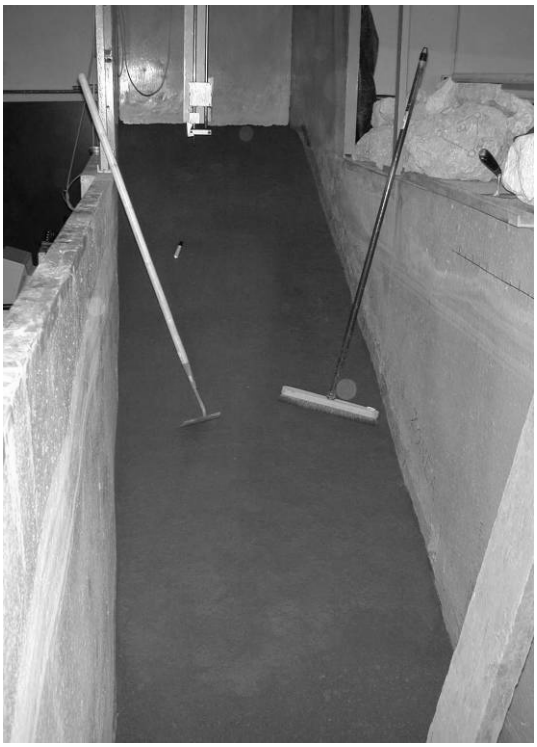

(a) Filled and compacted a bank slop.

(b) Laid the geotextile and geotube.

(c) Covered with concrete blocks.

(d) Testing.

Figure 3.11 The test procedure of RLGT.

3.3.2 The test arrangement of RRGT

The equipment layout of reinforced revetment using geotextile test (RRGT) is shown in Figure 3.12. The construction of compacted bank is the same as RLGT and to form a platform on the top of bank. In order to simulate the vertical surface of reinforced revetment, the geotextile is pre-processed into a geotextile bag. The procedures of geotextile bag established are expressed in Figure 3.13.

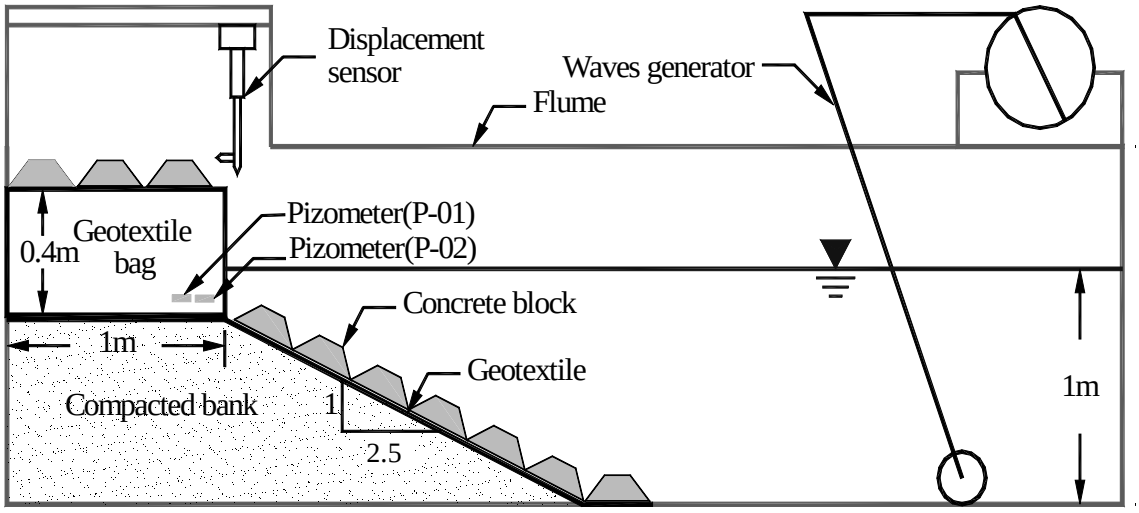

Figure 3.12 The equipment layout of RRGT.

(a) Fix the geotextile bag on rack.

(b) Fill and compact soil by layers.

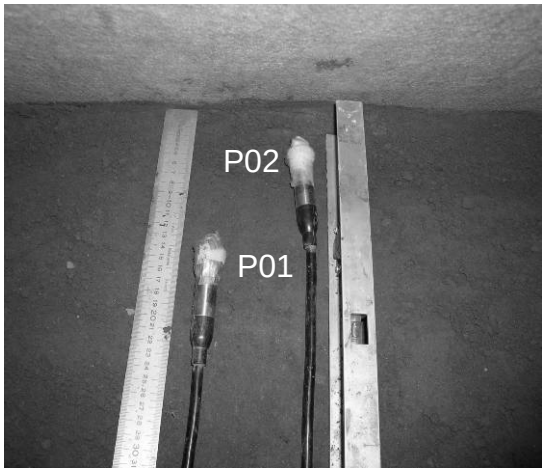

(c) Place two piezometers.

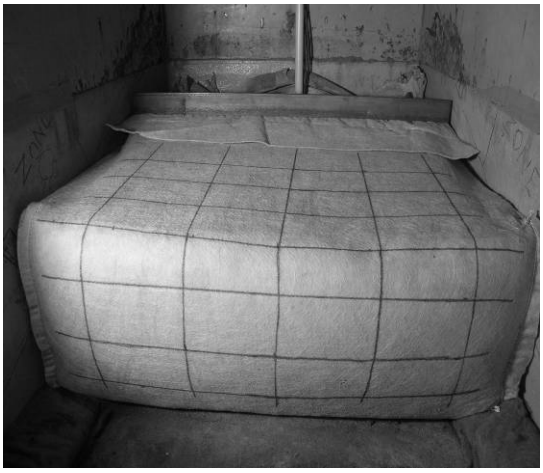

(d) Draw grids for monitoring displacement.

(e) Place the concrete blocks.

(f) Pour water 1m in depth.

Figure 3.13 The procedures of geotextile bags established.

3.3.3 The energy of wave action by wave generator

To vary the rotational speed of motor-transmission and to modify the distance between the connecting rod and the center of rotation flywheel could produce the different wave energy. In order to decide the appropriate wave frequency and amplitude, the prior test was carried out.

1. Wave frequency

Figure 3.14 is show the result of prior test, which indicates that the first peak will be generating around 10 Hz of the frequency of motor-transmission for every test curves. The wave period of about 2 seconds corresponds with one of the real conditions in situ, like waves produced by winds or boats. Therefore, 10 Hz is adopted as the motor-transmission frequency in this experiment.

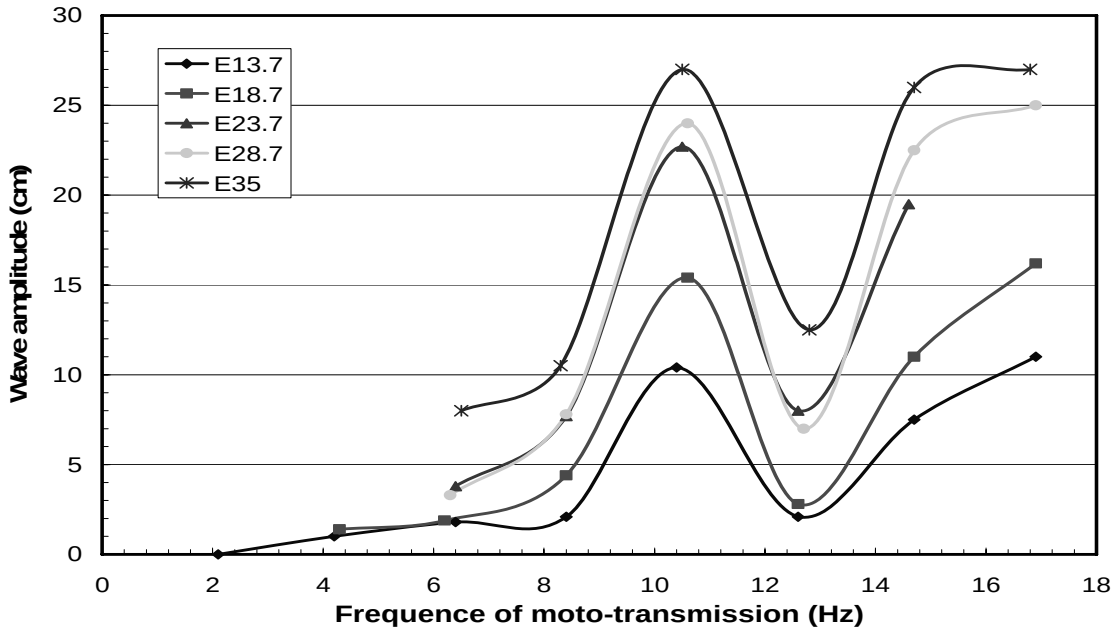

Figure 3.14 The relationship of wave amplitude and frequency.

2. Wave frequency

In order to simulate the waves from small to large, there are preset several different distances between the connecting rod and the center of rotation flywheel which applied successively. Figure 3.15 is the diagram of wave energy. The test duration for each wave energy is variable from 1 to 2 weeks, according to the response of the piezometers and displacement of concrete block.

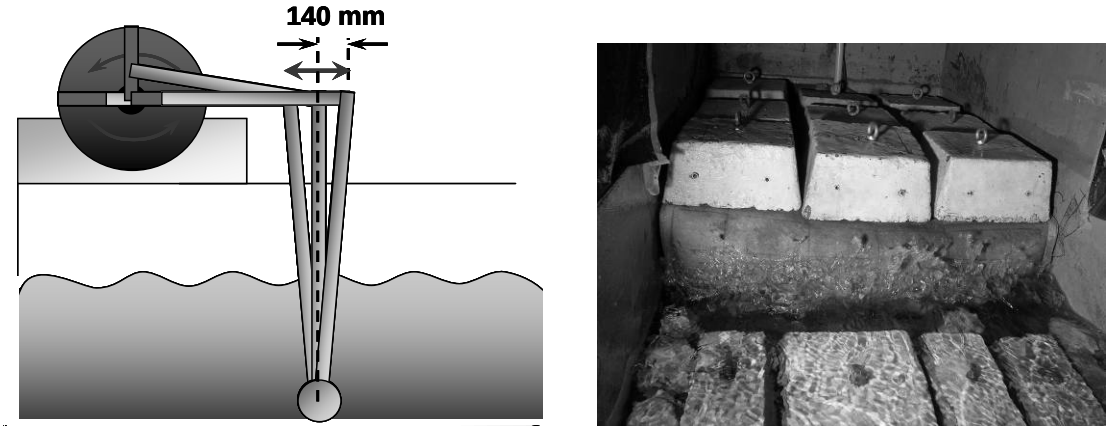

(a) E140.

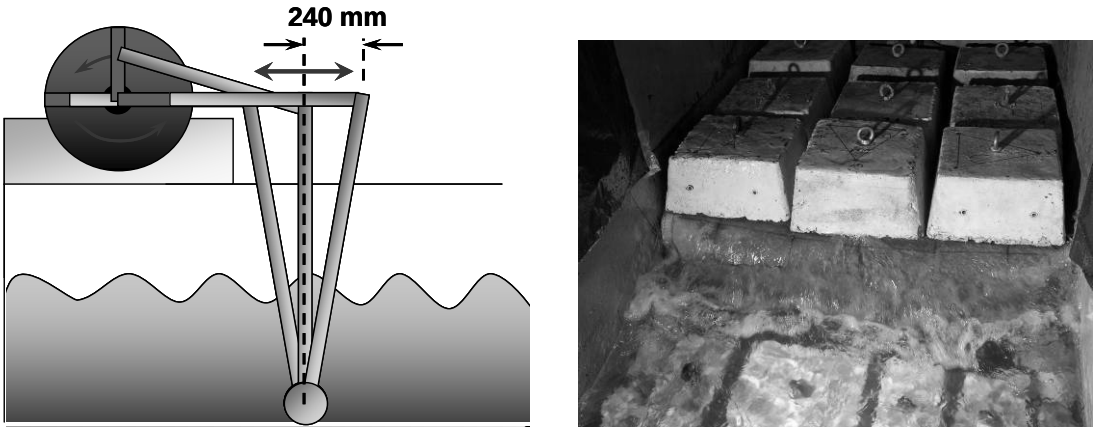

(b) E240.

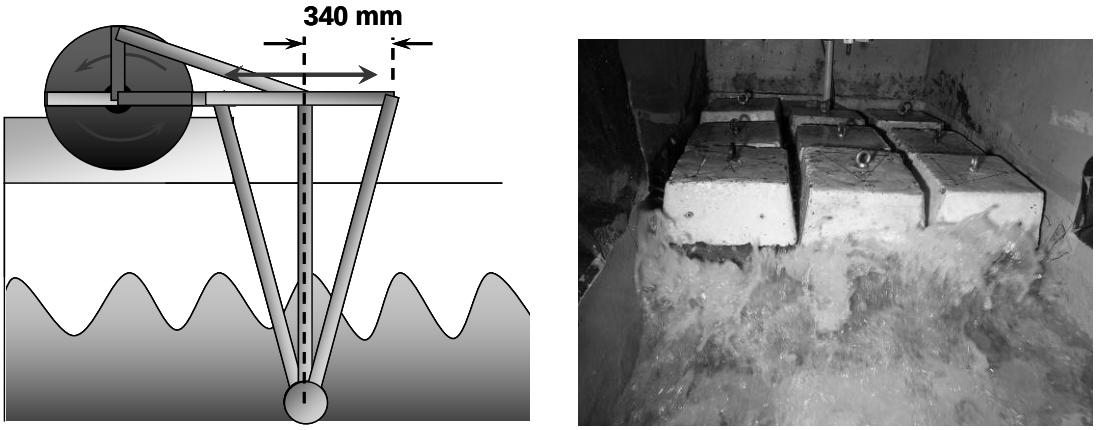

(c) E340.

Figure 3.15 Illustration of the wave energy.

3.4 Test results of RLGT

Five experiments were carried out in this subject (Table 3.3). For Test 1 and Test 2 was constructed a bank with a slope of 2H in 1V and covered by riprap (each rock 25 to 35 kg) on the geotextile, the others were placed the concrete blocks on the geotextile which laid on a bank slop of 2.5H in 1V. The cover area of every concrete block is 31 cm × 31 cm with 15 cm height, and 34 kg weight. The test results will be described and concluded in following sections.

Table 3.3 The list of RLGT tests.

No.	Geotextile type	Bank slop	Cover block	Wave energy
Test 1	BF400	2H : 1V	Riprap rock	E140, E190,E240, E340
Test 2	SF1100	2H : 1V	Riprap rock	E140, E190,E240, E340
Test 3	BF400	2.5H : 1V	Concrete block	E240, E340
Test 4	SF1100	2.5H : 1V	Concrete block	E240, E340
Test 5	BF400	2.5H : 1V	Concrete block	E240, E340

3.4.1 The variation of water turbidity

The water turbidity can be measured during the test without stopping the waves. It is a non-destructive measurement that indicates when the soil reaches a stabilised state.

As shown in Figure 3.16, Figure 3.17, and Figure 3.18, water turbidity increases at the beginning of the test and then decreases quickly. Under the small wave action (E ≤ 240 mm), the turbidity decrease is faster than under great wave action and the residue value is almost zero. This is because under great wave action, the perturbation of water is relatively violent. The quantity of soil particle washed-out is large and the fine suspended particles do not sediment easily. For this season, the measured turbidity decreases slowly and keeps constant, but does not decrease to zero even there is no more erosion.

According to the results of the five tests, the variations of turbidity between BF400 (Test 1, 3, and 5) and SF1100 (Test 2 and 4) are insignificant. In some test, the turbidity is higher but it decreases down to very low value in any case. It seems that the thickness of geotextile is unobvious to the influence on the water turbidity although the observed erosion behavior is unlike. Turbidity measurements are not enough accurate to distinguish the difference of erosion between both geotextiles. On the other

hand, the turbidity parameter is not adopted to evaluate any mass of soil erosion, but is a good indicator to determine the tendency of soil erosion.

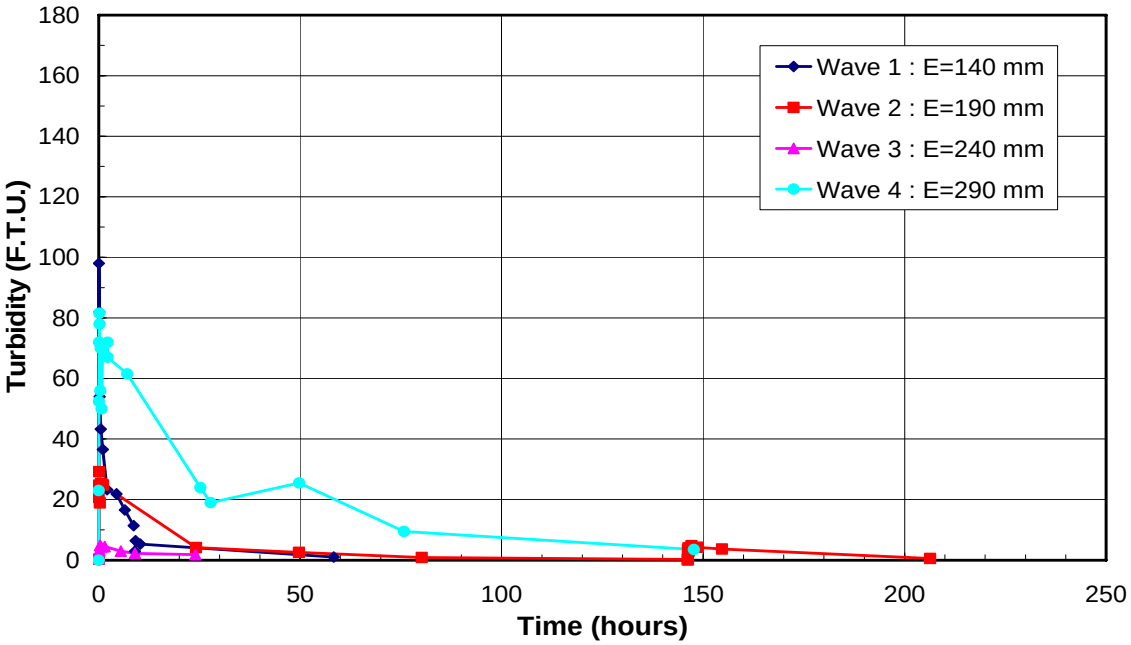

Figure 3.16 Variation of water turbidity during the test (Test 1, BF400).

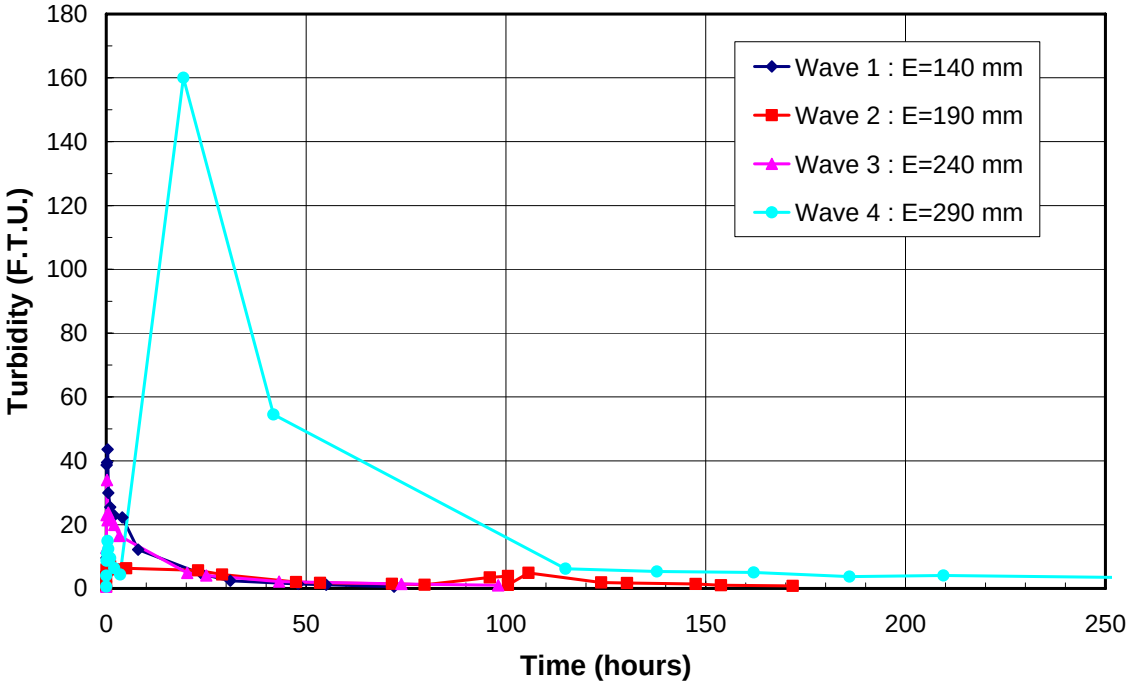

Figure 3.17 Variation of water turbidity during the test (Test 2, SF1100).

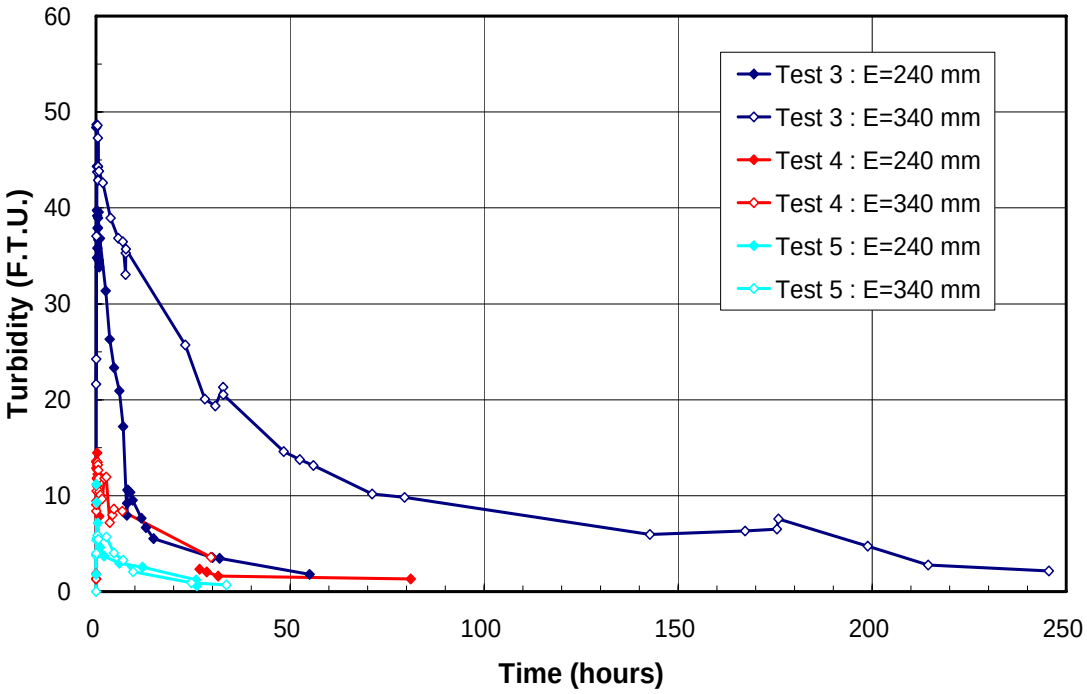

Figure 3.18 Variation of water turbidity during the test (Test 3 to Test 5, BF400).

3.4.2 The variation of pore water pressure

In this study, two electric piezometers were used to measure the variation of pore water pressure during test. For Test 5, piezometers 1 (P01) was placed under the geotextile covered 5 cm of soil and submerged about 20 cm from the static water level. Piezometers 2 (P02) was fixed on the geotextile surface and had a distance of 16 cm from the static water level. The situation of two piezometers is diagrammed in Figure 3.19. And the results of Test 5 as show in Figure 3.20 and Figure 3.21.

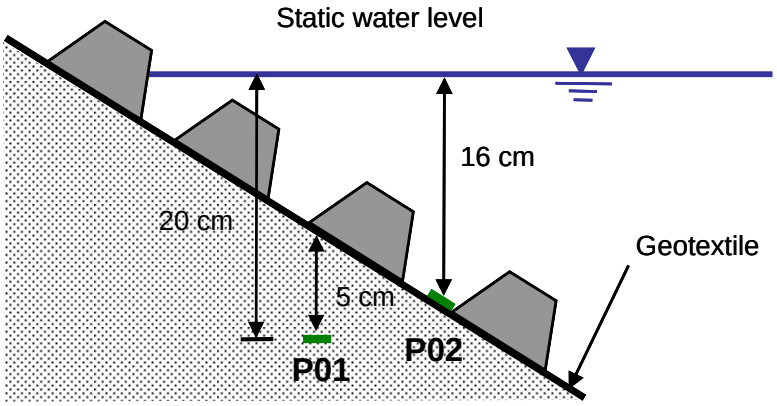

Figure 3.19 Schematic diagrams of two piezometers of Test 5 (BF400).

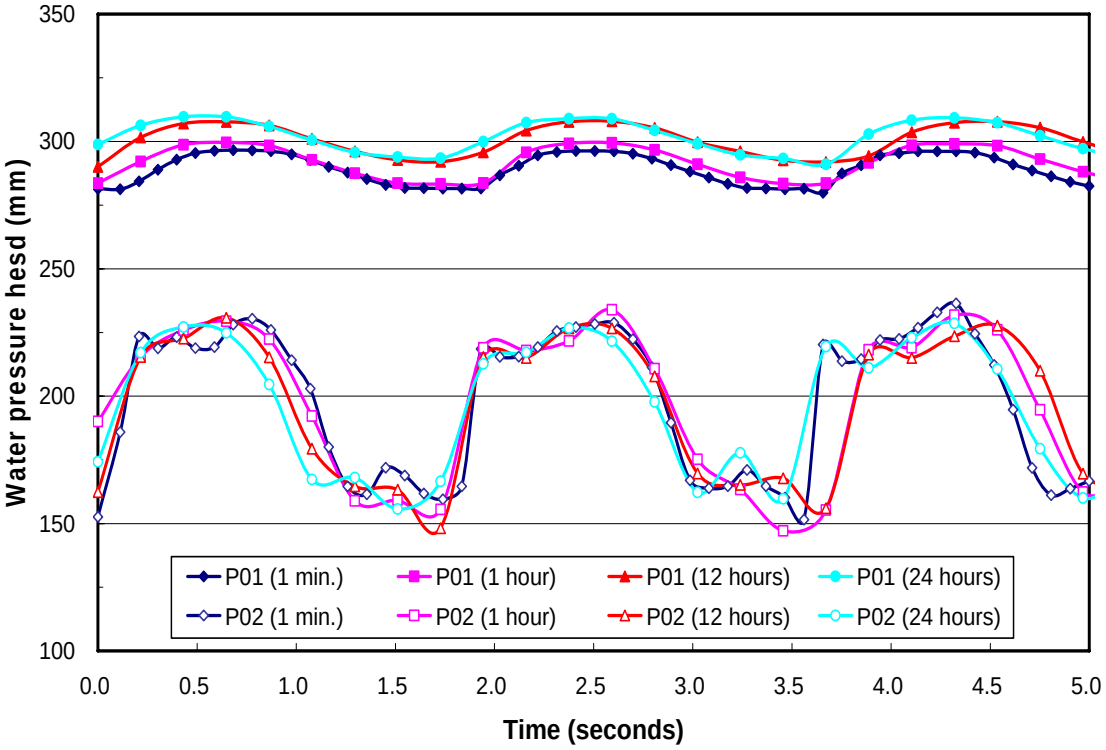

(a) After test beginning from 1 hour to 24 hours.

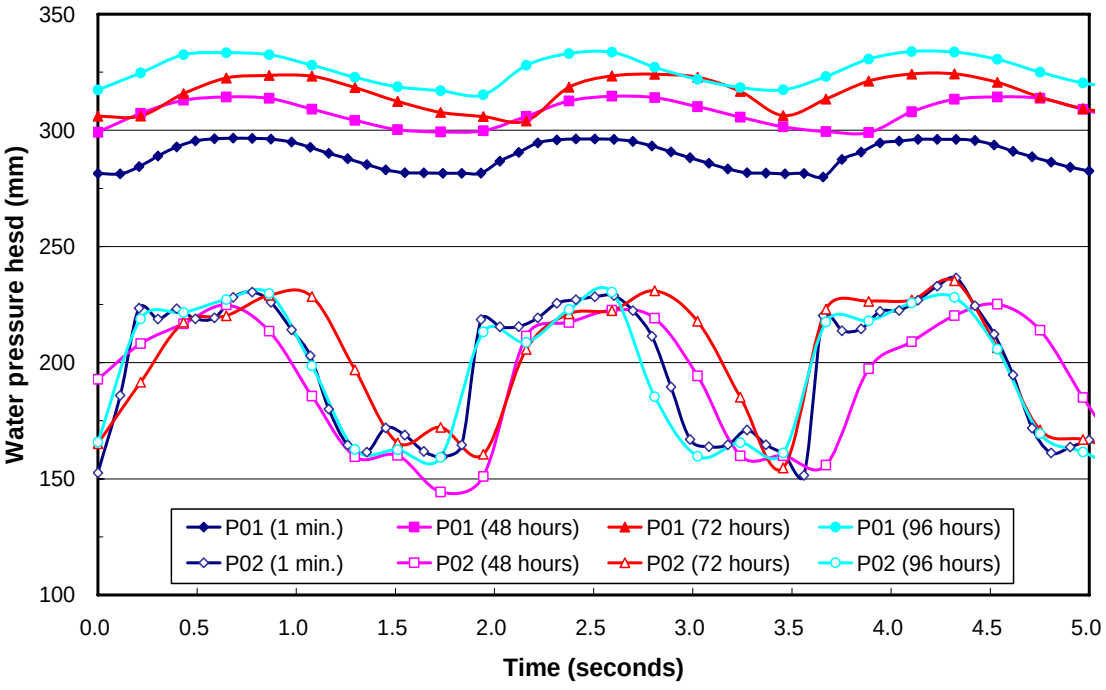

(b) After test beginning from 48 hours to 96 hours.

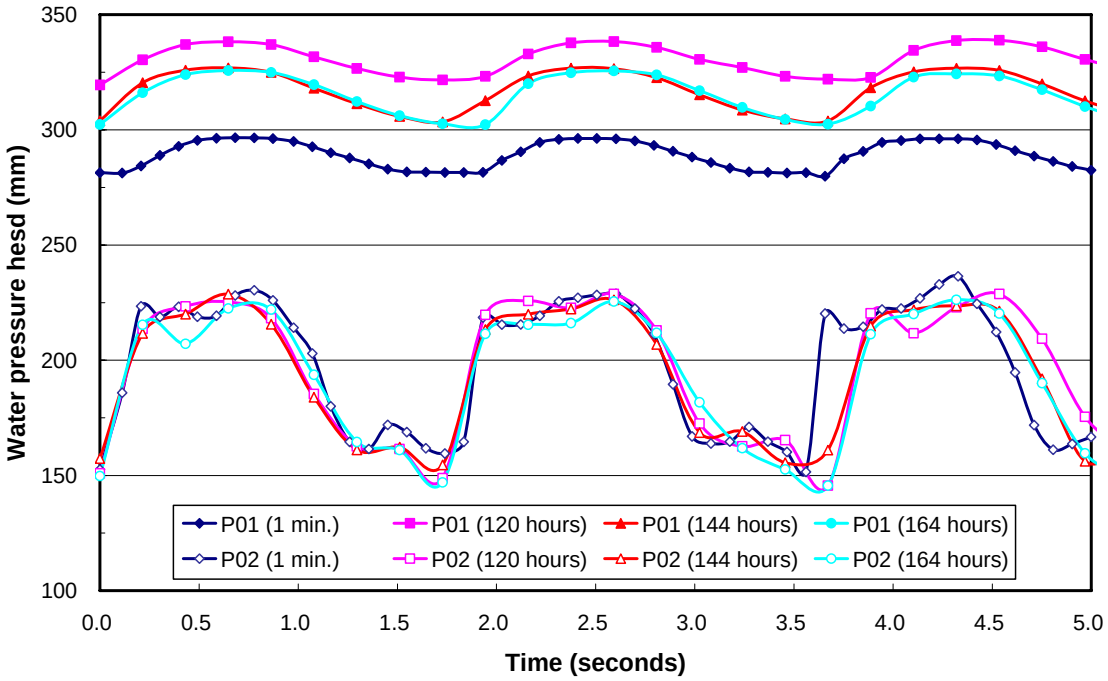

(c) After test beginning from 120 hours to 164 hours.

Figure 3.20 The variation of water pressure head duration 5 seconds of Test 5 under small wave action (E240).

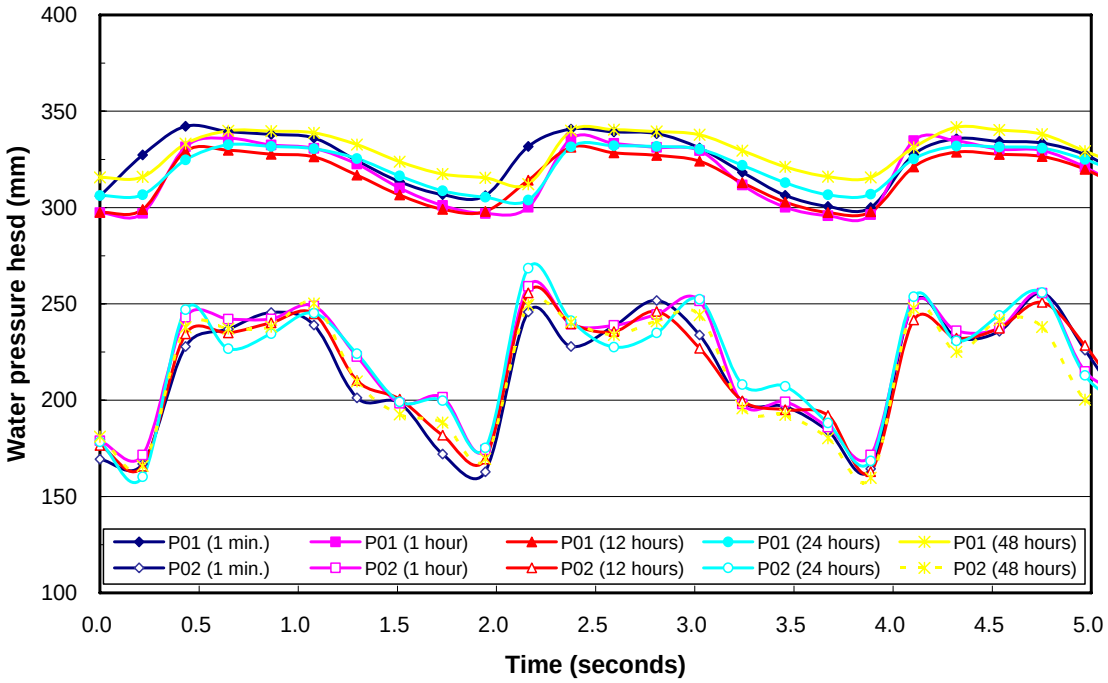

(a) After test beginning from 1 hour to 48 hours.

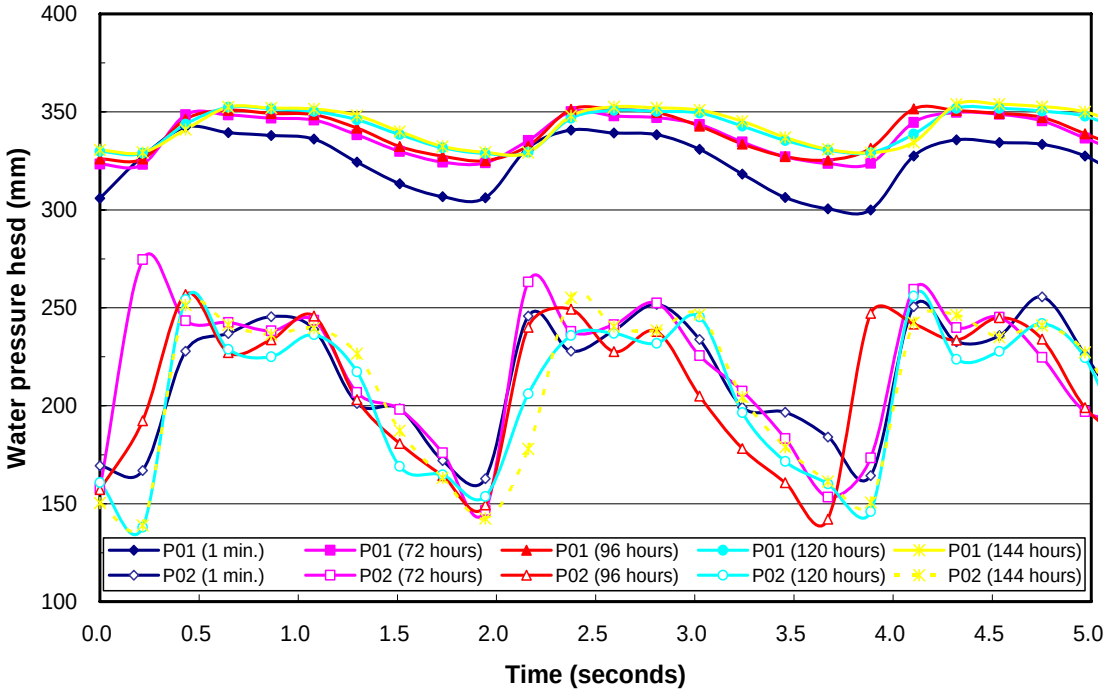

(b) After test beginning from 72 hours to 144 hours.

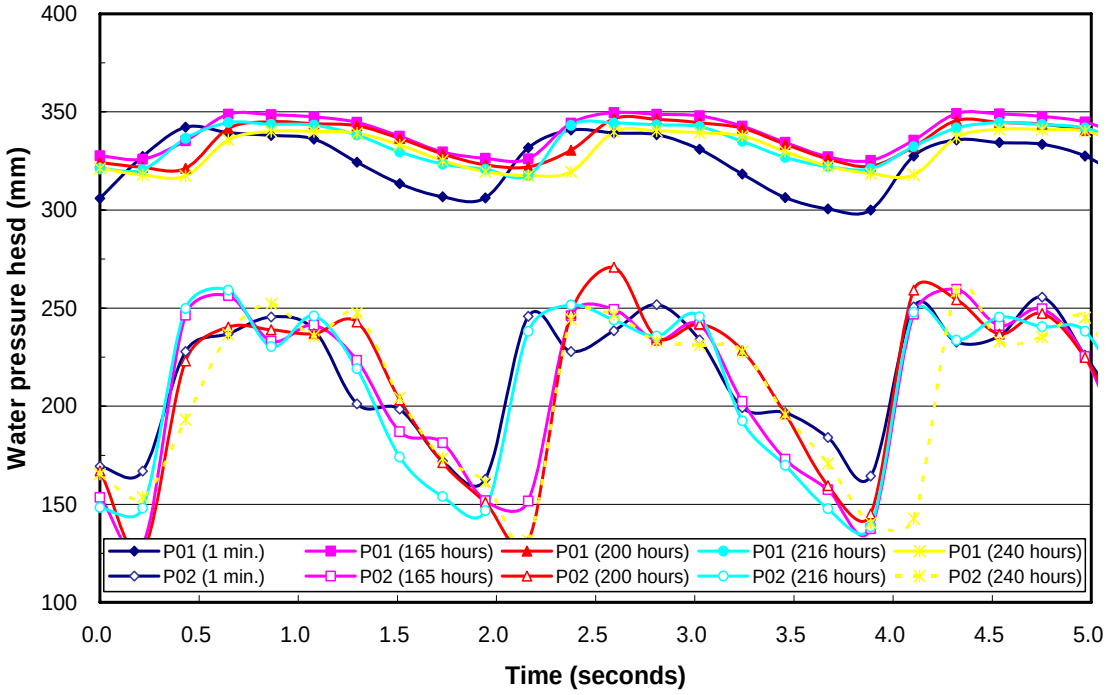

(c) After test beginning from 165 hours to 240 hours.

Figure 3.21 The variation of water pressure head duration 5 seconds of Test 5 under great wave action (E340).

The frequency of wave is about 2 seconds during the test that is conform to the described before. As show in Figure 3.20, under the small wave action, the amplitude of P01 is about 23 mm, P02 is about 75mm. The water pressure head of P01 increases quite obviously that the test duration until 120 hours. That is because the fine soil particles on the surface of bank would be migrate toward the geotextile under the wave action. The fines particles are sustained and blocked within the fibers or pass through the geotextile. And then, the coarse grain particle would be remain behind the geotextile and formed a natural filter layer gradually. For this reason, the increase of the pore water pressure is limited. After 120 hours of test duration, the water pressure head would be decrease and then maintain a constant (see Figure 3.20(c)). It seems that the natural filter layer formed.

Figure 3.21 is the variation of water pressure head under great wave action (E340). The frequency is still 2 seconds; the amplitude of P01 is 48 mm and P02 is 110 mm that are larger than the condition of small wave action. The variation of water pressure head is insignificant in different test duration due to the natural filter layer that was formed. That is to say the eroded soil might be slight and consequently the water turbidity decrease quickly (see Figure 3.18).

The behavior of soil erosion is complicated, it need more evidences to support above-mentioned argument. As following, attempts make use of more results of the test to explain the behavior of soil erosion.

3.4.3 The displacement of cover blocks

In order to survey the variation of topography of the bank, several reference points were marked on the riprap rocks or the concrete blocks. Periodically, the waves are stopped in order to carry out a topographical survey of the reference points. Displacement of each point can thus be calculated. Figure 3.22 shows the reference points of Test 1 and Test 2 that used in displacement measurements. There are ten observe rocks and marked three reference points for each. All of the reference points located in the zone subject to wave action. A device running along guide rails and fitted with 3 displacement sensors can give orthogonal co-ordinates X, Y and Z of each point on the blocks. Their position can therefore be plotted against the time in order to analysis their displacement mechanism. For each blocks, the displacements were evaluated by the mean value of its three reference points.

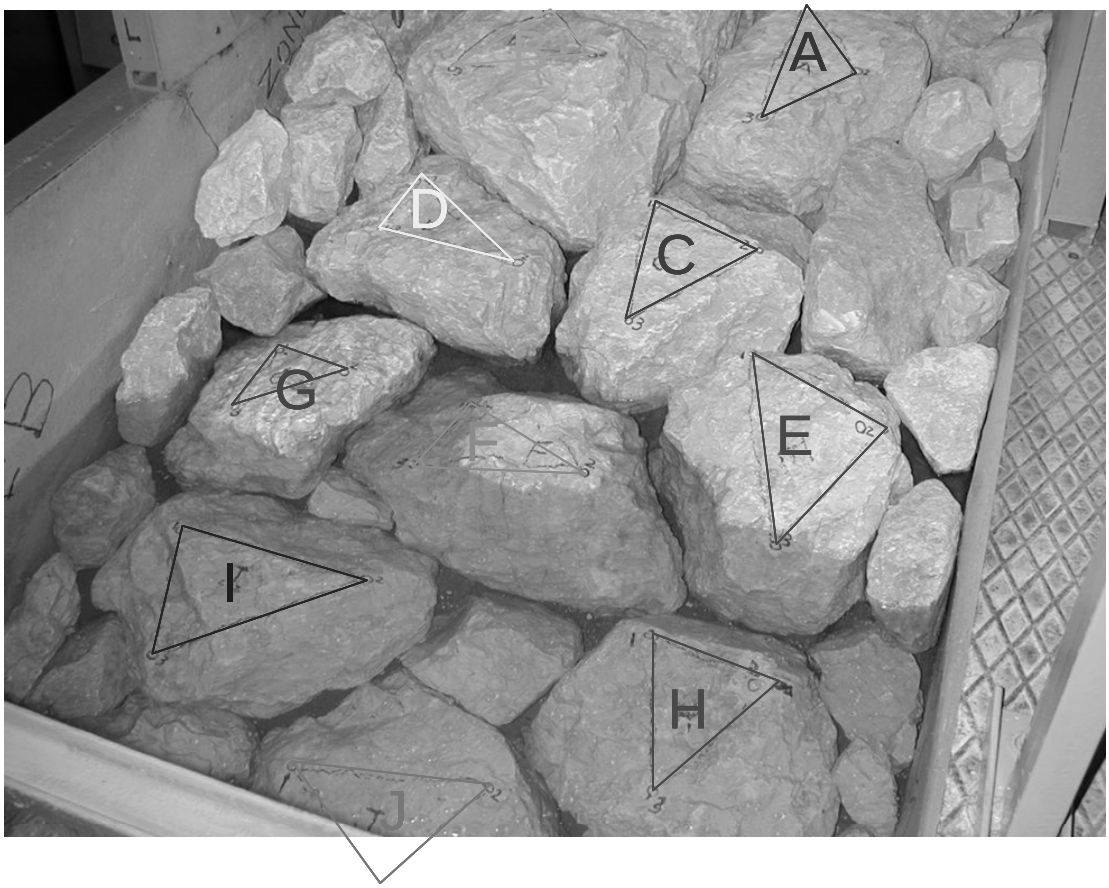

Figure 3.22 Reference points of Test 1 and Test 2 used in displacement measurements.

The horizontal displacements (in the X direction) are presented in Figure 3.23. For Test 1, the different wave energy seems did not have a noticeable effect on X displacement, yet the horizontal displacement increases with increasing the wave energy in Test 2. Moreover, except A, B, and C, the other rocks all have a tendency to slide along the slope. This phenomenon is more obvious after E290.

Figure 3.24 expresses the displacement of Test 2 in X-Y plan after E290 wave action. In order to shows the variation clearly, the displacements amplified by a factor of 6. As shown, A, B, and C blocks moved backward, the other rocks were all moved forward to the dip direction of slop. In addition, Y direction is limited to water flume wall, the displacements of Y direction are neglected. Hence, this experiment can be simplified as 2- D system, only considers the displacement alone X and Z direction.

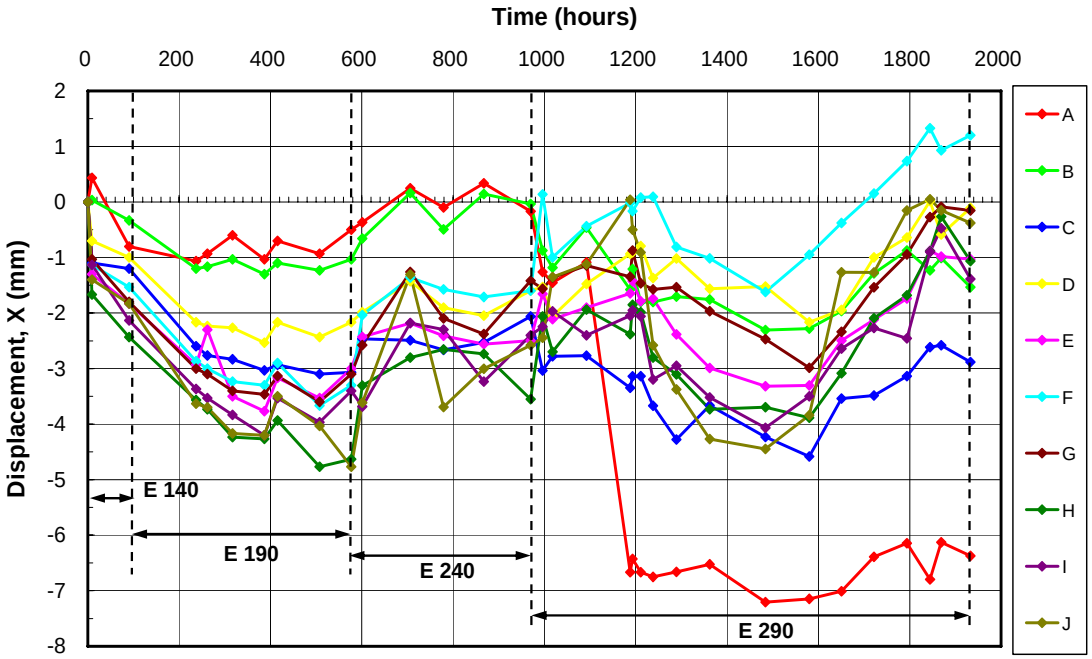

(a) Test 1

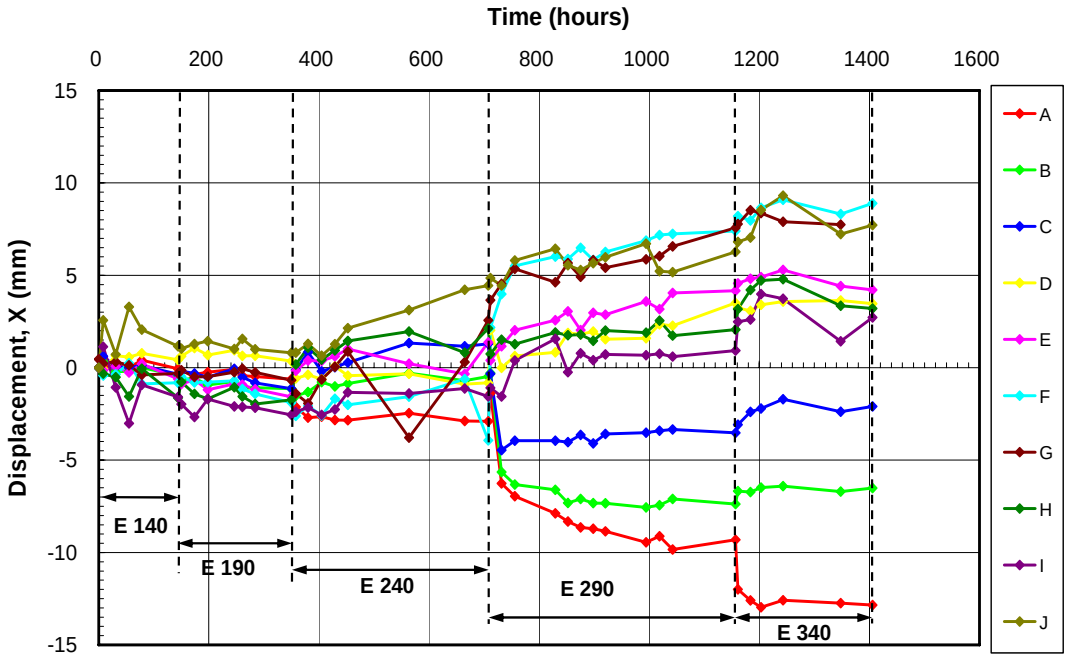

(b) Test 2

Figure 3.23 The displacement of Test 1 and Test 2 in X-direction.
(X>0: displacement outward from the bank)

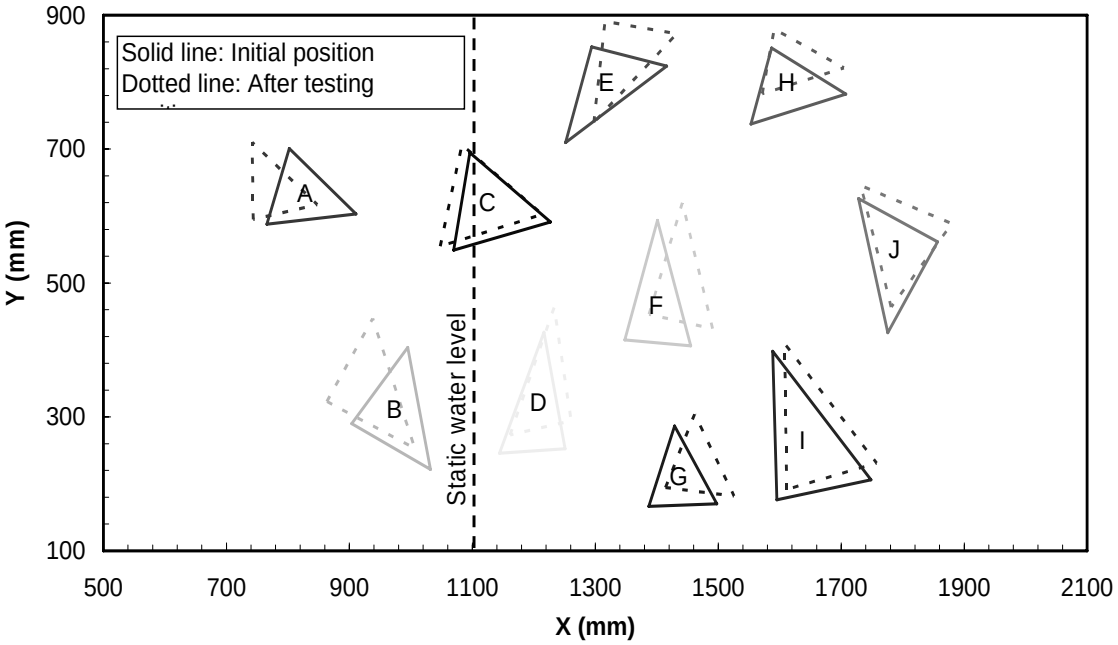

Figure 3.24 Projection of displacements in the horizontal plan X-Y, Test 02, E290 (displacements amplified by a factor of 6).

Examples of vertical displacements (in the Z direction) are presented in Figure 3.25. As shown, the settlement is unobvious under the small wave action (≤ E240), yet it increased suddenly under the wave action in E290 and tended towards stability after 150 hours. Moreover, the settlement almost maintains in a constant even increase the wave energy to E340 and therefore E290 is the critical wave energy for this experiment.

Figure 3.26 expresses the displacement of Test 2 in X-Z plan after E290 wave action. The displacements amplified also by a factor of 6. The most significant displacements correspond to the blocks located in the upper part of the bank, in the zone subject to wave action (block A and B). Those located below the average water level undergo practically no displacement. Those in the lower part tend to rise (blocks E and F).

To compare with Figure 3.16 and Figure 3.17, the water turbidity is larger in E290 than the other wave energy and decrease to a constant after 150 hours. The response seems in accordance to with the variation of displacement.

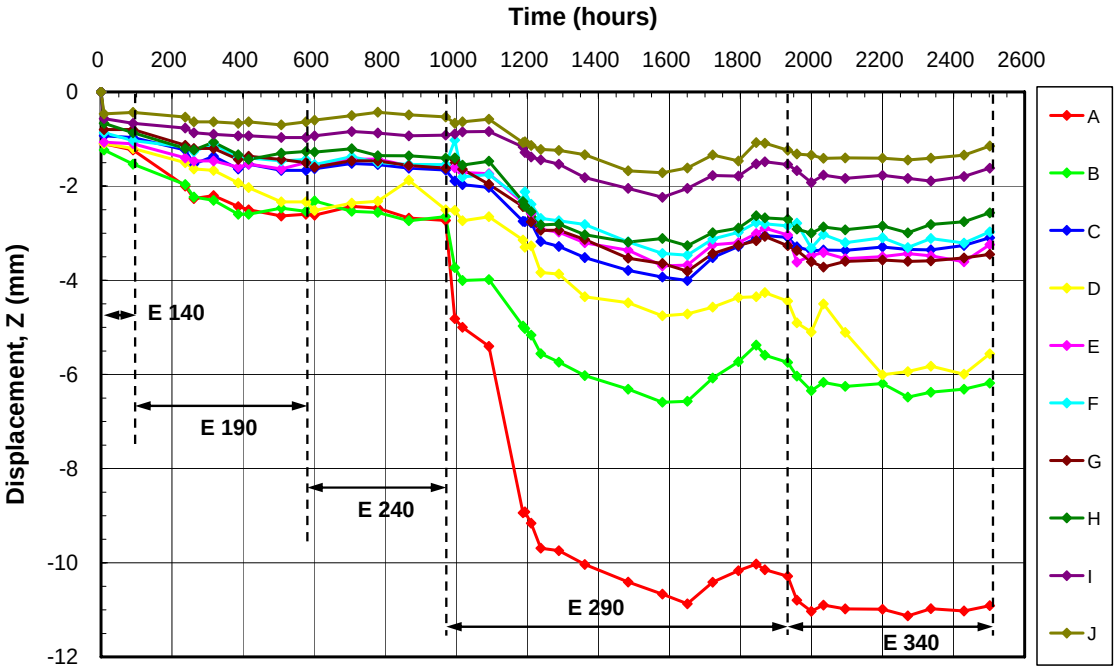

(a) Test 1.

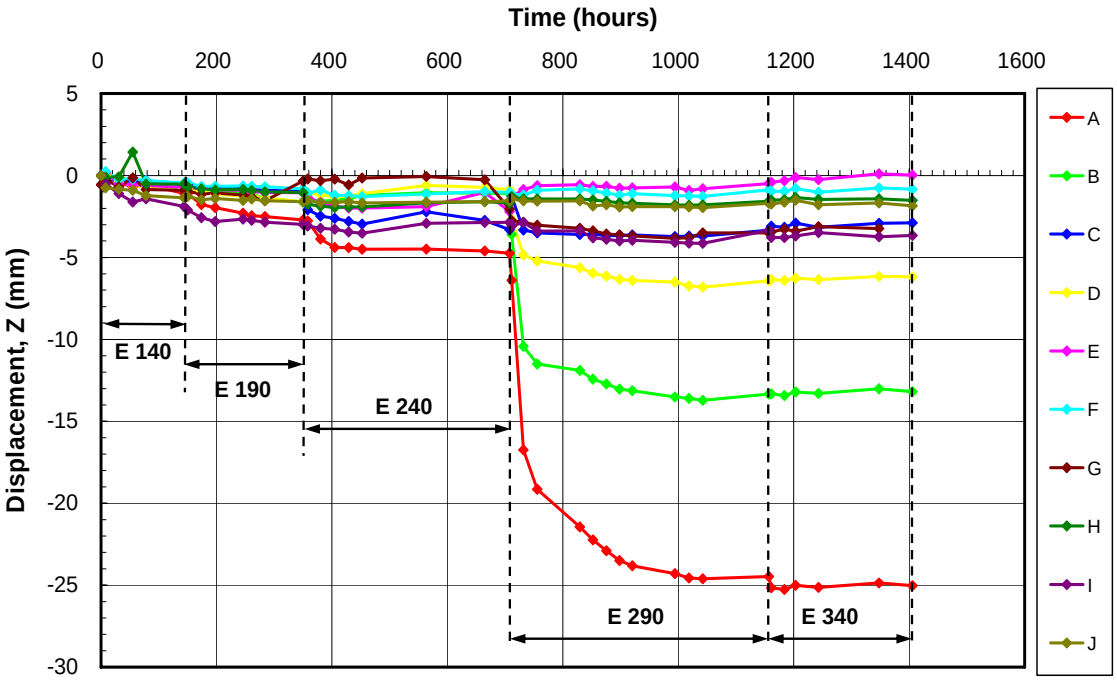

(b) Test 2.

Figure 3.25 The displacement of Test 1 and Test 2 in Z-direction.
(Z<0: settlement)

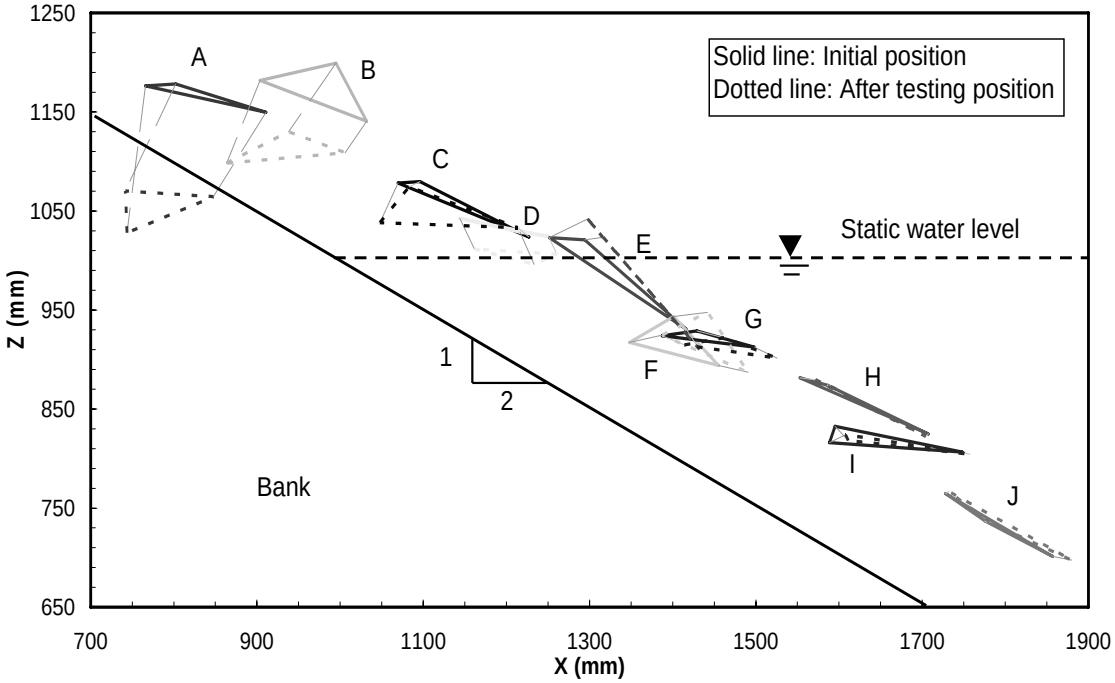

Figure 3.26 Projection of displacements in the vertical plan X-Z, Test 02, E290 (displacements amplified by a factor of 6).

A substantial difference in the amplitude of the displacements for the different geotextiles is observed. With the SF1100, the displacements are roughly twice as large as those obtained with the BF400. To observe the soil surface of bank after removed the riprap rocks and geotextile cover, no matter Test 1 or Test 2 can find that have a serious soil collapse zone at the upper part of the bank (Figure 3.27). This caused a significant displacement of blocks A and B. These collapse locations are in the intersection of the slope and the platform on the top of bank, and furthermore they are in the extremity of wave action. In this region, the geometry of the bank is discontinuous and the variation of pore water pressure is complex, it is understandable to produce a large hydraulic collapse.

In order to determine the stability of slop, the factor of safety of slope against sliding was calculated. For non-cohesive soil subjects to the tangential groundwater flow, the infinite slope model was used to evaluate the factor of safety of slope against sliding. It is defined as following

$$FS = \frac{\gamma_s'}{\gamma_{sat}} \times \frac{\tan\phi'}{\tan\theta} = \frac{9.87}{19.68} \times \frac{\tan 35.4}{\tan 26.6} = 0.71 \qquad (3\text{-}1)$$

Hence, such factor of safety may not be enough to prevent the local hydraulic collapses. Because of this reason, Test 3, 4, and 5 adopted the gradient of slop in 2.5:1 (FS ≈ 1.0) and to compact the bank slop as far as smooth.

(a) Test 1.

(b) Test 2.

Figure 3.27 Hydraulic collapse of soil at the upper part of the bank

Test 3 and Test 4 covered the concrete blocks on the geotextile. We also selected ten monitor blocks and marked three reference points for each block in order to measure the displacement. The situation of these monitor blocks are shown in Figure 3.28. As showing, block A and B are located in above the maximum level of wave, block I and J are located in blow the minimum level of wave and the others are placed on the zone that subjected to the wave action.

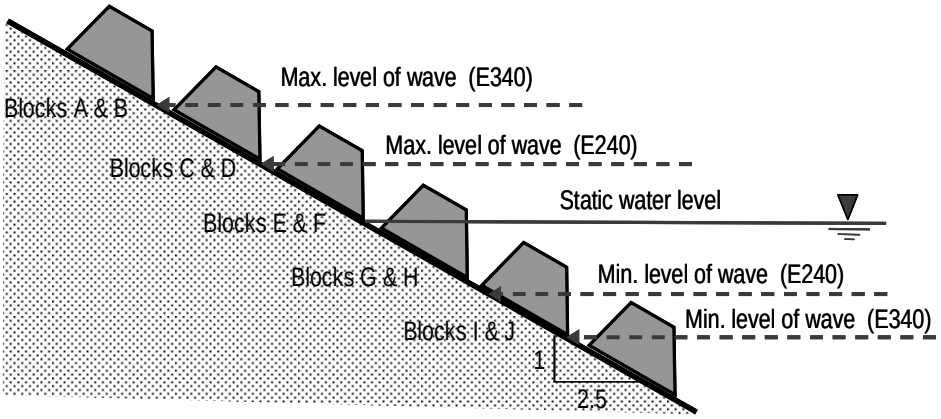

(a) Schematic diagram of the monitor blocks section.

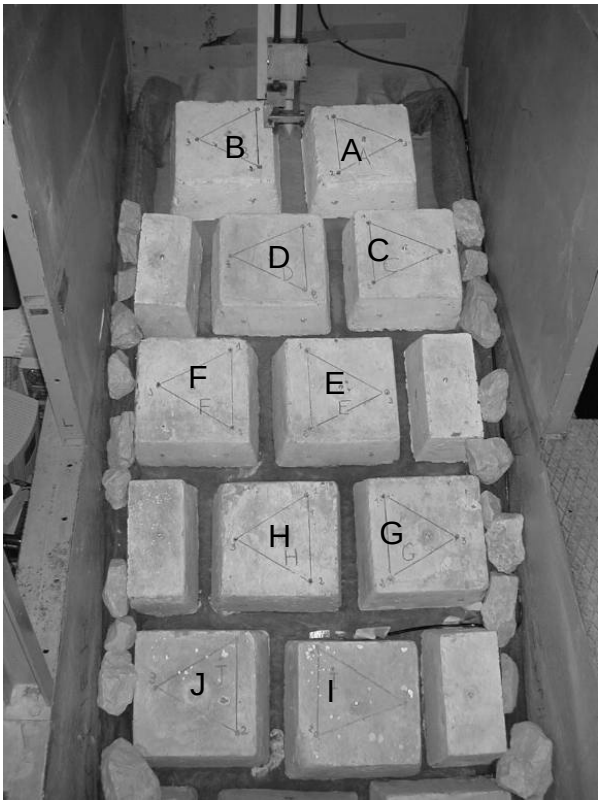

(b) The conference points layout.

Figure 3.28 The displacement reference points of Test 3 and Test 4.

The displacement of block A and B are almost no moved; block I and J located over the capacity of displacement measure roller and therefore can be surveyed only one reference point. The horizontal displacements of the others are presented in Figure 3.29. In order to shows the variation clearly, the displacements are amplified by a factor of 10. The blocks have a tendency to slide along the bank slope, but the displacement is slighter than Test 1 and 2. That is because the slope is more gradual than Test 1 or 2.

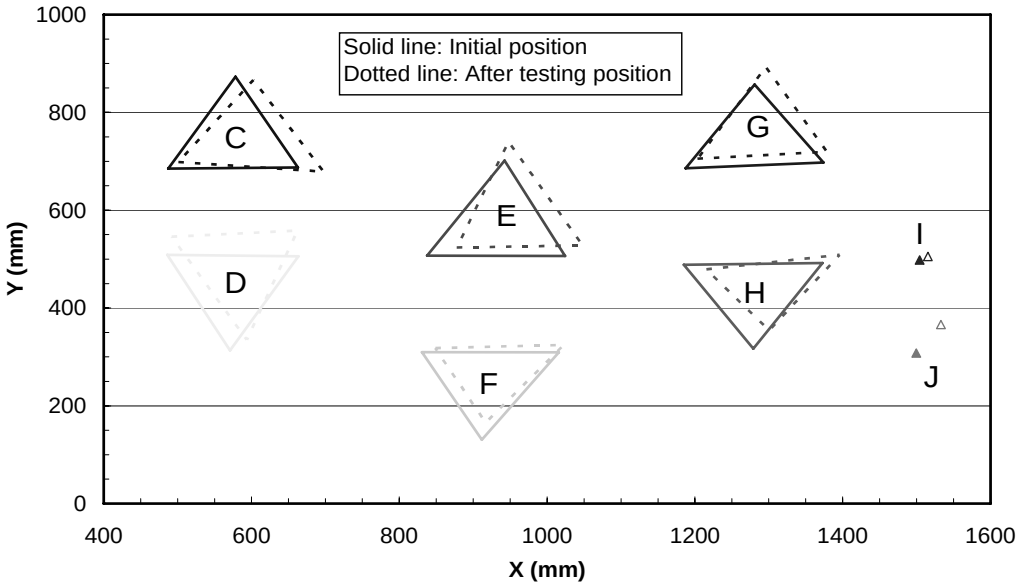

(a) Test 3

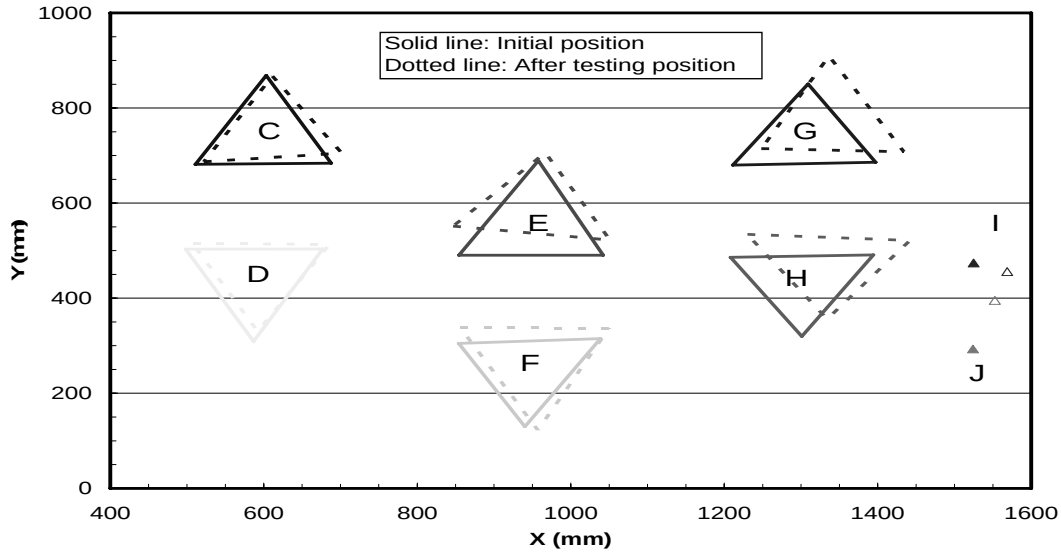

(b) Test 4

Figure 3.29 The displacements in the X-Y plane after Test 3 and Test 4 (displacements amplified by a factor of 10).

Figure 3.30 express the variation of vertical displacement of Test 3 and Test 4. The settlement is insignificant under the small wave (E240) and increases suddenly when subjected to the large wave in Test 3. Compare the result of Test 3 with Test 4, the settlement of Test 4 that used the thick geotextile (SF1100) is smaller than Test 3 that used the thin geotextile (BF400). As the same phenomenon of Test 1 and Test 2 (Fig. 3.24), except the blocks A and B which serious settlement cause from the hydraulic collapse. However, it is seems that the thick one displayed the better performance of the two geotextiles but it is not quite obvious. The result of the test accords with the suggestion of Hoare (1984). Under the bi-directional cyclic flow, used the thick non-woven geotextile can be get better protection.

To observe the soil surface of bank after removed the cover of concrete blocks and the geotextile as shown in Figure 3.31. At the upper part of the bank, between block A, B and block C, D, a local soil collapse zone can be find but it is not serious. The situation of bank surface below block A and B is seems no change, that is why the displacement of block A and B are insignificant. In addition, there are several local erosion areas on the zone subjected to the influence of waves and that could produce the displacement. Besides, the bank roughly still keeps steady. Consequentially, to improve the bank smooth and gradual can avoid soil hydraulic collapse effectively.

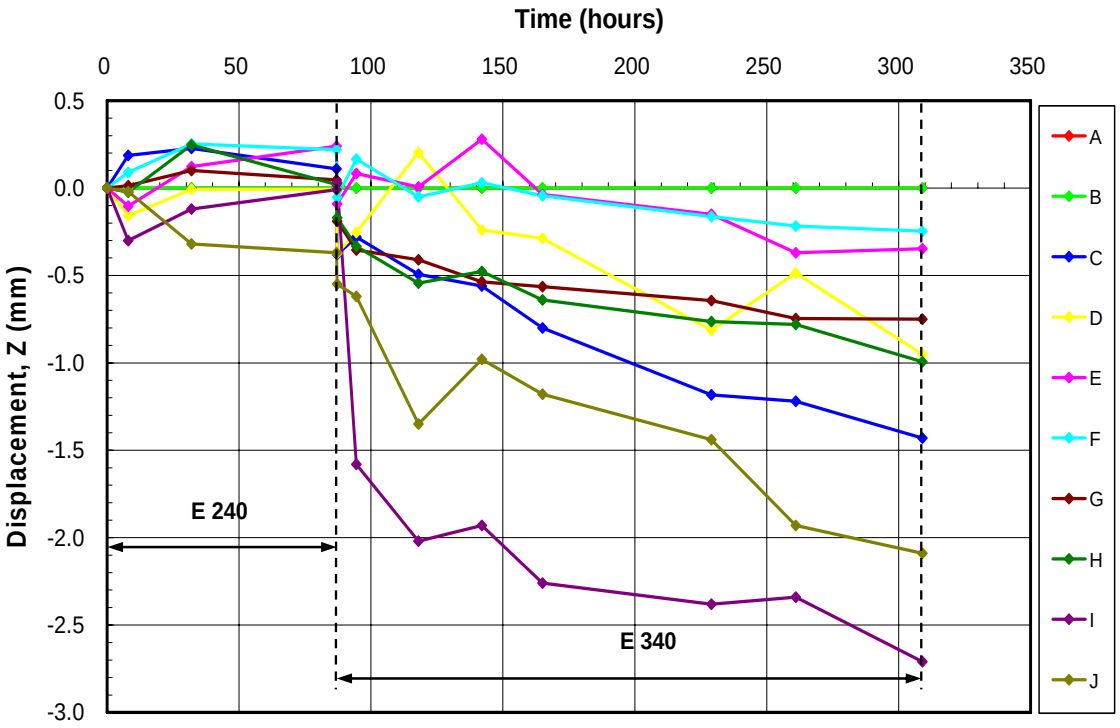

(a) Test 3

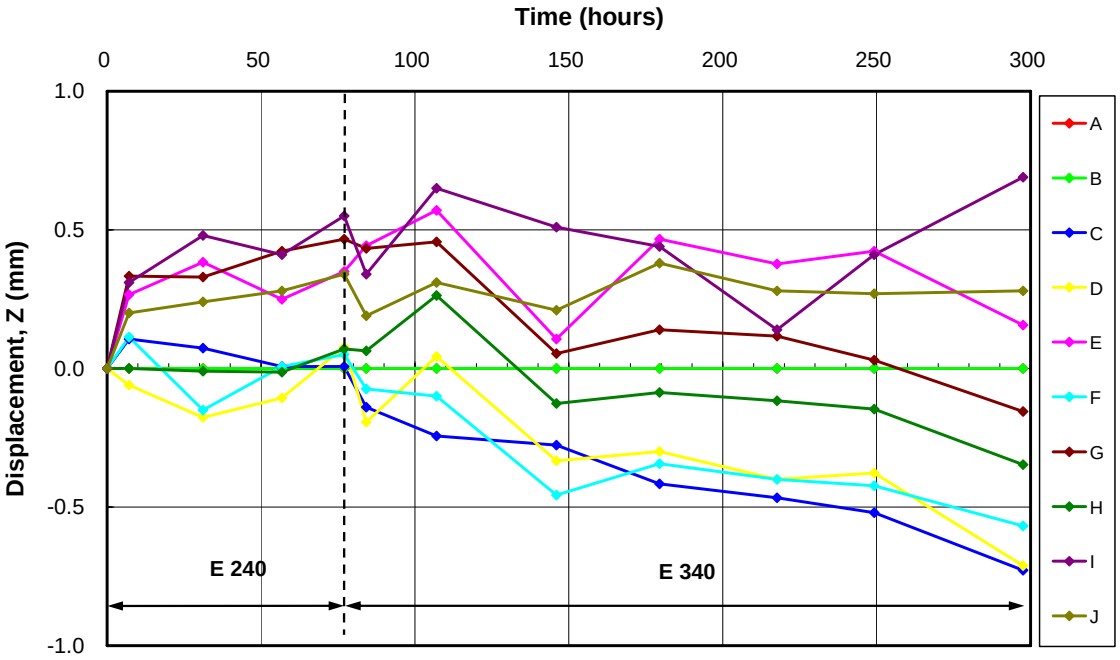

(b) Test 4

Figure 3.30 The displacement of Test 3 and Test 4 in Z-direction.

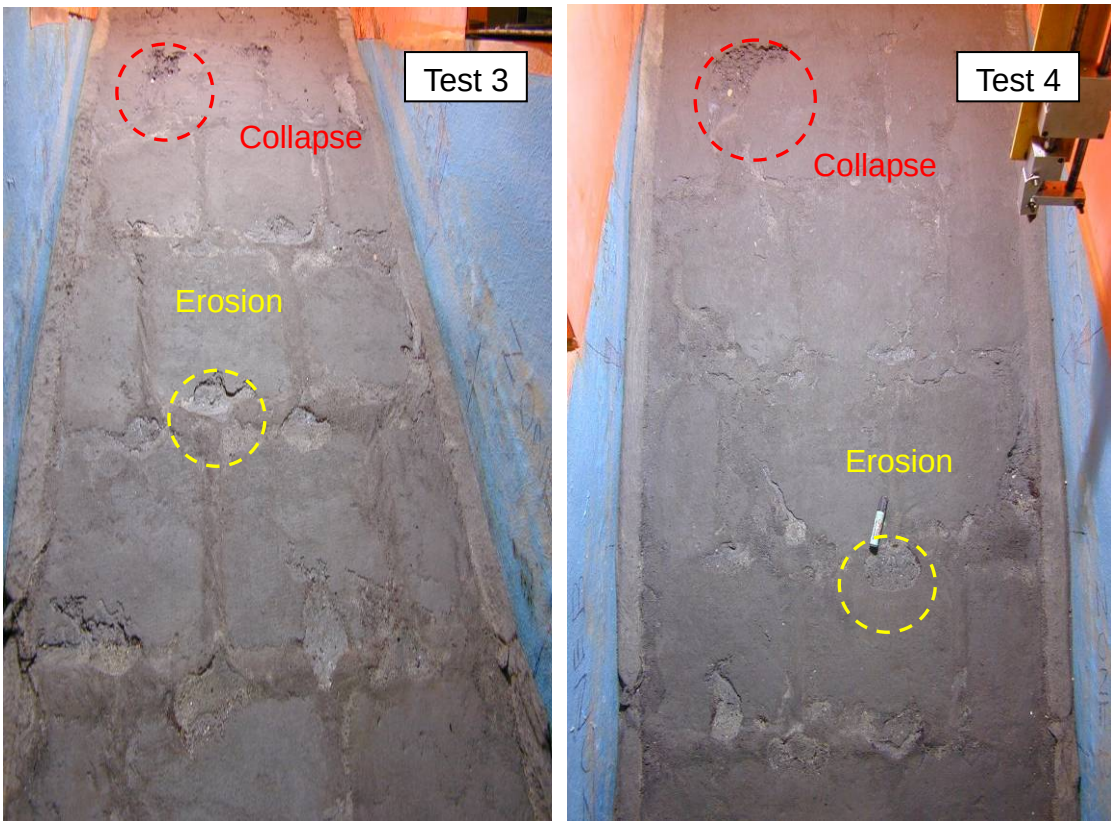

Figure 3.31 The situation of bank surface after testing (Test 3 and Test 4).

3.4.4 Observations after cover blocks removed

After each test, the blocks left clear imprints on the surface of the geotextile. At the upper part of the bank, the textile between the cover block is clean and there is no soil deposit on the surface of geotextile (Figure 3.32(a)). That is because the waves impact the bank, the up-rush water flow into the geotextile to increase the pore water pressure and caused the hydraulic collapse. And then the down-rush water flow along the slope on the top and bottom side of the geotextile (see Figure 3.32(b)). The water flow on the bottom side of the geotextile will take away the soil eroded and flow toward the water side. In the area which covered with block on the geotextile, the fine particle will fill within the textile and caused the color of geotextile to become dark. On the contrary, in the area not covered with blocks, fine particles will pass through the geotextile easily and will be taken away by down-rush flow above the geotextile continuously, and as a result, the surface of geotextile will become clean.

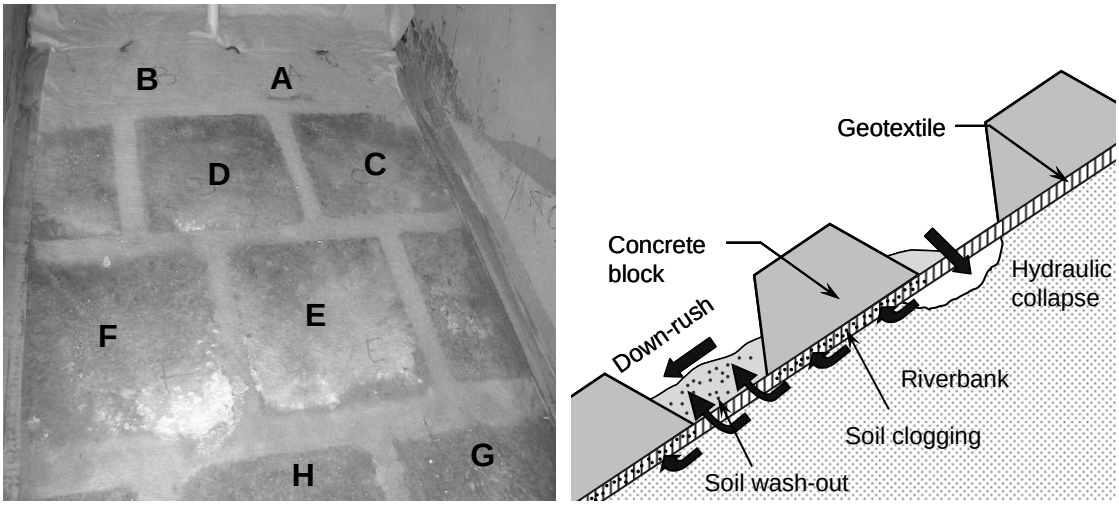

(a) The surface state. (b) Erosion mechanism diagram

Figure 3.32 The upper part state of geotextile surface after testing (Test 5).

Furthermore, at the lower part of the bank, the geotextile surface which contact with the cover blocks cleaner than the other area (Figure 3.33(a)). This phenomenon is contrary to the upper part of the bank. Because the effect by waves impacts at lower part is relatively slight and the surface of geotextile washed by down-rush flow is unapparent. Additionally, water flow down along the bank from the upper part of the bank and carry the particles of soil eroded into the lower part. In the area not covered

with blocks, water flow through the geotextile easily and takes away the fine particles to clog or pass through the geotextile (Figure 3.33(b)). Moreover, the washed out soil deposits on the surface of geotextile between the cover blocks due to the slow flow velocity in lower part (Figure 3.34). For those reasons, the color of the geotextile surface between the cover blocks is darker than the other area.

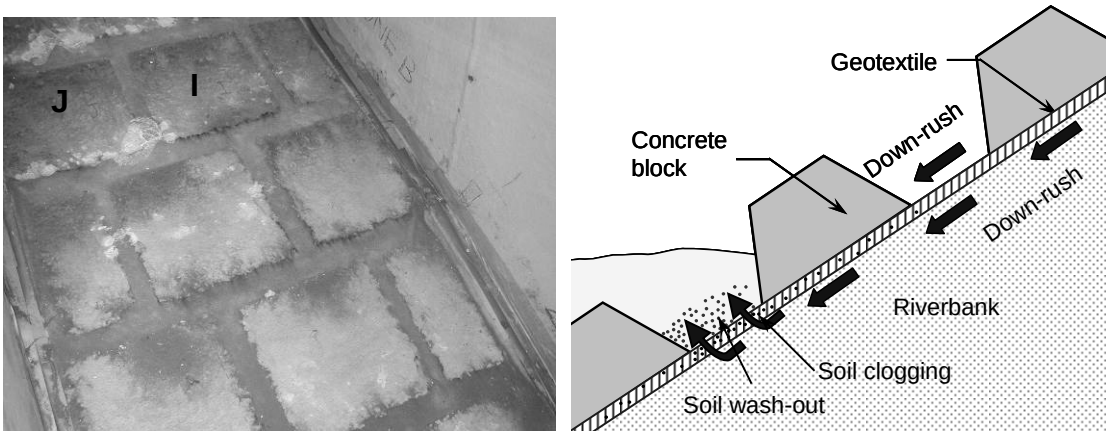

(a) The surface state. (b) Erosion mechanism diagram

Figure 3.33 The lower part state of geotextile surface after testing (Test 5).

Figure 3.34 The eroded particles deposited on the surface of geotextile (Test 3).

Then the geotextile was removed and observed the surface of bank (Figure 3.35).

The soil under the cover blocks maintains the original appearance, but there are several soil erosion area between the cover blocks zone. Therefore, the good cover by concrete blocks or riprap rocks can be prevented the soil erode effectively.

Figure 3.35 The eroded particles deposited on the surface of geotextile (Test 3).

3.4.5 The variation of soil particle size distributions

Due to the fact that the displacements were apparent in Test 2, several soil specimens were taken from below the riprap rock covered (good contact) and between the riprap rock covered (no confining) respectively. Figure 3.36(a) shows the state of the soil specimen was taken from no confining area: the right part of the specimen is close to the water side and the left part is the bank side. Within the depth of 15 mm on the right part, the loss of fine soil particle is obvious, yet the state of the soil seems alike with the initial state after 30 mm from the right part. Hence, the influence depth that subjected to wave action is about 15 mm to 30 mm. However, the soil specimens took from the good contact area by riprap rock show Figure 3.36(b) that there was less significant influence on the soil state.

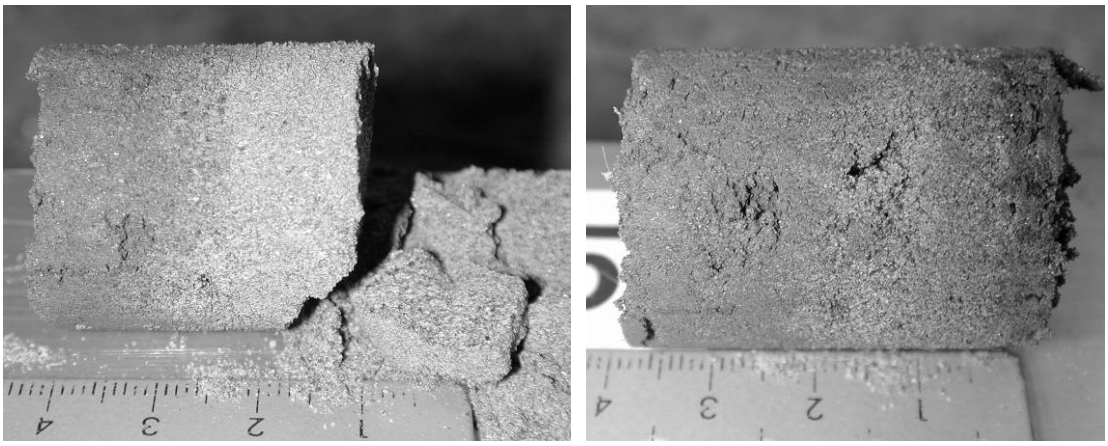

(a) Between the riprap rock. (b) Below the riprap rock.

Figure 3.36 The state of soil specimen (Test 2).

Moreover, the grain size analysis made on the soil underlying the geotextile, varies considerably between the zones considered. For example, some fine particles remained in the areas directly under the rocks (Figure 3.37); the variation of soil granulometric curve is insignificant. Inversely, the variation of soil granulometric curve between riprap blocks is very obvious (Figure 3.38). Hence, the quality of the contact between soil and the geotextile is the key factor. Good contact is promoted when the force acting normal to the interface (due to the weight of the cover blocks) is large. The safety of the bank is totally dependent on this normal force because of the cohesionless nature of the soil. Besides, the good contact could reduce the water flows through the surface of soil, and to prevent the fine particle further erosion. Between the rocks it appears that all the fine particles have been removed from the surface soil, leaving sandy areas. However, a mechanism of self-filtration of the granular medium has developed which ensures the stability of the remaining soil.

Additionally, the soil erosion on the upper part of the bank is more serious than the lower part. As above-mentioned, when the waves strike the revetment, water flows into the bank and flows down along the interval between the riprap rocks. In consequence, the fine particle migrated together with water flow down and causes the serious soil erosion. The fine particles migrated to the lower part of the bank, a part of particles was deposit, and a part was washed-out through the geotextile. Because of this reason, the soil erosion on the upper part of the bank was obvious.

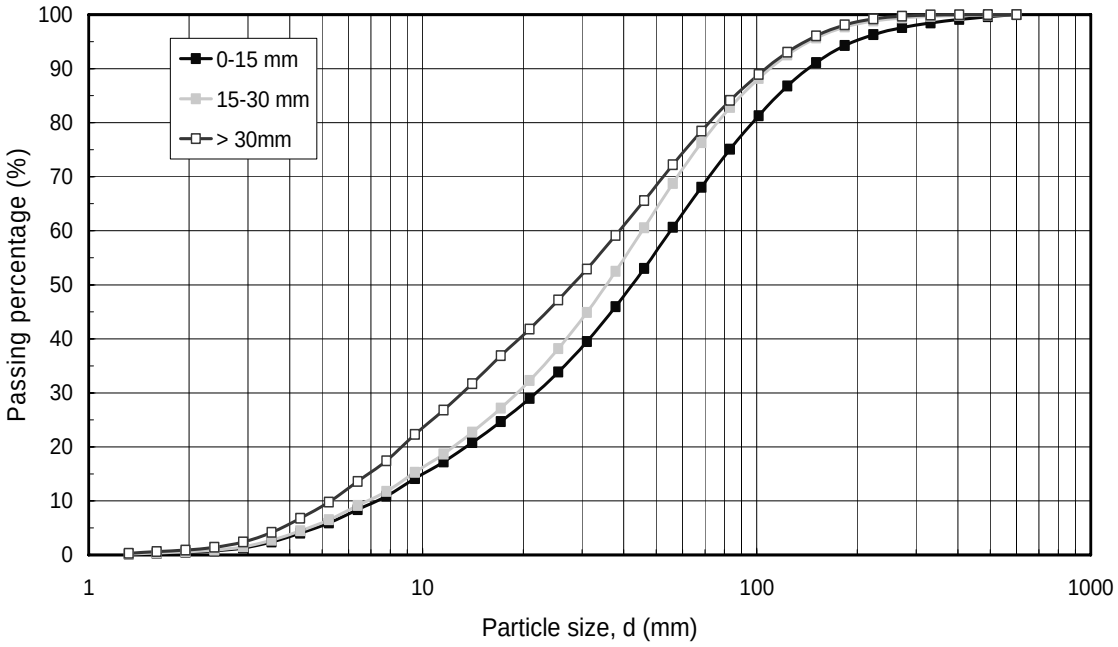

(a) Sampling from the upper part of the bank.

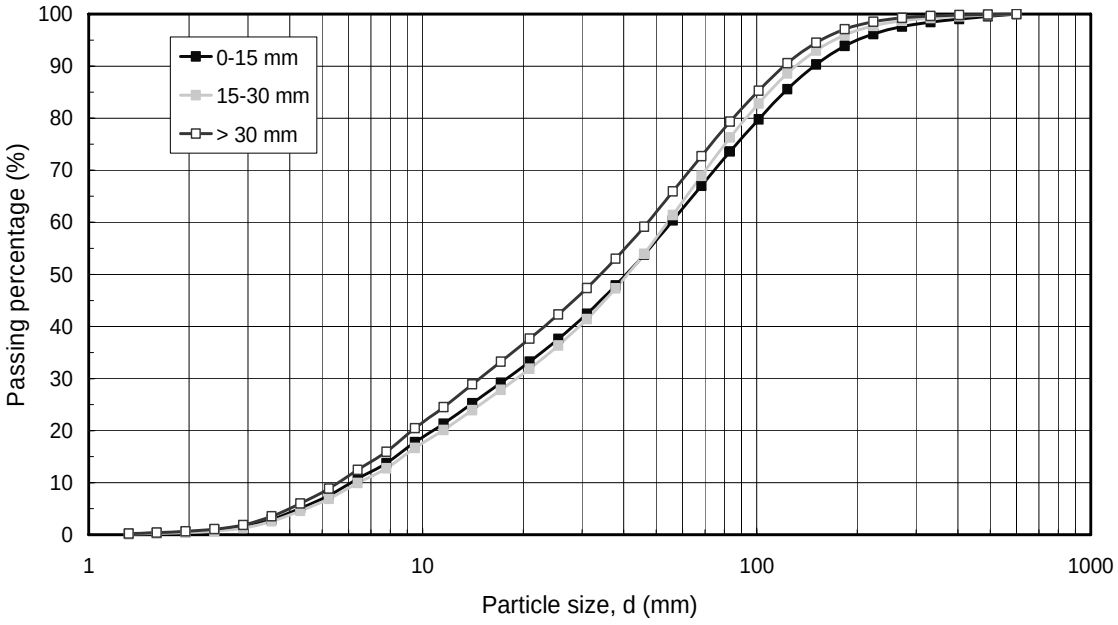

(b) Sampling from the lower part of the bank.

Figure 3.37 Grain size distribution of sampling under riprap (Test 2).

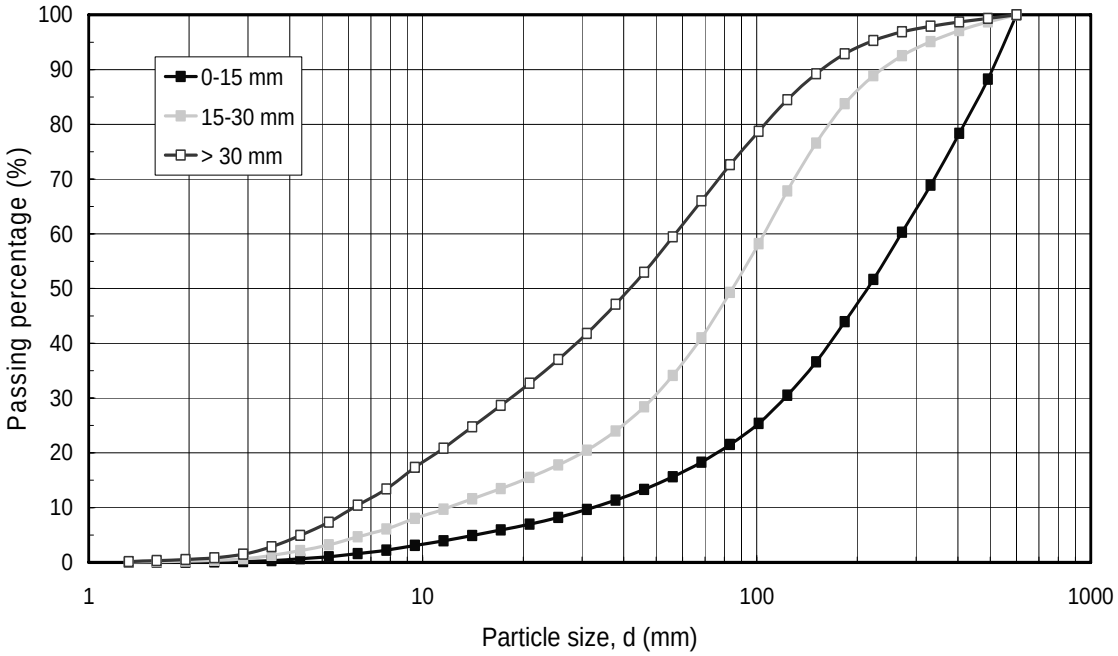

(a) Sampling from the upper part of the bank.

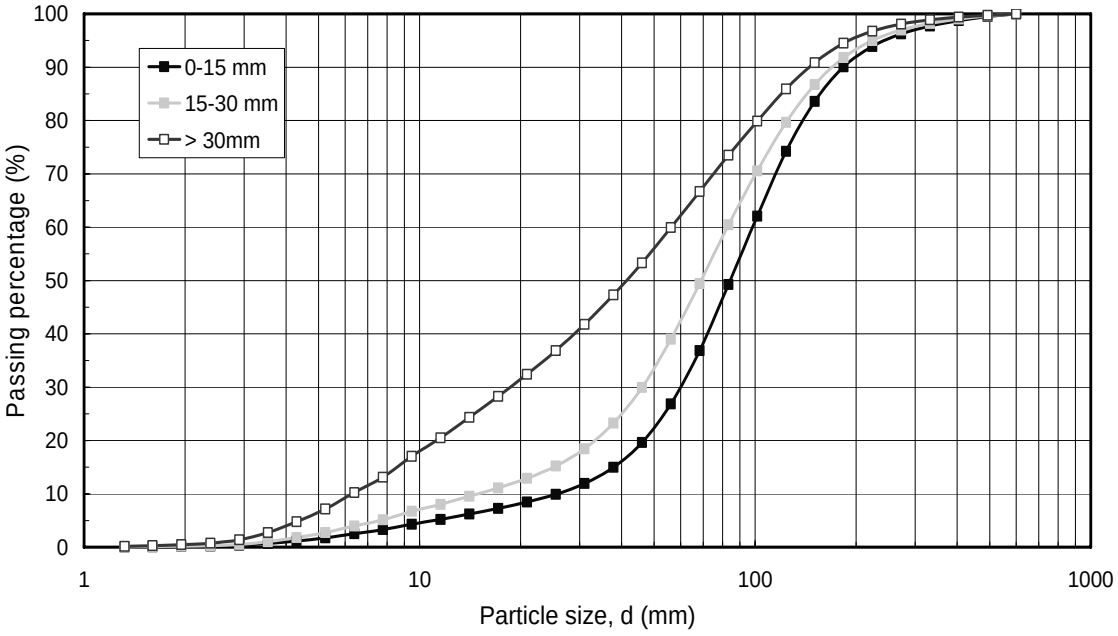

(b) Sampling from the lower part of the bank.

Figure 3.38 Grain size distribution of sampling between riprap (Test 2).

3.4.6 Summary

According to the performance of above-mentioned, the soil erosion mechanism of revetment laying geotextile subjected to the wave action can be explaining as follows and expressing in Figure 3.39:

1. When the wave surging (Figure 3.39(a)), the up-rush water will strike the bank, a part of water falling on bank to produce the pore water pressure increase and there is a consequent erosion of soil. Moreover, the upward flow will wash the surface of textile.

2. When the wave ebb (Figure 3.39(b)), the down-rush flow in the vicinity of geotextile will produces the tangential hydraulic force. A part of eroded soil migrates to the lower part due to the tangential flow. On the surface of geotextile, the down-rush flow will wash the textile clean.

3. On the other side, the tangential flow will take away the soil eroded to the lower part along the interval of cover block. The finer soil particles pass through the geotextile and the coarse one may deposit to form a natural filter layer.

4. When the wave action continues, the water flow circulation will go on. The soil in the upper part of the bank will be eroded and to cause the cover blocks settlement; the blocks in the lower part tend to rise due to the soil deposit.

5. Until the natural filter layer formed, the behavior of erosion and deposit will stop and the riverbank become more and more stable.

The cyclic water flow in the vicinity of geotextile is complex. In the zone that subjected to wave action, the water flow direction in upper part of the bank is mainly perpendicular to the geotextile (perpendicular flow), in middle part of the bank is mainly parallel to the geotextile (tangential flow), and it is an association of the perpendicular flow with the tangential flow in the lower part of the bank.

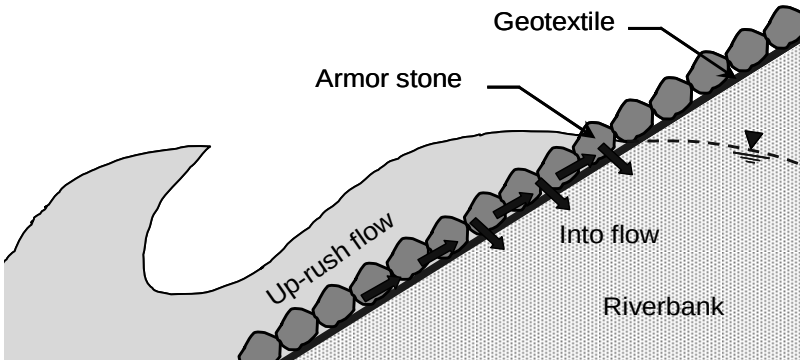

(a) Wave surging.

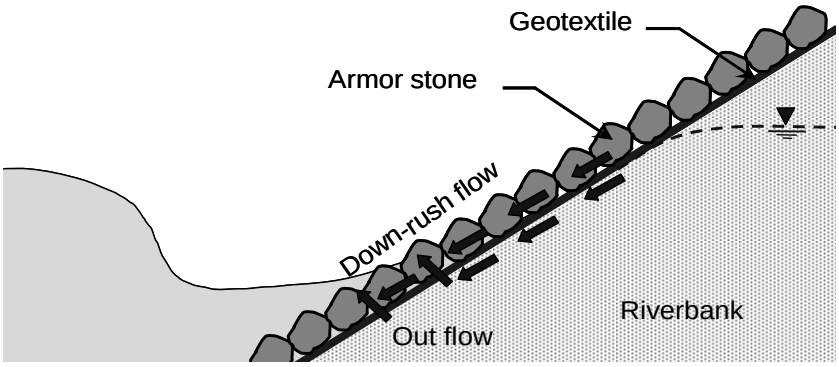

(b) Wave ebbing.

Figure 3.39 The water flow in the vicinity of geotextile.

Furthermore, under the tangential flow (middle part), it seems that there is no great difference between the two geotextile, although overall the SF1100 (thick geotextile) displayed better performance, it perhaps the thicker geotextile can offer better damping effect to retard the tangential hydraulic force acting on the soil surface. As pointed out by Bouthot et al. (2002), for the same opening size of geotextile, the constriction number (m) of thick geotextile is larger than the thin one and is less suited for perpendicular flow condition and it was observed at the upper part of revetment in this test. However, the opening size of those two geotextiles is suitable to maintain the soil of bank. The retention criteria of Heerten (1982), DGEC (1986), and Ragutzki (1973) suggested are too conservative. According to the result of the variation of pore water pressure, those two geotextiles are conforming to the permeability criteria.

Besides the criteria of permeability and retention, the quality of the contact between soil and the geotextile is an important factor too. Good contact could well maintain the state of soil.

3.5 Test results of RRGT

Two experiments were carried out in this subject. In order to understand the erosion behavior of reinforced revetment using geotextile, water turbidity, pore water pressure, displacement of geotextile bag were measured during the test. The results of the experiment are discussed in the following sections.

3.5.1 The variation of water turbidity

The water turbidity near the vertical geotextile face was measured during the test at regular times and the results are shown in Figure 3-40. As shown, the peak value of water turbidity increases with an increasing energy of wave. The progress of turbidity expresses that the erosion is most serious in the beginning of the experiment. As the experiments goes on, erosion tends to stabilize. Under the large wave energy action, the water turbidity decrease is slower than subjected to the small wave energy. In this experiment, the turbidity of the smallest wave energy (E150) decreases and becomes constant after 2 days. For E250 this occurs about after 4 days, and for the largest wave energy (E350) it needs 5 days. This result is alike with the result of RLGT.

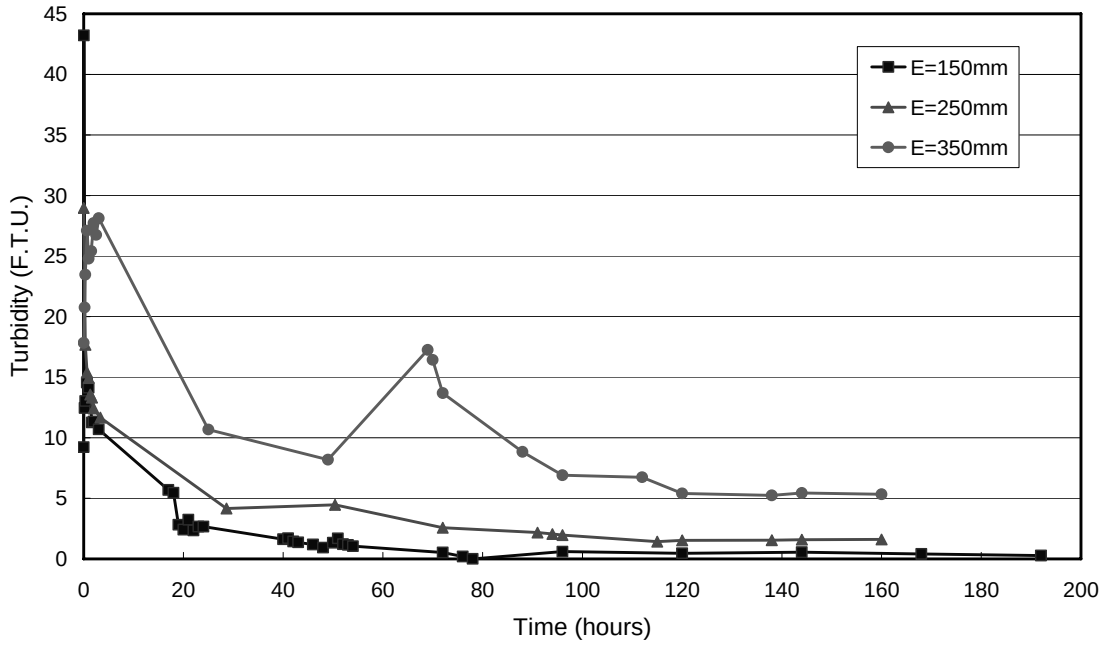

Figure 3.40 Turbidity versus time.

3.5.2 The variation of pore water pressures

Two piezometers are buried in the geotextile bag in order to measure the variation of pore water pressure in the experiment process for determining the clogging of geotextile. The P01 is placed and located in 15 cm behind the geotextile bag's vertical face of the water side; P02 is located in 5 cm behind the same vertical face (see Figure 3.13(c)). Those two piezometers are placed in same elevation (in the middle of the geotextile bag) and covered the soil with 20 cm thick. Furthermore, the two piezometers were submerged 2 cm under the static water level.

Figure 3.41 show the variation of pore water pressure head during the test. For P02, the water pressure head increases as the wave energy increases. However, it seems that the variation of P01 is irregular under the small wave energy action. That is because the piezometers located in 2 cm under the static water level, but the water level within the soil may be lower than free water side, P01 was probably not fully saturated. Then its answer is not correct. Once the wave energy increases, the water level will rise and flood the piezometers. Hence, the performance of pore water pressure is regular that subjected to the higher wave energy action. Besides, the pore water pressure head of P02 that subjected to the wave energy in E150 decreased slowly with time. That is on account of the water evaporated from the flume during the test. After the test of E150, the measured water level was found 2 cm lower.

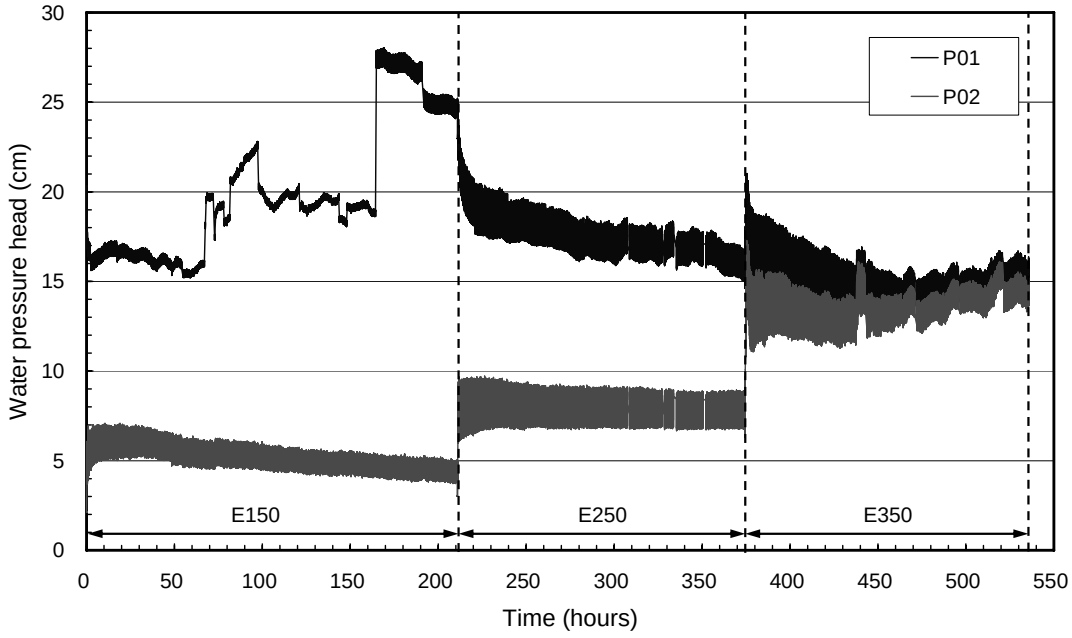

Figure 3.41 The variation of water pressure head during testing.

In addition, the amplitude of pore water pressure increases with an increasing energy of wave action. And the amplitude of P02 is larger than P01. That is because the P02 is close to the water side that the variation of pore water pressure is more sensitive than P01. The pore water pressure head of P02 shows that the variation of amplitude is quite stable, which serves as good indication that the filtering process of geotextile at the water side has been clean and that there is no clogging or blocking.

3.5.3 The displacement of geotextile bags

In order to monitor the variation of displacement, twenty reference points were marked on the top of geotextile bag and also twenty reference points on the geotextile bag surface of the water side (see Figure 3.42 for details). Five vertical sections in view of the reference points can be cut.

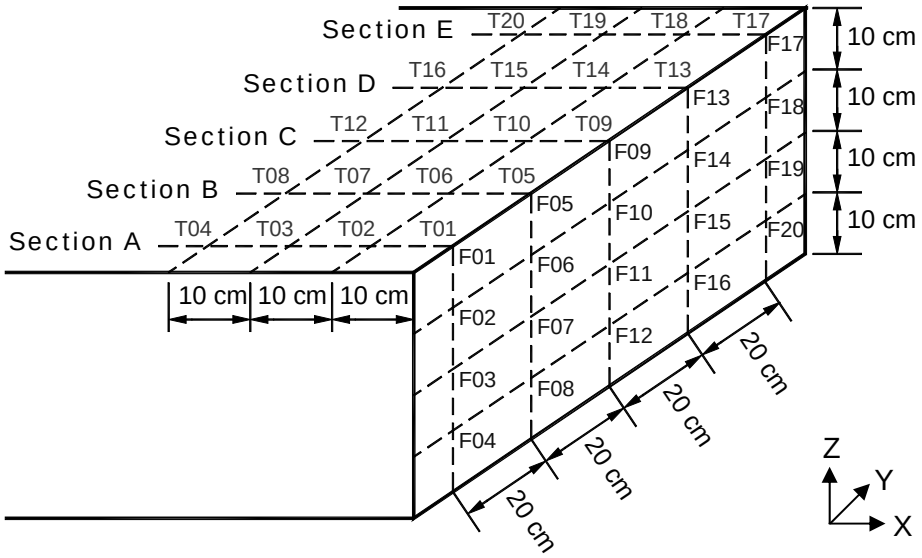

Figure 3.42 Illustration of the reference points of geotextile bags for measuring the displacement.

The displacements are periodically recorded during the test. On the top of the geotextile bag which the displacement of Z direction is more interesting, because it presented the variation of settlement during the test (see Figure 3.43). The most part of settlement takes place in the initial stage of each wave energy action, and the curves are more and more gentle as the test goes on. The settlement increases with an increasing energy of wave. This is due to the large wave energy that induces the large pore water pressure and consequently to produce greater settlement. The greater settlement takes place by the water side (T01, T05, T09, T13, and T17). Due to the

boundary on both sides that contact with the wall of the flume, the deformation of the central part of the geotextile bag is greater. The ultimate topography of the geotextile bag's top is diagramed in Figure 3.44 by Surfer V6.02. It shows that most of the settlement took place in range of 20 cm of near the water side. That is to say the influence range of the wave action is about 20 cm from the water side.

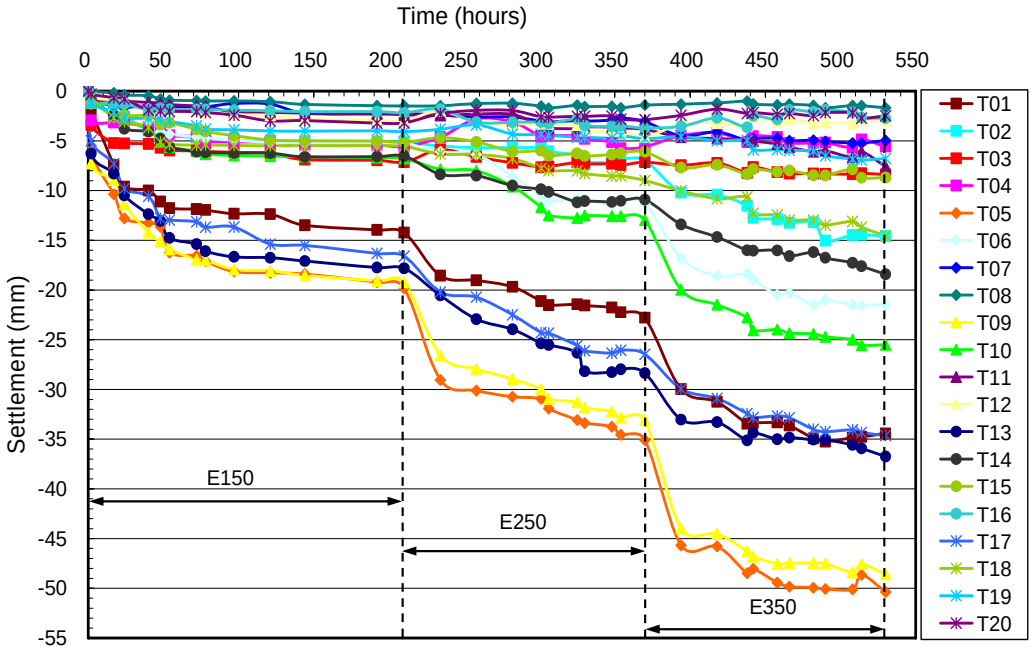

Figure 3.43 The variation of settlement on the top of the geotextile bag.

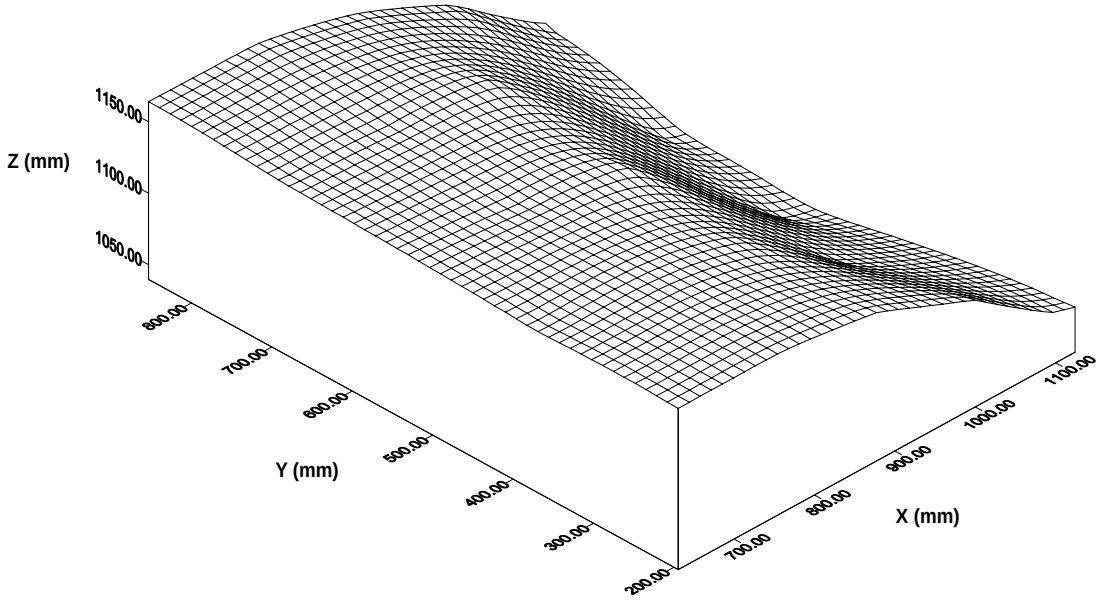

Figure 3.44 The ultimate topography of the top of the geotextile bag.

In addition, the X-direction displacement of the vertical face of the geotextile bag on the water side express the variation of deformation of the vertical face. The result of monitoring is presented in Figure 3.45. The interpretation is more complicated because the deformation at the water side involves both horizontal and vertical displacement. Consequently, the time-curve of the displacement is irregular. Experiment outcomes, however, also indicate that as the experiment time increases the deformation which becomes more significant. Those curves gradually level up. The greater of the impact energy of the waves generated the greater deformations. The figure indicated that the greater deformation took place in the middle and the lower part of the vertical face of the geotextile bag. Besides, the points of the crest F01, F05, F09, F13 and F17, show negative horizontal displacement, indicating the wall has deformed inwardly with a large settlement. Hence, the settlements of these five points are more important as shown in Figure 3.42 (T01, T05, T09, T13 and T17).

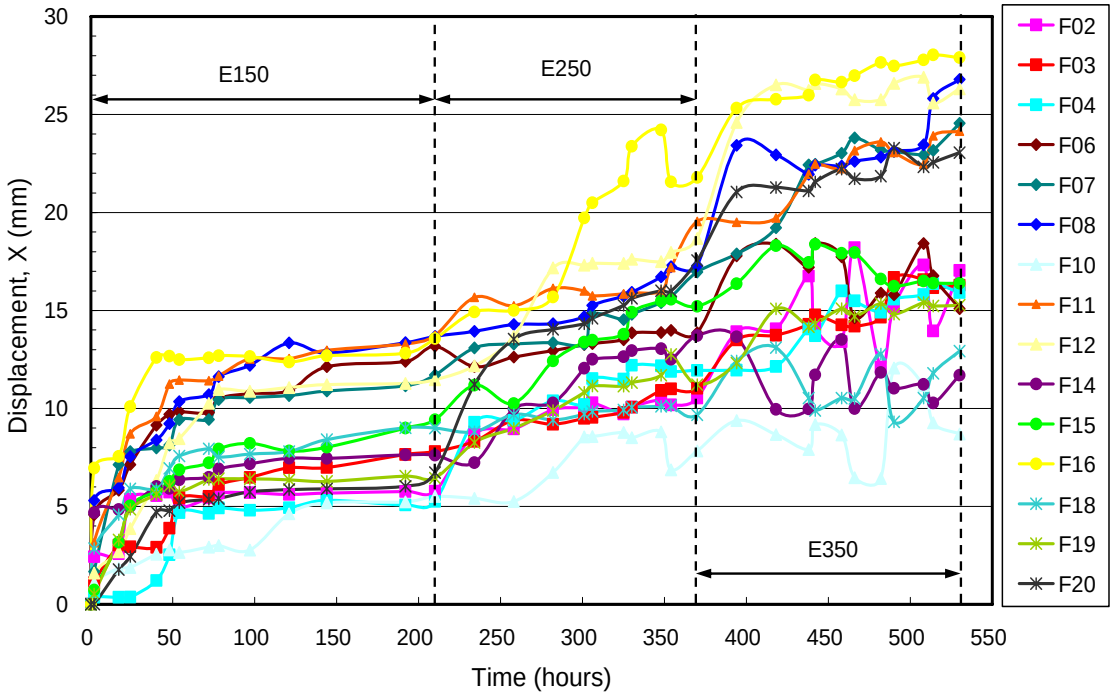

Figure 3.45 The variation of displacement on the water side surface of the geotextile bag.

In order to know the progress of the displacement during testing, the variation of settlement of Section C by time is shown in Figure 3.46. Figure 3.47 shows the combination of X and Z displacement, giving an idea of the slope of the bag face. The other sections are presented in Appendix I.

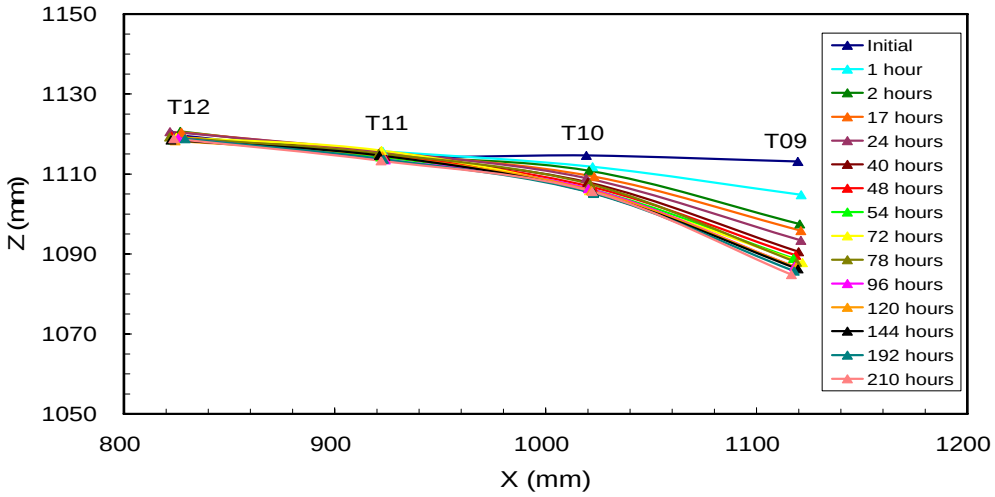

(a) E150

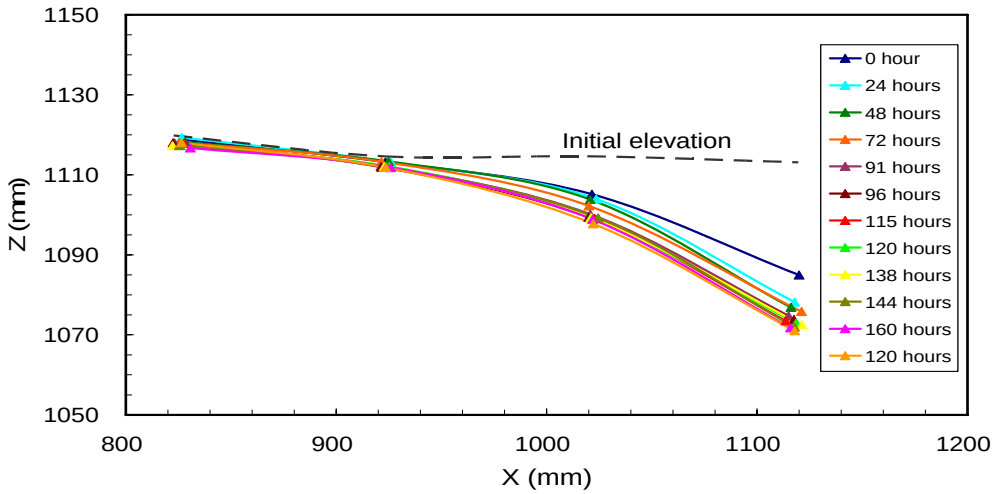

(b) E250

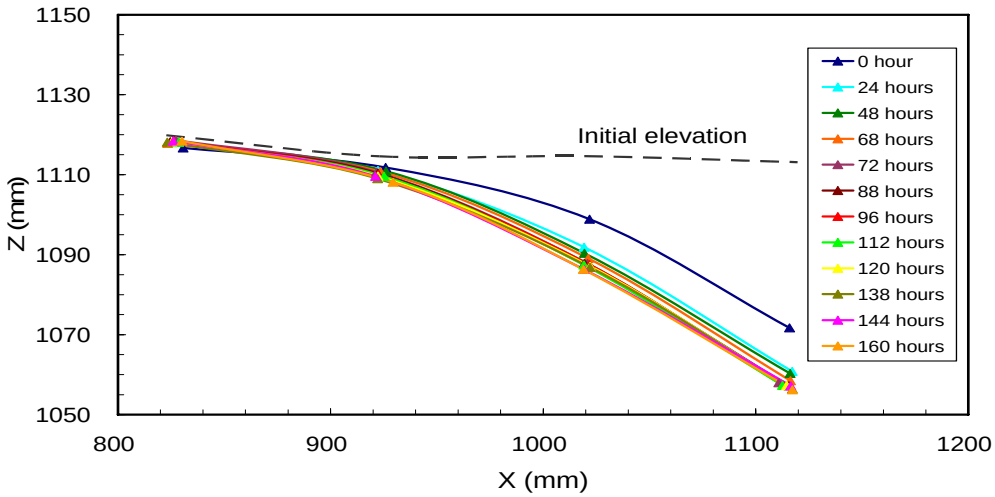

(c) E350

Figure 3.46 The variation of settlement on the top of the geotextile bag (Section C).

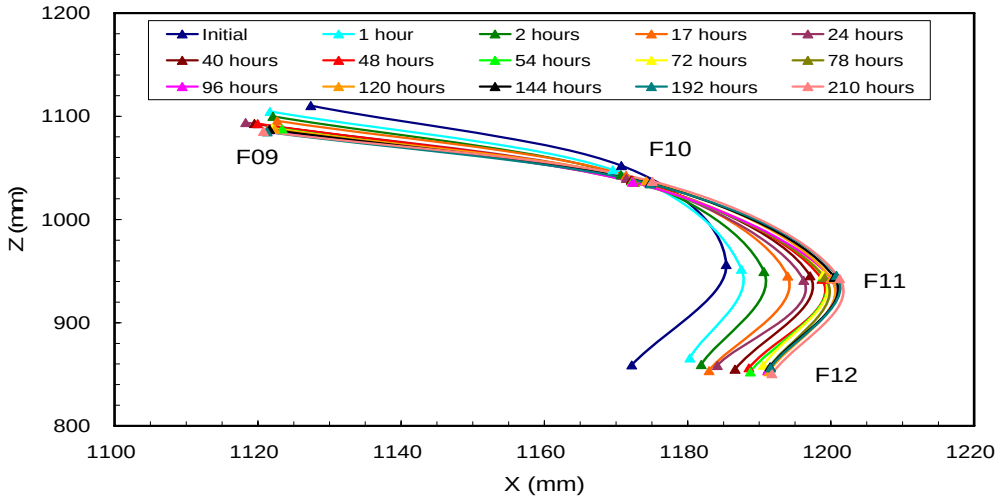

(a) E150

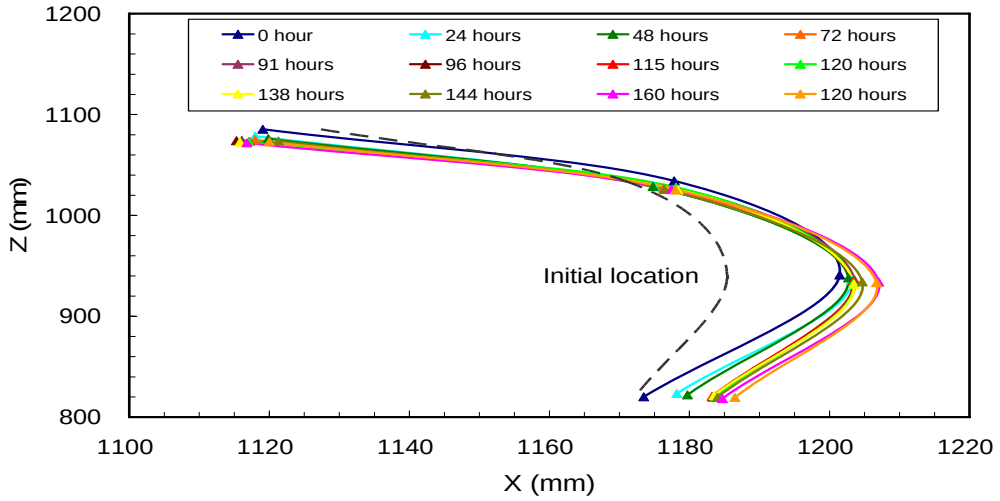

(b) E250

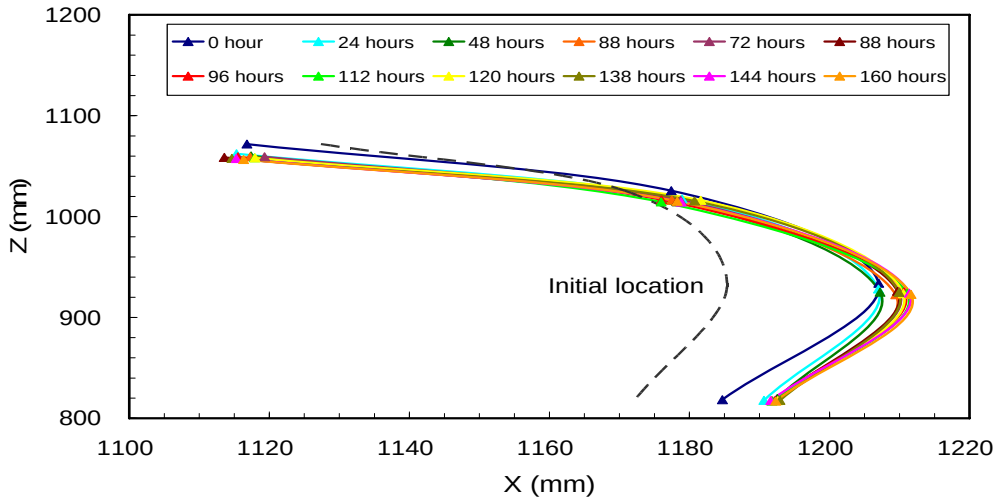

(c) E350

Figure 3.47 The variation of the shape of the bag face (Section C).

As shown in Figure 3.46, the largest settlement took place in T09. During the test, the total settlement reaches 57.5mm: 50 % (28.3 mm) occurred for the phase E150, 24.1 % (13.9 mm) for E250, and 26.9 % (15.5 mm) for E350. For each wave energy action, there are more than 50 % of settlement occurred while the first 24 hours of the test and it tends to stable after 120 hours. It indicated that the critical state of settlement of the geotextile bag while just beginning of the wave action.

Figure 3.47 presented the appearance similar to Figure 3.46. The maximum deformation took place at F11 and F12 and there is more than 50 % of displacement occurred while the first 24 hours for each wave energy.

3.5.4 Observation after testing

Figure 3.48 shows the appearance change of the geotextile bag before and after the test. The vertical face of the geotextile bag on the water side presented two different parts. Upper the static water level, the textile was cleaner than the lower part. That is because the surface of textile was washed repeatedly by wave action and there was no soil erosion continuously behind the geotextile. By opening the geotextile and it was found that there were several areas of the natural filter formed behind the geotextile (see Figure 3.49) in the zone subjected to the wave action. But in the zone under the static water level, the textile is dark and no natural filter area is observed.

(a) Before the test (b) After the test

Figure 3.48 The appearance of the geotextile bag before and after test.

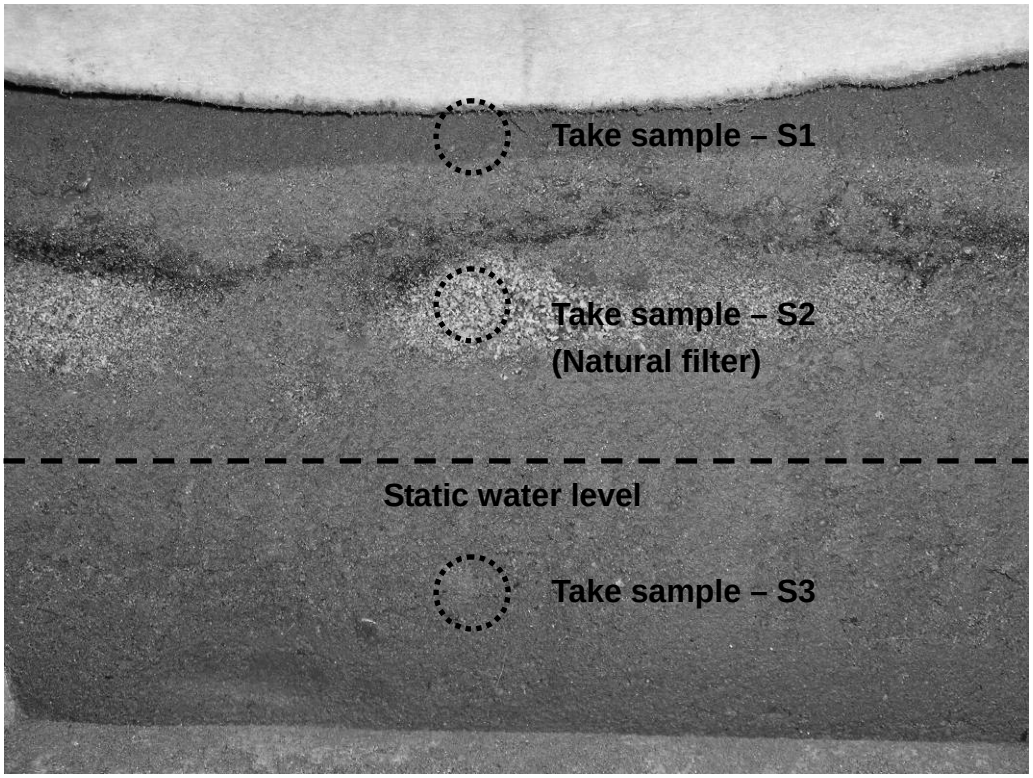

Figure 3.49 Natural filter areas formed behind the geotextile.

As Figure 3.49 shows, three soil specimens were taken from different parts of the vertical face. Figure 3.50 presents the state of soil specimen taken from the middle part (subject to the wave action). Within depth a thin layer on the left side (water side), the fine particles of the soil has been eroded and filtered out, and the cohesion has lowered as a result. Yet the soil behind the water side contains more fine particles and can stands on its own.

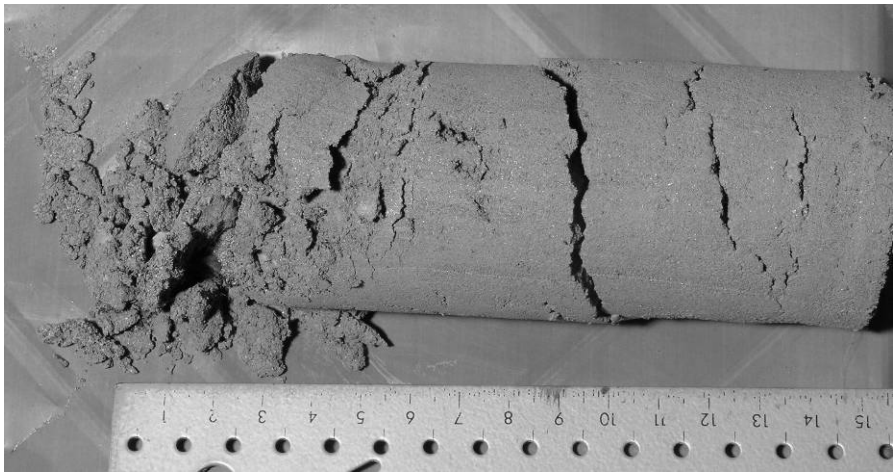

Figure 3.50 The state of soil specimen (S2).

3.5.5 The variation of soil particle size distributions

Figure 3-51 shows the particle size distribution of the soil specimens S02. Within 30 mm from the water side, the grain size distribution of this thickness does not show so large different with the original soil particle distribution as for sample taken in test 2 of RLGT (Figure 3.37). This means that the thickness of the natural filter layer is very thin and unfortunately the specimen analyzed was too thick (30 mm) to explain the real observed situation. After 30 mm from the water side, the particle size distributions are alike with the original soil. Moreover, Figure 3.52 shows the particle size distribution of the soil specimens S03 and the variation of soil state is insignificant.

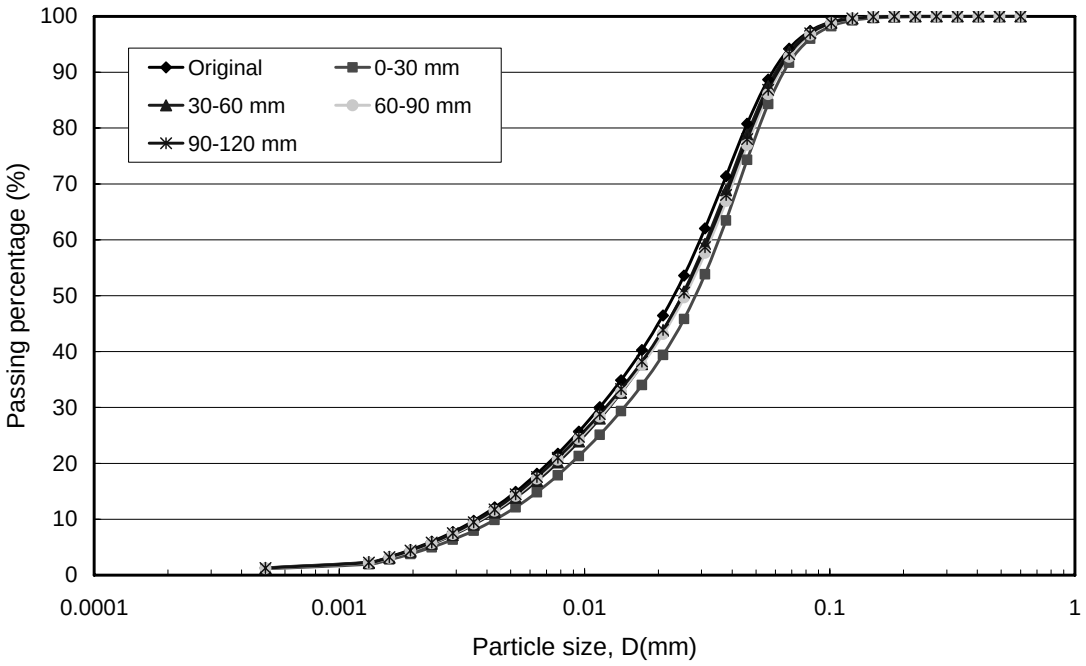

Figure 3.51 The particle size distribution of sample S2.

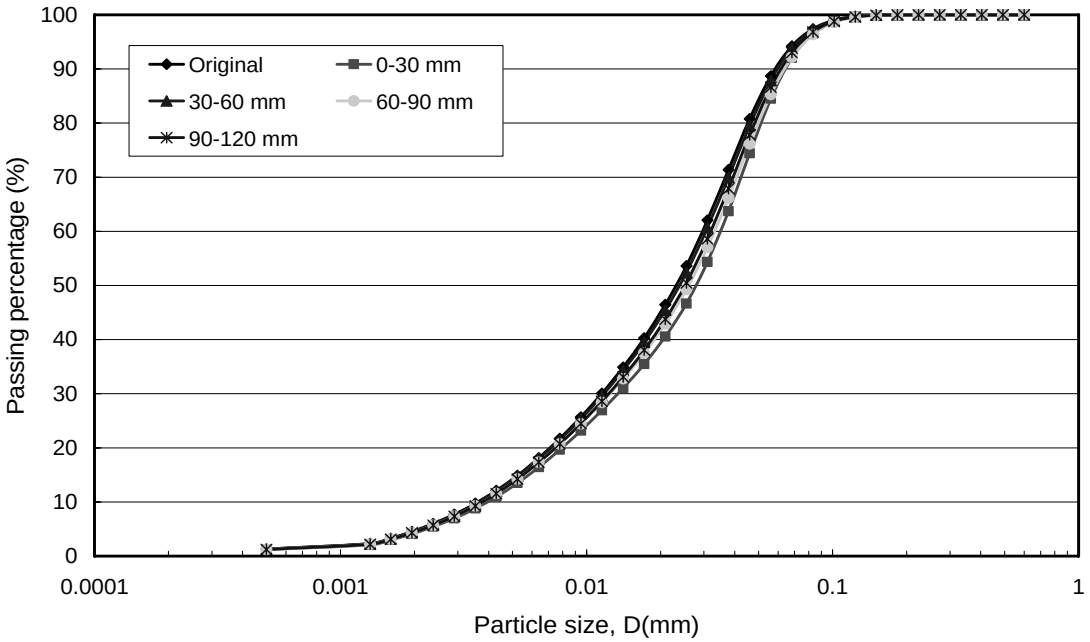

Figure 3.52 The particle size distribution of sample S3.

3.5.6 Summary

From the RRGT experiment results, the conclusions are described as follows:

1. The water in the flume was quite turbid during the preliminary stage of the experiment with eyes observation. The water turbidity obtained from the turbidity meter was also quite high. As the time of the experiment increases, however, the turbidity gradually dropped, indicating the fact that the soil within soil bag was no longer eroded. Once the eroded soils were gradually sedimentated at the bottom of the flume, the water became clear. After that the turbidity stabilizes, if the wave energy increases, the water becomes turbid again and the turbidity quickly increases, signifying the fact that the soil in the soil bag is being eroded again. As the time goes on, however, the turbidity gradually drops and the water becomes clearer. Under the action of greater wave energy, it takes longer for the turbidity to decrease, and it will stabilize at a constant that is higher than that of lower wave energy.

2. The amplitude of pore water pressure increases with an increasing energy of wave action. And the amplitude of P02 is larger than P01. The farther it is away from the water side, the less significant the amplitude will be, so that the amplitude becomes immune to tidal changes.

3. The fine particles that filled in the textile or deposited behind the geotextile were easier to wash out due to cyclic flow action. So the clogging and blocking would not take place.

4. There was more than 50 % of the settlement took place in the first 24 hours of the experiment when the waves action. As the time goes on it gradually alleviates. Once the impact energy of the wave increased, the settlement also increased. The greatest settlement took place on the water side. Deformation of X-direction at water side face was similar as the settlement at the top of the geotextile bag. The greatest deformation of X-direction took place at the middle part near the static water level.

5. The closer it is to the water side, the more obvious the fine particles lost. So the content of fine particles decreases.

6. A natural filter layer formed in the zone that subjected to the wave action. This phenomenon is alike to the observation result of RLGT. Hence, the soil-geotextile system can form the natural filter layer under the short term bi-directional cyclic flow.

Chapter 4 Long-term bi-directional flow test

As mentioned in Chapter 1, due to the fluctuation of water table, a revetment using geotextile has a zone subject to bi-directional flow. The infiltration rate of water through the soil-geotextile system is a function of the hydraulic gradient between the water levels within and outside of the revetment. Under this condition, soil particles may migrate from the soil into the geotextile that modifies the properties in this zone of soil. The study of this zone and its hydraulic characteristics are essential to understand the filtration mechanism. However, most of the research considered simpler conditions than real in-situ conditions such as bi-directional or cyclic flow due to the fluctuation of water table caused by sea waves, boats, or periodic draw-down of water for irrigation purposes. In order to understand the filtration function of a geotextile subjected to cyclic flows, a series of laboratory tests are performed in this study, with an apparatus capable of simulating bi-directional cyclic flows, thereby examining the appropriateness of the current criteria.

4.1 Test equipment

The bi-directional cyclic flow apparatus (Figure 4.1) was developed at National Taiwan University, with some modifications of the perpendicular cyclic flow model of ENEL, Italy (Cazzuffi et al. 1999). This apparatus is capable of simulating cyclic flow normal to the soil-geotextile interface. It consists of a cyclic wave generator, an acrylic sample chamber, a water reservoir and wash-out collecting tank, and a vertical pressure application system.

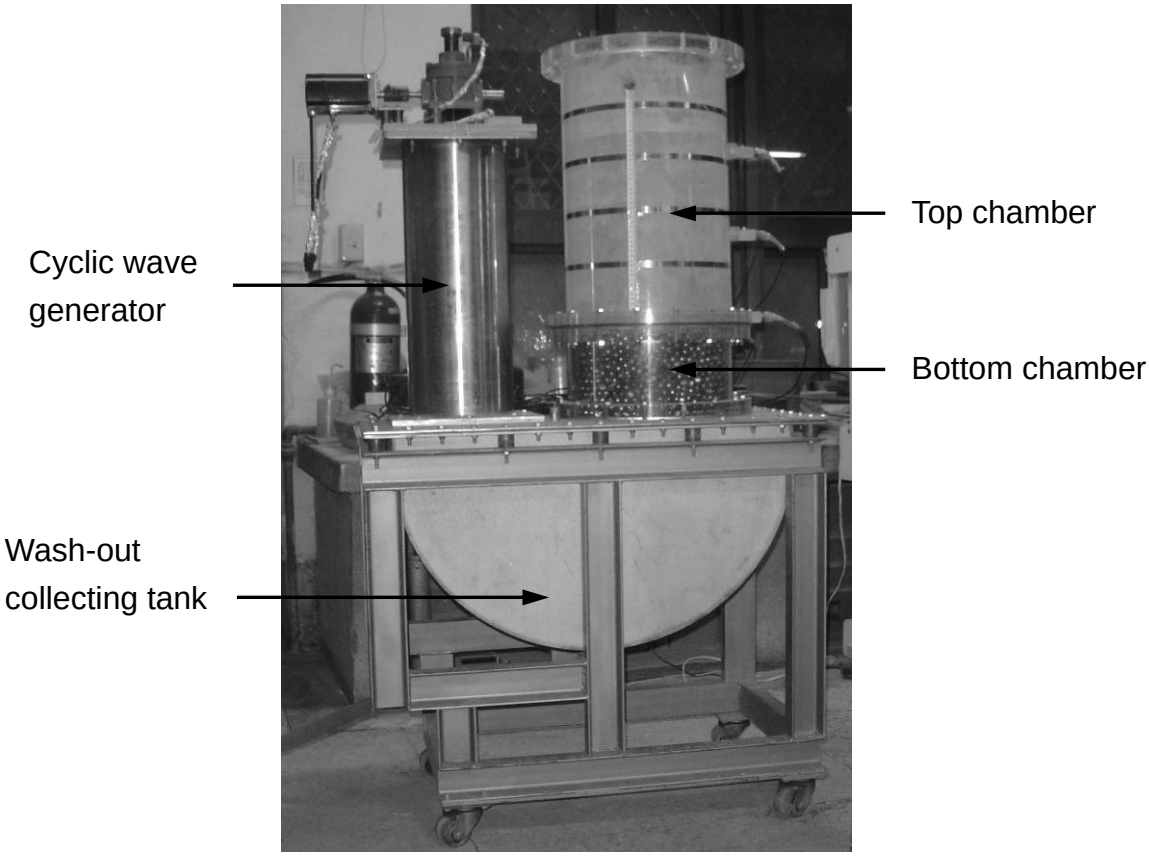

Figure 4.1 Front view of the bi-directional cyclic flow apparatus.

1. Sample chamber

Figure 4.2 shows the detailed schematic view of the internal setup of the sample chambers. The specimen cylinders consist of the upper and the lower acrylic chambers that is convenient to observe the state of soil erosion. The lower chamber contains marbles simulating the secondary armor layer in a revetment and a porous steel plate is placed below the lower chamber to maintain the marbles. A geotextile is laid on the marbles and is clamped between the upper and the lower chambers and then the soil specimen is filled in the upper chamber. There are four pore pressure transducers (P01, P02, P03 and P04) placed at different positions to monitor the fluctuation of pore pressure. The measured pore pressures can provide information regarding various phenomena such as blinding, clogging, or blocking. There is another porous steel plate places on the top of soil specimen in order to apply the vertical pressure. In addition, two LVDT (Linear Variable Differential Transformer), S01 and S02, are mounted on the top of a porous steel plate to obtain the average settlement during testing. The type of the pore pressure transducer that used is KYOWA PGM-05KG and the type of LVDT is KYOWA DT-30F. The specification of those instruments is presented in Appendix II.

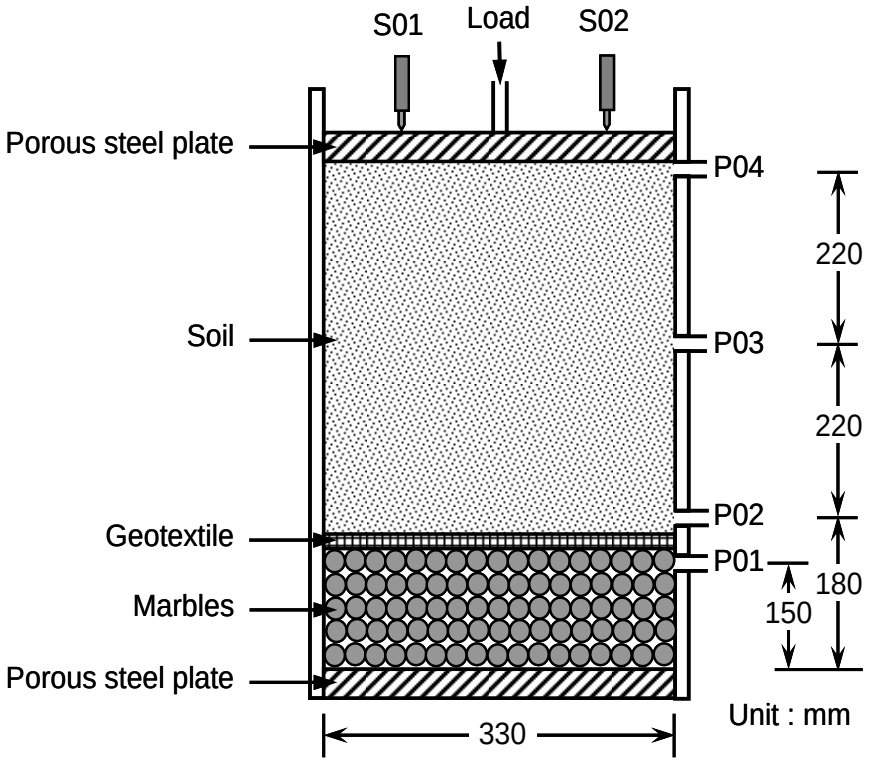

Figure 4.2 Detailed schematic view of the internal setup of chambers.

2. Cyclic wave generator

The cyclic wave generator activated by a piston whose action can simulate the cyclic wave loadings applied on a revetment. The piston of the cyclic wave generator is propelled by a stepper motor and the variation of the stroke length and the speed of the stepper motor are controlled by an automatically controlled system. In this test, the stroke length of the piston is adopted to be 9cm. Hence, the volume of water flow into/out the soil specimen is fixed during testing.

3. Steel water tank

Under the cyclic wave generator and sample chamber is a steel water tank. There is a water inject/drain valve in the bottom of the water tank. For being apt to collect soil particle that washed out, the bottom of water tank has a circular shape. In order to avoid the influence of air while testing, there is an air exhaust valve on the top of the water tank. Before testing, open the air exhaust valve to let air discharge while injecting water so as to ensure that there is not air in the water tank.

4. Vertical pressure application system

In order to understand the influence of vertical pressure on the bi-directional cyclic flow condition and to avoid the soil specimen lifted up while testing when the

water flow upward, vertical pressure is necessary and is applied by an hydraulic jack is necessary. The vertical pressure application system is shown in Figure 4.3. In this study, there are two vertical total stress were adopted 70 kPa and 140 kPa , respectively.

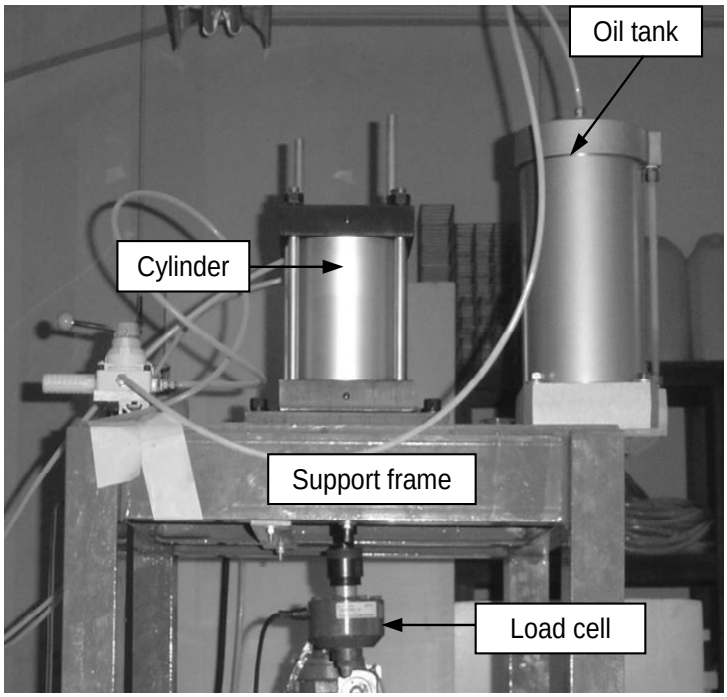

Figure 4.3 Vertical pressure system.

4.2 Test materials properties

In order to understand the effect of the fine content of soil on the filtration behavior of geotextile, one geotextile with eight compositions of soil are used. Their engineering properties are described below.

4.2.1 Soil material

The soil used in this test is composed of various weight proportions of coarse sand, silt and clay. Their grain size distributions and properties are shown in Figure 4.4 and Table 4.1, respectively.

1. Coarse sand

In this experiment, the primary soil that is adopted is Vietnam sand. The

properties of sample were obtained from laboratory tests. The specific gravity (Gs) of Vietnam sand is 2.66. The classification of the soil sample is SP (poorly-graded sand) based on Unified Soil Classification System (USCS). The maximum void ratio is 0.76~0.77. The minimum void ratio is 0.56~0.57.

In order to avoid the influence of the fine particle content of the original Vietnam sand on whole fine particle content of the testing soil specimen, the Vietnam sand was washed and filtered out the fine particle that are smaller than 0.074 mm before used.

2. Silt soil

The silt soil is obtained from some alluvial soil from Xindian Creek (Taipei), with liquid limit 25.9% and specific gravity 2.68. In order to get the silt soil, the alluvial soil was pretreated. After soil samples are taken from the site, the original soil are dried and the coarse particles that larger than 0.074 mm are filtered out by sieving test. The fine particles collected are mixes with water and the particles are let for sedimentation. According to the theory of water pluviation method, silt particles sedimentate earlier than the clay particles. After that, the slurry is dried and the non-cohesive soil that sedimentated in the bottom is collected: this is the silt soil adopted. The liquid limit (LL) by Atterberg Limits testing is 25.9% and non-plastic for this silt. According to Unified Soil Classification System, the classification of this silt sample is ML (low plasticity silt).

3. Clay soil

The clay soil is sampled from the sediment of Keelung River (Taipei), with a liquid limit (LL) of 39.0%, a plastic limit (I_p) of 26.4%, and a specific gravity (Gs) of 2.60. According to Unified Soil Classification System, the classification of this silt sample is CL (low plasticity clay). The sediment soil is pretreated following the same way as above-mentioned and the cohesive soil that sedimentated on the top is collected after the slurry is dried.

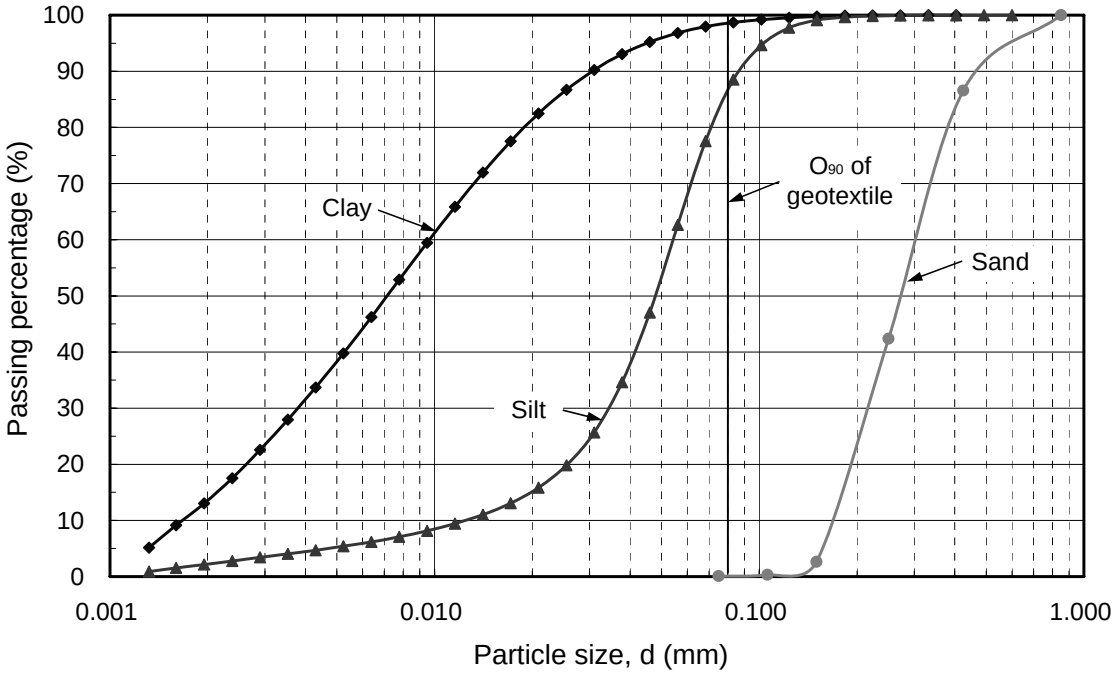

Figure 4.4 Particle size distributions of soils for cyclic flow test.

Table 4.1 Grain sizes and properties of soils

Soil	d_{50} (mm)	d_{80} (mm)	d_{85} (mm)	d_{90} (mm)	Gs	LL (%)	I_P (%)	USCS
Sand	0.270	0.380	0.408	0.470	2.66	-	-	SP
Silt	0.048	0.070	0.079	0.084	2.68	25.9	NP*	ML
Clay	0.007	0.019	0.023	0.030	2.60	39.0	26.4	CL

*NP: Non-plastic

Seven soil specimens were prepared by mixing those soils with various proportions. Their components by weight, soil classification symbol, and hydraulic conductivity are tabulated in Table 4.2. For the mixture of G-01 to G-05, the percentage of silt content increases from 0% to 20%. For G-06 and G-07, the total amounts of fine particle content (less than 0.074mm) are both 10%. However, G-06 contains 6.5% of silt and 3.5% of clay, and G-07 contains 3.5% of silt and 6.5% of clay. It can be seen from Table 4.2 that the hydraulic conductivity reduces as the fine content increases, especially reduced significantly by a small amount of increase in the clay content.

Table 4.2 The proportion of soil specimem

Test No.		Vertical Pressure (kPa)	Sand (%)	Silt (%)	Clay (%)	Classification (USCS)	k_s (m/s)
G-01	a	70	100	0	0	SP	4.38×10^{-3}
	b	140					
G-02	a	70	95	5	0	SP	3.25×10^{-3}
	b	140					
G-03	a	70	90	10	0	SP-SM	1.43×10^{-3}
	b	140					
G-04	a	70	85	15	0	SM	8.33×10^{-4}
	b	140					
G-05	a	70	80	20	0	SM	4.38×10^{-4}
	b	140					
G-06	a	70	90	6.5	3.5	SP-SM	8.41×10^{-5}
	b	140					
G-07	a	70	90	3.5	6.5	SP-SC	7.22×10^{-6}
	b	140					

Seven soil specimens were prepared by mixing those soils with various proportions. Their components by weight, soil classification symbol, and hydraulic conductivity are tabulated in Table 4.2. For the mixture of G-01 to G-05, the percentage of silt content increases from 0% to 20%. For G-06 and G-07, the total amounts of fine particle content (less than 0.074mm) are both 10%. However, G-06 contains 6.5% of silt and 3.5% of clay, and G-07 contains 3.5% of silt and 6.5% of clay. It can be seen that the hydraulic conductivity reduces as the fine content increases, especially reduced significantly by a small amount of increase in the clay content.

Moreover, the particle size distribution for those seven soil specimens shows in Figure 4.5. As shown, the average particle diameter (d_{50}) is almost same for each test specimen but the effective particle diameter (d_{10}) is decrease from specimen G-01 to G-05. For G-06 and G-07, the effective particle diameter is close to G-03 but the percentage of particle content which smaller than d_{10} is different. Besides, the geometrical stability of soil was evaluated that used the criterion of Kenney and Lau (1985, 1986). According to the result of analysis (Figure 4.6), except G-06, other specimens are all stable.

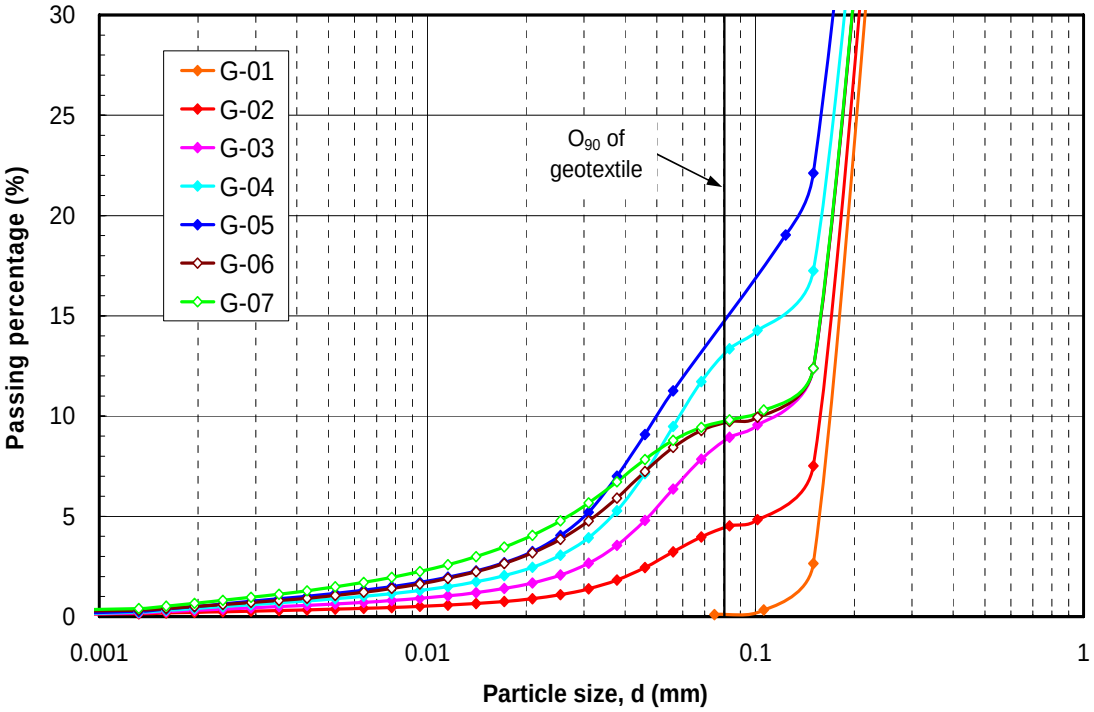

	d_{10} (mm)	d_{15} (mm)	d_{40} (mm)	d_{50} (mm)	d_{60} (mm)	d_{85} (mm)	d_{90} (mm)	Cu	I_p (%)
G-01	0.180	0.180	0.240	0.270	0.302	0.408	0.470	1.7	-
G-02	0.170	0.170	0.230	0.265	0.298	0.402	0.466	1.8	-
G-03	0.110	0.150	0.215	0.255	0.285	0.400	0.452	2.6	-
G-04	0.059	0.115	0.209	0.240	0.280	0.392	0.447	4.7	-
G-05	0.048	0.082	0.200	0.230	0.275	0.388	0.438	5.7	-
G-06	0.105	0.150	0.215	0.255	0.285	0.400	0.452	2.7	-
G-07	0.092	0.150	0.215	0.255	0.285	0.400	0.452	3.1	5

Figure 4.5 Particle size distributions of test specimens.

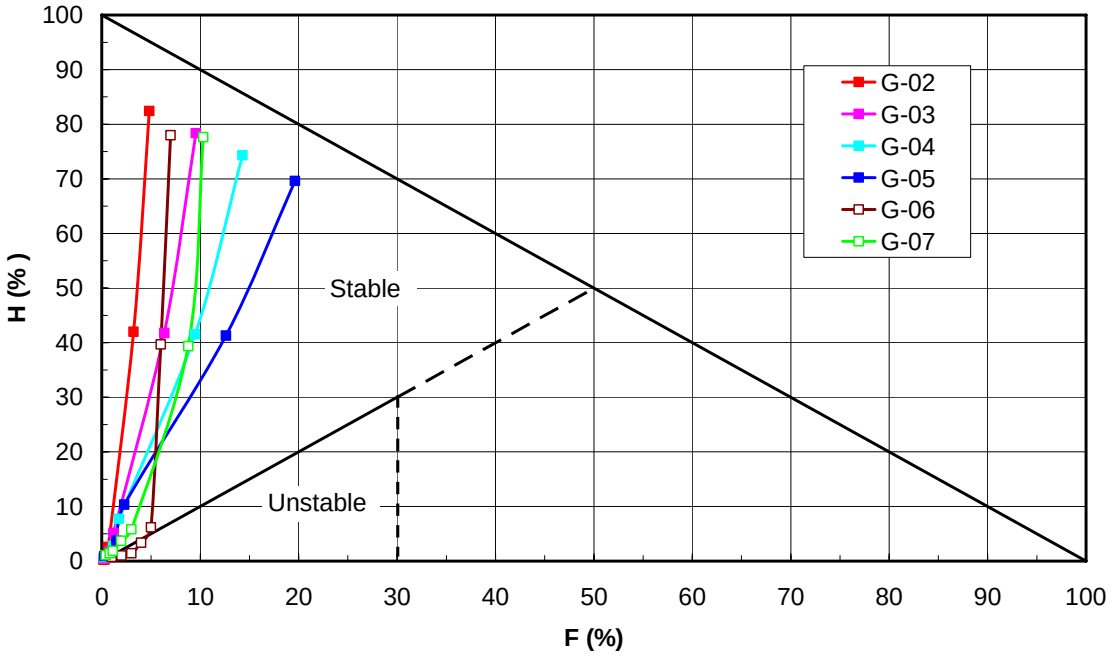

Figure 4.6 The result of analysis of the internal stability of soil filter by the criterion of Kenney and Lau (1985).

4.2.2 Geotextile material

In regard to the geotextile for testing, Hoare (1984) proposed to adopt thin heat-bonded geotextiles for uni-directional water flow conditions and thick needle-punched geotextiles for bi-directional flow conditions. In addition, according to the suggestion of Giroud et al. (1998), a two-layer non-woven geotextile is suitable for protecting river or coastal revetment. In view of this, this study employed a thick two-layer needle-punched geotextile for a series of tests (BF400). The geotextile is same as the one of the geotextile that adopted in Chapter 3 and the material properties of BF400 list in Table 4.3.

Table 4.3 Geotextiles characteristics

Name	Mass Specific Filter layer (g/m^2)	Thickness of Filter layer (mm)	O_{90} (microns)	Number of Constrictions	Permeability (m/s)
BF400	170	1.7	80	25	2.5×10^{-3}

4.2.3 Examination of the materials used with the current design guidance

1. Permeability criteria

According to the filtration criterion that described in Chapter 2, Equation 2-9 was used for examining the appropriateness. For non-cohesive soil specimens such as G-01 to G-06, the permeability of the geotextile must be greater than 10 times that of the soil. On the other hand, the permeability of the geotextile must be greater than 100 times that of the cohesive soil (G-07). Since the coefficient of hydraulic conductivity of the geotextile, k_g, is 2.5×10^{-3} m/s, and according to the permeability of each specimen that are listed in Table 4.2. It is apparent that the geotextile for G-01, G-02, and G-03 are unsatisfied the permeability requirement.

2. Retention criteria

In regard to the retention, the values of the relevant parameters of the testing materials were substituted into the criteria listed in Table 2.2 and Figure 2.7. The results also satisfied the retention requirement. The parameters of soil particle distribution have shown in Figure 4.4 for each test specimen. Regarding G-05 and G-07 as the example because of the specimen of G-05 contains the most silt soil and G-07 contains the most clay soil, the result examined is listed in Table 4.4.

Though this geotextile satisfied the above requirements, it would be tested under bi-directional flow conditions designed in this study, thereby examining the adequacy and applicability of the preceding criteria.

Table 4.4 The examined results of the retention criteria of test materials under cyclic flow.

References	Base soil type	Retention criterion	Examining Result	
			G-05	G-07
Heerten (1982)	non-cohesive soil	$O_{90} < d_{50}$	OK	OK
DGEC (1986)	$d_{40} > 60\mu m$	$O_{90} < d_{90}$	OK	OK
Ragutzki(1973)	not confined	$O_{90} \le (0.5 \sim 0.7) \times d_{50}$	OK	OK
PIANC (1987)	$Cu > 5$	$50\mu m < O_{90} < d_{90}$	OK	-
	$Cu < 5$	$50\mu m < O_{90} < 0.7 \times d_{90}$	-	OK
ASPG (1985)	$d_{40} > 60\mu m$	$O_{90} \le 1.5 \times d_{10} \times \sqrt{Cu}$ $O_{90} \le d_{60}$	OK	OK
CFGG (1986)	loose sand ($Cu>4$)	$O_{90} < 0.6 \times d_{85}$	OK	-
	loose sand ($Cu \le 4$)	$O_{90} < 0.48 \times d_{85}$	-	OK
Holtz(1998)	$d_{50} \ge 74\mu m$	$O_{90} \le d_{15}$	OK	OK
Mlynarek (2000)	See Fig. 2.7	$O_{90} < 0.8 \times d_{50}$ or $150\mu m < O_{90} < d_{50}$	OK	OK

Note: $O_{90} = 80\mu m$

G-05:	$d_{10} = 48\mu m$	$d_{15} = 82\mu m$	$d_{40} = 200\mu m$
	$d_{50} = 230\mu m$	$d_{60} = 275\mu m$	$d_{85} = 388\mu m$
	$d_{90} = 438\mu m$	$Cu = 5.7$	$I_p = 0$
G-07:	$d_{10} = 90\mu m$	$d_{15} = 130\mu m$	$d_{40} = 190\mu m$
	$d_{50} = 210\mu m$	$d_{60} = 230\mu m$	$d_{85} = 350\mu m$
	$d_{90} = 380\mu m$	$Cu = 2.6$	$I_p = 5$

4.3 Test procedure

In order to investigate the effect of normal pressure on the filtration function of the geotextile under bi-directional cyclic flow, loading was applied on the top of specimen at 70 kPa and 140 kPa, respectively. The wave period applied ranged from long to low periods, i.e., at 600, 300, 150, and 75 seconds, respectively. The testing procedure is summarized briefly as follows:

1. After the apparatus had been set up, the soil at optimum water content was divided into eight layers of equal weight and placed in the upper chamber. Each layer of soil is compared until it reaches the maximum dry density. With these eight layers, the total height of the soil specimen is 45cm. The maximum dry density and the optimum water content were obtained by the Standard Proctor Compaction Test (ASTM D698). The test results are shown in Figure 4.7.

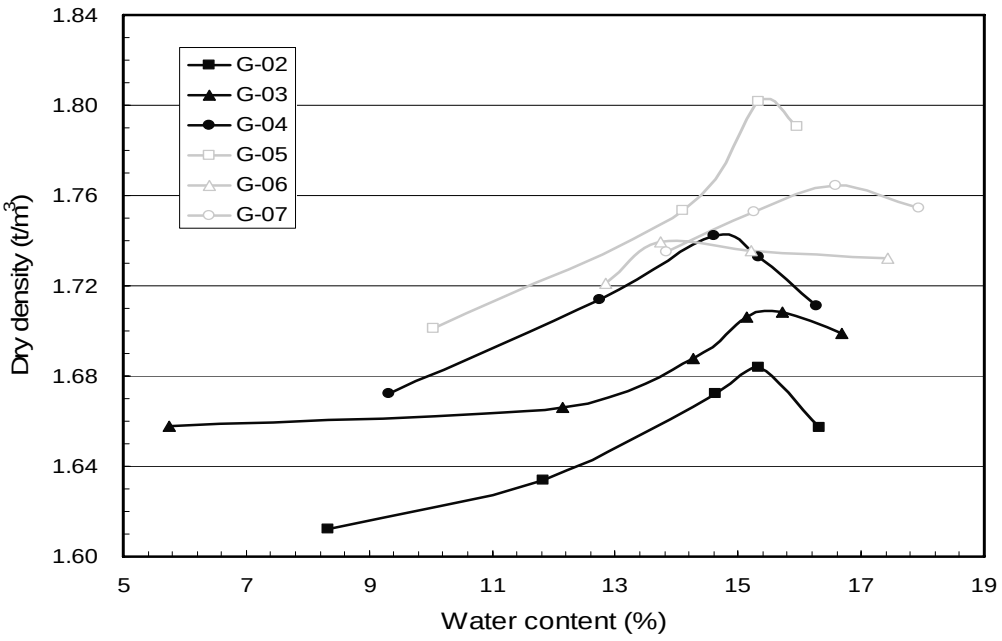

Figure 4.7 The Standard Proctor Compaction Test curves.

2. The loading device is fixed to the chamber and normal stress was then applied incrementally by step of about 10% to 20% of the maximum normal load. The subsequent increment of loading is added only after the settlement induced by the previous loading had become stable and the pore water pressure is equal to the static water pressure by piezometers.

3. The specimen was then saturated with water gradually from the bottom until the water reached the top of the specimen. According to the suggestion of Chew et al. (2003), this procedure was repeated three times in order to ensure full saturation. Alternatively, the pore pressures recorded by the four transducers could be compared with the elevation of the transducers to examine whether the specimen was fully saturated.

4. Under the constant normal pressure, 70 kPa or 140 kPa, the specimen is then subjected to cyclic flows in the order of 600, 300, 150 and 75 sec/cycle of wave period, respectively. The volume of the water flow into/out keeps constant for each wave period, so that the flow velocity within soil specimen increases from 600 sec/cycle to 75 sec/cycle. The test duration for each constant period is at last 48 hours and until the variation of pore water pressure become stable. Figure 4.8 illustrates the period and amplitude of each cyclic flow applied. Comparing with the large flume test (described in Chapter 3), the wave periods that adopted in this test are the long-term periods and the flow velocity within soil is consequently lower than large flume test.

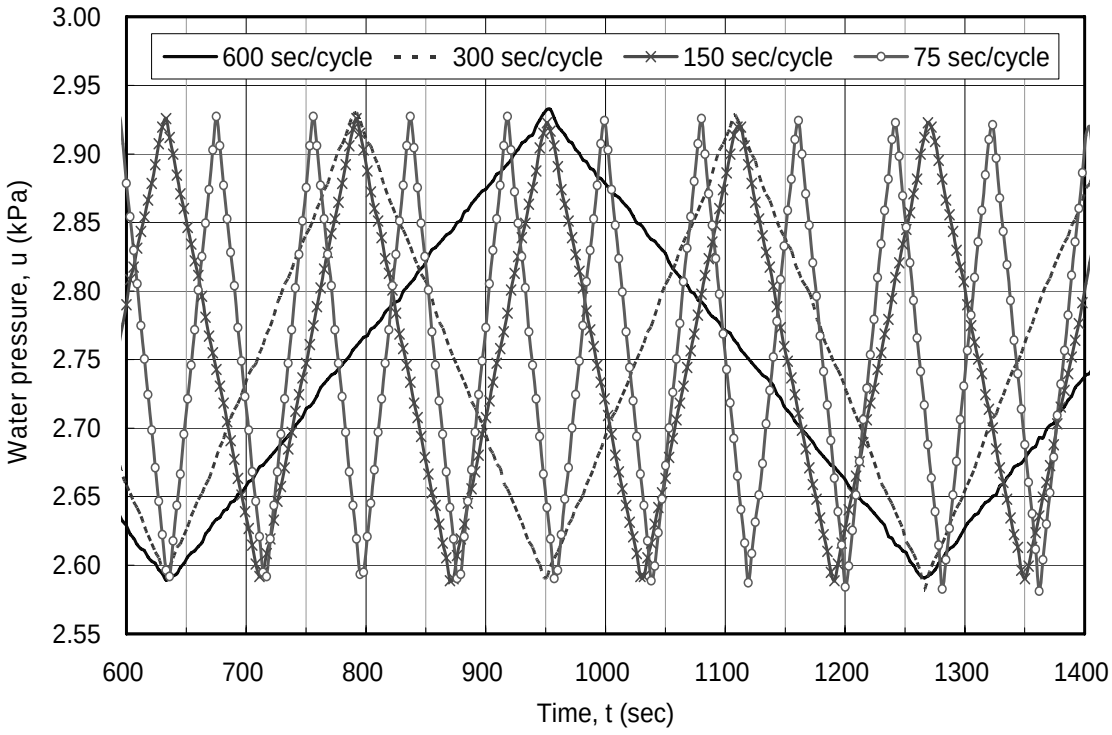

Figure 4.8 The period and amplitude of cyclic flows applied (no soil in the chamber).

4.4 Test results

During the test, the pore water pressures at various levels in this soil are recorded in order to examine the conditions such as clogging, blocking or boiling that might occur in the filtration system. The settlement measured can also be compared with the pore water pressure to find if there exists a relationship between them. In addition, the grain size distribution of the soil, before and after test, is compared with the soil washed-out in the collecting tank to have a better understanding of the mechanism.

4.4.1 Pore water pressure

1. Pure sand (G-01):

Figure 4.9 shows the pore water pressure response of wave periods of pure sand at 600, 300 sec/cycle, and 150 sec/cycle, respectively. The pore water pressure response at 75 sec/cycle was absent because the piezometers were broken during the test with this period.

As shown, the peak value of pore water pressure increases as the wave period decreases (flow velocity increases). This is due to the pore water pressure has not dissipated completely when the next cycle of flow comes up in the case of smaller period of flows (high flow velocity). The effect of normal stress on the response of pore water pressure can also be seen from Figure 4.8. For pure sand under various normal stresses, the difference in pore pressure is not significant. This implies that pure sand has a quite stable structure under the action of normal stress.

In regard to the different of pore water pressure between P01 and P02, is nearly the same during testing. This indicates that the geotextile without clogging and blooding while testing.

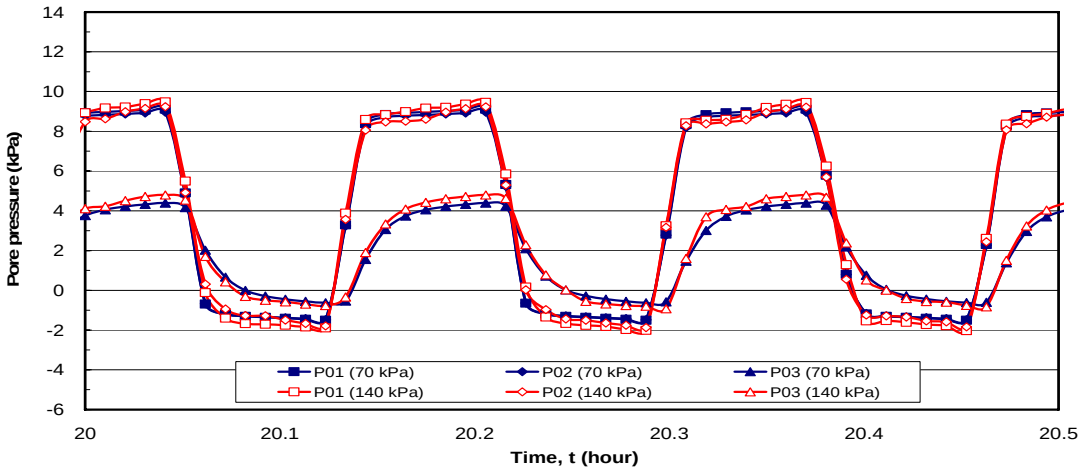

(a) 600 sec/cycle

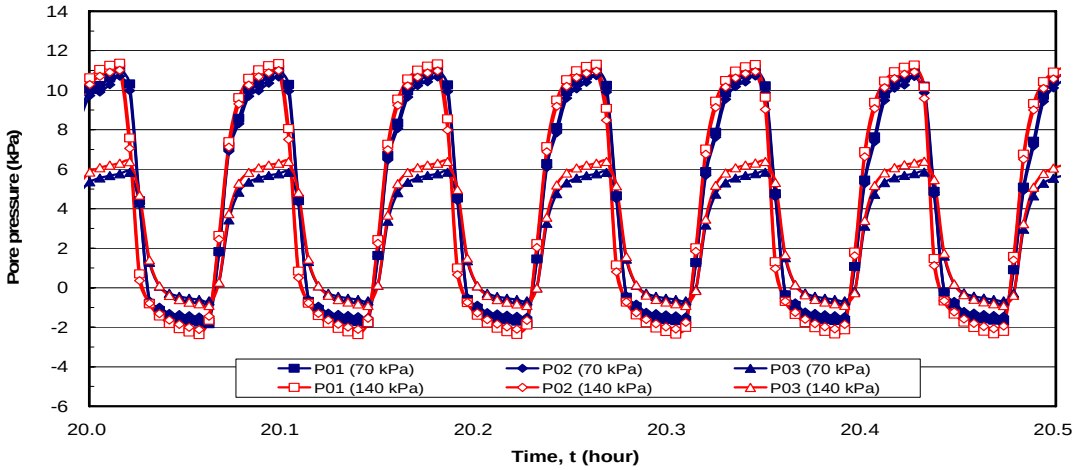

(b) 300 sec/cycle

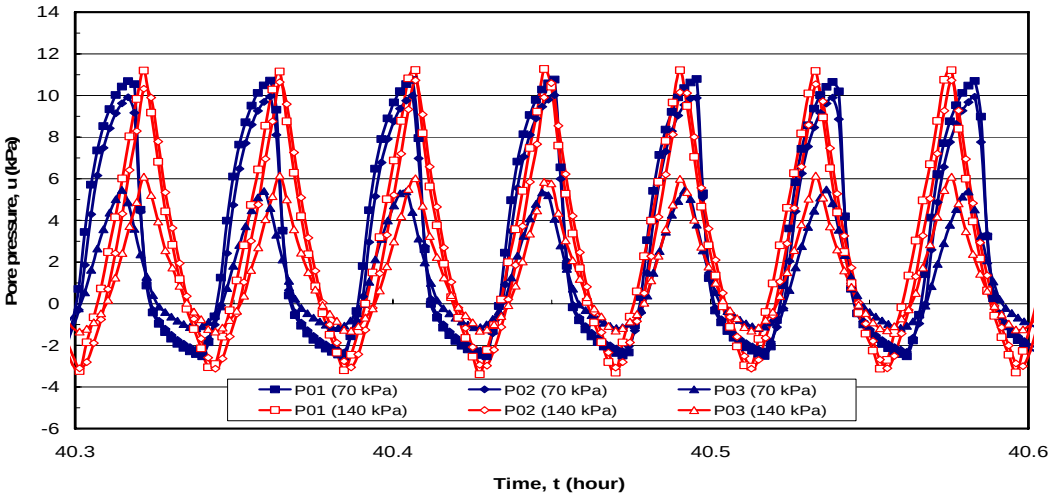

(c) 150 sec/cycle

Figure 4.9 Pore water pressure of pure sand (G-01).

2. Silty sand (G-02 ~ G-05):

Figure 4.10 to Figure 4.13 present the pore water pressure response for specimens of different amount of silts under the wave period at 600 sec/cycle and 150 sec/cycle, respectively. They illustrate that the fine particle content may cause the peak value of pore pressure to increase. In regard to the effect of the wave period, pore water pressure in the long period condition (low flow velocity) has enough time to transmit and hence is lower than that in the short period condition (high flow velocity). Moreover, for silty sand, it is quite observes that the effect of normal pressure on the response of pore water pressure. The high normal pressure induces a high pore water pressure response. This is because fine particles are more compressible than sand and are susceptible to forming a denser structure when under a load. A denser structure, therefore, tends to produce a higher response of pore water pressure than an incompressible stable structure.

In addition, in the long period condition such as 600 sec/cycle, the amplitude of pore water pressure is uniform during testing and the value of P01 and P02 is close. That is because the flow velocity is low under the condition in long period and not enough to cause the soil particles migrate. Hence, the soil structure is stable. However, for test G-02 at 300 sec/cycle of the wave period, a phenomenon is noteworthy that is the response of pore water pressure is not uniform during testing (see Figure 4.14). During the time of certain hour after the test began, pore water pressure decreased along time. Afterwards it remained constant. The specimen of G-02 contain small silt content (5%), the fine particle filled within the void of sand is not enough to form a denser structure even if applies the high overburden pressure. In the beginning of testing, the pore water pressure will increase gradually. Once the pore water pressure increases to a certain value, the fine particle will becomes to migrate freely. In some position which the most of fine particle losses may causes the local soil boiling (As shown in Figure 4.15). Moreover, the permeability of soil specimen increases due to the fine particle losses and to reduce the pore water pressure when the flow rate keeps constant. The same situation takes place at test G-03-a that contains 10% of silt soil and applies the lower normal stress of 70 kPa. In this condition, it was not enough limited the fine particles moved and the local soil boiling was observed at the 300 sec/cycle wave period. Consequently, the pore water pressure reduces in early stage of testing. However, for test G-03-b that the high normal stress (140 kPa) was applied and formed a denser soil structure than G-03-a. The fine particle moves is not intense and local soil boiling was unobserved. Hence, the pore water pressure distribution is uniform during testing.

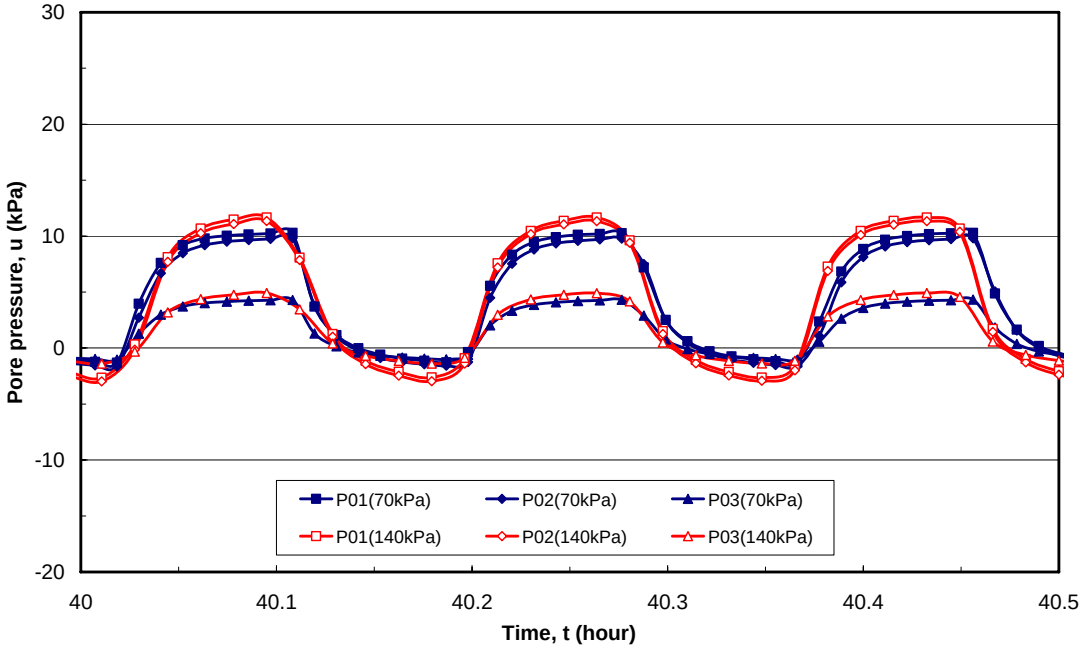

(a) 600 sec/cycle

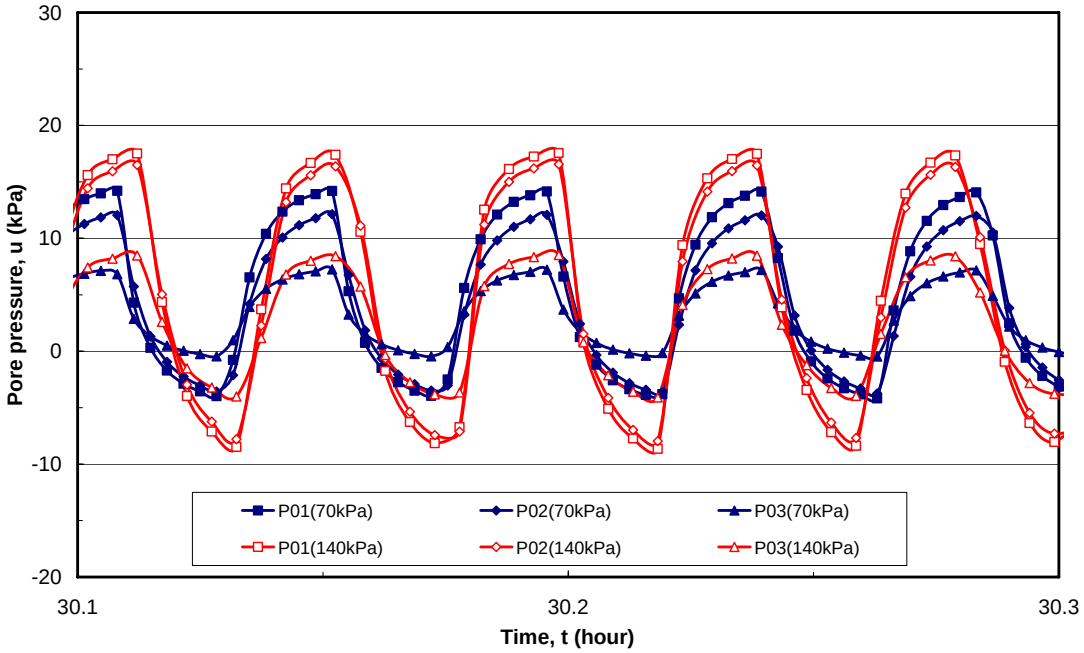

(b) 150 sec/cycle

Figure 4.10 Pore water pressure of silt sand (G-02, 5% of silt content).

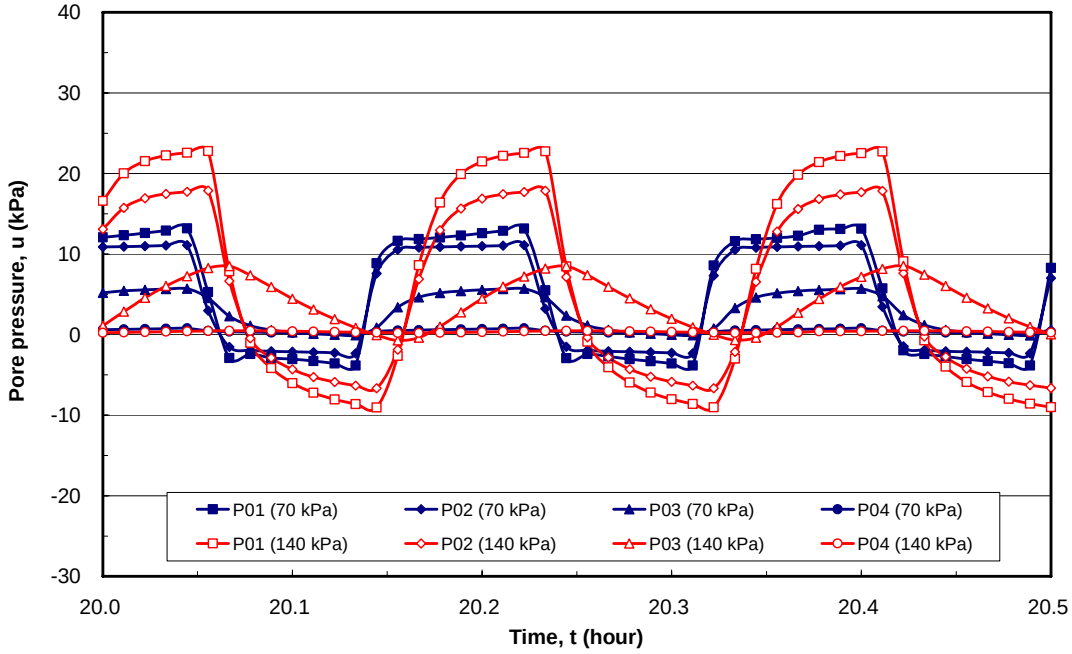

(a) 600 sec/cycle

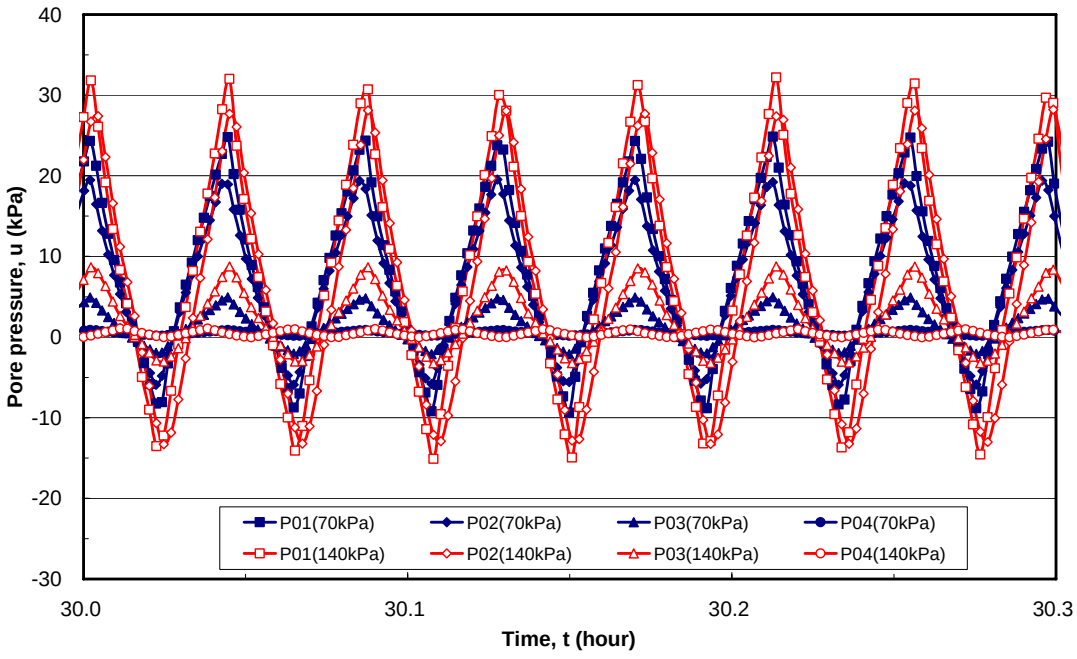

(b) 150 sec/cycle

Figure 4.11 Pore water pressure of silty sand (G-03, 10% of silt content).

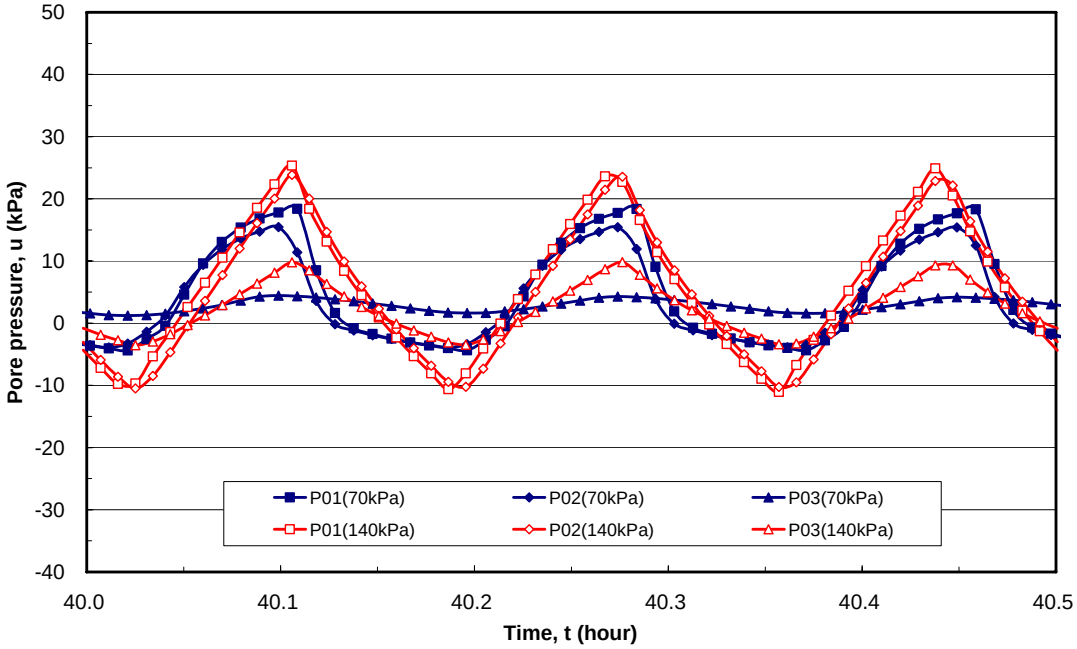

(a) 600 sec/cycle

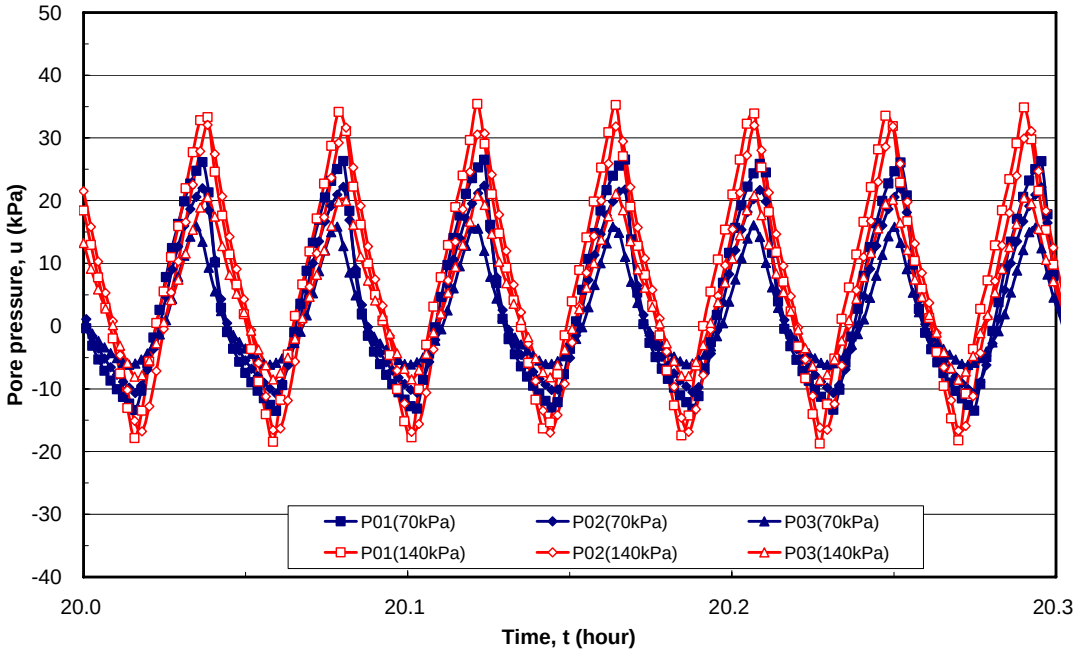

(b) 150 sec/cycle

Figure 4.12 Pore water pressure of silty sand (G-04, 15% of silt content).

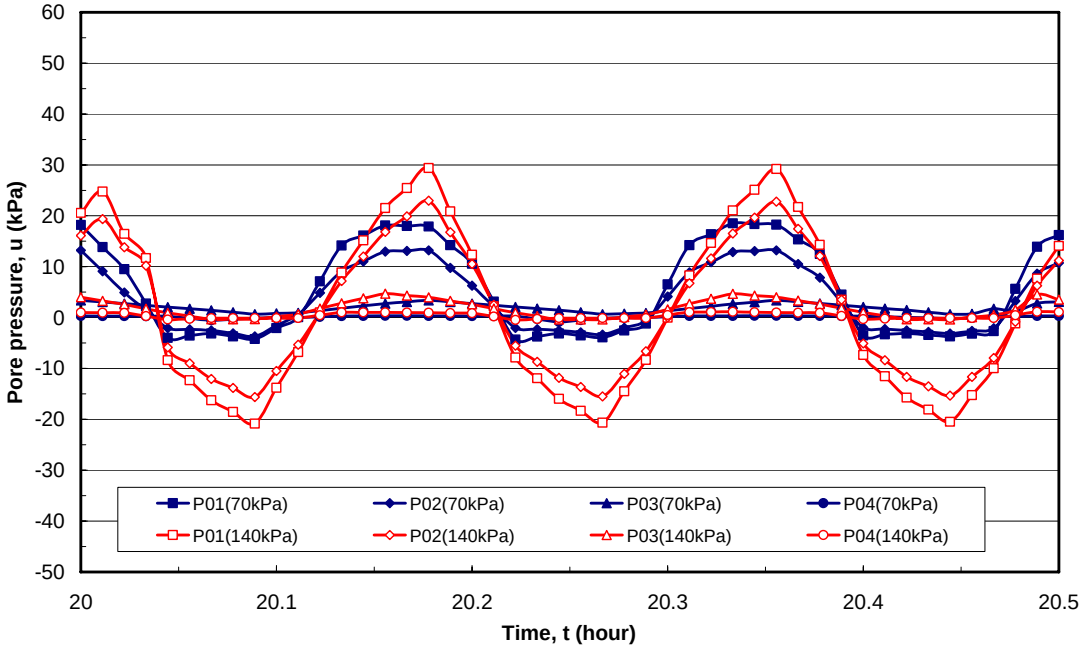

(a) 600 sec/cycle

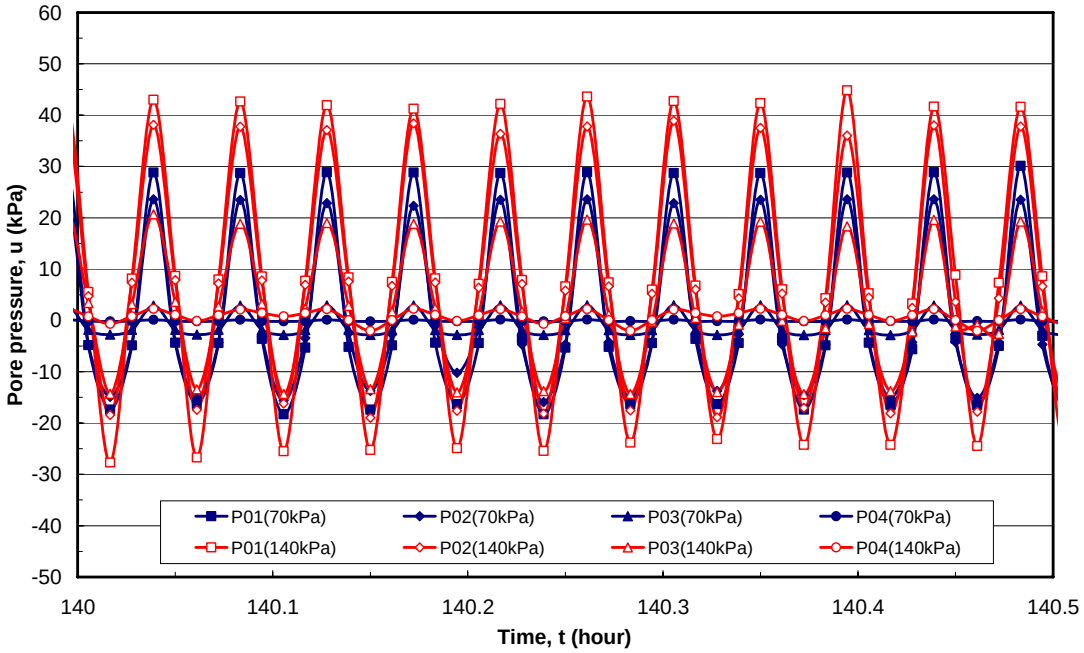

(b) 150 sec/cycle

Figure 4.13 Pore water pressure of silty sand (G-05, 20% of silt content).

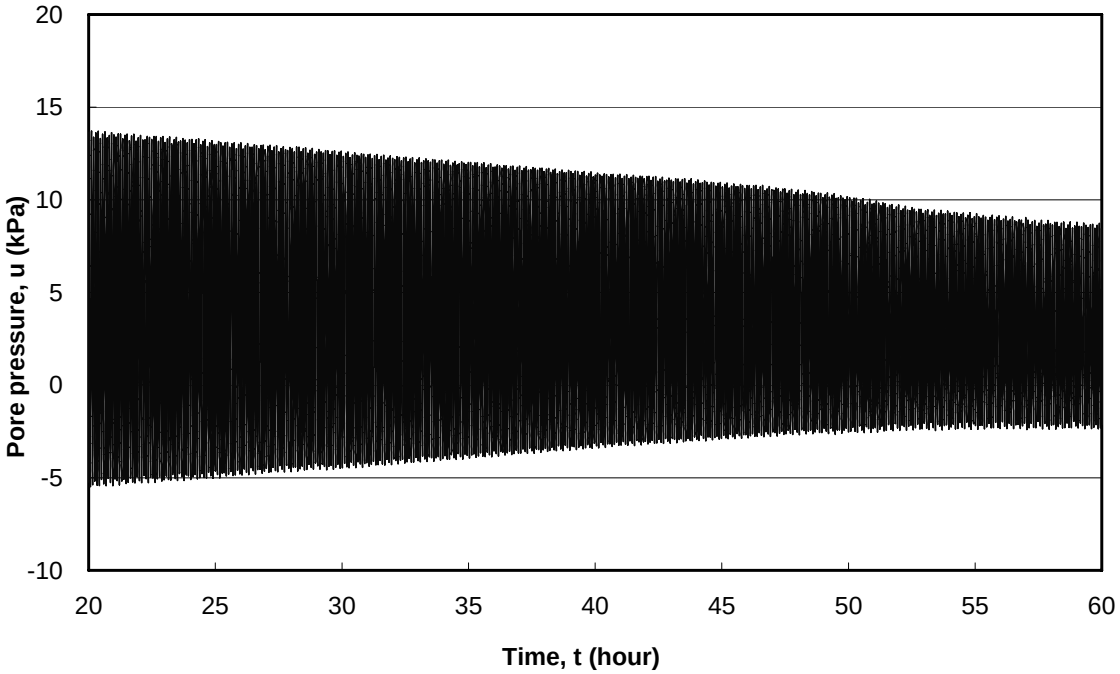

(a) G-02-a (silt content: 5%, normal stress: 70 kPa)

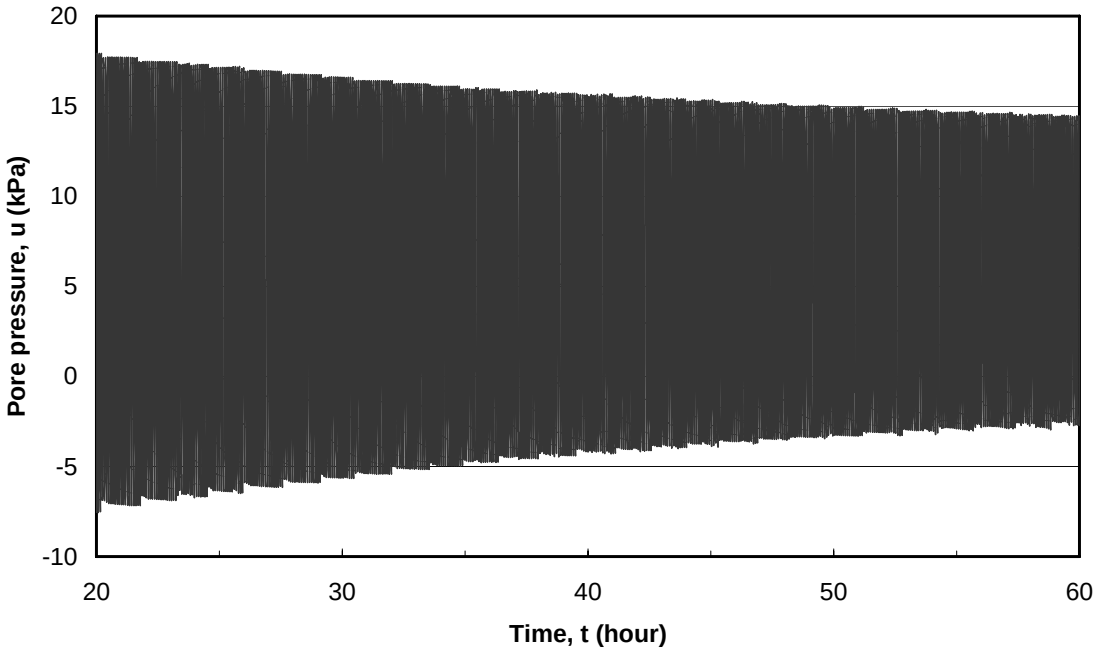

(b) G-02-b (silt content: 5%, normal stress: 140 kPa)

Figure 4.14 The pore pressure (P02) of G-02 at 300 sec/cycle.

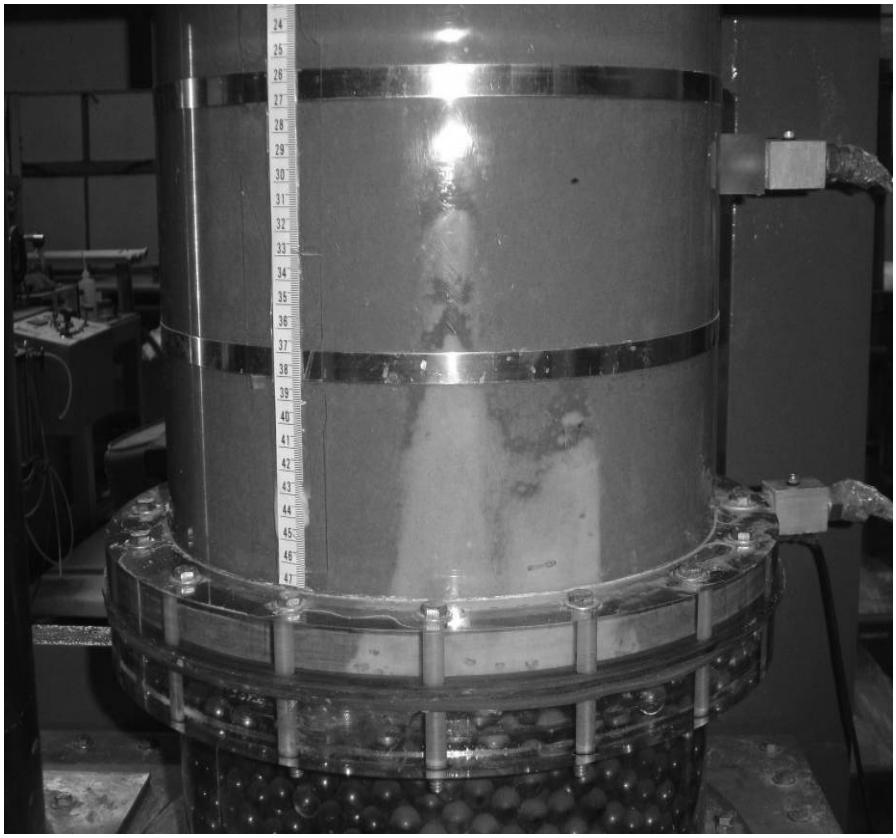

Figure 4.15 Local soil boiling (G-02-a).

For test G-04 and G-05 that respective contain 15% and 20% of the silt content, the fine particle could be filled within the void of sand and formed a denser structure than G-02 and G-03. The soil structure is more stable when suffers the bi-directional cyclic flow. Therefore, the amplitudes of pore water pressure are uniform when the wave period keeps constant and the local soil boiling was unobserved during testing.

In additional, in regard to the shape of pore water pressure variation, it can be seen that the pore water pressure distribution curve is more gradual when it reaches the maximum and minimum pore pressure under long-period cyclic flow (600 sec/cycle), especially for test G-01, G-02, and G-03. However, the variation curve of pore water pressure seems steeper and with a clear peak value under short-term cyclic flow action, such as 150sec/cycle or 75 sec/cycle. Figure 4.16 shows the variation of pore water pressure with cycles. It is quite obvious to express the different curve shape of pore water pressure distribution. For large period the pressure is quite constant as the flow is constant too. If the period is divided by 2, the velocity is multiplied by 2. Then the pressure should increase (multiplied by 2) and should be constant again during upwards flow. The maximum value is reached only at the end of the cycle. As the

period is again reduced twice, the maximum pressure does not increase twice. It is assumed that air remains entrapped inside the specimen after preparation. The compressibility of the air reduced the amplitude of the pressure and the shape of its variation.

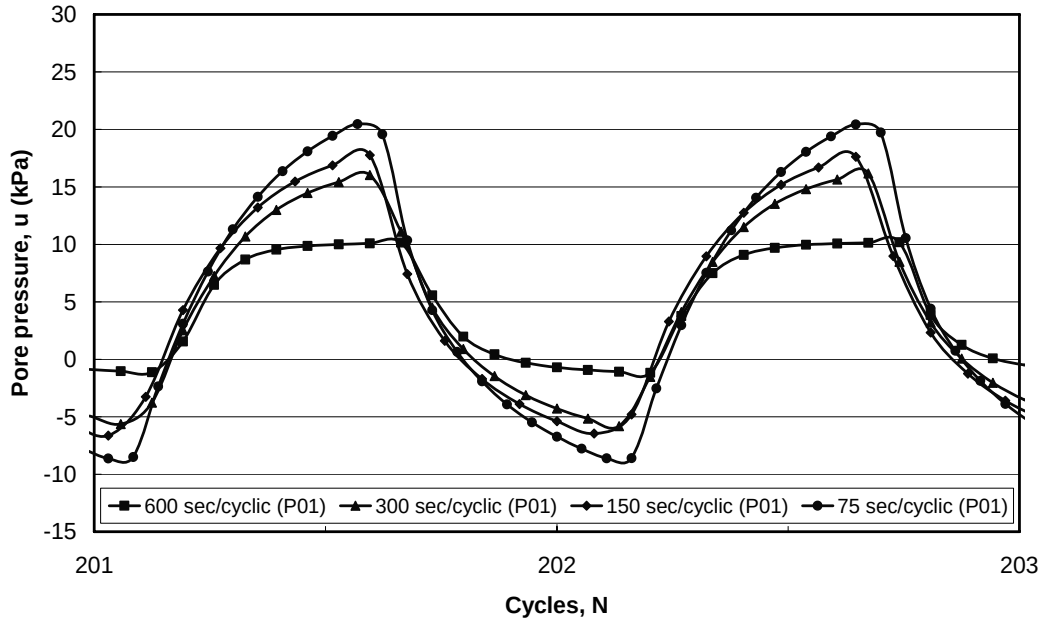

(a) G-02-a (Silt content: 5 %, Normal stress: 70 kPa)

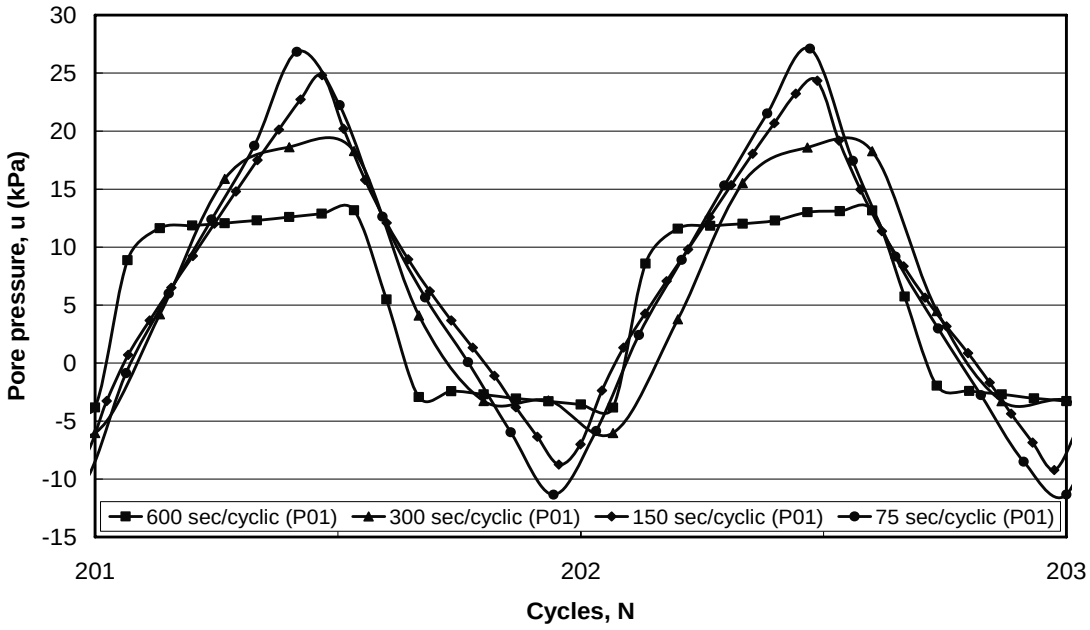

(b) G-03-a (Silt content: 10 %, Normal stress: 70 kPa)

Figure 4.16 The variation of pore water pressure versus cycles

3. Clayey-silty sand (G-06 and G-07):

According to the result of silty sand, 10% of silt content is the threshold that whether the local soil boiling happen or not. In order to understand the effect of clay content upon the pore water pressure, G-06 and G-07 are carried out and composed of different ratio of clay and silt content but the amount of fine particle keeps in 10%.

Figure 4.17 shows the variation of pore water pressure of G-06. Compare Figure 4.17 with Figure 4.11, the specimen with higher clay content results in higher pore water pressure due to the low hydraulic conductivity of the clay when the amount of fine particle keeps constant. Moreover, the local soil boiling was also observed at 300 sec/cycle of wave period under the low normal stress (70 kPa) and caused the variation of pore water pressure was non-uniform during testing.

Figure 4.18 shows the variation of pore water pressure of G-07. It can be seen that the peak value of pore water pressure higher than G-06. That is causing lower permeability because the content of clay of G-07 is greater than G-06. On the other side, there is no local soil boiling happen in the process of testing of G-07. Because of the clay particles are apt to flocculate, the particle is not easy to migrate. In addition, the cohesion of clay will limit the particles migrate. This proves that increases the clay content will be reducing the potential of local soil boiling but increases the pore water pressure at the same time.

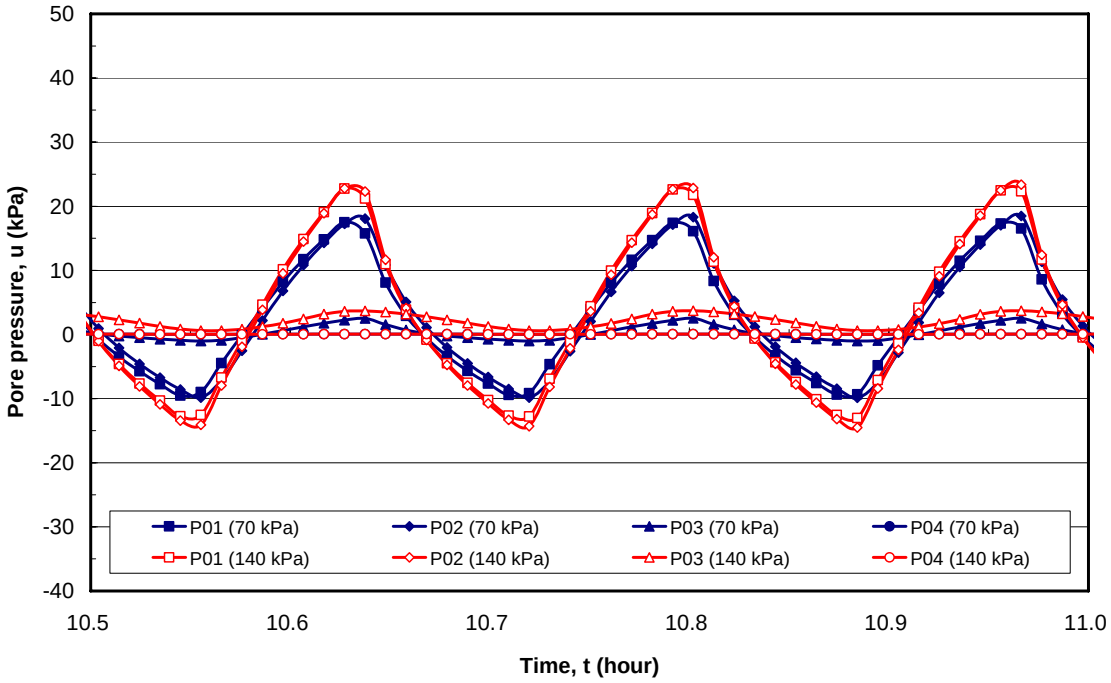

(a) 600 sec/cycle

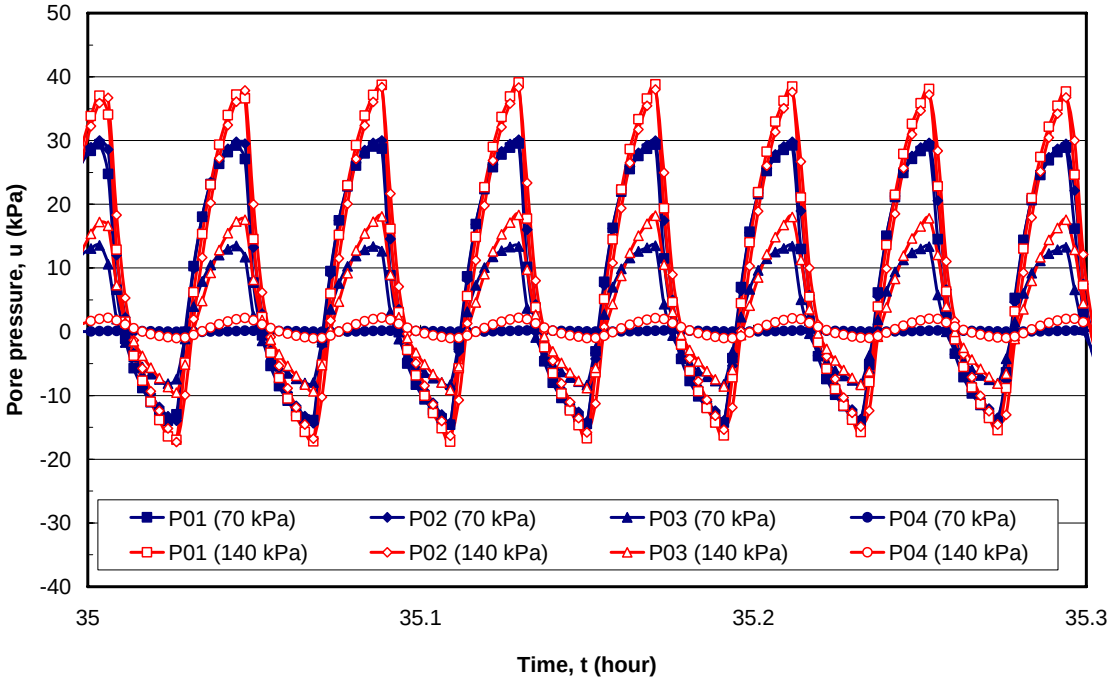

(b) 150 sec/cycle

Figure 4.17 Pore water pressure of clayey-silty sand (G-06, 6.5% of silt and 3.5% of clay content).

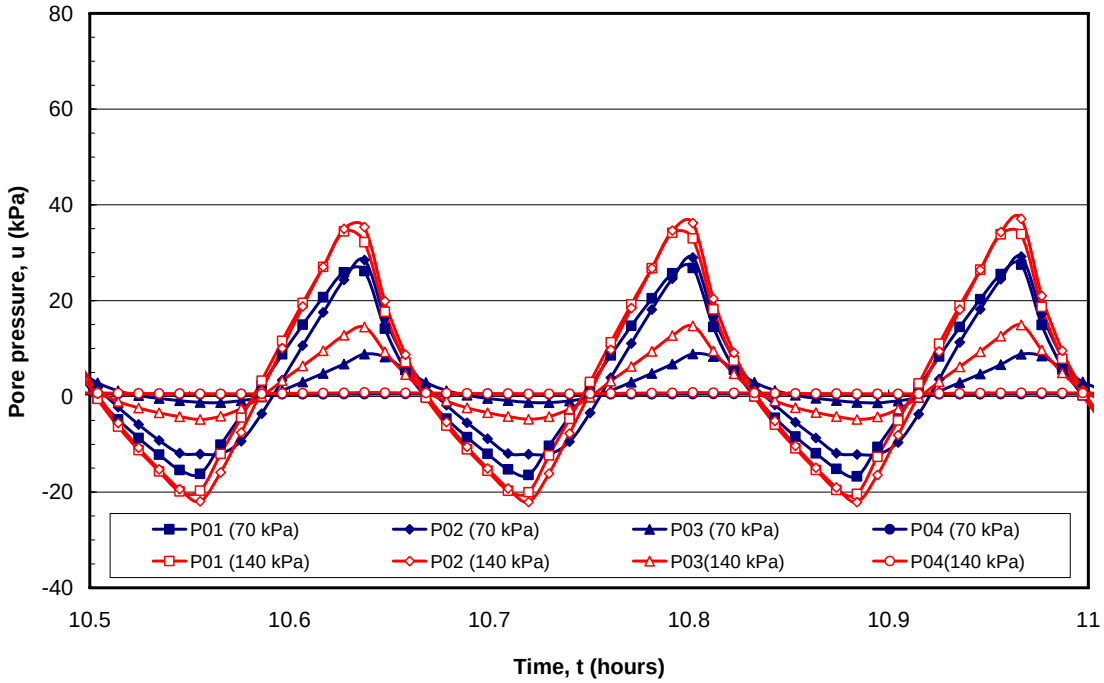

(a) 600 sec/cycle

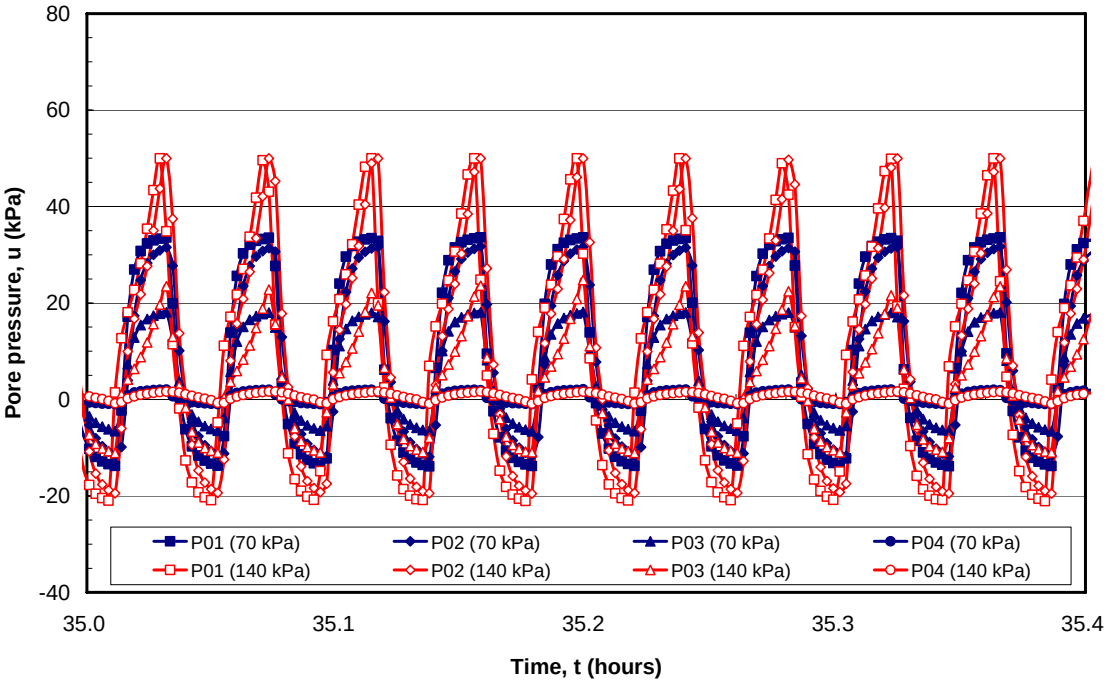

(c) 150 sec/cycle

Figure 4.18 Pore water pressure of clayey-silty sand (G-07, 3.5% of silt and 6.5% of clay content)).

4.4.2 Cyclic flow gradient index

To measure pore pressure can provide some information regarding various phenomena such as clogging, blocking, or soil loss. In this study, the cyclic flow gradient index, I, is introduced to examine the hydraulic conductivity behavior.

$$I = \frac{i_{P(n+1)}}{i_{P(n)}} \tag{4-1}$$

$$i_P = \frac{u_{P1} - u_{P2}}{\rho_w \times g \times L} \tag{4-2}$$

where $i_{P(n)}$ and $i_{P(n+1)}$ are the hydraulic gradients at peak pore pressure between the two piezometers, P01 and P02, in the n^{th} and the $(n+1)^{th}$ cycles, respectively. The values u_{P1} and u_{P2} are the peak pore pressures at P01 and P02, respectively. The density of water is denoted as ρ_w, g is the acceleration of gravity, and L is the distance between P01 and P02.

The value of I indicates the variation in hydraulic conductivity in the filter. According to Darcy's law, if flow rate (q) and flow section area (A) remain constant, the permeability (k) is inversely correlated with the hydraulic gradient (i). For this test, when the hydraulic gradient between the piezometers P01 and P02 increases (I>1.0) that means decreasing the permeability of soil-geotextile system between P01 and P02 and indicates that the soil-geotextile system is clogged. On the contrary, if the hydraulic gradient decreases (I<1.0), the permeability of soil-geotextile system increases and indicates that the fine particle within the soil-geotextile system is washed-out or piping is occurred. If the internal structure of soil-geotextile system between P01 and P02 has no change, the hydraulic gradient may be kept constant with time so that a constant value of I can be maintained ($I \approx 1.0$). Hence,

$I > 1.0$: Clogging

$I = 1.0$: Stable

$I < 1.0$: Washed-out or Piping

1. pure sand

As discussed in previous section, for pure sand, no soil particle clogs or blocks within geotextile during testing. Hence, to evaluate the I value for pure sand is insignificant.

2. silty sand

Figure 4.19 shows the variation of I value of G-02 and G-04 under 70 kPa normal pressure and the wave period at 600 sec/cycle and 300 sec/cycle, respectively. As show in Figure 4.19(a), I value is close to 1.0. That is because the soil structure is stable under slow cyclic flow and clogging or blocking is not take place within the geotextile. The same result can be obtained under 140 kPa of the normal pressure.

For specimen G-02 at wave period of 300 sec/cycle under 70 kPa normal pressure, denoted by solid squares in Figure 4.19(b), the variation of I value is wider in the beginning. For those points that I value large than 1.0 indicate that the clogging happens in the soil-geotextile system and I value smaller than 1.0 indicate that the fine particle washed-out. This shows that under bi-directional cyclic flow, the soil-geotextile system alternates between fine particles loss and clogging. Local soil boiling happening will accelerates this phenomenon of particle clogs or washed-out until the system is stable. After that, the permeability of soil-geotextile system will keeps constant and the different of pore water pressure between P01 and P02 will be reduced. Consequently, the I value approaches to 1.0. The same result can be obtained by specimen G-03 under 70 kPa of the normal stress. It presents the soil of silt of low content that with the lower density under the low normal stress, an independent fine particle can move freely and clogs the soil-geotextile system or washed-out. But this phenomenon of particle clogs within geotextile or washed-out is impermanent and soil boiling occurs will accelerates this phenomenon.

For specimen G-04 at wave period of 300 sec/cycle, denoted by hollow squares in Figure 4.19(b), a constant value of I can be maintained during testing. Because of the soil specimen with high content silt, fine particle is not easy to migrate and clogging or blocking is unlikely to occur at any point.

In additional, the I values at wave period of 150 sec/cycle and 75 sec/cycle are all very close to 1.0 for each test. That is to say that the clogging or blocking will not happen at the shorter wave period.

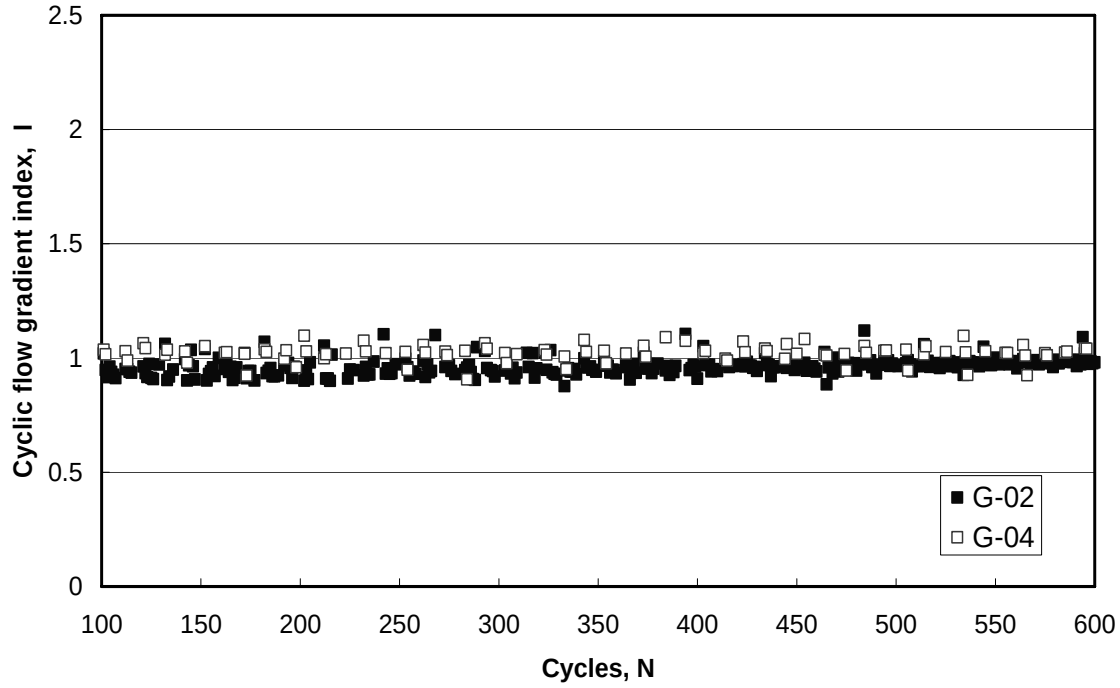

(a) 600 sec/cycle

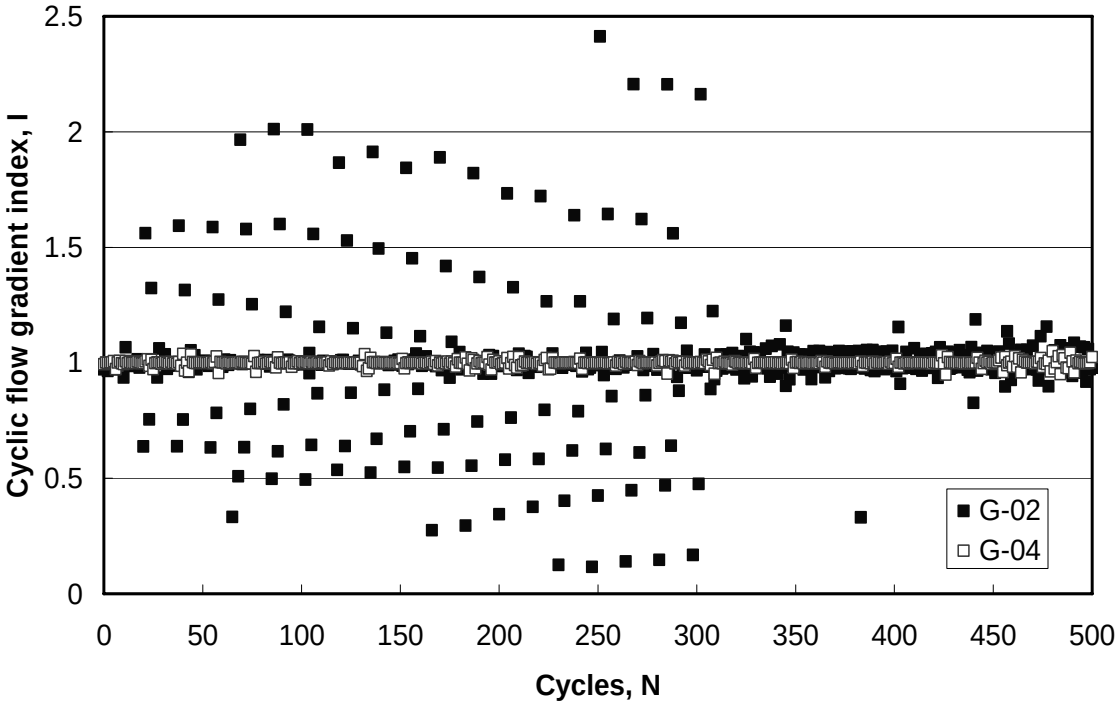

(b) 300 sec/cycle

Figure 4.19 The cyclic flow gradient index of G-02 and G-04 under 70 kPa.

3. clayey-silty sand

Figure 4.20 shows the I values of specimens G-06 and G-07 at wave period of 300 sec/cycle and under normal pressure of 70 kPa. For specimen G-06, denoted by solid squares, the range of most hydraulic gradient ratios is narrow, from 0.97 to 1.1 over the course of testing. For specimen G-07, denoted by hollow squares, the range is wider than G-06, from 0.9 to 1.1. But anyway, the I value of clay-silty sand are all very close to 1.0 even if soil boiling occurs in G-06. Therefore, it implies that, for clayey-silty sand under bi-directional cycle flow, clogging or blocking is unlikely to occur at any point, irrespective of the clay content of soil. This also infers that the mechanism is quite different from that in uni-directional flow condition.

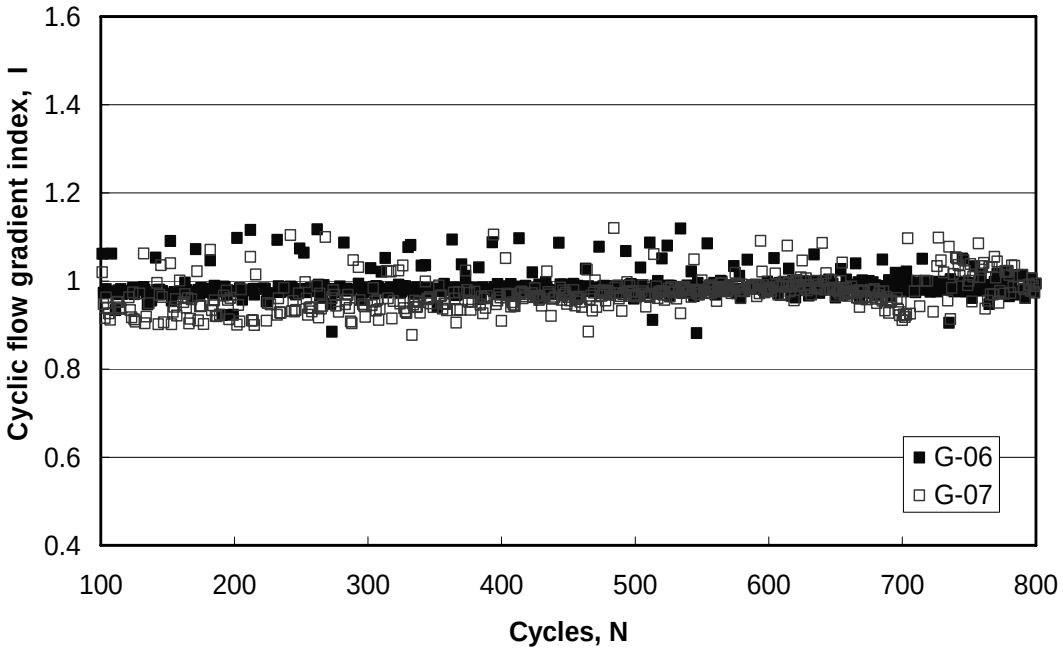

Figure 4.20 The cyclic flow gradient index of G-06 and G-07 under 70 kPa.

4.4.3 Settlement

1. Pure sand (G-01)

For pure sand (as shown in Figure 4.21), the curves of settlement versus time are nearly the same irrespective of normal pressures. As discussed previously, the difference in pore water pressure for pure sand under different normal pressure is negligible. It can thus be concluded that the sand can form a so stable structure that the particles are not able to move easily under cyclic flow. Consequently, the settlement is insignificant.

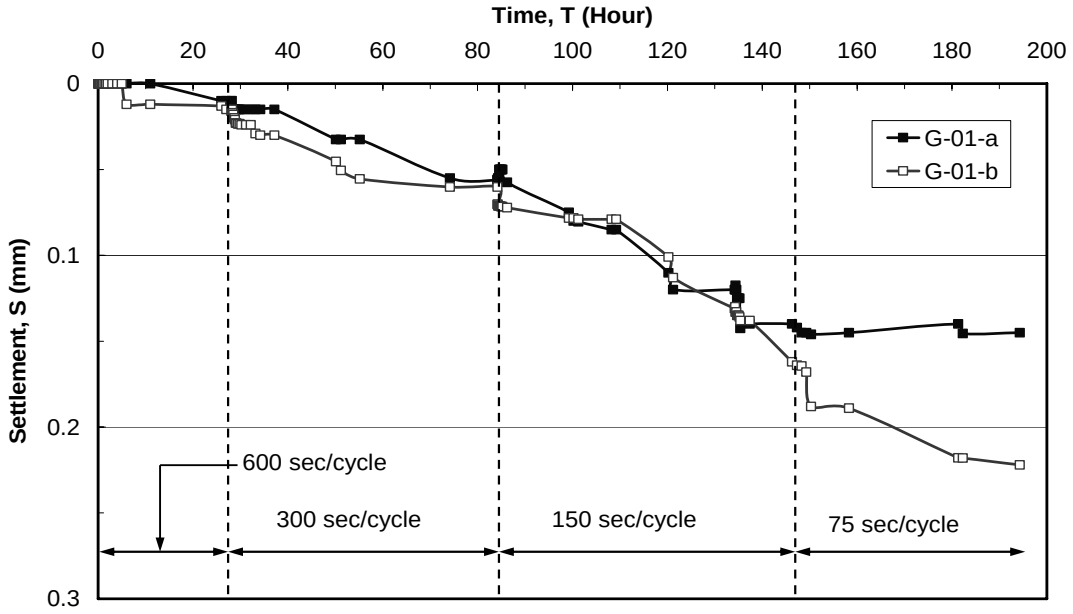

Figure 4.21 Settlement curves of pure sand.

2. Silty sand (G-02~G-05)

Figure 4.22 presents the curves of settlement versus time under the different vertical pressure by silty sand (G-02, G-03, and G-05). They show that the settlement under 140kPa of vertical pressure is small than that under 70kPa. That is because the soil structure is relatively loose when low load is applied. The particles can move more easily and tend to result in more settlement. In particular, for G-02 and G-03-a, the settlements increase dramatically during the action of 300 sec/cycle wave period. The corresponding pore pressure response has shown in Figure 4-14 is measure at P02 for G-02 and G-03. It is obvious that the pore pressure reduces when the settlement falls suddenly. This is because the upward water flow induces pore pressure and reduces the effective stress in the soil to be small enough to cause the coarse and the fine particles to separate and migrate intensely away from the geotextile to produce local boiling. As the water flows downwards again, the soil particles then migrate towards the geotextile and some fine particles passing through the geotextile, are collected in the wash-out tank. Furthermore, the boiling causes the fine particles to suspend on the coarse particles. As the water flows downwards, the heavy coarse particles precipitate relatively fast. In this situation, rearrangement of soil particles is so significant that it causes a sudden settlement until the stable soil structure formed. After soil structure becomes stable, settlement will tend to mitigate. In additional, as shown in Figure 4.22(b), there are large different between G-03-a with G-03-b. That is because the soil boiling happened in G-03-a. For this reason, soil boiling is one of the important factors that to cause soil settle.

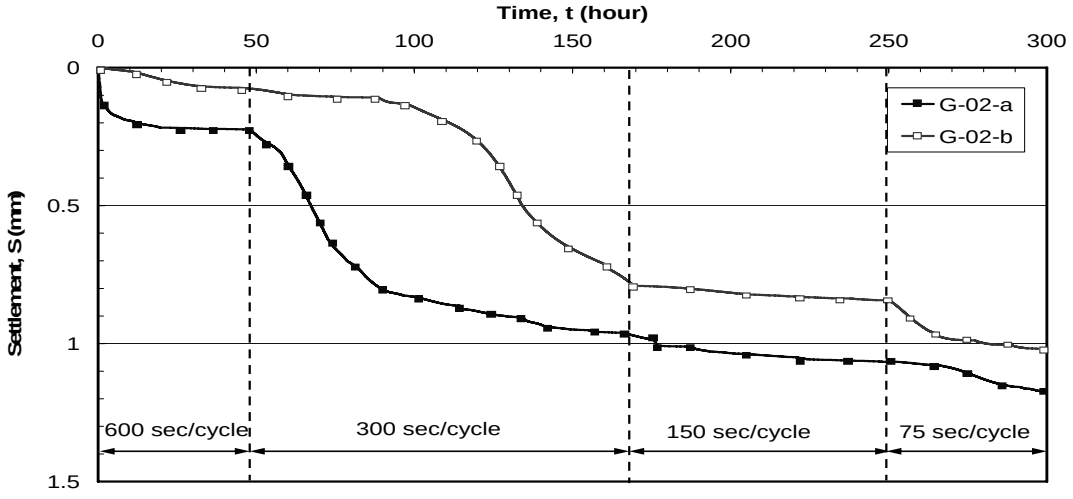

(a) G-02

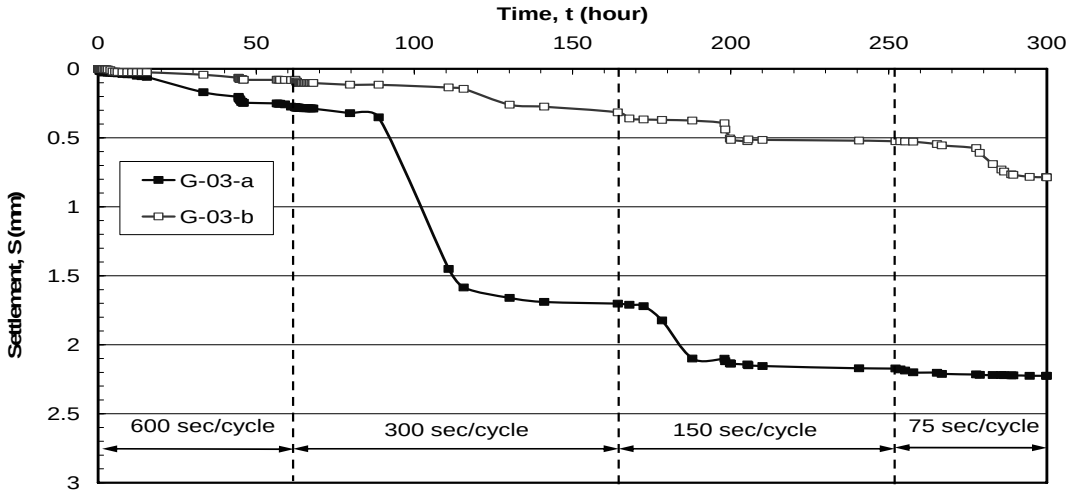

(b) G-03

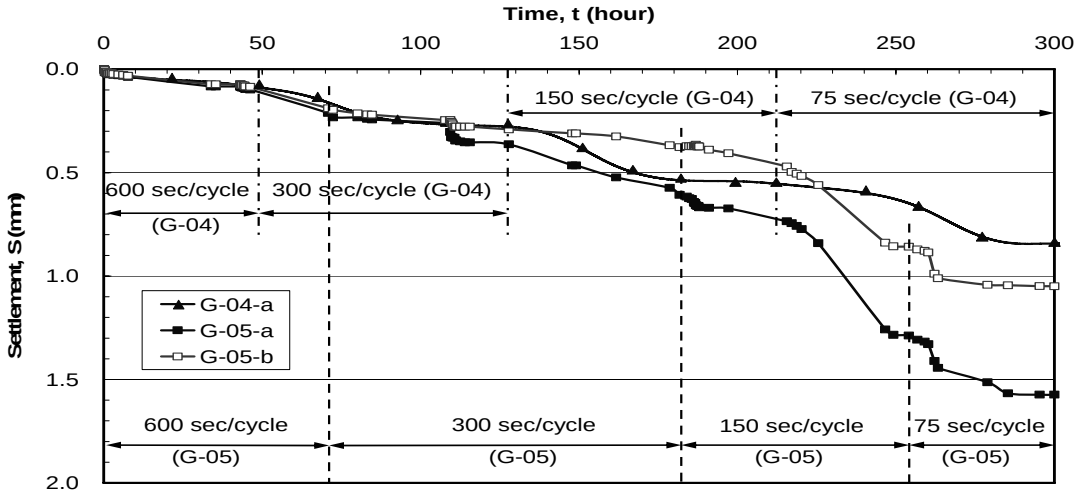

(c) G-04 and G-05

Figure 4.22 Settlement curves of silty sand.

To compare the settlement of G-04-a, with G-05-a (see Figure 4.22(c)), the settlement increases with increasing amount of silt when the vertical pressure keeps constant. Because of the soil with higher silt content is subject to more settlement as more fine grained soil particles are likely to be washed out.

3. Clayey-silty sand (G-06 and G-07)

The variation of settlement for clay-silty sand shows in Figure 4.23. To compare the settlement of G-06-a with G-07-a, it is not surprising that more clay content will reduce the settlement due to the effect of the cohesion to combine soil particles and to restrain rearrangement and boiling to occur. However, comparing the settlement of G-03-a with G-06-a, those content the same percentage of fine particle, 3.5% of clay content is not enough to avoid the soil boiling. In additional, specimen of G-06 contents the finer particle than G-03 and the fine particle is easier to pass through the geotextile to cause the larger settlement.

From the above results, it can be seen that the normal pressure and the clay content of soil play important roles in the settlement behavior of the soil-geotextile filtration system.

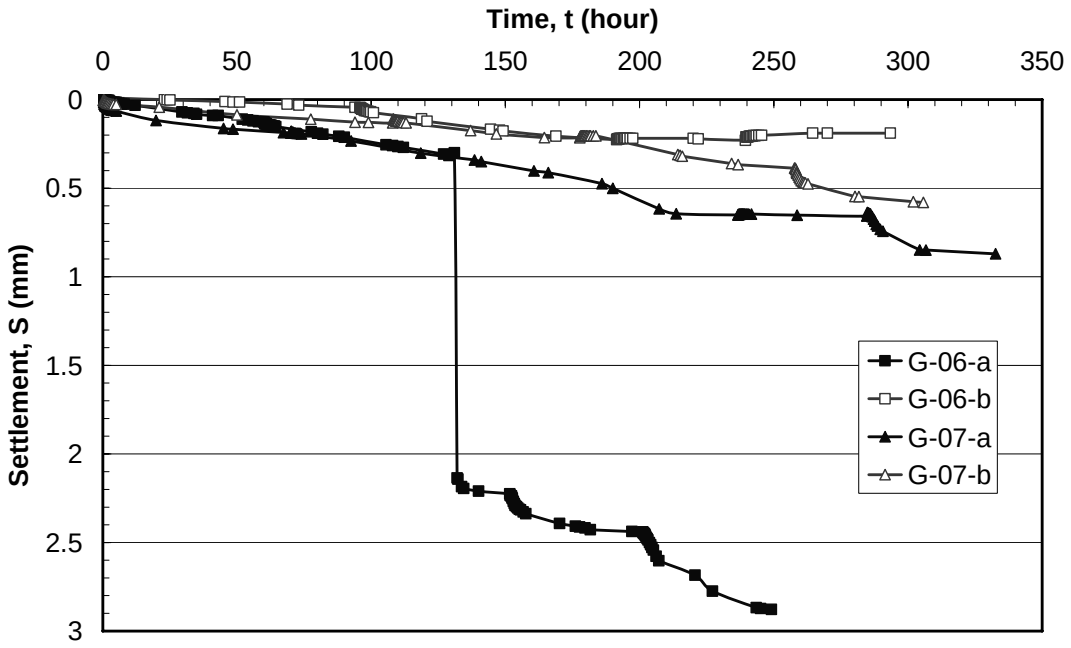

Figure 4.23 Settlement curves of clayey-silty sand.

4.4.4 The change in the amount of fine particles

In order to justify the above mentioned mechanism, some soils are taken from three positions in the chamber to evaluate their particle size distributions. The top position is above the boiling zone; the middle position is within the boiling zone; and the bottom position is in the vicinity of the geotextile. Table 4.5 shows the amount of fine particles smaller than 0.074 mm before and after testing. It shows that the percentages of fine particles of all these samples are changed after testing. At the bottom position, some fine particles are washed out or moved to other places, therefore, the fine content decreases after testing. At the middle and bottom positions, the fine content reduces more for low normal pressure than for high normal pressure. Besides, soil boiling induces the fine particle to move upwards; hence the fine content increases at the top position and decreases in the middle position. For cases where no boiling occurs, the change in fine content is not significant at the top and middle positions. It is obvious that soil boiling is the main cause of a significant settlement when the specimen is under low vertical stress.

Table 4.5 The percentage of fine particle content (d<0.074mm) at different positions after testing

Test No.		Vertical stress (kPa)	Soil boiling	Fine particle content (%)			
				Before Testing	After testing		
					Top	Middle	Bottom
G-02	a	70	Yes	5	7.29	4.03	3.94
	b	140	Yes	5	6.26	5.11	4.07
G-03	a	70	Yes	10	11.74	6.63	4.01
	b	140	No	10	9.63	8.93	8.12
G-04	a	70	No	15	15.89	14.51	11.61
	b	140	No	15	15.47	15.49	14.35
G-05	a	70	No	20	22.14	19.26	17.77
	b	140	No	20	21.08	20.44	18.47
G-06	a	70	Yes	10	10.68	5.24	5.15
	b	140	No	10	9.84	9.56	8.44
G-07	a	70	No	10	9.97	9.59	8.82
	b	140	No	10	10.09	9.42	9.07

4.4.5 Soil washout

1. Amount of soil washout

After testing, the soil washout is collected and the amount collected per square meter is shown in Table 4.6. For pure sand, G-01, there are only small amounts of soil collected under various normal pressures. This is due to large particles being able to form a stable structure under normal pressure. For G-03, a greater amount of soil is collected under low normal pressure than high normal pressure, because small effective stress has difficulty in confining soil particle effectively. As stated previously, boiling occurs in this situation and particle rearrangement is obvious. In this situation, the silt disperses in the water and moves more easily under lower normal pressure. Hence, for non-cohesive soil, settlement results from particle rearrangement and soil loss.

Table 4.6 The weight of soil washout per square meters (unit: g/m^2)

Test number	Normal pressure (kPa)	
	70	140
G-01	79.6	63.2
G-02	421.0	352.2
G-03	5096.1	490.6
G-04	4351.6	513.6
G-05	5517.5	570.4
G-06	389.3	409.2
G-07	486.4	465.2

As to the effect of clay content, it can be seen by comparing the results of G-03 and G-06. The cohesive soil submerged in the water would form aggregates so that the soil particles could not move easily. That is why, though both specimens of G-03 and G-06 induced boiling under low normal pressure, the wash-out soil collected from G-06 is less than G-03. Apparently, this is due to the specimen of G-06 having a higher clay content than the specimen of G-03. Hence, the settlement in the cohesive soil was

due primarily to particle rearrangement which is dissimilar to non-cohesive soil as stated previously. Moreover, the clay content also influences the amount of the wash-out, as known from the results of G-06 and G-07.

It is also found that the settlement has no direct relation with the amount of soil loss; and the settlement is not completely related to boiling. There must be other factors such as pore water pressure that caused the structure to be altered.

2. Grain size distribution of soil washed-out

In order to know the different of fine particle size distribution between the wash-out soil and the fine soil prior to testing, the grain size analysis was executed with laser granulometric. The result of analysis for silty sand test under the low normal pressure presents in Figure 4.24. As shown, the difference between the original and the wash-out is obvious. The particle size distribution of washed out soil is more uniform than the original silty soil. For test G-02-a and G-03-a, the mean particle diameter, d_{50}, of the wash-out soil is close to the original. But there is some portion of particles larger than the original. As above-mentioned, test G-02-a and G-03-a, soil boiling was happened in 300 sec/cycle wave period and was caused the soil particle violent to migrate then produced some larger particles to be washed out. To compare the particle size distribution of G-02-a and G-03-a with G-04-a and G-05-a, it can be explained that the larger particles are washed out due happening of soil boiling. Moreover, compared with the geotextile opening size, O_{90}, there is more than 30% of particle size larger than O_{90} for test G-02-a and G-03-a but for G-04-a and G-05-a have only less than 10%. Hence, the geotextile used under this situation that no soil boiling happen is suitable to retain the most of soil particle.

Figure 4.25 shows the variation in fine particle size distributions between the wash-out soil and the soil prior to testing for clayey-silty specimens. The symbols, G-06-0 and G-07-0, denote the original particle size distribution of the fine content of G-06 and G-07, respectively. The difference between the original and the wash-out is obvious. For example, the mean particle diameter, d_{50}, of the wash-out soil is smaller than that of the original. Moreover, the variation in particle size distributions in the wash-out soil under different normal pressure is insignificant. Compared with the geotextile opening size, O_{90}, there is less than 10% of particle size larger than O_{90} for this situation that no soil boiling happened. In particular, boiling occurred in the specimen of G-06-a and caused more particles ($\approx$20%) larger than O_{90} to pass through the geotextile. In summary, the wash-out soil has particles which are mostly finer than the original soil, but also has some portion of particles larger than the geotextile opening size due to happening of soil boiling.

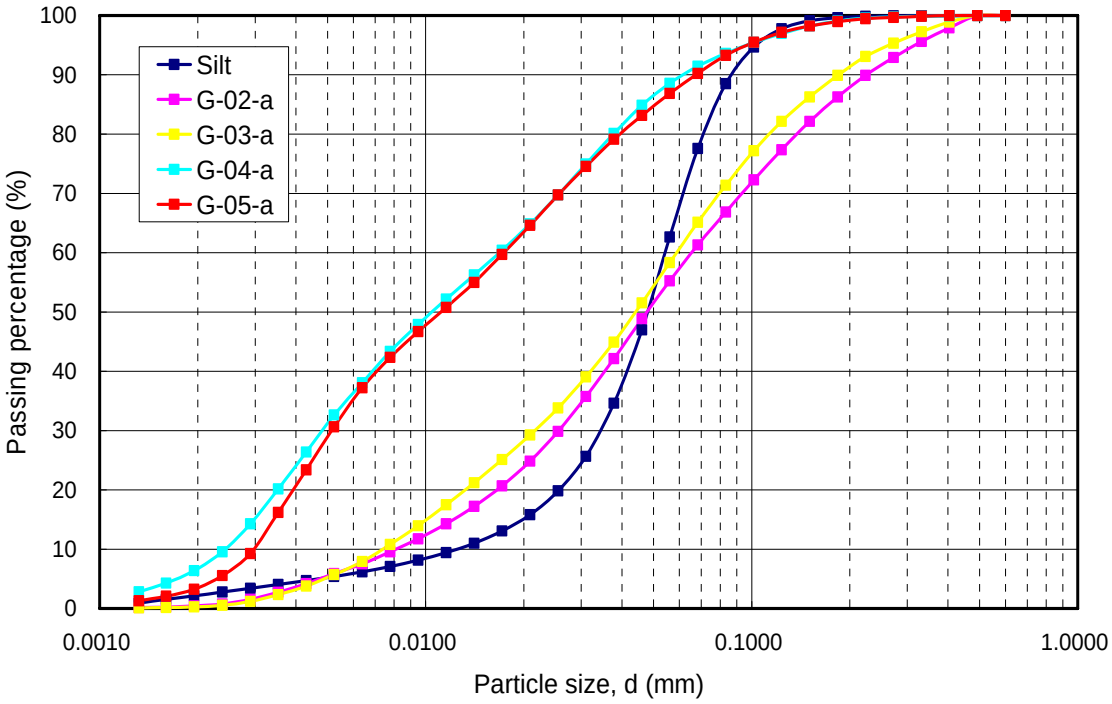

(a) Passing percentage vs. particle size

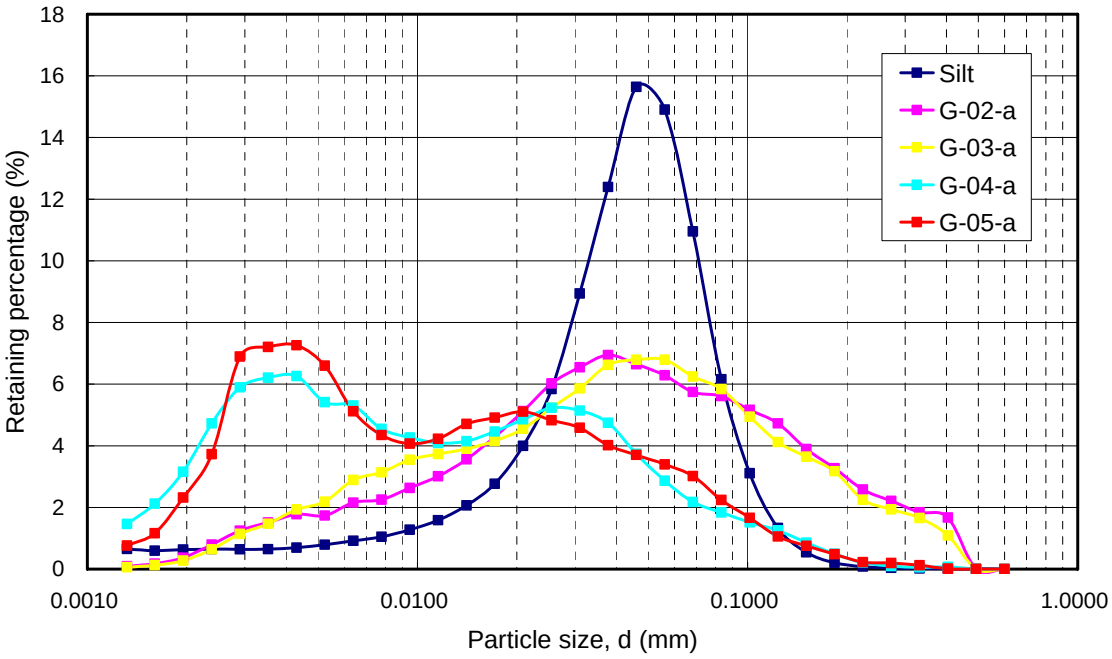

(b) Retaining percentage vs. particle size

Figure 4.24 The particle size distribution of soil washout on silty sand test.

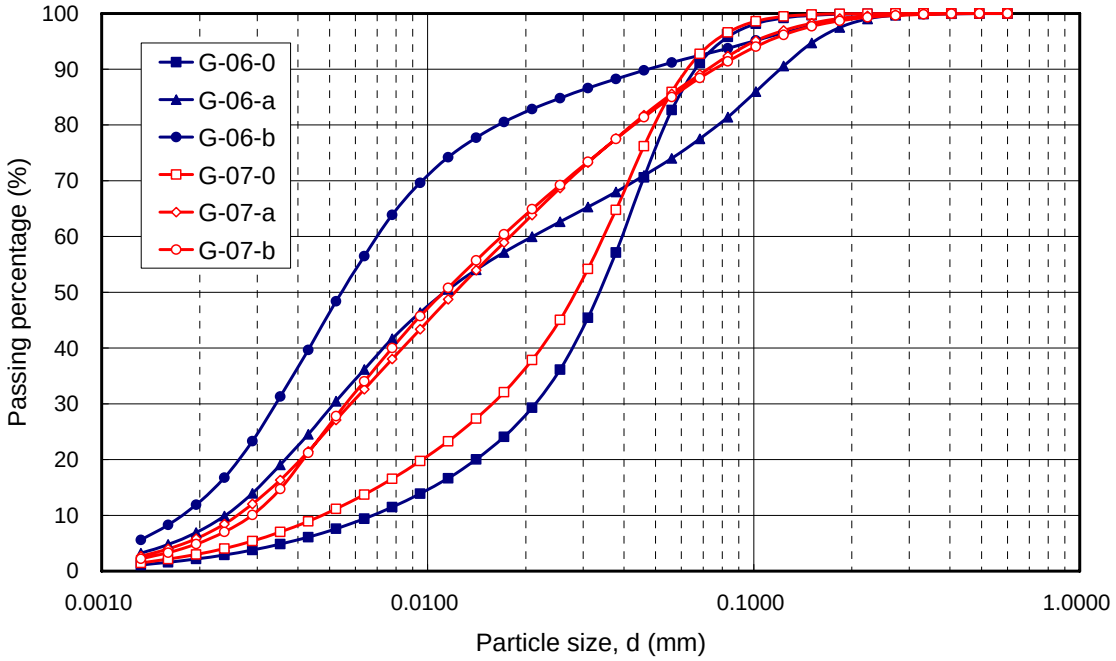

(a) Passing percentage vs. particle size

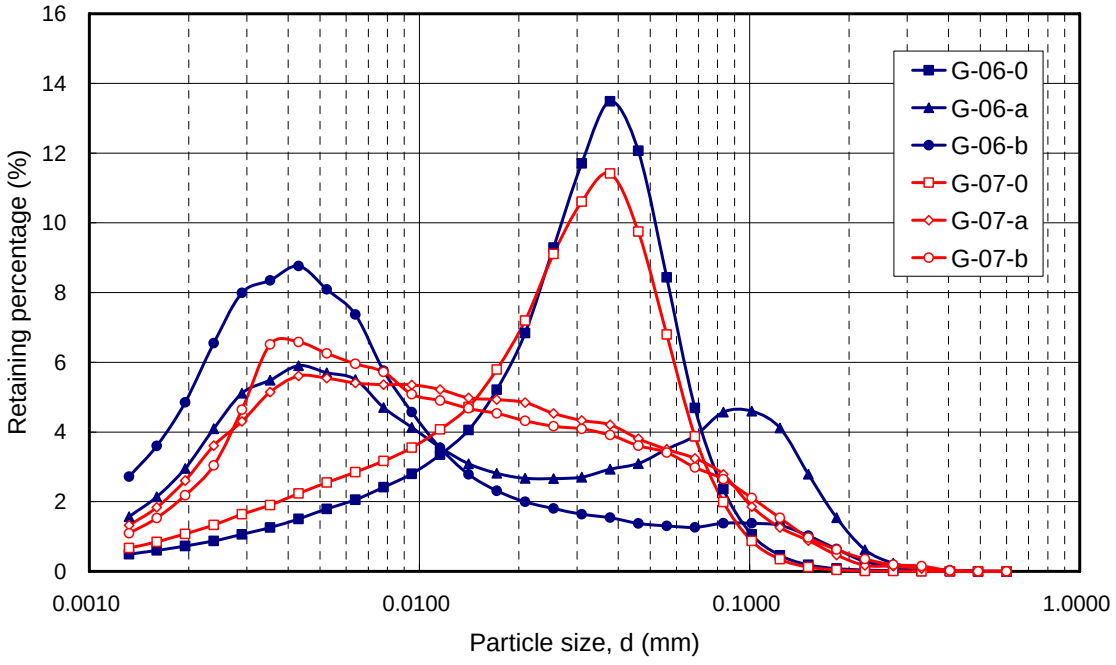

(b) Retaining percentage vs. particle size

Figure 4.25 The particle size distribution of soil washout on clay-silty sand test.

4.5 Observation by the stereomicroscope

After testing, a stereomicroscope was utilized to observe the clogging condition in the geotextile. Figure 4.26 shows the surface of geotextile which is in contact with the marbles after testing, as observed by naked eye. It can be seen that the area where the marble locates is darker than that of other areas. In order to understand the reasons, two pieces of geotextile were cut to observe the surface state by stereomicroscope after testing.

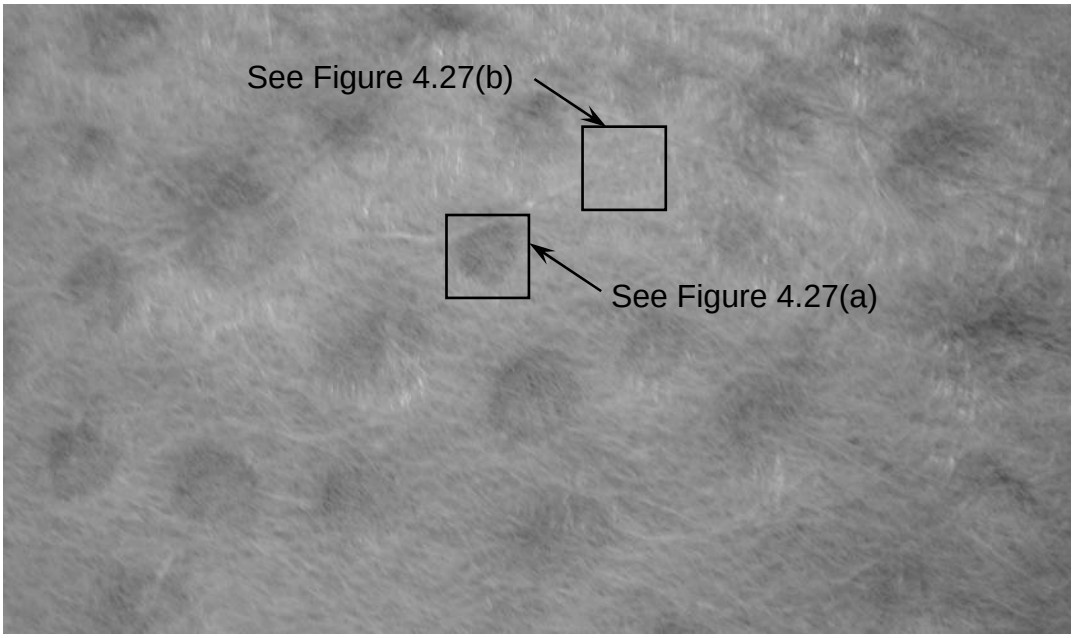

Figure 4.26 The surface state of geotextile after testing (G-04-a) (Chung, 2007).

Figure 4.27(a) shows the microphenomenon of geotextile surface state that locate in the dark area and Figure 4.27(b) shows the observing phenomenon in the clean area, respectively. It is easy to find some soil particles adhered to the fibre of geotextile in the dark area while no or very few particles are visible in the clean area.

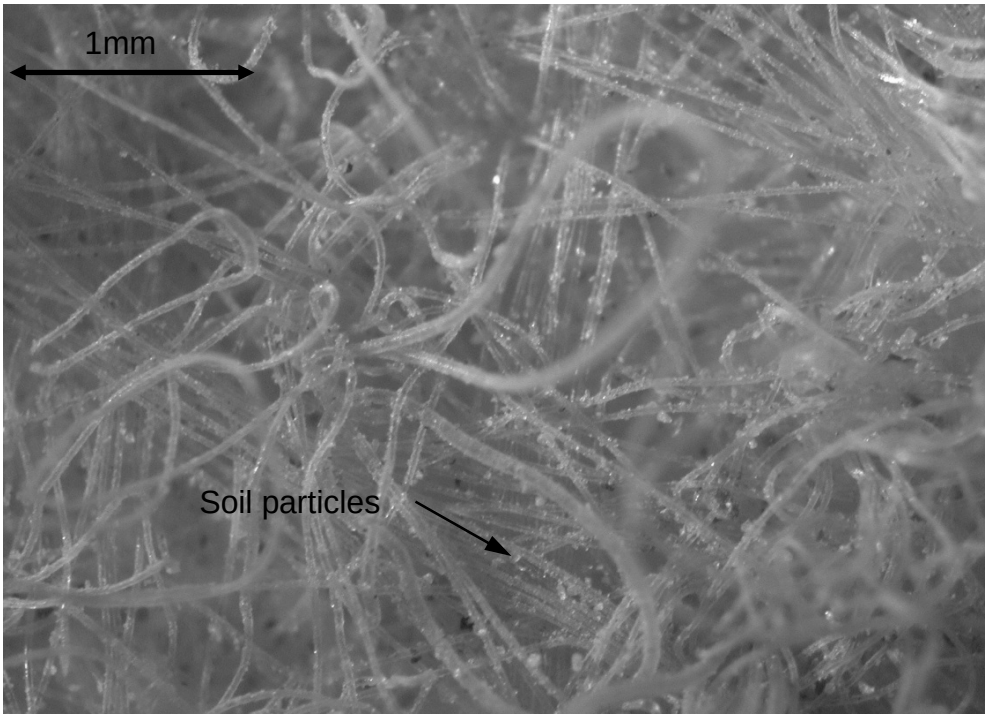

(a) Locate in the dark zone (contact with marble)

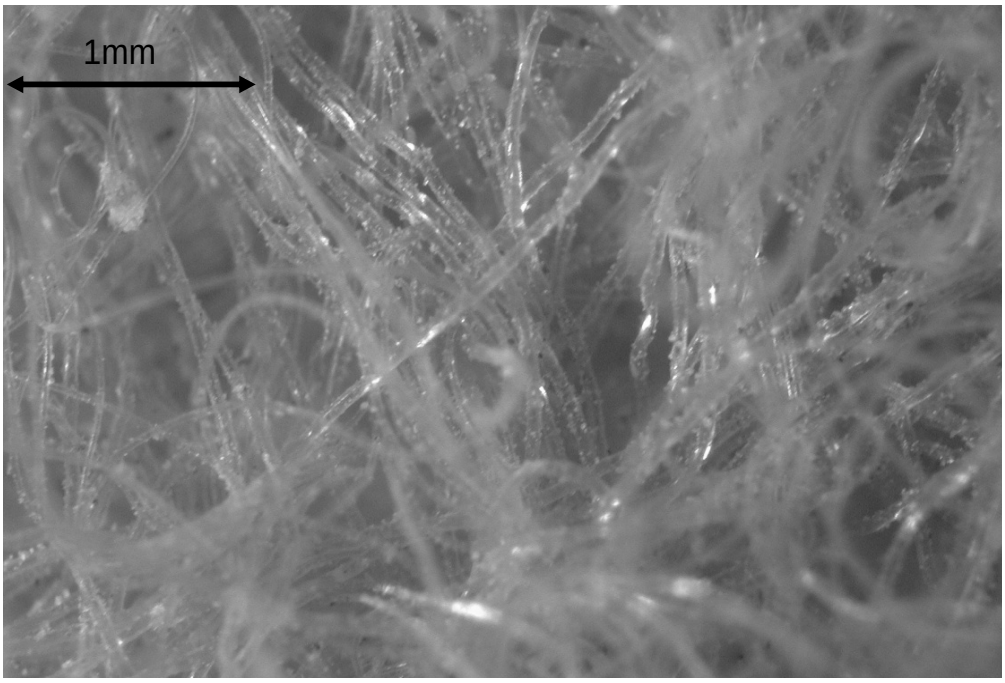

(b) Locate in the clean zone (no contact with marble)

Figure 4.27 Observation the surface state of geotextile by stereomicroscope (Magnification ratio: 25) (G-04-a) (Chung, 2007).

Figure 4.28 explains that the different behaviour between the area in contact with

rocks and the area not in contact with rocks. When the water flows downwards, the soil particles migrate towards the geotextile and some fine particles clog within the geotextile and some pass through the geotextile (see Figure 4.28(a)). As the water flow upward, water will pass through the fibre and take away the fine particle that clogs within the geotextile between where the marbles locates. But the geotextile in the marbles location is difficultly washed by the upward flow because of constraining by the marbles (see Figure 4.28(b)). This phenomenon will take place continuously with the cyclic flow until the soil-geotextile filtration system is stable.

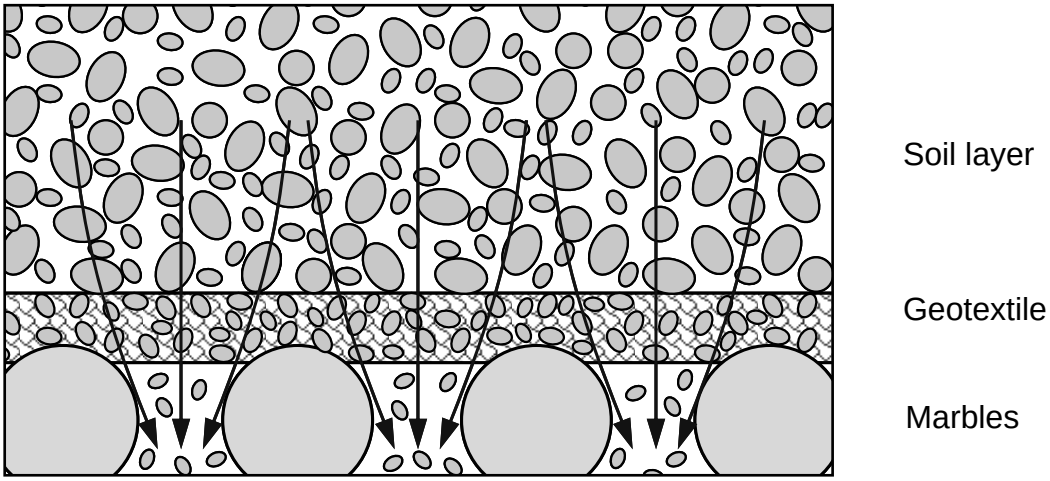

(a) Downwards flow

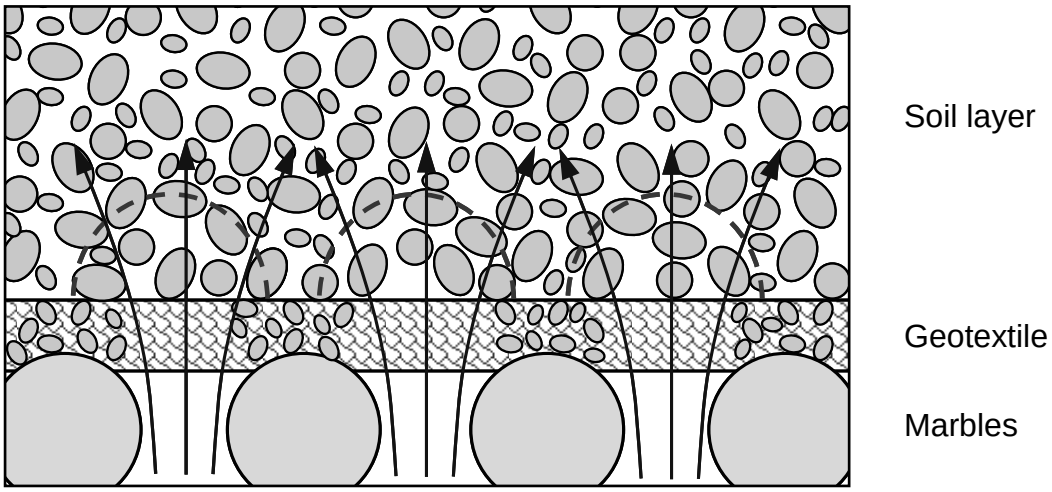

(b) Upward flow

Figure 4.28 The fine particles migrating behavior under cyclic flow

As above-mentioned, the geotextile between marbles is not almost clogged by fine particle. In order to investigate the soil erosion behaviour behind the geotextile where contact with soil, soil-geotextile sample is taken carefully from the area where between the marble after testing of G-06-a and the soil structure is observed by stereomicroscope (see Figure 4.29). It can be seen that a bridge network is formed behind the geotextile in the area between the marbles. In this area, as most fine particles are washed away and the cohesion of soil is lost and a hollow space is generated. Consequently it is difficult to keep sand while sampling. Outside the bridge network zone, the soil specimen contents the fine particles and is the cohesive soil. Hence, the bridge network was formed under the long-term bi-directional cyclic flow and to avoid the soil erosion and further settlement.

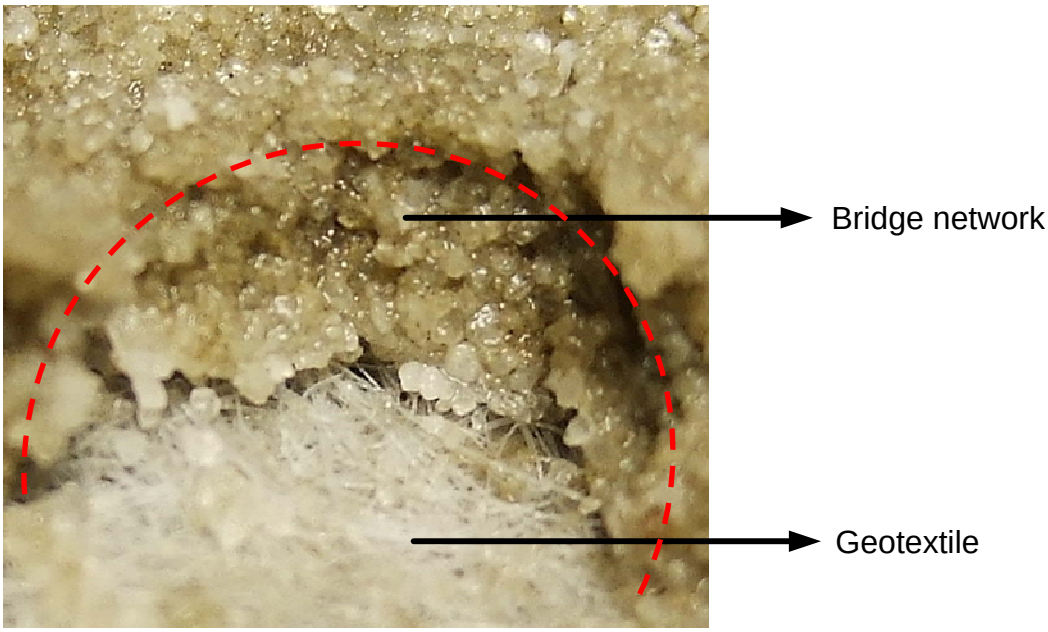

Figure 4.29 Bridge network formed behind the geotextile (G-06-a) (Chung, 2007).

Moreover, Figure 4.30 shows the microphenomenon of the cross section of geotextile after testing of G-3-a, G-6-a, and G-7-a, respectively. The initial soils in G-03, G-06, and G-07 tests have about 10% of fine particle (<0.074mm) but the microphenomenon of geotextile section after testing is large different: For test G-03-a, the amount of fine particle which adhere to the fiber of geotextile is smaller than for G-06-a and G-07-a. This can explain most of fine particle that clogged within the geotextile is washed out due to the soil boiling and to produce larger settlement and larger amount of soil washed out than the other two tests. On the contrary, for specimen of G-07-a which contents higher amount of cohesive soil, there are many

fine particles adhere to the fiber of geotextile. It will reduce the void within geotextile and causing the pore water pressure to increase. This is the reason why the pore water pressure of G-07-a is higher than G-06-a and G-05-a under the same wave period.

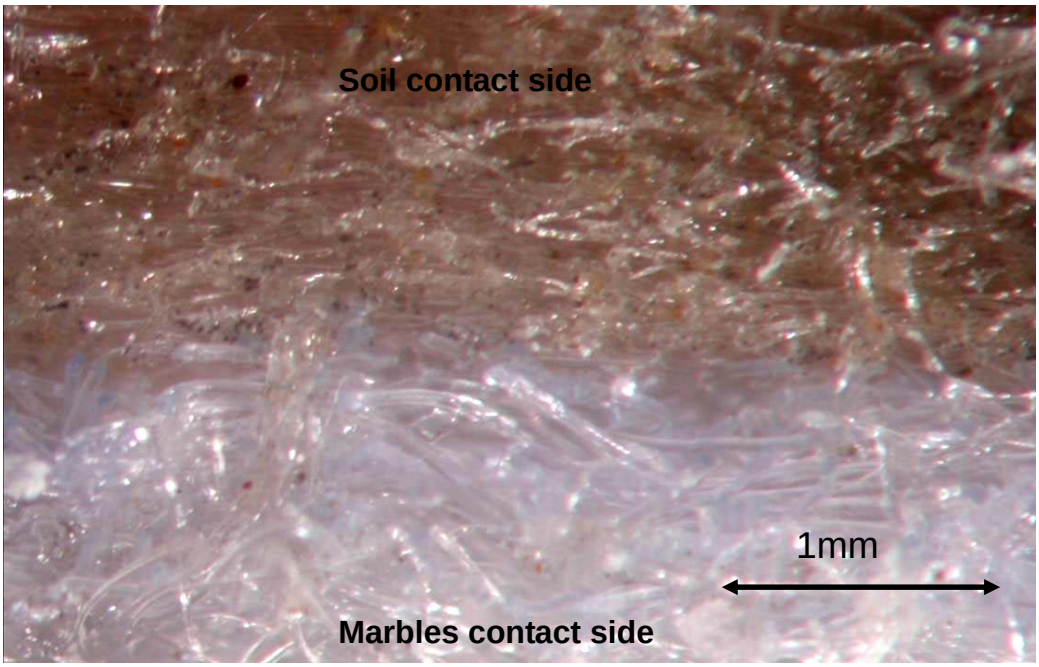

(a) G-3-a

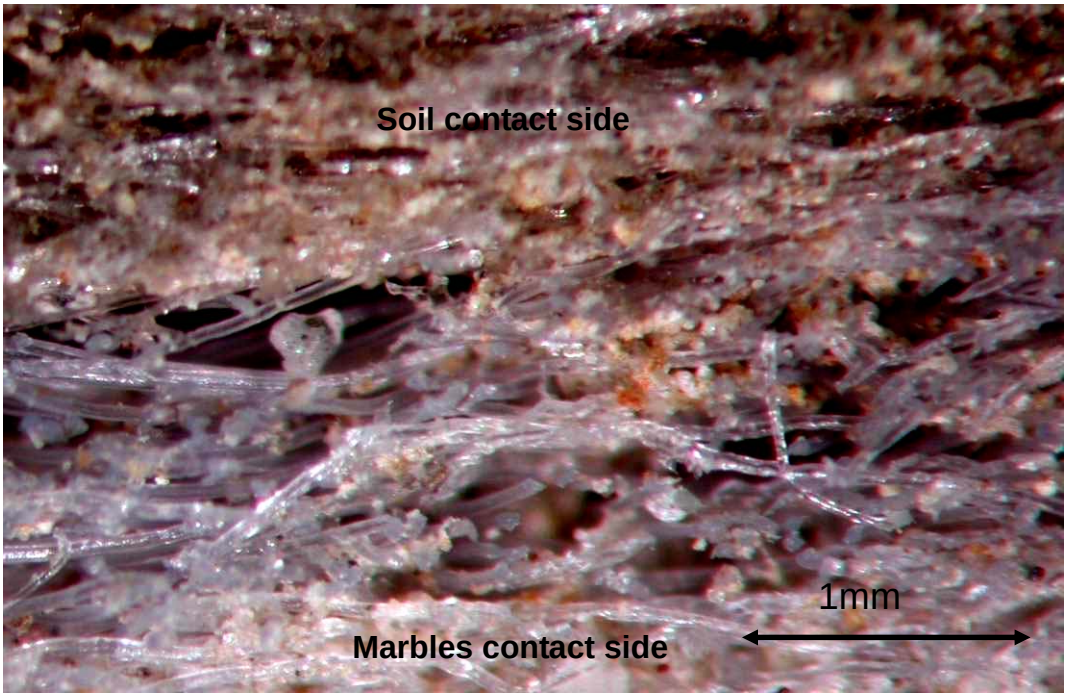

(b) G-06-a

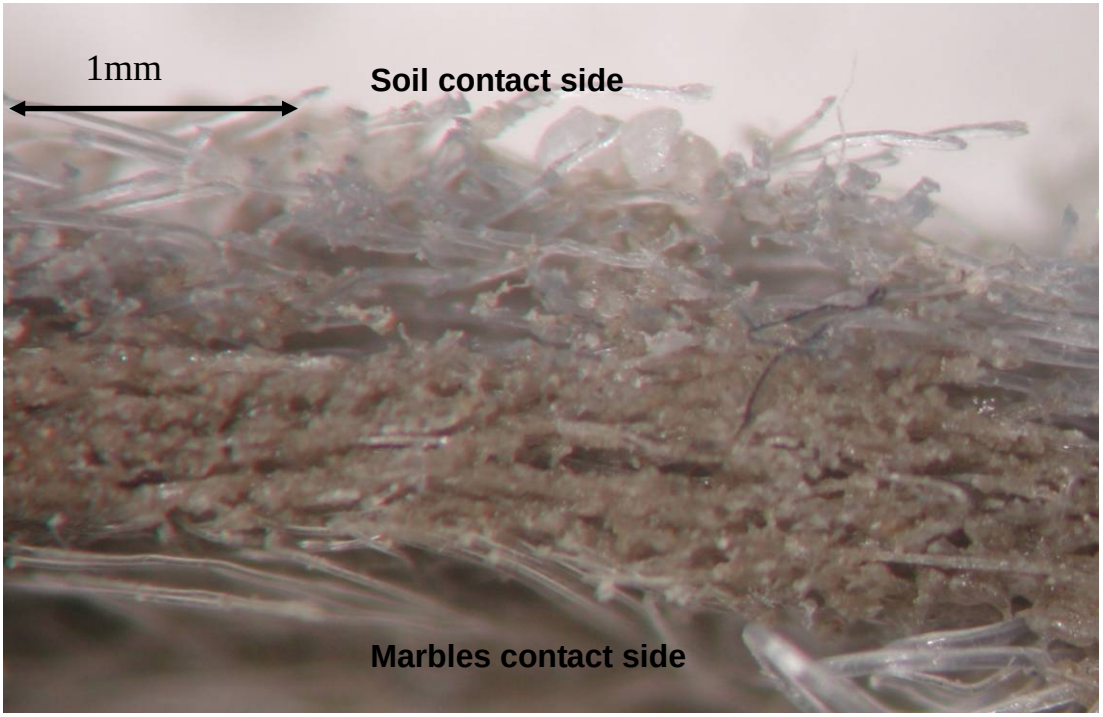

(c) G-07-a

Figure 4.30 The microphenomenon of the cross section of geotextile (Magnification ratio: 25) (Chung, 2007).

4.6 Summary

This research presents a study on the filtration characteristics of the geotextile under bi-direction cyclic flow. The apparatus adopted in this research is specifically designed to simulate in-situ conditions including overburden pressure, cyclic flow period and soil composition. The behaviors of non-woven geotextile with sandy soils of various fine particle contents were tested. The related information such as the settlement of the soil and the pore water pressures at various depths were recorded. The specimens and the grain size distribution of the soil before and after the test were examined. Also, the microphenomenon of the geotextile using a stereomicroscope after testing is observed. The results from this study are summarized as follows:

1. For the same soil specimen, the peak pore water pressure increases as the cyclic flow period decreases. The peak value also increases when increasing the amount of cohesive soil in this specimen. This is due to the low permeability of cohesive soil and the excess pore water pressure which has no enough time to dissipate over a short period condition and also.

2. For pure sand, the soil structure is quite stable under various normal pressures. In consequence, the difference in pore water pressure, settlement, and the amount of soil loss are insignificant.

3. For silty sand under low normal pressure, fine silty particles may migrate, clog within geotextile, or washed out. Consequently, in the beginning of testing the cyclic flow gradient index had a wide distribution. But this phenomenon was gradually eliminated as the cycles increased. On the other hand, for sandy soil with some amount of clay, the cyclic flow gradient index was close to unity during testing, which implies that clogging, blocking, or soil loss is less likely to occur for this kind of soils.

4. For silty sand, a low normal stress (70kPa) could not confine soil particles effectively and the cyclic flow induced pore pressure reducing the effective stress to be small enough to cause soil boiling. The boiled particles were easily washed out and caused significant settlement. On the other hand, a higher clay content and high normal pressure will reduce settlement.

5. The settlement has no direct connection with the amount of soil loss. The settlement of non-cohesive soil is derived from soil particle rearrangement and soil loss. For cohesive soil, the settlement results mainly from particle rearrangement. There might be other factors, such as soil structure change induced by pore water pressure that also need to be studied in the future.

6. For all specimens that without soil boiling happening, the average particle size, d_{50}, of the wash-out soil is smaller to that of the original fine particles. Besides, the particle size distributions of the wash-out soils are about the same. However, boiling occurring might cause some larger particles to pass through the geotextile. Hence, the retention and permeability criteria for bi-directional cyclic flow condition should be examined more carefully.

7. The microphenomenon by the stereomicroscope explains that the bridge network will be formed behind the geotextile where between the areas without marble contact area under the long-term bi-directional cyclic flow.

Chapter 5 Tangential erosion test

As described in Chapter 3 for full-scale flume test with wave action, the erosion due to perpendicular flow in the zone under the static level is insignificant and seems to be not influenced by the action of waves. In fact, the effect of tangential flow on this zone has stronger influence than the perpendicular flow. Based on this observation, a parallel erosion test (PET) equipment was developed to study the behavior of tangential erosion. In addition, this equipment can also be used for probing into the internal erosion behavior of the soil under the uni-directional flow.

5.1 Test equipment

Figure 5.1 presents the layout of parallel erosion test system and Figure 5.2 shows the general view of this equipment. The equipment of parallel erosion test comprises two water tanks. Clean water is poured into the bottom water tank and meanwhile pumped into the upper water tank by a lift pump. After opening the valve, water flows into the steel cell room through the water pipe. Inside the steel cell room, sub-soil, geotextile, gravel, and rubber water bag are filled in sequence. The top of the rubber water bag is connected to a pressurization system in order to apply the vertical pressure. The elevation of the sub-soil that filled in the cell room equals to the bottom level of the water inlet and outlet, so that water will only flow through the gravel layer. Consequently, the water flow direction is parallel to the sub-soil surface, and hence this experiment is called parallel erosion test (PET). In order to measure the hydraulic gradient, the connector tube that connects to a water pressure head loss meter in the water inlet and outlet was set up separately. Water flows out and carries the eroded soil particles out of the water outlet. Hence, a turbiditymeter in the outlet was installed to survey the variation of water turbidity, and a flowmeter was installed to measure the water flow rate.

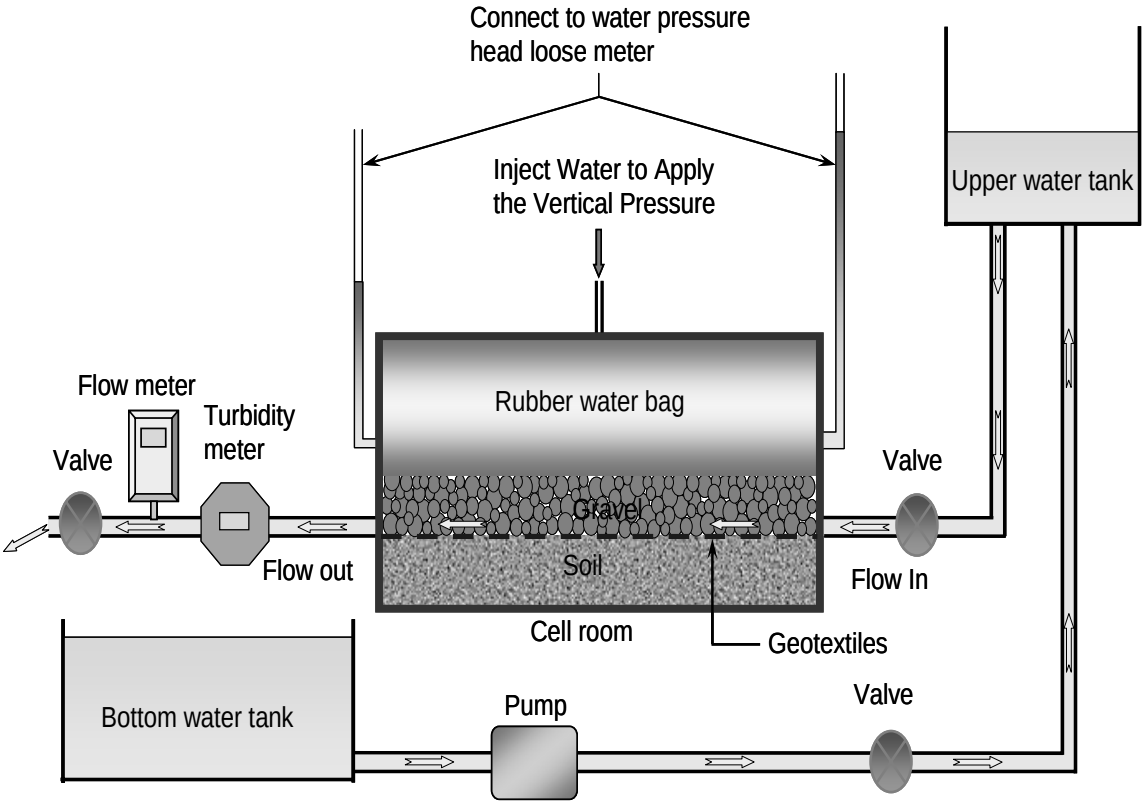

Figure 5.1 Illustration of the parallel erosion test equipments.

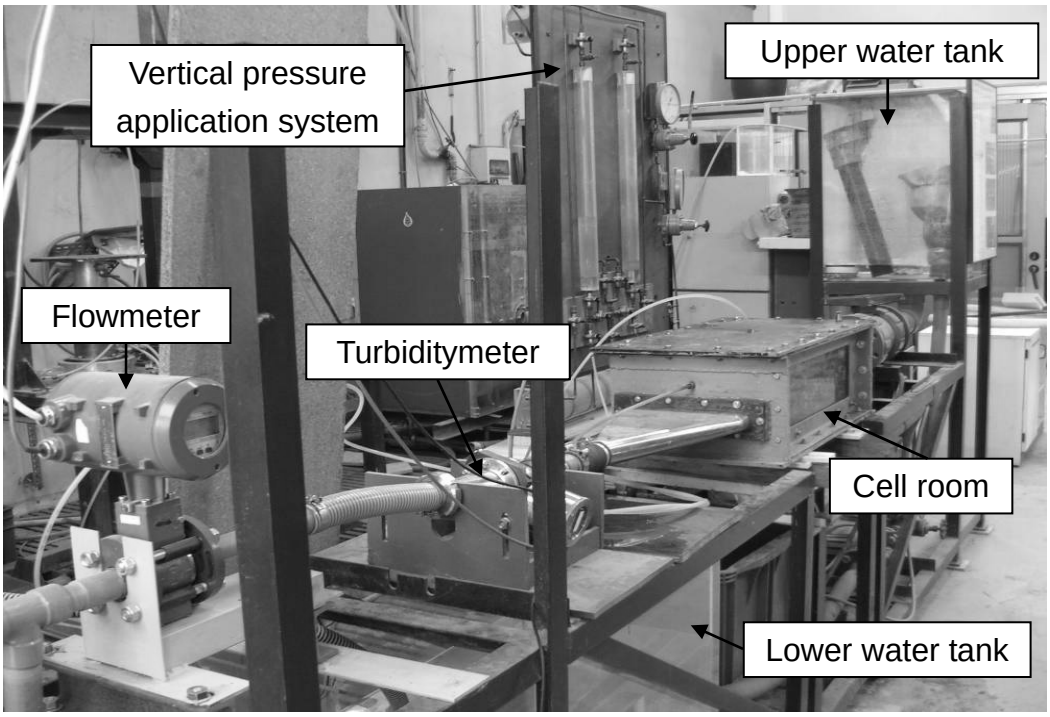

Figure 5.2 General view of the parallel erosion test equipment.

1. Steel cell room:

The dimension of the steel cell room is shown in Figure 5.3. As shown, the thickness of the sub-soil is 6 cm and filled the gravel 6 cm in thickness on the soil, and the interface of soil and gravel is geotextile. In order to observe the state of soil erosion, this cell room is equipped with an observation window made of transparent plexiglass on one side on which topographic reference lines were marked.

Moreover, two 5 cm long dense geotextile sheets above the soil in the end of flow in and flow out receptivity were laid in order to avoid the edge effect. The real erosion zone of soil is 550 mm × 300 mm. Besides, two pieces of geogrid were put on the water inlet and outlet in order to maintain the gravel particles.

Above the gravel is a rubber water bag, and the top of the rubber water bag connects to the pressurization system, which injects the water and applies the vertical pressure onto the gravel-soil system to simulate the overburden pressure in site.

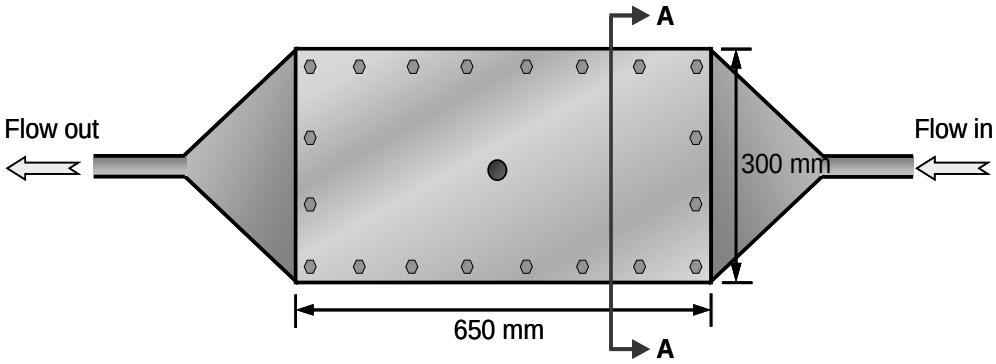

(a) The plan view of the cell room.

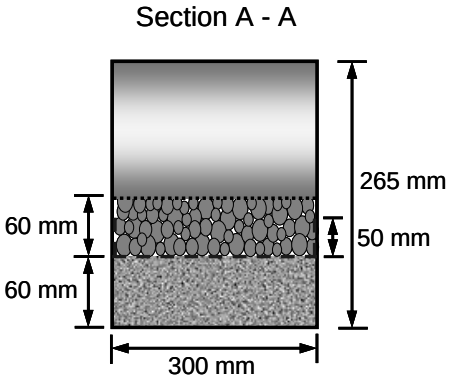

(b) The section of the cell room.

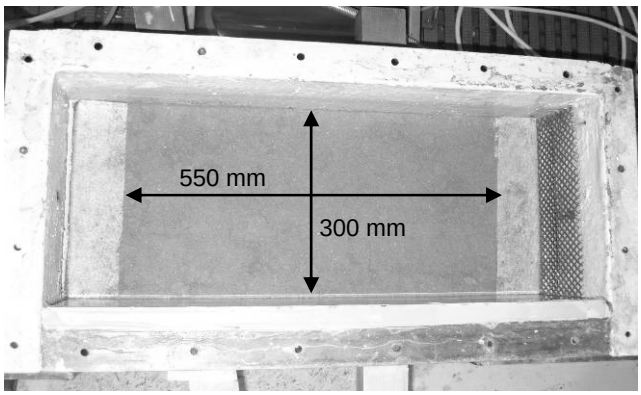

(c) The state of soil erosion surface.

Figure 5.3 The dimension of the steel cell room.

2. Water tank:

The test equipment is equipped with two water tanks. During the test, clean water was poured into the bottom water tank and pumped into the upper water tank by the lift pump. In order to control the hydraulic gradient and water flow rate, there is an adjustable overflow pipe at the upper water tank and a water valve before the entry of the water flow.

3. Monitoring devices:

In order to monitor the soil state more accurately and to define the timing of soil erosion, the monitoring system consists of several devices. Flowmeter is used to measure the flow rate while testing and to calculate the flow velocity. Turbiditymeter is used to monitor the variation of water turbidity by time and to convert it into the concentration of the soil particles in water. Furthermore, the water pressure head loss meter measures the change of water pressure head and transfers to the hydraulic gradient.

Additionally, the water turbidity in the upper tank was measured regularly during the test by using a manual turbidity measurement device (see Figure 3.4). This is to confirm that the water flow into the cell room is clean.

5.2 Test materials characteristics

The main test materials for this study are the sub-soil, the gravel and the geotextiles. Their physical characteristics are described as follows.

5.2.1 Sub-soil material

The sub-soil used in this experiment was non-cohesive fine silty sand collected from the sedimentary deposit of the river Isère. As the location where the soil sampled is different from that of the material used of Chapter 3, the soil material characteristics are different. The grain size distribution and the particle size parameters of sub-soil are presented in Figure 5.4. In this study, the dry unit weight of sub-soil adopted in $\gamma_d = 16.4 \text{kN/m}^3$ for all tests.

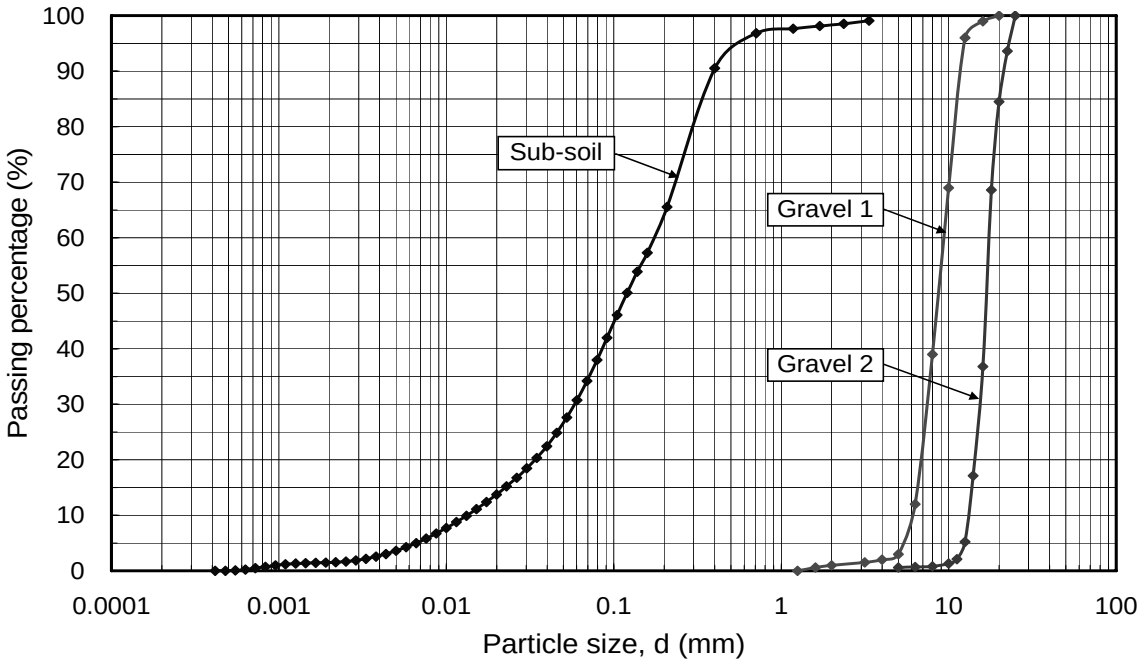

For sub-soil:

d_{10} = 0.013 mm d_{15} = 0.021 mm d_{30} = 0.059 mm d_{50} = 0.120 mm

d_{60} = 0.180 mm d_{85} = 0.320 mm d_{90} = 0.390 mm Cu = d_{60}/ d_{10} = 14

For Gravel 1:

d_{10} = 6.0 mm d_{15} = 6.5 mm d_{60} = 9.1 mm Cu = d_{60}/ d_{10} = 1.5

k = 15.8 cm/s (for i = 1.0) n_F = 0.44

For Gravel 2:

d_{10} = 12 mm d_{15} = 14 mm d_{60} = 18 mm Cu = d_{60}/ d_{10} = 1.5

k = 27.1 cm/s (for i = 1.0) n_F = 0.47

Figure 5.4 Grain size distribution and the particle size parameters of the sub-soil and gravels.

5.2.2 Gravel material

As there are often armor stones covered on the surface of the riverbank, the gravel was filled on the soil/geotextile to simulate the function of the armor stones. Also, in order to understand the influence on erosion behavior of the gravel size distribution, in this test two types of gravels that have different particle size distributions were chosen, as shown in Figure 5.4. The particle size of Gravel 2 is larger than Gravel 1 but the

uniform coefficient (Cu) is almost the same. They are all uniform graded gravels.

Moreover, to analyze the geometrical stability of gravel, the criteria by Kenney and Lau (1985, 1986) were used, which consists in checking the condition of soil filter between the large and the small particles. According to the result of analysis (Figure 5.5), Sub-soil, Gravel 1, and Gravel 2 are all internally stable.

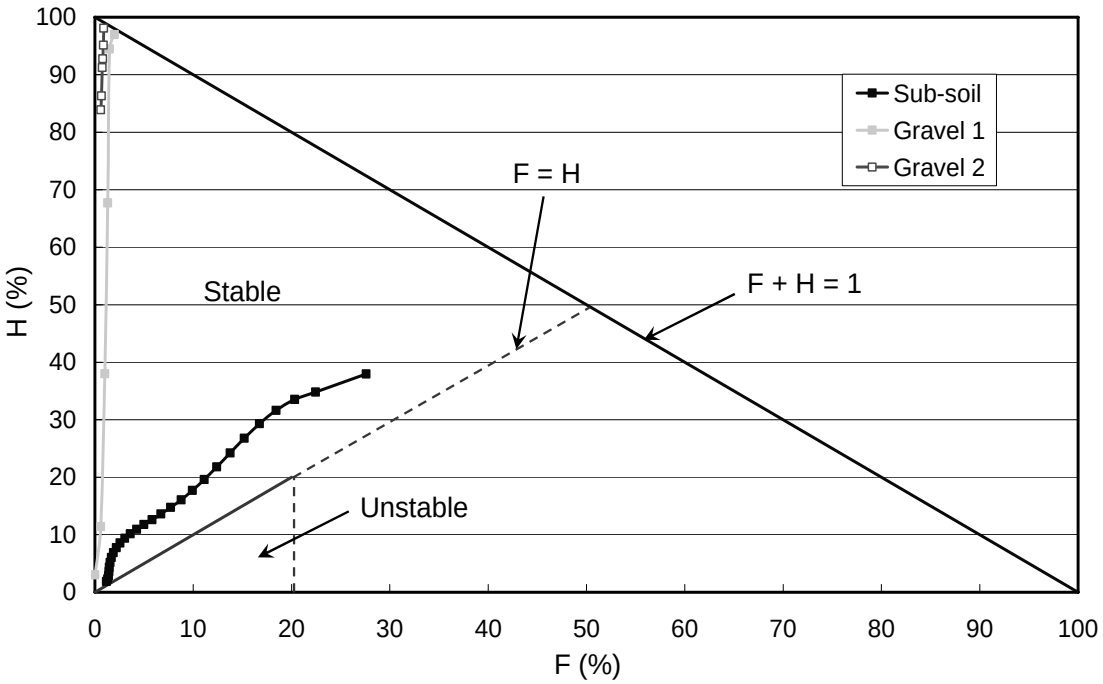

Figure 5.5 The result of analysis of the internal stabling of soil filter by the criterion of Kenney and Lau (1985).

5.2.3 Geotextile material

Four types of geotextiles were used in this experiment. Their thickness is almost the same but the opening size and the manufacturing approach is different. GTX1 is a woven and heat-bonded geotextile and the opening size is the largest. The manufacturing approach of GTX2 is same with GTX1 but the opening size is smaller than GTX1. GTX3 is a woven geotextile and GTX4 is a non-woven and needle-punched geotextile with the smallest opening size than the others. The thickness and the opening size of these four geotextile are presented in Figure 5.6.

They are too thin for geotechnical application like bank protection, but selecting those three woven geotextiles is because their size of opening are well known (square

mesh like sieves). For this study, focus is put on the influence of the opening size of geotextile on soil erosion behavior. Moreover, according to the general filtration criteria, when the opening size too small, less than 100 μm ($d_{45} \approx 100\mu m$), should not produce erosion. For that, a thin non-woven geotextile (GTX4) was selected.

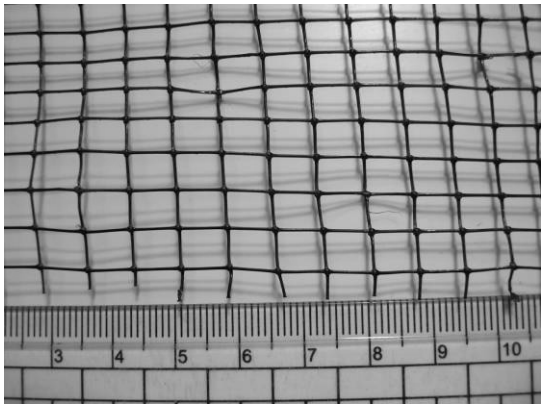

(a) GTX1 (Woven and heat-bonded).

Thickness : t_{GT} = 1.0 mm
Opening size : O_{90} = 7.0 mm

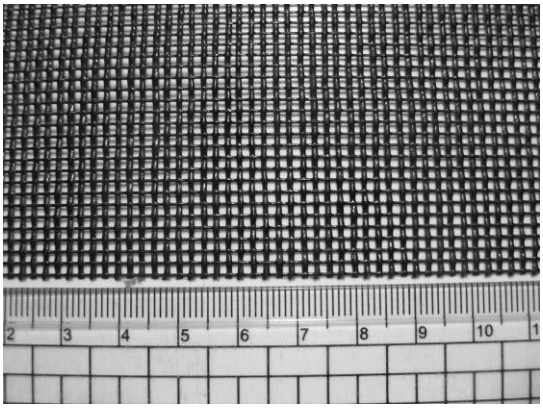

(b) GTX2 (Woven and heat-bonded).

Thickness : t_{GT} = 1.0 mm
Opening size : O_{90} = 1.07 mm

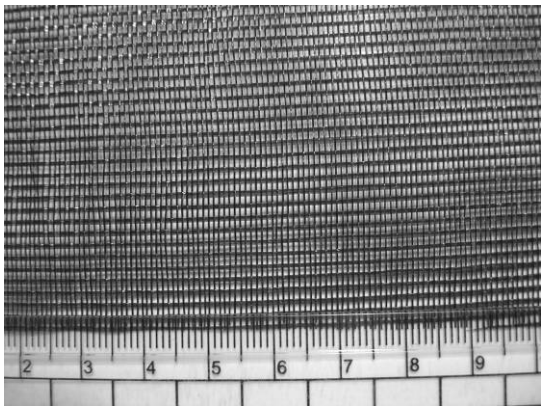

(c) GTX3 (Woven).

Thickness : t_{GT} = 0.8 mm
Opening size : O_{90} = 0.6 mm

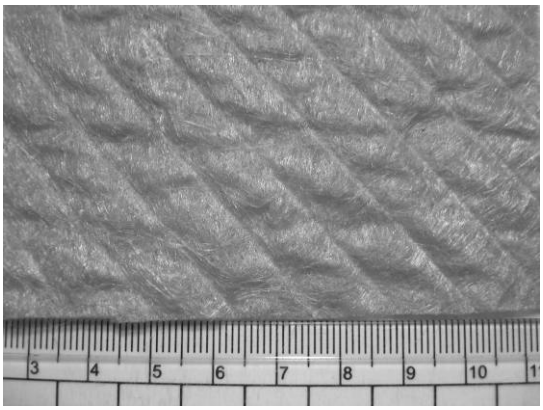

(d) GTX4 (Non-woven and needle-punched).

Thickness : t_{GT} = 1.3 mm
Opening size : O_{90} = 0.11 mm

Figure 5.6 The characteristics of the geotextiles used.

5.3 Tests performed

Six sets of PET experiment were conducted in this study. Their details are shown in Table 5.1.

Table 5.1 Details of PET performed

No.		Test quantity	Test number	Vertical pressure	Gravel	Geotextile
SET01	A	7	T01 ~ T07	50 kPa	Gravel 1	Non
	B	3	T08 ~ T10	10 kPa	Gravel 1	Non
SET02		6	T11 ~ T16	10 kPa	Gravel 2	Non
SET03		4	T17 ~ T20	10 kPa	Gravel 2	GTX1
SET04		7	T21 ~ T27	10 kPa	Gravel 2	GTX2
SET05		4	T28 ~ T31	10 kPa	Gravel 2	GTX3
SET06		4	T32 ~ T35	10 kPa	Gravel 2	GTX4

In SET01 and SET02 geotextile was not laid on the interface of the sub-soil and gravel, and in other tests GTX1, GTX2, GTX3, and GTX4 were laid. In order to understand the influence of the vertical pressure, in SET01-A and SET01-B, 50 kPa and 10 kPa of the vertical pressure was applied separately by the rubber water bag, respectively. Except SET01, all tests applied the same vertical pressure (10 kPa). Besides, in SET01, Gravel 1 was filled on the sub-soil and in the other tests Gravel 2 was filled.

In each test, the flow rate was increased from the small to the large phase gradually and the flow rate of each stage was carried out for more than 30 minutes. The water turbidity was recorded automatically every 3 seconds and the flow rate recorded every 15 seconds while testing. The water turbidity was converted into the concentration of soil particle in water and the flow rate was converted into the flow velocity by the process that will be describe in details in the next section.

5.4 Test data conversion and annotation

As mentioned above, the PET equipment comprises several devices. They are used to measure the water pressure loss, the water turbidity, and the flow rate while testing.

1. Hydraulic gradient, i:

It is easy to convert water pressure head loss data into the hydraulic gradient.

$$i = \frac{\Delta h}{L} \tag{5-1}$$

Where Δh is the water pressure head loss between the flow inlet and outlet and L is the length of flow path.

Figure 5.7 shows the relationship between the hydraulic gradient and the water turbidity with time. As the soil is in the state of non erosion, the hydraulic gradient keeps constant (see Figure 5.7 (a)). Once the soil reaches the state of erosion, the variation of hydraulic gradient is irregular with time (see Figure 5.7 (b)). With the flow velocity, the air within the gravel could be taken out and stayed in the connector tube of the water pressure head loss meter. Moreover, the air within the sub-soil also could be taken out due to soil erosion and influence the measure of water pressure. Hence, in this test is difficult to define soil erosion classification from the hydraulic gradient and therefore this study adopts the flow velocity to classify the soil erosion state and to compute the soil erosion rate.

However, if the measuring system of water pressure in the future experiment is modified, the variation of investigation water pressure should be accurate.

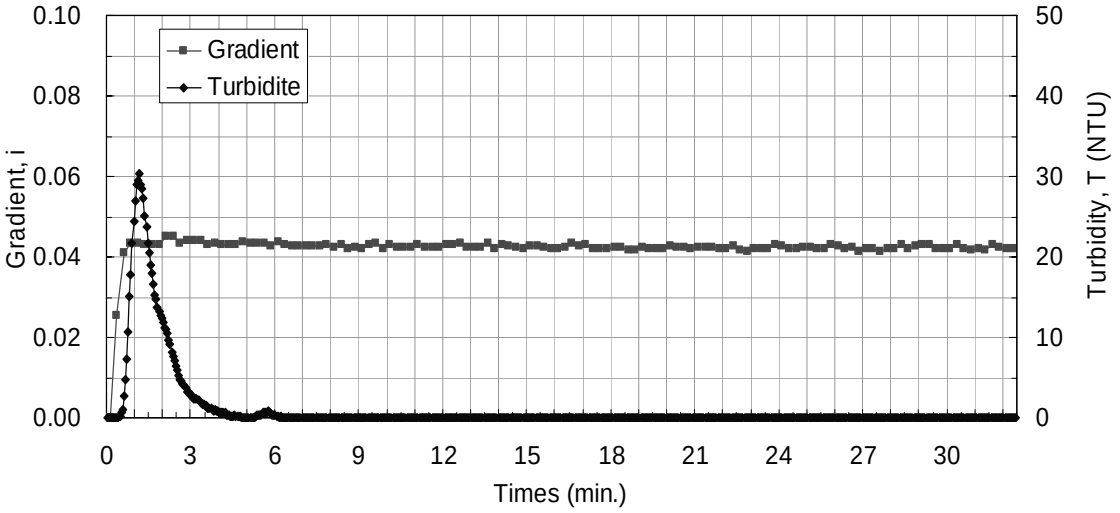

(a) Non erosion state

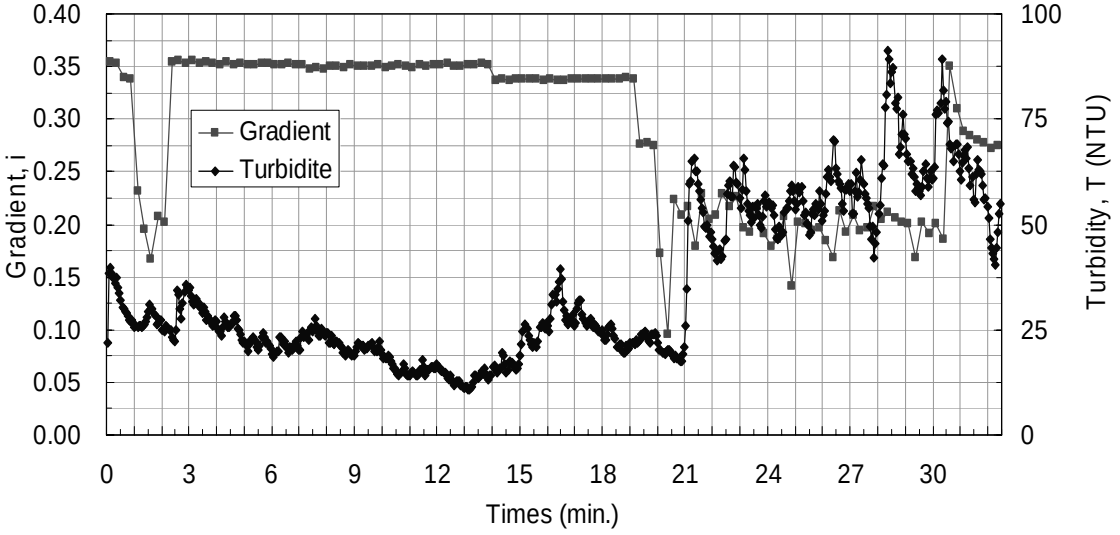

(b) Erosion state

Figure 5.7 The variation of hydraulic gradient and water turbidity with time.

2. Flow velocity, v:

According to the test data by flowmeter and adopting the following equation to convert the flow rate into the velocity.

$$v(cm/s) = \frac{q(cm^3/s)}{A_c(cm^2)} \tag{5-2}$$

Where q is the flow rate per unit time, A_c is the flow cross section area.

In this study, the unit used for q is liter per second, and A_c is considered to be the cross section of gravel. So

$$A_c = 30\text{cm} \times 6\text{cm} = 180\text{cm}^2$$

3. Concentration of soil particle in water, C:

In order to obtain the relationship between the measurement of water turbidity and the concentration of soil particles contained in water, several measurements of turbidity were taken with a turbiditymeter by sampling from 20 liters of clean water containing various predetermined quantities of soil particles. Figure 5.8 presents the test result of the primary experiment.

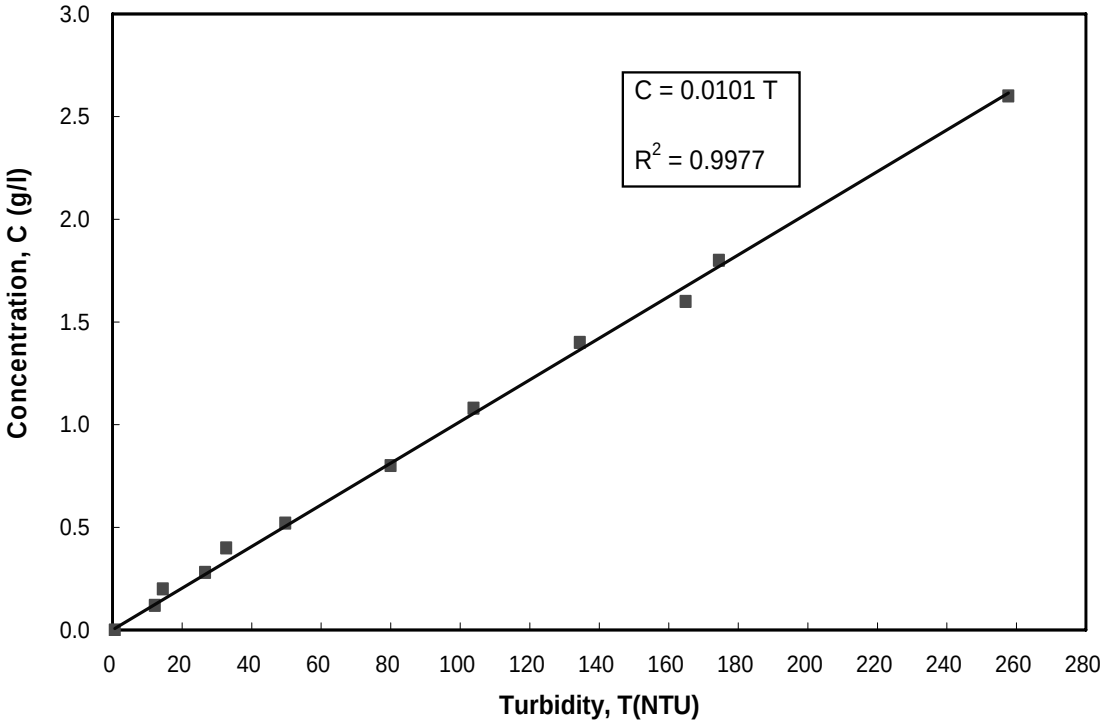

Figure 5.8 The relationship between water turbidity and concentration.

The correlation between water turbidity and concentration presented as follows.

$$C(g/l) = 0.0101 \times T(NTU) \tag{5-3}$$

T : Turbidity

4. Soil erosion rate, m':

The mass of soil erosion (m) while testing can be calculated by the following equation:

$$m(g/cm^2) = \int_0^t \frac{C(g/cm^3) \times q(cm^3/s)}{A_e(cm^2)} dt \tag{5-4}$$

Where A_e is the area of soil erosion surface. As shown in Figure 5.3, the soil erosion surface is 55 cm × 30 cm = 1650 cm^2. And t is the test time.

The soil erosion rate (m') is the mass of soil erosion by unit time. It is defined that

$$m' = \frac{C \times q}{A_e} = \frac{dm}{dt} \tag{5-5}$$

Figure 5.9 shows the variation of mass of soil erosion "m" with time for different flow velocities. When the soil is in the non erosion state, "m" keeps constant after the peak turbidity value as the water turbidity is zero (example on Fig. 5.7a); when the soil erosion occurs, the mass of soil erosion increases with time and the increase rate of mass of soil erosion relates to the severity of soil erosion. The slope of the mass of soil erosion curve was defined by the average soil erosion rate (m*). In order to reduce the influence on erosion rate of the peak water turbidity in the initial stage of testing, this research adopts the average slope of mass of soil erosion curve from 5 minutes to 30 minutes for every interval of 5 minutes of test period. That is to regard as the average soil erosion rate under this flow velocity.

$$m'(g/cm^2/s) \approx m^* = \frac{\Delta m}{\Delta t} \tag{5-6}$$

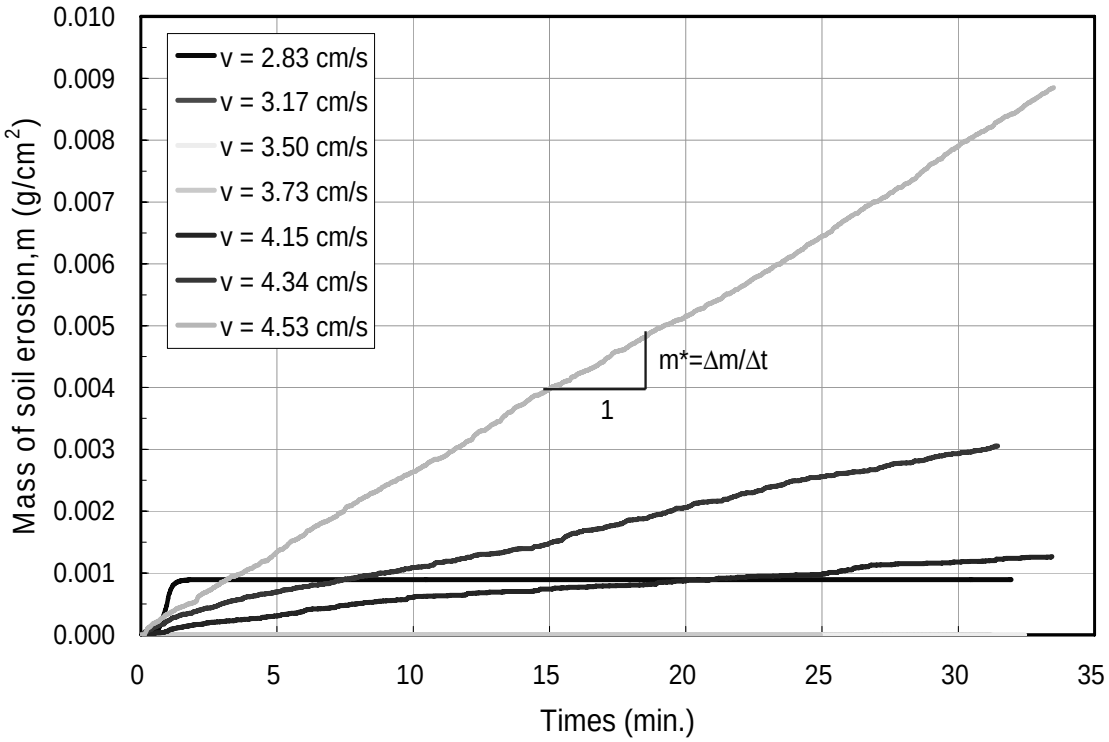

Figure 5.9 The variation of the mass of soil eroded with time.

5.5 Soil erosion observation and classification

Figure 5.10 shows the variation of water turbidity and flow velocity with time. As shown, there is a peak value at the initial stage of testing. That is probably due to the sudden increase of flow velocity which washed away the soil particles that adhered to gravel surface or deposited in the water pipe, and caused transient increase of water turbidity. According to the variation of water turbidity by time, the following three soil erosion states can be summarized:

1. Non erosion:

After the peak water turbidity of the initial stage, if no soil particles continued to be washed out by water, the water turbidity will decrease with time. As Figure 5.10 (a) shows, water turbidity decreased to zero after the peak point, meaning that the water outflow is clean and without any soil particles and consequently no soil erosion occurred. Hence, under this condition, the soil is in the non erosion state.

2. Steady erosion:

As shown in Figure 5.10 (b), the water turbidity also decreased but could not decay to zero after the peak turbidity. The residual turbidity keeps constant with time. In addition, by observing the state of the soil through the observation window of cell room it can also be found that particles are migrated by flow. It presents that the follow-up water outflow included a fixed quantity of soil particles. In other words, the sub-soil was eroded and the erosion rate remains unchanged under the fixed flow velocity. It can say that the soil is in the state of steady erosion.

3. Failure erosion:

The water turbidity increases with increasing flow velocity. Figure 5.10 (c) shows that the water turbidity is high and the variation is irregular with time when the flow velocity keeps constant. This shows that the water contains a large quantity of soil particles. On the other hand, the soil has undergone obvious erosion as observed through the transparent plexiglass while testing. Under this condition, the soil is in the failure erosion state and will produce failure quickly.

Under the smaller flow velocities, non soil erosion occurred. With the increase of the flow velocity, the soil begins to erode gradually. The critical flow velocity (v_c) was defined that the flow velocity when the soil begin to erode. In addition, the flow velocity when the soil situated between steady erosion and failure erosion is named the failure flow velocity (v_f).

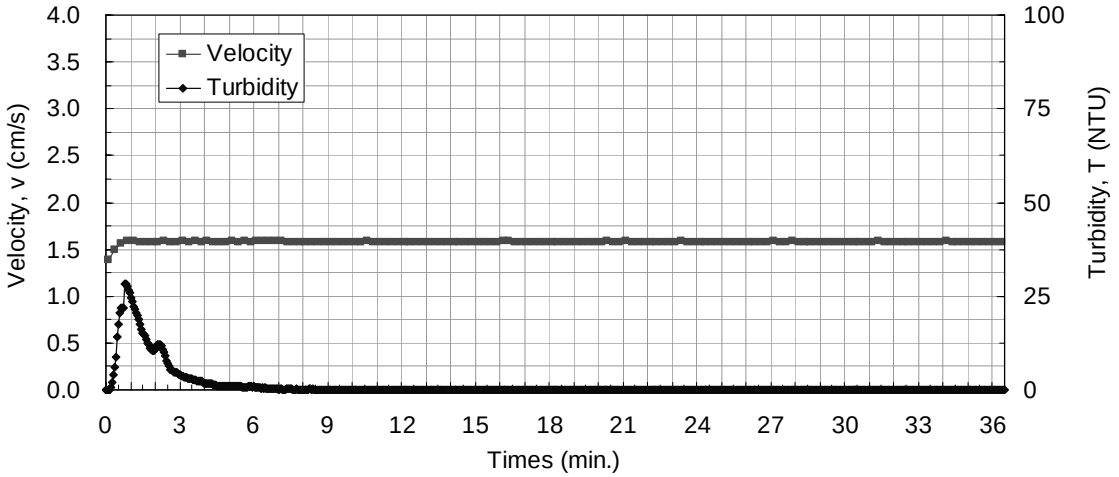

(a) Non erosion state

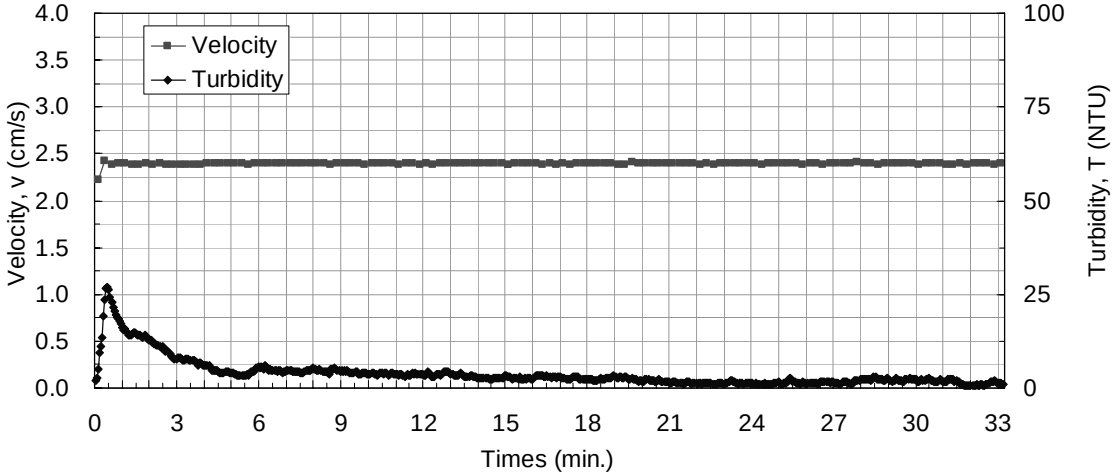

(b) Steady erosion state

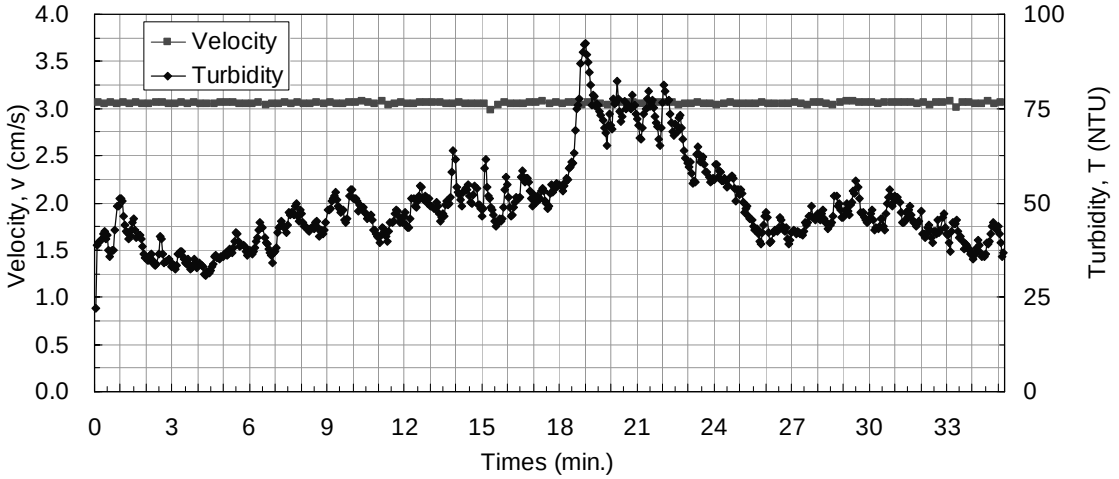

(c) Failure erosion state

Figure 5.10 Types of soil erosion states.

5.6 Test results of PET

5.6.1 Correlation between water turbidity and flow velocity

Figure 5.11 presents the variation of water turbidity and flow velocity with time of T12 (SET02) and the other figures are given in Appendix III. It can be seen that have peak water turbidity in the initial stage for each flow velocity and the peak value is depending on the range of velocity increases. In order to classify the soil erosion by the theory as described in Section 5.4.1, Figure 5.11 was split into several figures in accordance with different velocities and shown in Figure 5.12. It is clear to know that the critical velocity (v_c) seems between 1.38 cm/s and 2.04 cm/s and the failure velocity (v_f) seems between 2.37 cm/s and 2.74 cm/s. In addition, the same conclusion can be drawn by the monitoring result through the observation window (see Figure 5.13). But if v_c and v_f need to be determined more accurately, it is necessary to carry on more tests and collect more data.

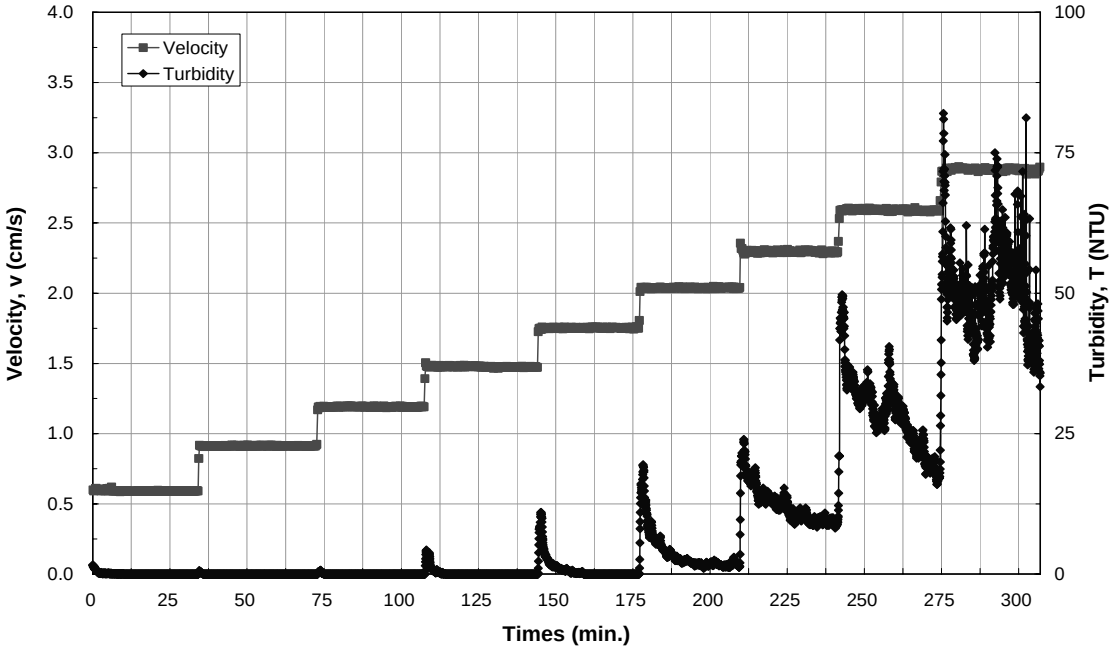

Figure 5.11 The variation of turbidity and velocity with time (T12).

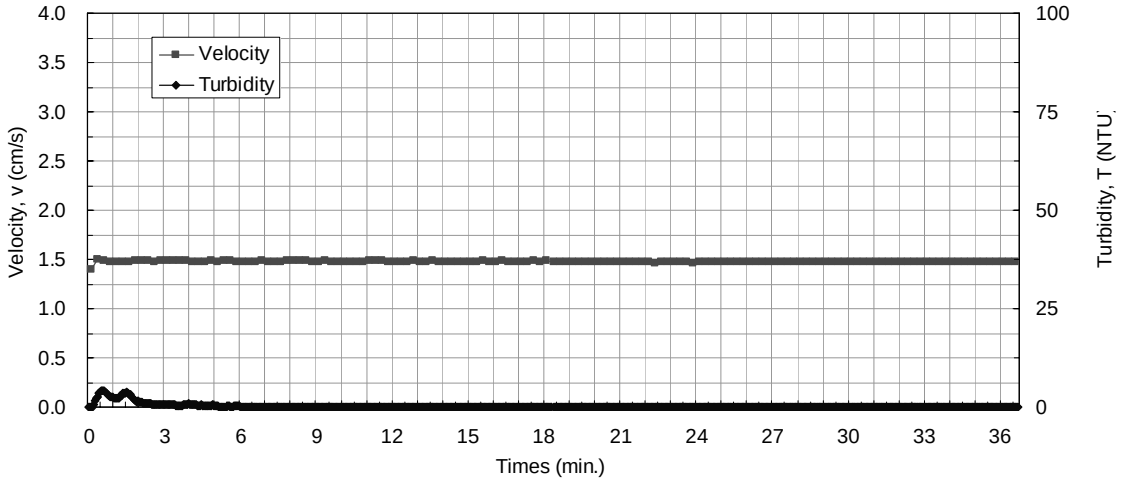

(a) v = 1.48 cm/s (Non erosion)

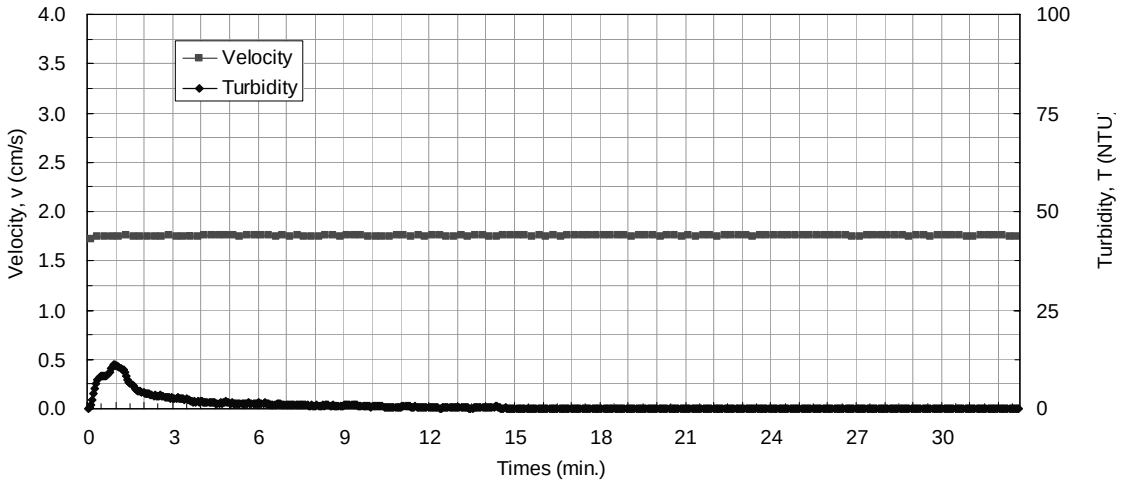

(b) v = 1.75 cm/s (Non erosion)

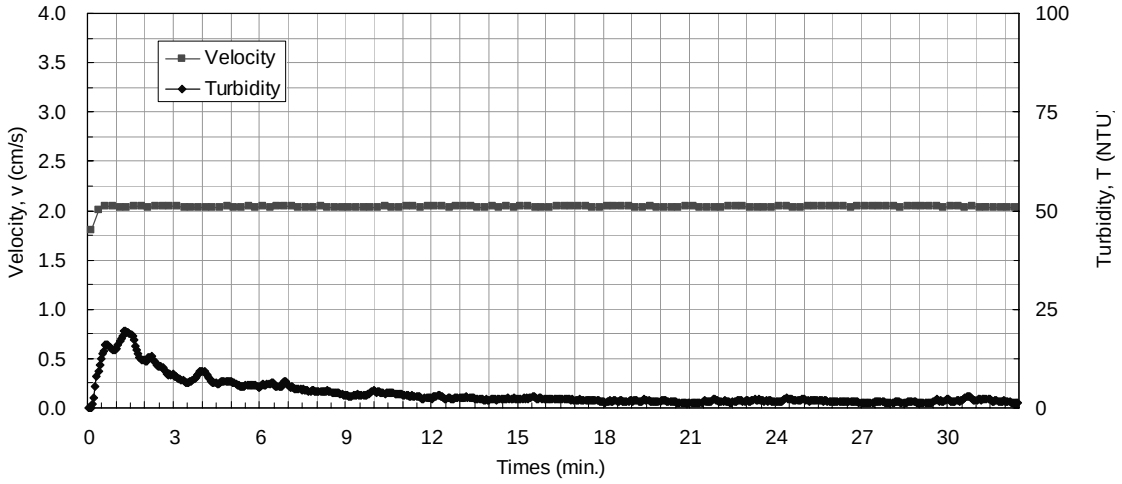

(c) v = 2.04 cm/s (Steady erosion)

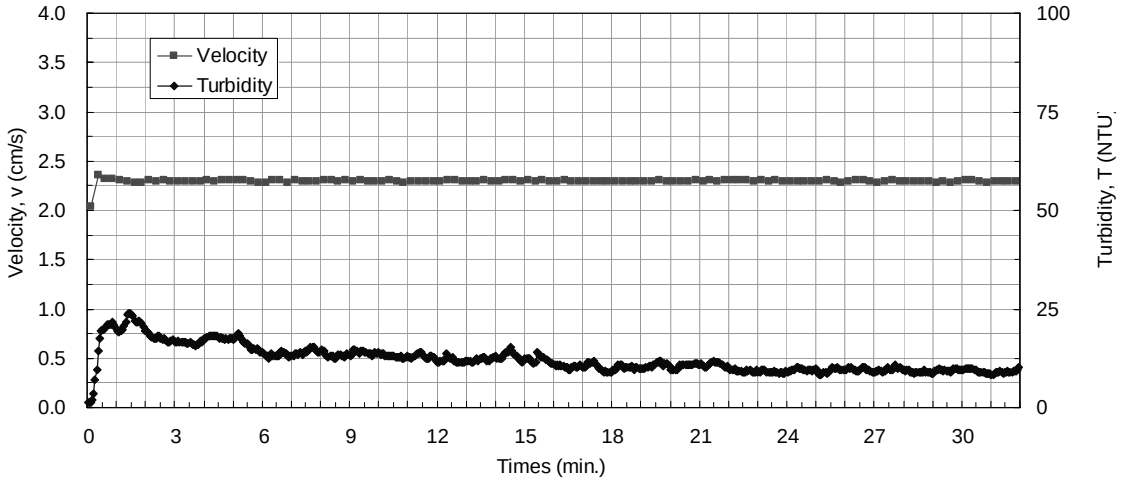

(d) v = 2.28 cm/s (Steady erosion)

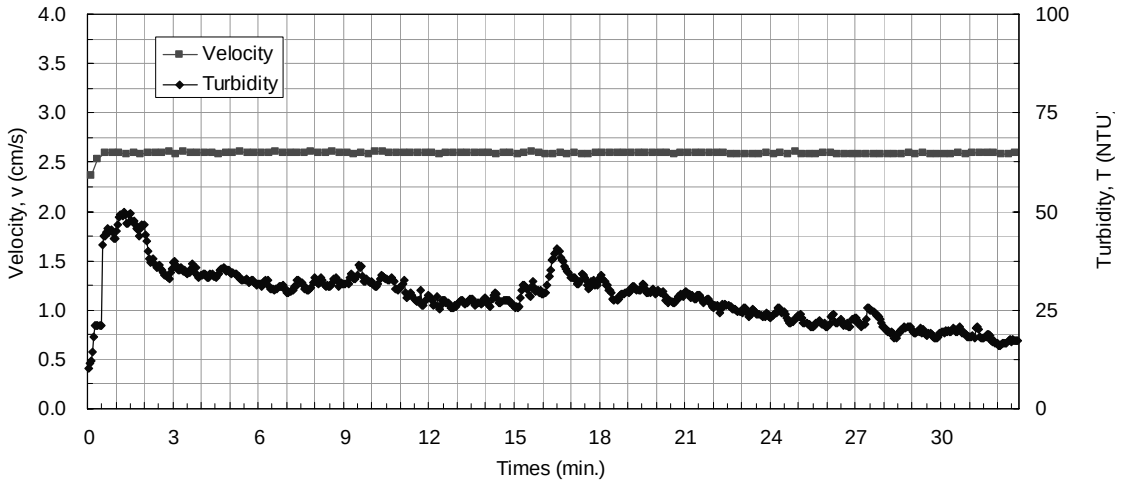

(e) v = 2.59 cm/s (Failure erosion)

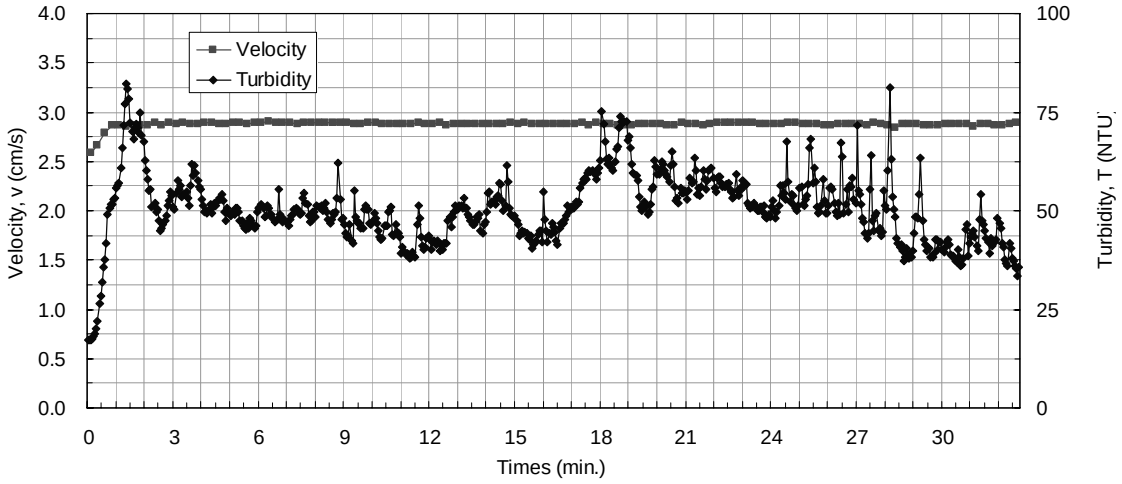

(f) v = 2.88 cm/s (Failure erosion)

Figure 5.12 The variation of water turbidity with time (T12) for each velocity.

(a) v = 1.48 cm/s (Non erosion)

(b) v = 1.76 cm/s (Non erosion)

(c) v = 2.04 cm/s (Steady erosion)

(d) v = 2.28 cm/s (Steady erosion)

(e) v = 2.59 cm/s (Failure erosion)

(f) v = 2.88 cm/s (Failure erosion)

Figure 5.13 The variation of soil erosion state (T12)

5.6.2 Determination of critical velocity and failure velocity

Ten tests were carried out in SET01. In order to understand the impact of the overburden pressure on soil erosion behavior, 50 kPa of vertical stress was applied in 7 tests and 10 kPa in was applied in the other 3 tests in SET01. The test result of these 10 tests is summarized in Table 5.2.

Table 5.2 The soil erosion classification of SET01 (Gravel 1).

Test No.	σ_v (kPa)	Velocity (cm/s)									
T01	50	0.68	1.18	1.50	2.04	2.42					
T02	50	0.69	1.18	1.50	2.02	2.46	2.73	2.91			
T03	50	0.63	1.07	1.53	1.84	2.34	2.76				
T04	50	0.57	0.90	1.39	1.69	2.11	2.28	2.74	3.14		
T05	50	0.35	0.91	1.40	1.82	2.28	2.84	3.24			
T06	50	0.56	1.38	2.04	2.37	2.74	3.01				
T07	50	0.80	1.60	2.48	2.89	3.11					
T08	10	0.34	0.68	1.02	1.35	1.69	2.02	2.39	2.78	3.06	
T09	10	0.47	0.75	1.14	1.48	1.80	2.13	2.48	2.83	3.24	
T10	10	0.26	0.62	0.89	1.22	1.58	1.91	2.31	2.55	2.80	3.20

: Non erosion : Steady erosion : Failure erosion

As presented in Table 5.2, the difference in soil erosion state is insignificant under different vertical stress. It can be determined that the critical velocity, v_c = 2.0 cm/s, and the failure velocity is v_f = 2.7 cm/s.

The result of SET01 expresses that the influence of vertical stress is insignificant. For this reason, in SET02 to SET06, 10 kPa of the vertical stress was applied. In SET02 greater size of gravel (Gravel 2) was used than in SET01 and 6 tests were carried out. In SET03, 04, 05 and 06 Gravel 2 was also used, but GTX1, GTX2, GTX3 and GTX4 were laid, respectively between the sub-soil and gravel. As the same

method proposed before, critical velocity and failure velocity were determined in each test. The test results are presented in Table 5.3.

Table 5.3 The critical velocity and failure velocity for each set of test.

No.	Gravel	O_{90} (mm)	Geotextile	Critical velocity v_c (cm/s)	Failure velocity v_f (cm/s)
SET01	Gravel 1	-	Non	2.0	2.7
SET02	Gravel 2	-	Non	2.0	2.3
SET03	Gravel 2	7.0	GTX1	2.0	2.5
SET04	Gravel 2	1.07	GTX2	2.9	3.3
SET05	Gravel 2	0.6	GTX3	2.6	3.3
SET06	Gravel 2	0.11	GTX4	4.0	-

Both SET01 and SET02 have no geotextile covering the soil, and only the gravel is laid to protect the sub-soil. According to the proposal of Terzaghi (1922) on the gravel-soil filtration system (see Eq. (5-8)), Gravel 1 and Gravel 2 are not suitable filtration materials for the sub-soil that used in this test. In consequence, the soil erosion was quite serious.

$$\frac{d_{15,gravel}}{d_{85,soil}} < 4 \tag{5-7}$$

Though in SET01 and SET02 different gravel was used, the critical velocity is the same, as the pore within the gravel is large enough for soil particles to pass through easily. Once the flow reaches the critical velocity, the particles on the sub-soil surface will be migrated and then separated from the soil mass. In SET02 the larger particle size of gravel was used, which formed the greater space of erosion on the surface of sub-soil, and then failure erosion occurred more easily. As shown in Table 5.3, the failure velocity of SET02 is smaller than SET01.

According to the proposition of Scherzinger (1984) that discussed in section 2.5.1, the critical erosion flow velocity ($v_{F,crit}$) of the gravel filter-subsoil interface is:

$$v_{F,crit} = Fr_{crit} \times n_F \times \sqrt{\frac{\gamma'_{sB} \times d_{50B}}{\rho_w}} \qquad (2\text{-}19)$$

In this test, Gravel 1 (n_F = 0.44) and Gravel 2 (n_F = 0.47) were used to cover on the sub-soil with γ'_{sB} = 16.4 kN/m^3 and d_{50B} = 0.120mm respectively and Fr_{crit} = 0.65 is adopted to evaluate the critical erosion flow velocity ($v_{F,crit}$). Hence,

For Gravel 1: $v_{F,crit} = 1.27 cm/s$

For Gravel 2: $v_{F,crit} = 1.36 cm/s$

To compare with the result that shown in Table 5.3, the critical erosion flow velocity ($v_{F,crit}$) that evaluated according to the theory of Scherzinger (1984) is lower than the critical velocity (v_c) that obtained from this test. Because of those two methods to decide the timing of soil erosion occurred are different. In PET test, the variation of water turbidity was adopted to decide the erosion critical velocity of sub-soil but for the theory of Scherzinger is unknown.

Moreover, according to the test result of Brauns (1985) (see Figure 2.13), the critical erosion hydraulic gradient ($i_{F,crit}$) for SET01 that used Gravel 1 is $i_{F,crit}$ = 0.109 and for SET02 that used Gravel 2 is $i_{F,crit}$ = 0.039. Although water head difference is unable to be accurately measured when the soil starts to erode due to limitations of water pressure head loss meter as mentioned above, the test data acquired before soil erosion can be documented as reference.

Figure 5.14(a) shows the variation of water turbidity under the hydraulic gradient i = 0.125 by SET01-T09. It can be seen that under this hydraulic gradient which larger than that obtained by Brauns ($i_{F,crit}$ = 0.109), the turbidity decrease to zero that expresses the sub-soil without erosion. Figure 5.14(b) shows the similar state by SET02 with SET01. The sub-soil under the hydraulic gradient (i = 0.042) that larger than that obtained by Brauns ($i_{F,crit}$ = 0.039) is stable. It indicates that the theory of Brauns (1985) is not suitable for all soil and how to define the soil erosion is a key point.

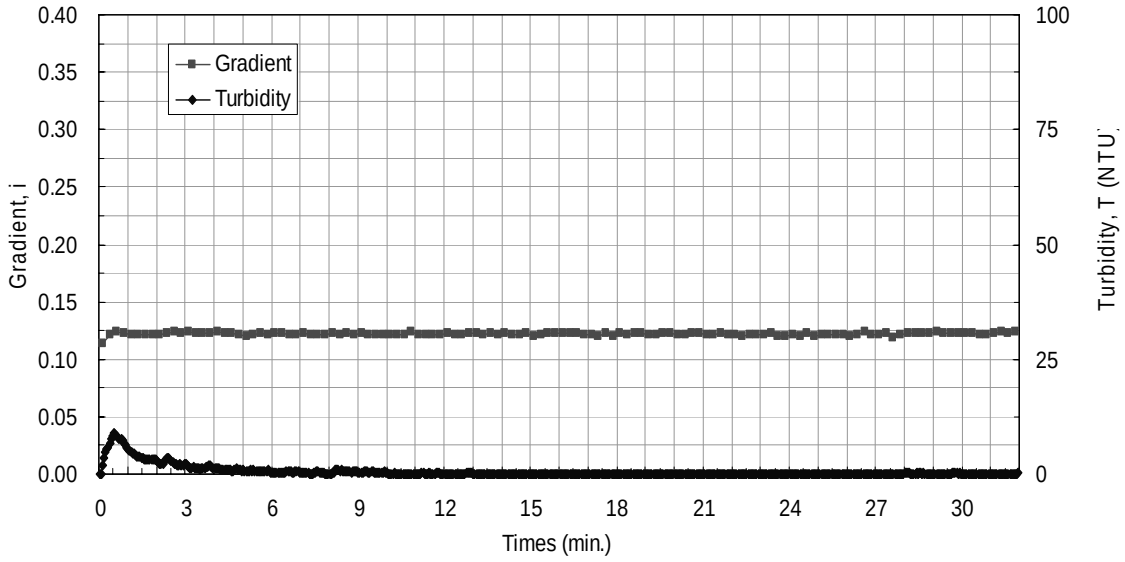

(a) SET01 (T09), i = 0.125

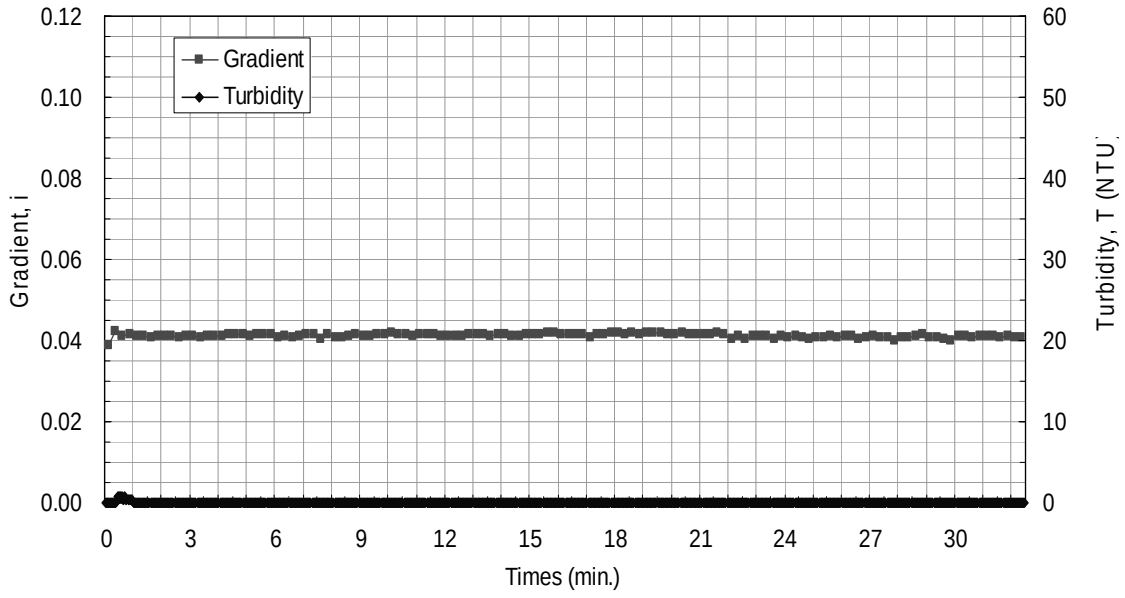

(b) SET02 (T13), i = 0.042

Figure 5.14 The variation of water turbidity with time.

In SET03, GTX1 was used to cover the sub-soil, but the opening size is larger than the soil particle size (see Figure 5.15), and consequently the critical flow is the same with SET01 and SET02. This indicates that the function of GTX1 on protecting the sub-soil is insignificant.

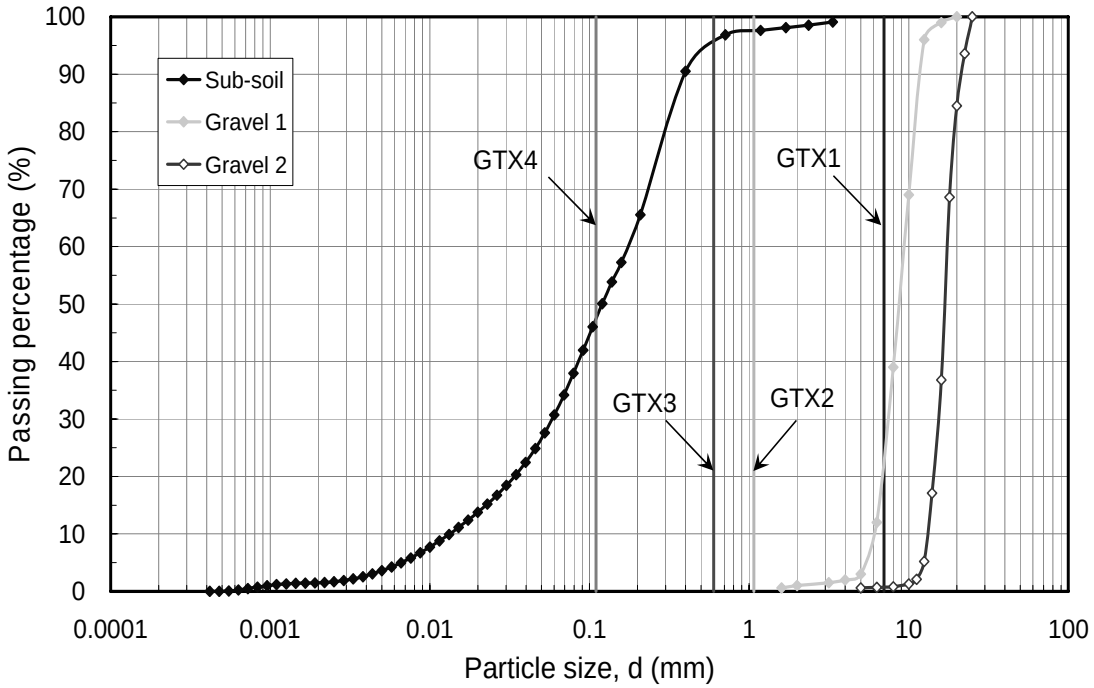

Figure 5.15 The relationship between the opening size of the geotextiles and the particle size distribution of the sub-soil and the gravels.

In SET04 is laid GTX2 between the gravel and the sub-soil. The critical velocity raise to 2.9 cm/s and the failure velocity is 3.3 cm/s. As shown in Figure 5.15, the opening size of GTX2 is almost the same with d_{98} of the sub-soil. The geotextile performed to protect sub-soil. Compared to the results of SET04 and SET05, it seems that the performance of GTX2 is better than GTX3 even if the opening size of GTX3 is smaller than GTX2. As Figure 5.15, it can be seen that the opening size of GTX3 almost equals to d_{95} of the sub-soil. As the relationship between opening size of geotextile and the particle size of sub-soil of SET04 and SET05 is very close, the effect on soil erosion of the opening size of GTX2 resembles GTX3. Nevertheless, the GTX2 is thicker than GTX3 and the diameter of fiber of GTX2 is larger than GTX3. Therefore, the fibers of GTX2 could retain fine soil particles like the weir under small flow velocity even through the soil particles have been departed the sub-soil surface and consequently have larger critical velocity than the thin geotextile (see Figure 5.16). However, as soon as the flow velocity increases continuously, the retaining effect of the fibers will not be obvious.

Moreover, the larger diameter of fiber can transmit the normal stress that applied

above to the surface of sub-soil well and to form a wider consolidation area. The soil particles which are located in the consolidation area are not easy to be eroded and will form the vault effect. Therefore, it is better than the thin fiber that the thick fiber resists the soil eroded which locate in the consolidation area (see Figure 5.17). Besides, for the identical opening size of geotextile, the percent opening area (POA) of woven geotextile that with the thick fiber is smaller than that with the thin fiber in the same cover area. For those reasons, to avoid the sub-soil erosion, use the woven geotextile that with thick fiber displayed better performance than thin one based on the same opening size of geotextile.

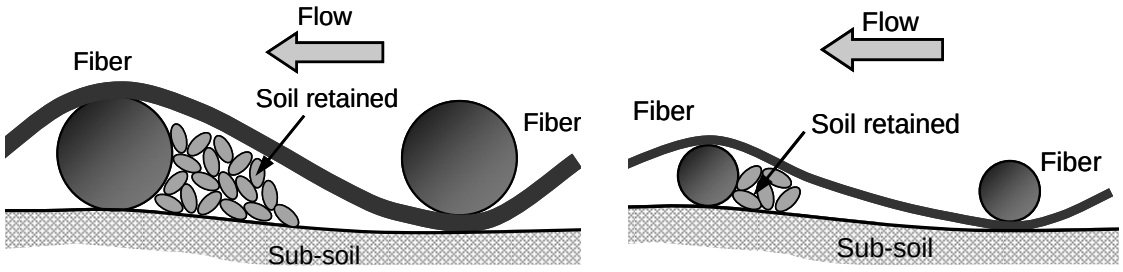

(a) Thick fiber (b) Thin fiber

Figure 5.16 The influence of fiber thickness of non-woven geotextile on retaining soil particle.

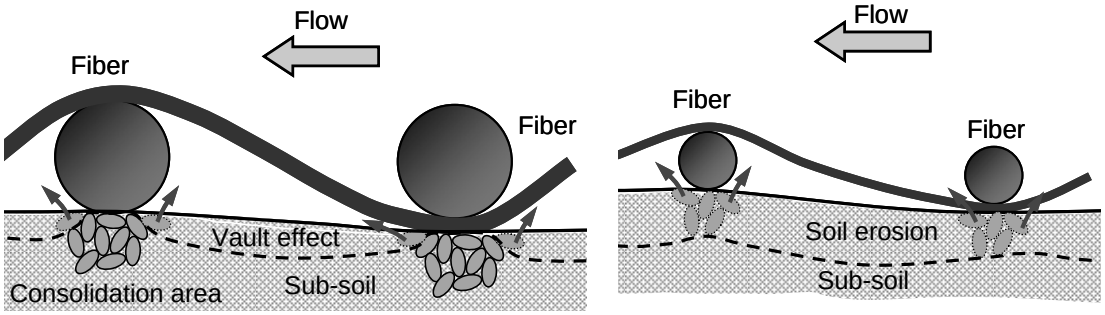

(a) Thick fiber (b) Thin fiber

Figure 5.17 The consolidation area and vault effect of non-woven geotextile.

Moreover, the critical velocity of SET06 is 4.0 cm/s. The opening size of GTX4 is 0.11 mm and almost equals to d_{50} of the sub-soil. It is clear that the relationship of opening size of geotextile and particle size of sub-soil is the key factor. According to

the retention criteria under uni-directional flow (see Table 2.1), the examination results of these four geotextiles used is shown in Table 5.4. In addition, the failure velocity of SET06 is absent in this study due to the limitation in flow velocity capacity of the PET equipment (v_{max} = 4.5 cm/s).

Table 5.4 The examined results of the retention criteria of test materials under the uni-directional flow.

References	Geotextile	Retention criteria	GTX			
			1	2	3	4
Calhoum (1972)	WN	$O_{95} < d_{85}$	NG	NG	NG	-
Ogink (1975)	WN	$O_{90} \leq d_{90}$	NG	NG	NG	-
	NW	$O_{90} \leq 1.8d_{90}$	-	-	-	OK
Schoeber and Teindl (1979)	WN and thin NW	$O_{90} \leq (2.5 \sim 4.5)d_{50}$	NG	NG	NG	OK
Giroud (1982)	WN NW	$O_{90} \leq (9 / Cu')d_{50}$	NG	NG	NG	NG
Heerten (1981)	WN NW	$O_{90} < 10d_{50}$	NG	OK	OK	OK
		$O_{90} \leq d_{90}$	NG	NG	NG	OK
Loudière et al. (1982)	WN NW	$O_{90} < d_{95}$	NG	NG	OK	OK
DGEC (1986)	WN NW	$O_{90} < 10d_{50}$	NG	OK	OK	OK
		$O_{90} < 2d_{90}$	NG	NG	OK	OK
Christopher and Holtz (1985)		$O_{95} < (1 \sim 2)d_{85}$	NG	NG	OK	OK

Note: WN = Woven ; NW = Non-woven

According to the test result, only GTX4 is well adopted to protect this sub-soil with uni-directional tangential flow. When the examination of the retention criteria was checked under uni-directional perpendicular flow (Table 5.4), some of them give us the same conclusion (Schoeber and Teindl (1979), Heerten (1981)). Moreover, the role of

the flow velocity is very important. Then these criteria for uni-directional perpendicular flow are not suitable for tangential flow.

Figure 5.18 shows the variation of the critical velocity (v_c) with the ratio of O_{90} of the geotextile to d_{90} of the sub-soil according to our test results. When $O_{90}/d_{90} < 1.0$ it is quite obvious that the critical velocity increases. Hence, the retention criterion of geotextile under uni-directional parallel flow can be proposed as below,

$$O_{90} < d_{90} \tag{5-8}$$

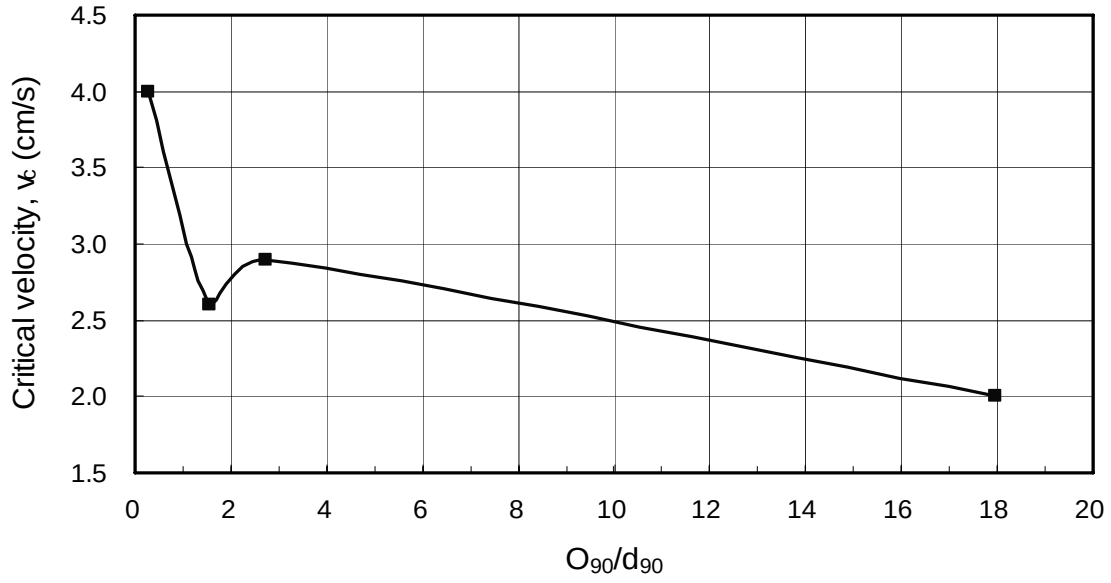

Figure 5.18 The variation of v_c with O_{90}/d_{90}.

5.6.3 Soil erosion rate and erosion equation

The variation of mass of soil erosion with time for each test was summarized in Appendix IV. Additionally, soil erosion rate of each test is also calculated according to the analysis procedure described in section 5.4.2. Figure 5.19 shows the relationship between the velocity and the soil erosion rate (m') of SET01. As shown, the influence in different vertical pressure is insignificant. This is because the vertical pressure is transmitted to the soil surface through gravel. However, as the water flows through and erodes the soil from space between gravel particles, the vertical pressure will not influence the behavior of erosion. Furthermore, the water flow induces pore pressure and reduces the effective stress small enough in the soil surface to cause the particles to

separate and to migrate intensely away from the sub-soil mass and to pass through the gravel. Hence, there is a close relationship between preventing the sub-soil erosion and controlling gravel cover area. That was already concluded in Chapter 3.

According to the test of Slot Erosion Test (SET) and Hole Erosion Test (HEL), the following equation of soil erosion rate was proposed by Wan and Fell (2003).

$$m' = \kappa \times (\tau - \tau_c) \tag{5-9}$$

Where κ is the coefficient of soil erosion, τ is the shear stress in the soil surface due to water flow, and τ_c is the critical shear stress.

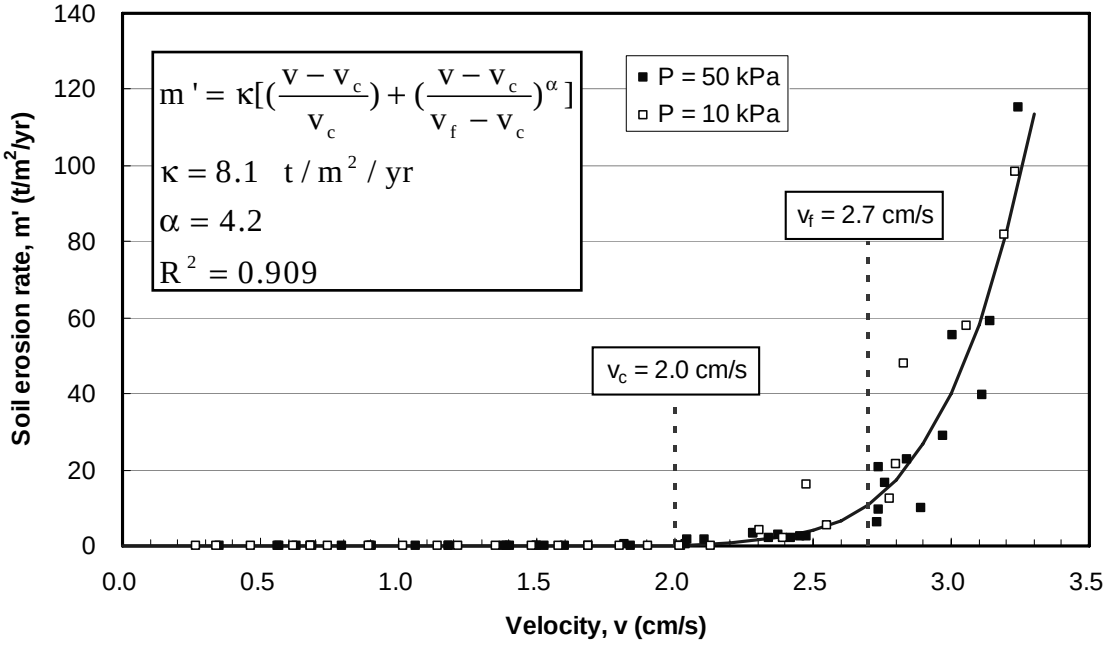

Figure 5.19 The relation of the velocity and the soil erosion rate (SET01).

For our test, the shear stress in the soil surface (τ) is unable to obtain but the flow velocity and water turbidity is measured during testing. As above-mentioned, the relationship of soil erosion rate and velocity can be obtained. As shown in Figure 5.19, the soil erosion rate curve is not linear and relate to critical velocity (v_c) and failure velocity (v_f). Hence, the soil erosion rate can be determined with the equation below,

$$m' = \kappa \times \left[(\frac{v - v_c}{v_c}) + (\frac{v - v_c}{v_f - v_c})^{\alpha} \right] \geq 0 \qquad v > v_c \tag{5-10}$$

Where κ and α are the soil erosion parameters, α is a non unit coefficient and the unit of κ depends on soil erosion rate (m'). The value of κ and α are related to the sub-soil/gravel particle dimension, the hydraulic condition, and the cover situation on the surface of sub-soil. To evaluate the soil erosion rate, there are four unknown parameters must be predetermined by test.

Figure 5.20 and Figure 5.21 present the result of regression curve of soil erosion rate equation of SET02 and SET03, respectively. The soil erosion parameters are summarized in Table 5.5.

Table 5.5 The soil erosion parameters of SET01, SET02, and SET03.

Test	Gravel	Geotextile	κ (t/m^2/yr)	α
SET01	Gravel 1	-	8.1	4.2
SET02	Gravel 2	-	7.0	1.8
SET03	Gravel 2	GTX1	1.2	5.6

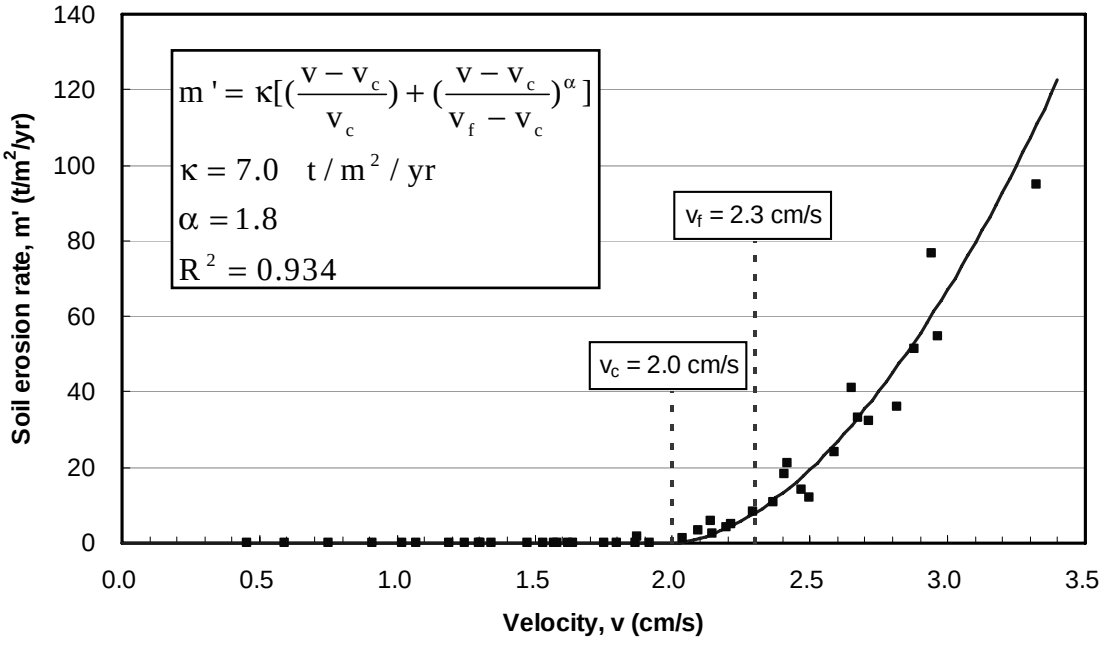

Figure 5.20 The soil erosion rate curve and equation (SET02).

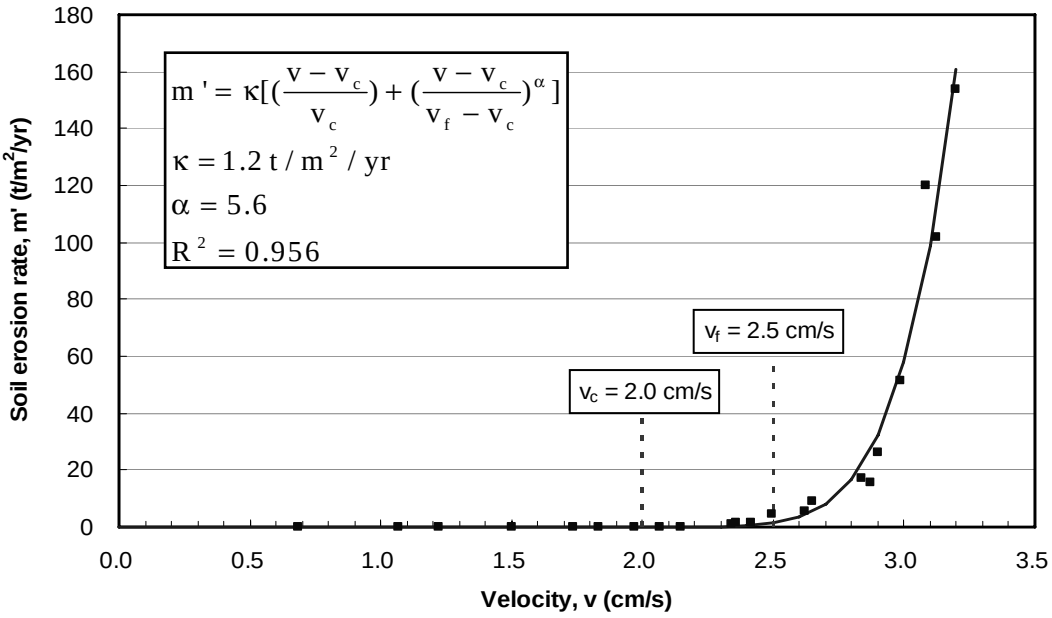

Figure 5.21 The soil erosion rate curve and equation (SET03).

Comparing the curves of soil erosion rate of SET01 with SET02 (see Figure 5.22), it can be seen that the erosion rate of SET02 increases faster than SET01 when the flow velocity is larger than v_c. That is because the gravel of SET02 (Gravel 2) is coarser, the aperture formed are larger. Then the mass of soil involved by erosion is larger too. Once the velocity increases to a certain value ($>v_f$), soil erosion becomes very serious, and the difference of the effect on retaining soil particles between the two gravels is not obvious.

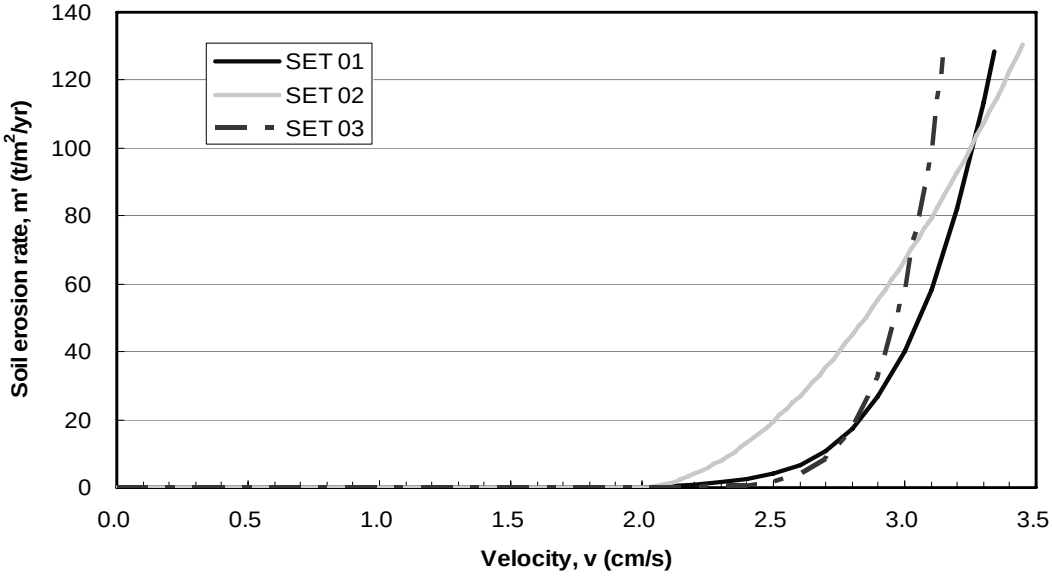

Figure 5.22 The curves of soil erosion rate of SET01, SET02, and SET03.

Figure 5.22 also shows the relationship of soil erosion rate between SET02 and SET03. In the initial stage when the soil starts to erode, the geotextile performs to protect the sub-soil and results in a smaller soil erosion rate (κ_{02} = 7.0 t/m^2/yr, κ_{03} = 1.2 t/m^2/yr). After a certain velocity, the soil erosion rate of SET03 suddenly accelerates and exceeds the erosion rate of SET02. Figure 5.23 shows the reasons. Under the smaller flow velocity, the fibers of geotextile develop the capacity of retaining soil particles due to the geotextile laying on the sub-soil. However, the mass of soil erosion increases with increasing flow velocity and therefore form a gap between sub-soil and gravel (see Figure 5.23) due to the fact that geotextile sustains the gravels. In this situation, the sub-soil eroded by the flow under the condition that almost has not been protected by the gravel and the geotextile and therefore could cause greater erosion rate than SET02. Hence, it is even more unfavorable to lay unsuitable geotextile than not to lay any geotextile on the sub-soil.

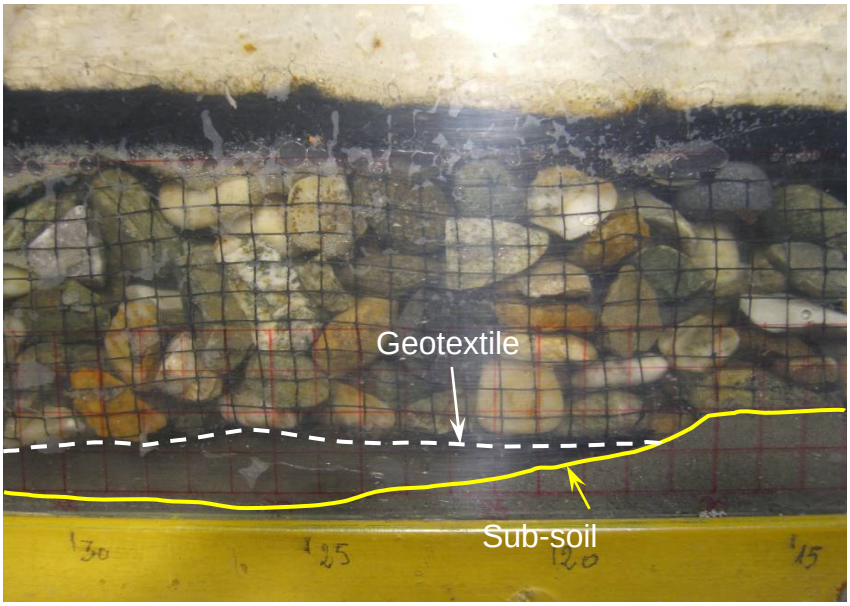

Figure 5.23 The profile of soil erosion (SET02).

Figure 5.24 presents the soil erosion rate curves of SET04 using GTX2. It can be seen that the soil erosion behavior is different from that of SET03. Once the flow velocity is larger than v_c, the soil erosion rate increases to a peak value as the flow velocity increases. Comparing v_c and v_f of SET02 with SET04, the efficiency of laying the GTX2 for protecting the soil erosion is obvious. When the flow velocity reaches v_c, soil erosion occurs and the mass of soil erosion increases progressively. While the particles of eroded soil are migrating, coarse soil particles would deposit on the

original sub-soil and form a natural filter layer gradually below the geotextile in the down stream of the cell room first. As soon as the natural filter layer has formed, the sub-soil will not continue to erode and the water turbidity will decrease (see Figure 5.25).

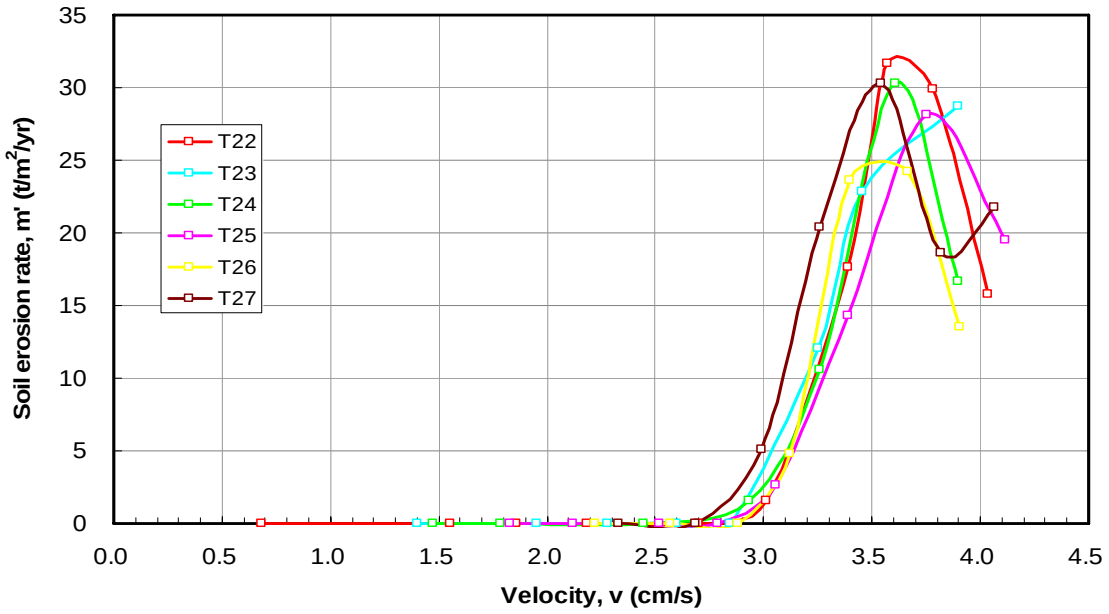

Figure 5.24 The soil erosion rate curves of SET04 tests.

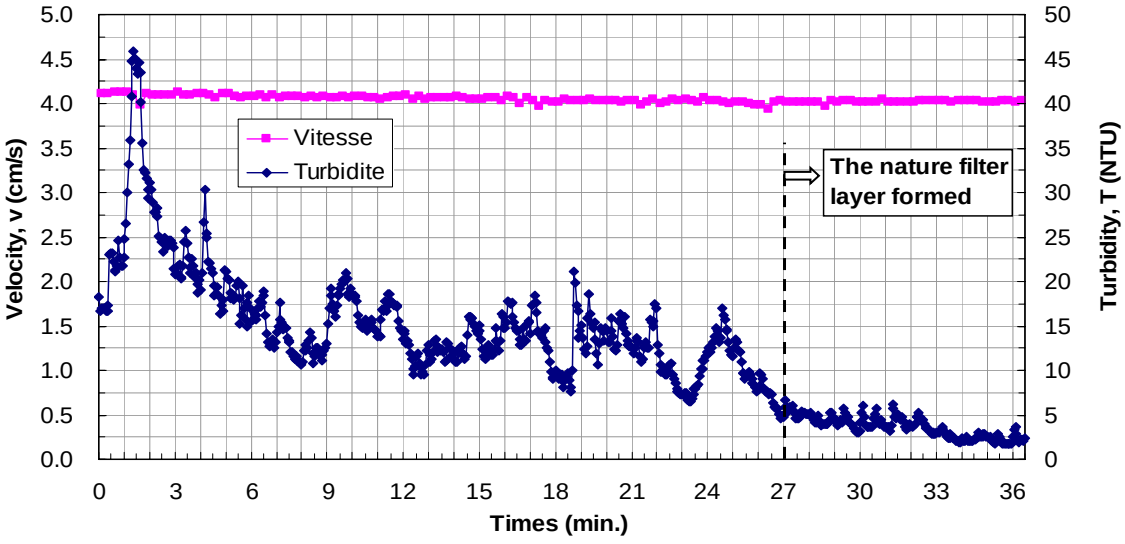

Figure 5.25 Water turbidity after the nature filter layer formed (T22).

Yet increases the flow velocity, in the down stream area that have already been formed a stable nature filter layer and the sub-soil will not be eroded again. But soil

erosion will take place in the up stream area where a natural filter layer is not yet formed. The state of the soil can be observed through the observation window of cell room that the “headward erosion” occurred on the soil surface (see Figure 5.26). Based on these reasons, the soil erosion rate not increases without end. Once a stable natural filter layer is formed completely (see Figure 5.27), even if flow velocity accelerates, soil erosion rate will not necessarily increases. The time needed to let soil erosion rate reach peak value does not only relate to the flow velocity but also depend on the duration of water flow. Under the smaller velocity (larger than v_c), the natural filter layer formed slowly, and it formed fast under the high flow velocity.

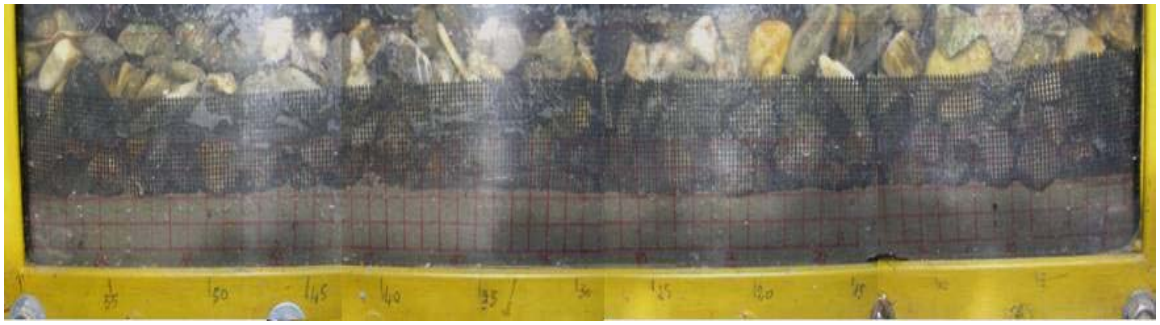

(a) v = 2.33 cm/s (Non erosion)

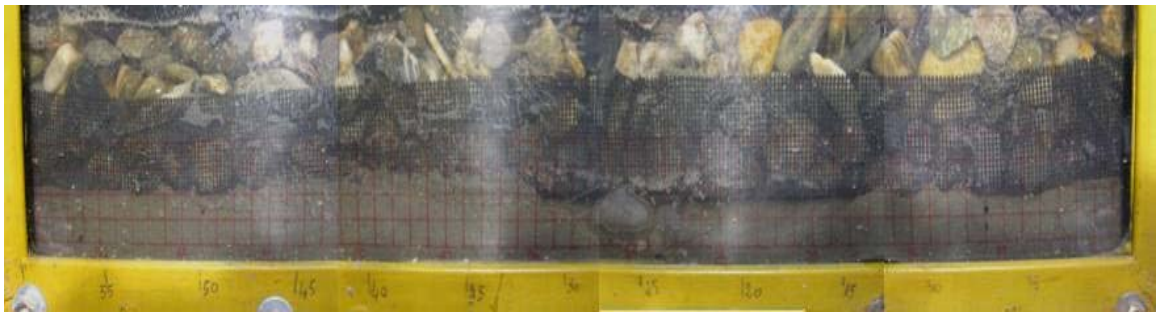

(b) v = 3.54 cm/s (Failure erosion)

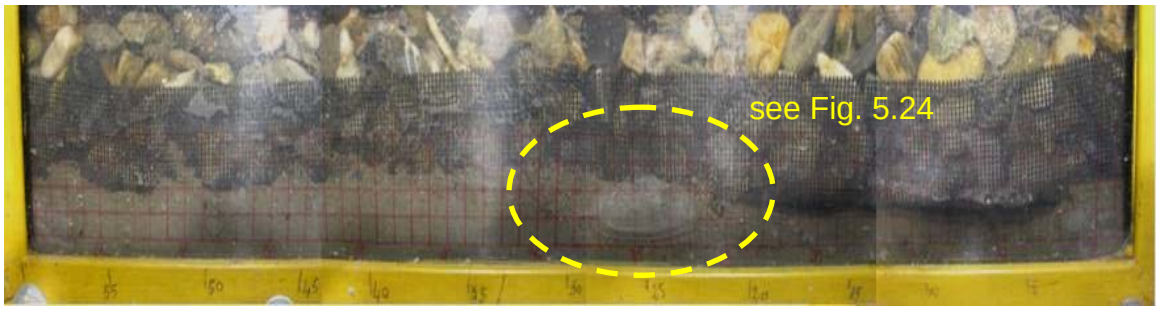

(c) v = 4.06 cm/s (Failure erosion)

Figure 5.26 Headward erosion behaviors (T27, SET04).

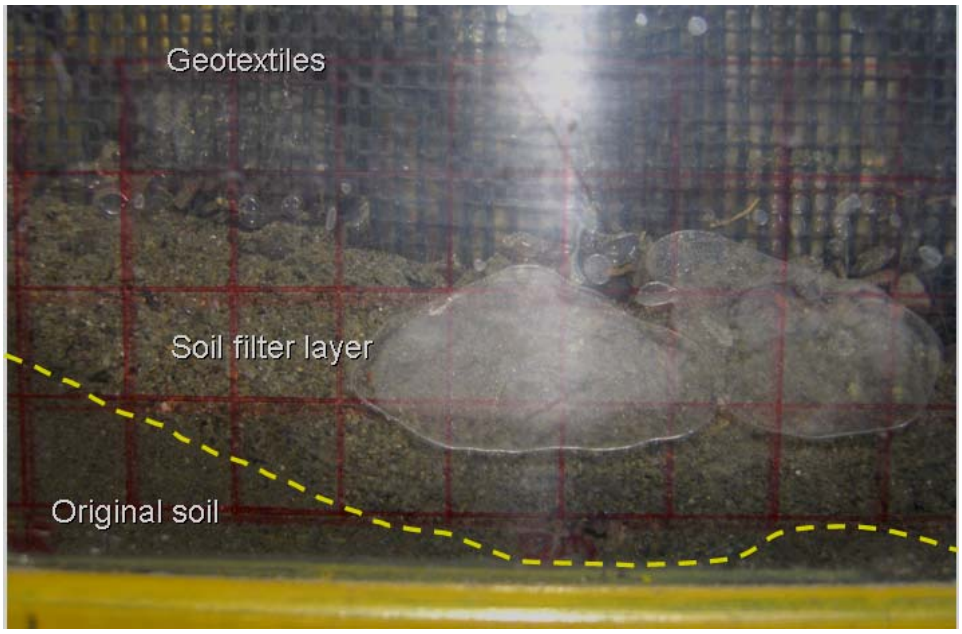

Figure 5.27 The detailed view of the nature filter layer formed (T27, SET04).

In addition, the post-peak erosion behavior is very complicated. It depends on the headward erosion behavior, such as in this test, once the headward erosion occurs and reaches the boundary of steel cell room, the soil erosion behavior will stop, and the decrease of soil erosion rate is inevitable. However, the in-situ condition, like this circulation behavior that soil erode in up stream and then the coarse particles deposits to form a natural filter layer in down stream will take place constantly, and consequently is more complicated for soil erosion rate.

Figure 5.28 presents the soil erosion rate of SET04. The erosion rate equation obtained only adopted the test data before the peak value. As shown, the soil erosion parameters κ = 13.93 t/m^2/yr and α = 0.96. The erosion rate curve is similar to a straight line.

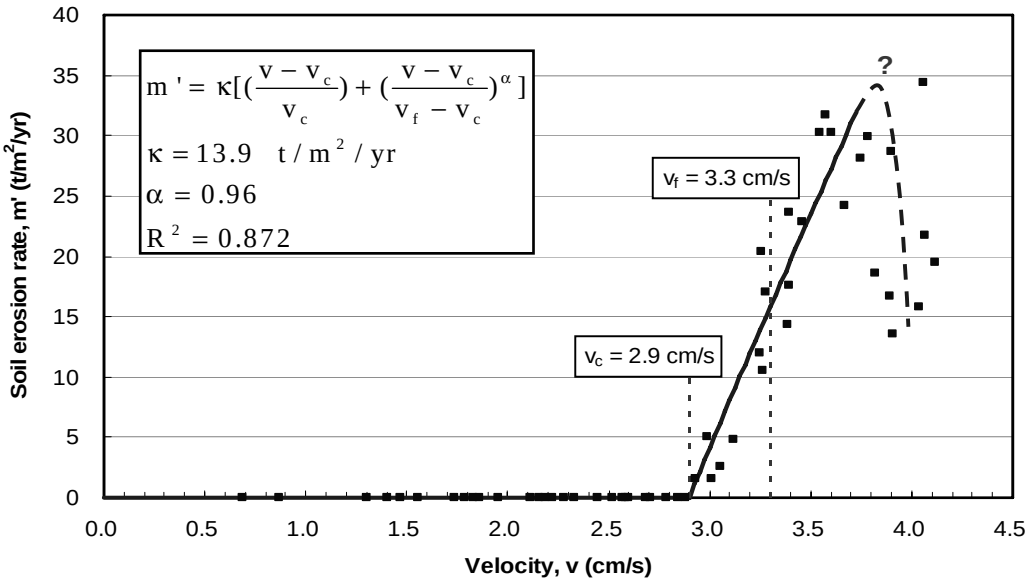

Figure 5.28 The soil erosion rate curve and equation (SET04).

In addition, the soil erosion rate curve and equation of SET05 are presented in Figure 5.29. Comparing the soil erosion curve of SET04 with SET05 (see Figure 5.30), there are very obvious differences on the performance of preventing soil erosion between GTX2 and GTX3. As shown, the soil erosion rate of SET05 is smaller than SET04 under the same flow velocity. That is due to the fact that the opening size of GTX3 is smaller than GTX2 which results in easier formation of a natural filter layer, even if the critical velocity of GTX3 is smaller than GTX2.

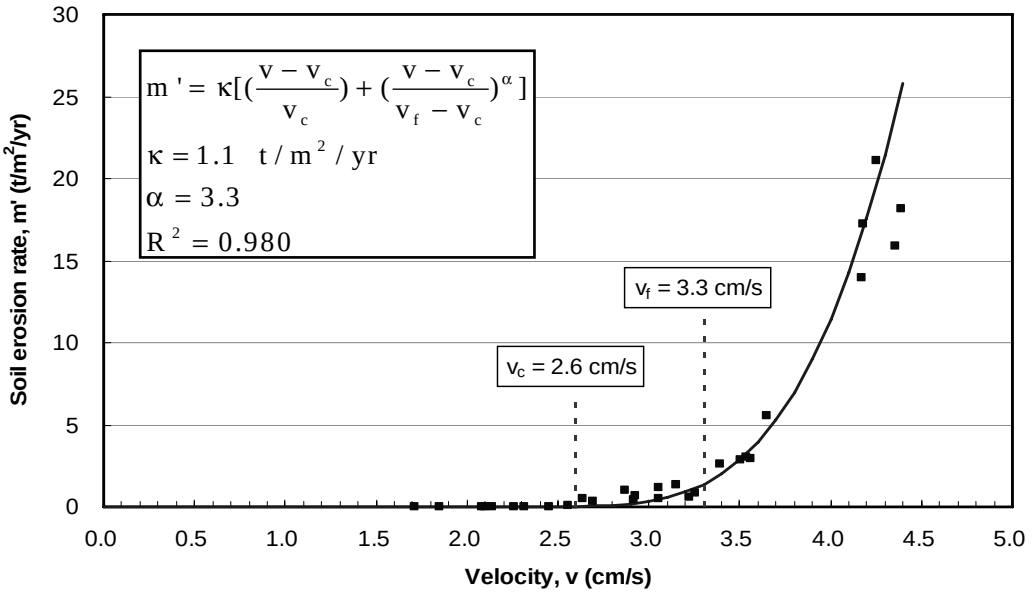

Figure 5.29 The soil erosion rate curve and equation (SET05).

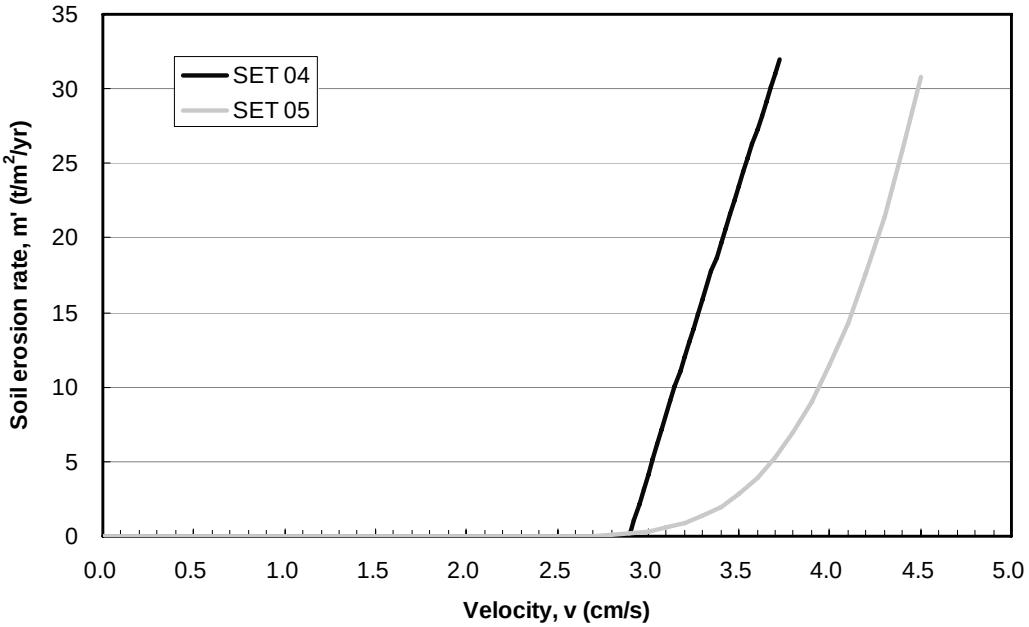

Figure 5.30 The curves of soil erosion rate of SET04 and SET05.

Figure 5.31 presents the test data and soil erosion rate curve of SET06. Because of the capacity limitation of the equipment of PET, the maximum velocity of the water supply system is 4.7 cm/s. Such a flow velocity is not enough to reach the failure velocity for SET06. Based on this reason, the equation form of soil erosion rate is different from those of other tests. However, the performance of preventing the soil erosion is more satisfactory than the other geotextiles used in this study.

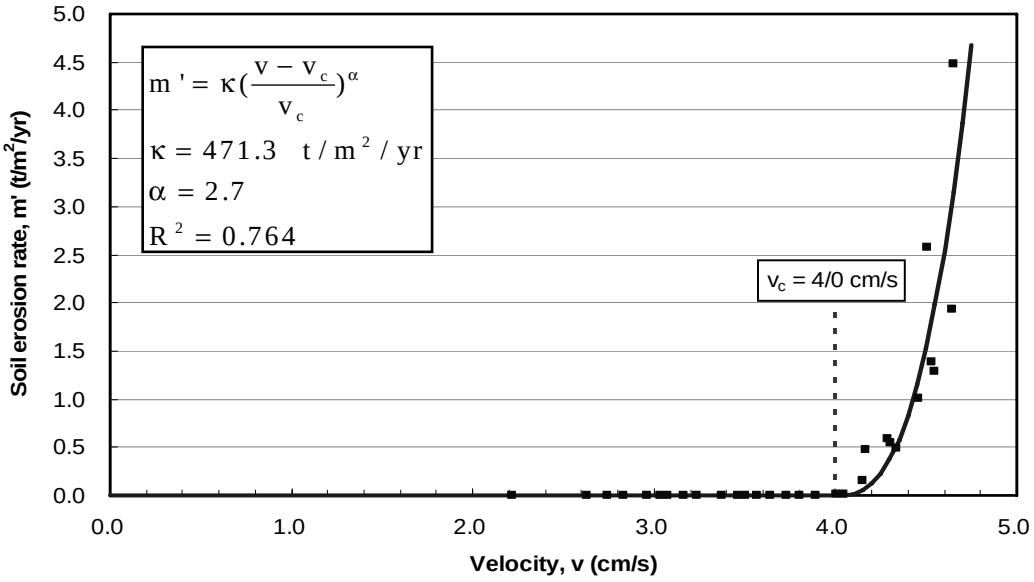

Figure 5.31 The soil erosion rate curve and equation (SET06).

5.6.4 Investigation of the particle size distribution of washout soil

The soil washed out is collected in several different flow velocities of T15 (SET02) and T16 (SET02). Table 5.6 summaries the amount of soil collected during 10 minutes of test duration and the soil erosion rate (m'_{10}) is evaluated.

Table 5.6 The amount of soil collected during 10 minutes.

Test No.	v (cm/s)	Erosion state	Amount (g)	m'_{10} ($t/m^2/yr$)	m'_{th} ($t/m^2/yr$)
T15	2.15	Steady erosion	8.02	2.59	2.76
	2.68	Failure erosion	94.66	30.56	29.05
T16	2.20	Steady erosion	13.52	4.36	4.28
	2.94	Failure erosion	141.82	45.79	48.64

m'_{th} : Calculate from the equation of soil erosion rate of SET02.

Comparing the soil erosion rate from the amount of soil collected (m'_{10}) with the soil erosion rate equation (m'_{th}), it can be seen that the results is close, proving that it is reasonable to predict the soil erosion rate with the equation.

In order to understand the relationship between the particle size of washed-out soil and flow velocity, particle size distribution analysis of the soil collected was conducted (see Figure 5.32). As shown, the particle size distribution of washed-out soil depends on flow velocity. Under the smaller flow velocity that sub-soil in the steady erosion condition, such as v = 2.15 cm/s and v = 2.20 cm/s, the maximum size of soil particle collected is 0.3 mm, and it is obvious that the size distribution of washed out soil is finer than the original sub-soil. The particles size of washed-out soil increases as the flow velocity accelerates. Once the flow velocity reaches 2.94 cm/s, the particle size distribution of soil washed out is similar to the original sub-soil.

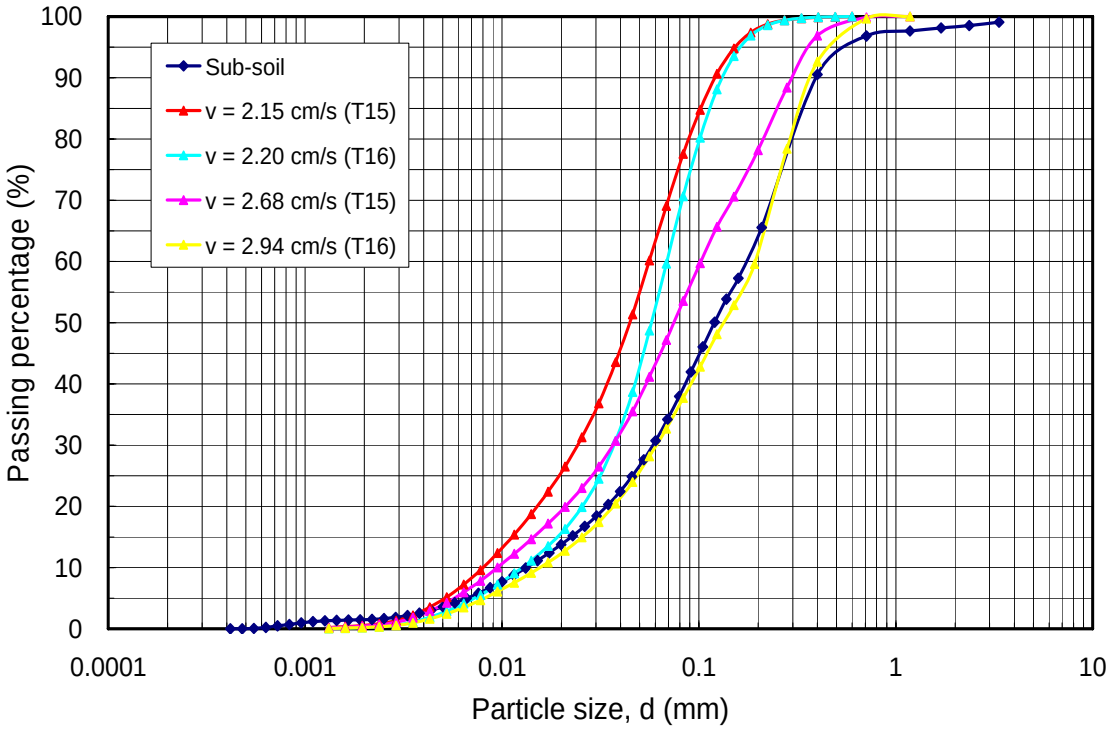

Figure 5.32 The granulometry of the soil washout.

5.7 Tangential erosion mechanism

As previously mentioned, the existence of geotextile applied on the sub-soil surface will influence the erosion behavior, and will present different soil erosion mechanism.

1. No geotextile or unsuitable geotextile used:

As described in SET01, SET02, and SET03, v_c is related to the sub-soil condition, such as particle distribution or cohesion. Moreover, v_f is related to the gravel condition covered on the sub-soil. Figure 5.33 shows the soil erosion mechanism of the sub-soil without the geotextile or with the unsuitable geotextile. Under the flow velocity that lower than v_c, the sub-soil is stable and no erosion is observed. If the velocity is larger than v_c, erosion will take place but the erosion rate is steady and the soil erosion rate is not large until the velocity reaches v_f. Once the velocity reaches v_f, the soil erosion rate increases suddenly and the mass of soil erosion is irregular with time. The failure erosion occurs on the surface of sub-soil and will be decisive on the failure of the riverbank.

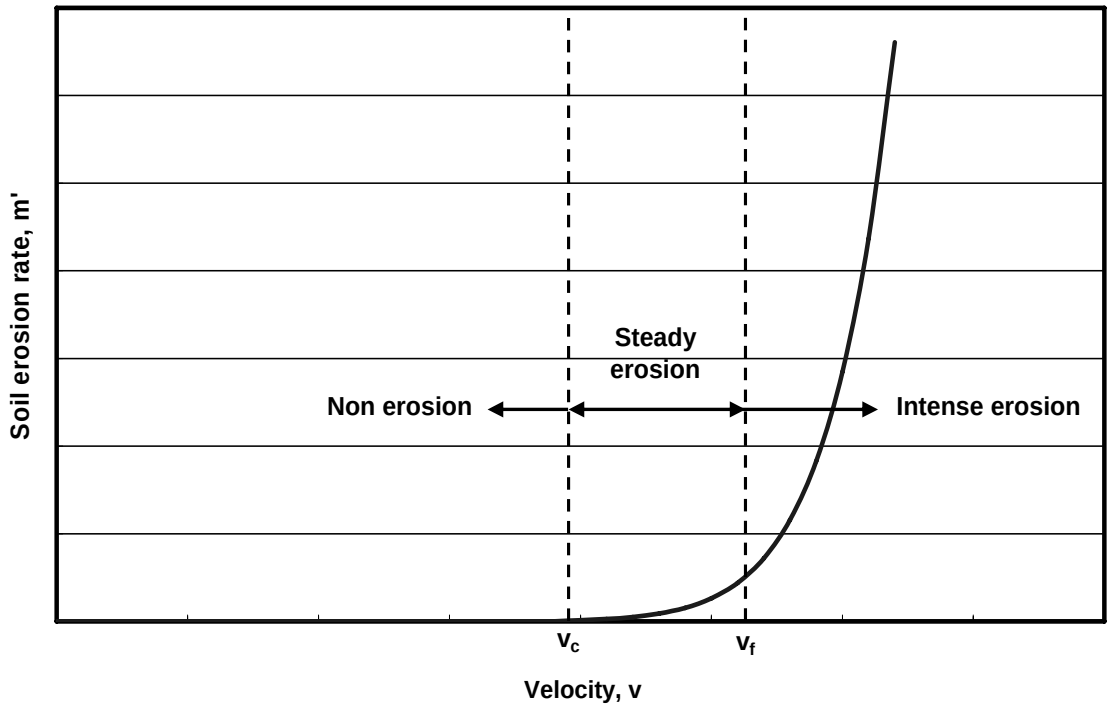

Figure 5.33 Tangential erosion mechanisms when without geotextile or unsuitable geotextile used.

2. Laying geotextile on the sub-soil

As described in SET04, SET05, and SET06, the value of v_c and v_f depends on the opening size and the thickness of geotextile and is also related to the production method of geotextile. Comparing with the results without geotextile, v_c and v_f increase are obvious. Comparing Figure 5.34 with Figure 5.33, it can be seen that the soil behavior is different when the velocity is larger than v_f (GTX2, GTX3). Due to the fact that geotextile covers the sub-soil, fine particles will be washed out and therefore soil erosion rate will increase. Moreover, a natural filter layer will be formed while the soil erosion occurs. At the same time, the headward erosion will take place. If the mechanism of headward erosion and down stream deposit which forms the natural filter layer takes place continuously, the soil erosion rate will keep constant. Besides, if the phenomenon of headward erosion stops and if the natural filter layer is formed, the soil erosion rate will reduce.

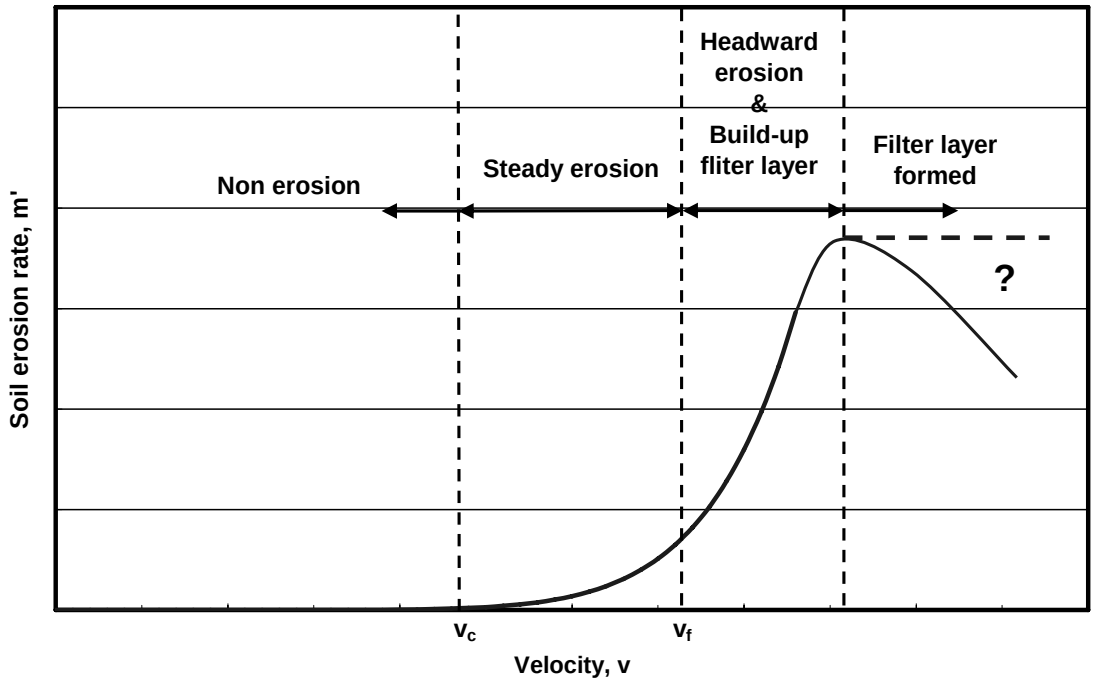

Figure 5.34 Tangential erosion mechanisms with geotextile.

5.8 Summary

Based on the previous discussions, some conclusions are reached as follows:

1. During the process of soil erosion, two characteristic flow velocities were introduced, the critical flow velocity (v_c) and the failure flow velocity (v_f), and were evaluated. When the flow velocity is lower than v_c, the sub-soil is stable and no soil erosion is observed. When the flow velocity is between v_c and v_f, the sub-soil is in the steady erosion state. Once the velocity larger than v_f, failure erosion will occur in the sub-soil and induce large mass of soil erosion.

2. The critical velocity and the failure velocity depend on the protection condition between the sub-soil and gravel. For the situation that no geotextile is used, v_c and v_f are correlate to the relation between the particle distribution of sub-soil and gravel. Moreover, v_c and v_f depend on the opening size and thickness of geotextile that used between the sub-soil and gravel.

3. If an unsuitable geotextile (too large opening size, too rigid geotextile) is used, not only the capability of resisting soil erosion will not be improved, but also soil erosion rate will increase due to the fact that the contact between gravels and sub-soil is impeded by the geotextile.

4. Using a suitable geotextile can decrease the soil erosion rate, and increase the critical velocity and failure velocity. a retaining criterion for uni-directional tangential flow was proposed as $O_{90} < d_{90}$.

5. In the situation of uni-directional tangential flow action, the revetment covered with geotextile can also form a natural filter layer. The time required for a natural filter layer to be formed depends on flow velocity, duration of water flow, geotextile condition, etc.

6. As mentioned in Chapter 1, the typical revetment using geotextile has a zone above the high water level and is subject to the uni-directional flow action. In this zone, the groundwater flow will induce soil particles to migrate toward the river side and cause internal erosion or piping. Part of soil particles will pass through the geotextile, and eroded soil particles will deposit behind the geotextile or clog up the fiber of geotextile (see Figure 5.35) and generate excess pore water pressure. The stability of the revetment decreases as the excess pore water pressure increases, while the internal erosion takes place continuously. On the other hand, the flow velocity of groundwater will decrease due to the clogging or blinding of geotextile. Once the flow velocity is lower than the critical velocity, internal erosion will stop and then the express pore pressure keeps constant. Hence, if one can know the express pore water pressure under the critical velocity, it is possible to examine the stability of the revetment in view of the above. This object is valuable to study by the parallel erosion test (PET) equipment in future.

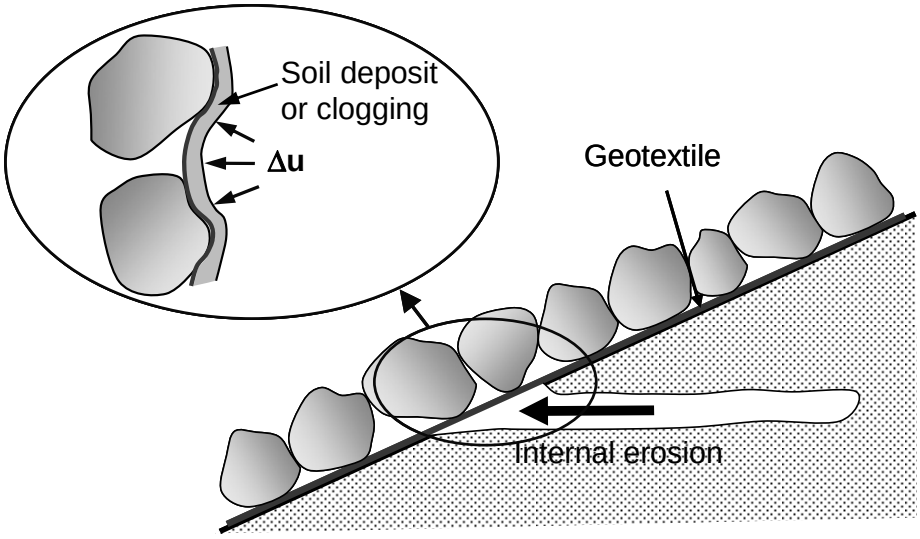

Figure 5.35 Schematic diagrams showing the internal erosion behavior.

Chapter 6 Conclusions and recommendations

According to the water flow direction, the revetment using geotextile can be divided into three zones. Zone 1 which above the high water level is in the uni-directional flow condition. Water flow in the vicinity of geotextile can be divided into two components, perpendicular flow (F_p), and tangential flow (F_t). Between high water level and low water level is zone 2, where the soil-geotextile interface is subject to bi-directional flow. For the short-term bi-directional cyclic flow, such as the hydraulic gradient caused by fluctuation of the water table due to sea waves or boats, the erosion behavior induced by the interaction of bi-directional cyclic perpendicular flow and tangential flow is complicated. Therefore, the full-scale flume test was performed. If the fluctuation of the water table is caused by tide or the aforementioned periodic drawdown of irrigation water, long-term bi-directional cyclic flow is generated. This study has developed a bi-directional cyclic perpendicular flow apparatus to model this flow situation. Finally, zone 3 is under low water level and the water flow along the revetment may cause parallel erosion. In order to understand the erosion behavior under this condition, the parallel erosion test was developed. Some conclusions drawn from the previous discussions of this research and suggestions to future works are as follows.

6.1 Conclusions

6.1.1 Short-term cyclic flow

1. The revetment laying geotextile that subjected to the wave action will cause different erosion behavior in the vicinity of geotextile. The water flow direction in the upper part of the revetment is mainly perpendicular to the geotextile (perpendicular flow) and causes local soil collapse due to pore water pressure increase. In middle part of the revetment is mainly parallel to the geotextile (tangential flow), the surface of geotextile is clean due to the tangential flow rush repeatedly and almost no soil particle clogging within the textile. Moreover, it is an association of the perpendicular flow with the tangential flow in the lower part of the revetment and it can be seen that a local natural filter layer formed under the geotextile in this study.

2. At the upper part of the revetment that subjected to the perpendicular flow, the thick geotextile that with higher number of constriction (SF1100) causes more serious soil collapse than thin geotextile that with the lower number of constriction (BF400).

3. According to the result of RLGT, BF400 and SF1100 are suitable to protect the revetment. Hence, the retention criteria of Heerten (1982), DGEC (1986), and Ragutzki (1973) suggested are too conservative.

4. Besides the criteria of permeability and retention, the quality of the contact between soil and the geotextile is an important factor too. Good contact could well maintain the soil.

5. The water turbidity obtained from the turbidity meter is high during the preliminary stage of the experiment, however, the turbidity gradually dropped as the time of the experiment increases. Moreover, under the action of greater wave energy, it takes longer for the turbidity to decrease, and it will stabilize to a constant that is higher than that of lower wave energy.

6. According to the result of RRGT, most of the deformation of the geotextile bag takes place in the first 24 hours of the experiment when the waves action and gradually alleviates as the time increases. The greatest settlement takes place on the water side and the greatest deformation of X-direction takes place in the middle part near the static water level. Moreover, increasing the impact energy of the wave also increase the deformation of the geotextile bag.

7. This full-scale model is a powerful product-testing tool, although cumbersome to bring into operation, is full of information for this type of study. The tests are unique because the hydrodynamic conditions generated in the bank are analogous to many real situations.

6.1.2 Long-term bi-direction cyclic flow

1. According to the test results, the soil-geotextile filter systems are stable for all of the specimens under large cyclic flow period, such as 600 sec/cycle. As soon as the cyclic period decreases to 300 sec/cycle, the soil specimens with small amount of silty content under lower normal pressure will causes soil boiling and produces large amount of soil washout and serious settlement. For this reason, the wave period is a key factor to design for the silty soil-geotextile filter system under cyclic flow condition.

2. The excess pore water pressure not having enough time to dissipate over a short period condition and also due to the low permeability of cohesive soil. Hence, the permeability of geotextile under bi-directional cyclic flow must be larger than that under uni-directional flow condition in order to dissipate the excess pore water pressure, especially for the short cyclic flow period. Moreover, the permeability of geotextile that used in cohesive soil must be also higher than that used in non-cohesive soil.

3. For pure sand, the soil structure is quite stable under various normal pressures. In consequence, the difference in pore water pressure, settlement, and the amount of soil loss are insignificant. Therefore, the permeability and retention criteria are suitable to design the pure sand-geotextile filter system.

4. For a well silty sand-geotextile filter system, except according with the filtration/drainage criteria, also need to prevent the local soil boiling in order not to produce large amount of soil washout and serious settlement. For this study, increasing the clay content (6.5%) or applying a higher normal pressure (140 kPa) are useful to prevent soil boiling.

5. For silty-sand under low normal pressure, an independent fine particle can move freely and clogs the soil-geotextile system or washout, and consequently produces the violent change of cyclic flow gradient index, *I*, in the beginning of testing. But this phenomenon of particle clogs within geotextile or washout is impermanent and soil boiling occurs will accelerates this phenomenon. Furthermore, the cyclic flow gradient index of clayey-silty sand specimen is quite close to 1.0 during testing. This implies that clogging, blocking, or particle loss is unlikely to occur during cyclic flow for clayey-silty sand.

6. As the gap-graded silty sand-geotextile filter system under lower normal pressure, the fine particle can moves easily within the void between coarse particles. If the geotextile is chosen based on the coarse particle distribution may cause large amount of fine particle loss. On the other hand, to choose geotextile based on fine particle distribution may cause the fine particle clogging. Hence, the retention and permeability criteria for bi-directional cyclic flow condition should be examined more carefully. Such as this soil condition, to determine the suitable material by testing was proposed.

7. According to the observation by stereomicroscope, there is some soil particles adhered to the fibre of geotextile that is contact with marbles and appeared darker colour. While no or very few particles are visible in the clean area that is not in

contact with marbles. It explains that the bridge network will be formed behind the geotextile where between the areas without marble contact area under the long-term bi-directional cyclic flow.

6.1.3 Tangential flow

1. In this study, water turbidity is adopted to estimate the soil erosion. According to the variation of water turbidity, the soil erosion into three classification were defined, non erosion, steady erosion, and failure erosion. When the flow velocity is lower than v_c, the sub-soil is stable and no soil erosion is observed. If the flow velocity is between v_c and v_f, the sub-soil is in the steady erosion state. Once the velocity larger than v_f, failure erosion will occur in the sub-soil and induce the large mass of soil erosion.

2. The critical velocity and the failure velocity are related with the particle size of sub-soil and gravel. For the situation that no geotextile is used, v_c is depend on the particle distribution of sub-soil and v_f is correlated to the particle distribution of gravel. In this study, the failure velocity increases as the gravel size decreases. In this situation that laying a geotextile between sub-soil and gravel, v_c and v_f increase as the opening size of geotextile decreases when the thickness of geotextiles are the same. Moreover, the critical velocity of thick geotextile is higher than thin geotextile when the opening size of geotextile is alike but they failure velocity is similar.

3. Under tangential flow condition, a suitable geotextile can form a natural soil filter layer below the geotextile and to avoid the sub-soil eroded. However, an unsuitable geotextile (too large opening size, too rigid geotextile) not only the capability of resisting soil erosion will not be improved, but also soil erosion rate will increase due to the fact that the contact between gravels and sub-soil is impeded by the geotextile. Hence, using geotextile to protect revetment should be chosen more carefully.

4. The thick and small opening size of geotextile displayed good performance in protecting revetment. According to the result of this test, a retaining criterion for uni-directional tangential flow is proposed as $O_{90} < d_{90}$.

6.2 Recommendations for future research

1. The quality of the cover block contact on the geotextile is one of the key factors of preventing the soil erode when the revetment is subjected to bi-directional cyclic flow. The effect of cover block on soil erosion of revetment requires more study to understand.

2. For the reinforced revetment using geotextile study, besides the deformation of geotextile bag and the change of pore water pressure and particle size distribution, it is quite important to know the variation of tension stress of the geotextile during wave action and is useful to understand the stress-strain mechanism of geotextile reinforced revetment under cyclic flow.

3. The critical velocity under the tangential flow depending on the particle size distribution of sub-soil. In order to understand the relationship between critical velocity and parameter of sub-soil, to use different graded of sub-soil and to carry out the tangential flow test for future research are needed.

4. In the uni-directional flow action zone, the stability of the revetment decreases as the excess pore water pressure increases, while the internal erosion takes place continuously. On the other hand, the flow velocity of groundwater will decrease due to the clogging or blinding of geotextile. Once the flow velocity is lower than critical velocity, the internal erosion will stop and then the express pore pressure keeps constant. Hence, if one can know the express pore water pressure under the critical velocity, it is possible to examine the stability of the revetment in view of the above. This object is valuable to study by the parallel erosion test (PET) equipment in the future.

List of references

ASTM D-5101-96 (1997), “Standard test method for measuring the soil-geotextile system clogging potential by the Gradient Ratio.” Annual Book of ASTM Standards, Section 4, Vol. 9, ASTM, Philadelphia, pp. 1016-1023.

Barsvary, A. K. and MacLean, M. (1981), “Engineering geotextiles, properties, use criteria, tests and list of acceptable products.” Report EM-45 Engineering Materials Office, Ministry of Transportation and Communications, Ontario, Canada.

BAW, Federal Institute for Waterway, Germany (1993), “Instruction card for the use of geotextilen filter in waterways.” Karlsruhe (in German).

Bertacchi, P. and Cazzuffi, D. (1985), “Geotextile filters for embankment dams.” Water Power and Dam Construction, December, pp. 11-18.

Bhatia, S.K. and Huang, Q., (1995), “Geotextiles filters for internally stable/unstable soils.” Geosynthetics International, Vol. 2, No. 3, pp. 537-565.

Blaza, J. (2002), “Stability of the banks – The behavior of the banks protected under the wave action.” The student training report, LIRIGM, Grenoble, France, 32 p (in French).

Bonelli, S., Brivois, O., Borghi, R., and Benahmed, N. (2006), “On the modeling of piping erosion.” Observation, analysis and modeling in complex fluid media, Special issue, Comptes Rendus Mecanique, Vol. 334, pp. 555-559.

Brauns, J. (1985), “Erosion in layered soil due to horizontal groundwater flow.” Water Management 75, Vol.10, pp. 448-453 (in German).

Calhoun, C. C. (1972), “Development of design criteria and acceptance specifications for plastic filter cloths.” Technical Report No. S-72-7, Army Waterways Experiment Station, Vicksburg, MI, pp. 6-55.

Caroll, R. G. (1983), “Geotextile filter criteria.” TRR916, Engineering Fabrics in Transportation Construction, Washington, D. C., pp. 46-53.

Cazzuffi, D., Faure, Y., and Fayoux, D. (1984), “Determine the characteristics of the geotextile filtration, comparison the results of various laboratories.” International Water Power and Dam Construction Conference “Materials for Dams 84”, Monte Carlo, Monaco (in French).

Cazzuffi, D., Mazzucato, A., Moraci, N., and Tondello, M. (1999), “A new test apparatus for the study of geotextiles behavior as filters in unsteady flow conditions: relevance and use.” Geotextiles and Geomembranes, Vol.17, No. 5-6, pp. 313-329.

CFGG, Committee French of the geotextiles and Geomembrances (1986), “General recommendation for using geotextiles on drainage and filtration.” French standards of tests, Boulogne Billancourt, April (in French).

Chang, D.T. and Nieh, Y.C. (1996), “Significance of gradient ratio test for determining clogging potential of geotextiles”, Recent Developments in Geotextile Filters and Prefabricated Drainage Geocomposites, ASTM STP, Vol. 1281, pp.113-131.

Chen, R.H. and Chen, C.N. (1986), “Permeability characteristics of prefabricated vertical drains”, Proceedings of the 3rd International Conference on Geotextiles, Vol. 3, Vienna, Austria, pp.785-790.

Chen, R. H., Ho, C. C., and Hsieh, A. T (2006), “Filtration behavior of geotextile under overburden pressure and bi-directional cyclic flow.” Proceedings of the 8th International Conference on Geosynthetics, 18-22 September, Yokohama, Japan, pp. 557-560.

Chen, R. H., Hsu, C. Y., and Ho, C. C. (2006), “Filtration behavior of geotextile in sandy soils subjected to bi-directional cyclic flow.” Proceeding of the 1st International GSI – Taiwan Geosynthetic Conference, December, Pingtung, Taiwan.

Chen, R.H., Kuo, J.T., and Lai, J.S. (2003), “Assessment of the failure of the revetment restoration work of Ho-Jin creek.”, Technical Report 484, Hydrotech Research Institute, National Taiwan University, 63 p. (in Chinese).

Chen, Y. H., Simons, D. B., and Demery, P. M. (1981), “Hydraulic testing of plastic filter fabrics.” Journal of Irrigation and Drainage Division, Proceedings of ASCE Vol.107, N IR3, pp. 307-324.

Chew, S. H., Tian, H., and Tan, S. A. (2003), “Erosion stability of punctured geotextile filters subjected to cyclic wave loadings – A laboratory study.” Geotextiles and Geomembranes, Vol.21, No. 4, pp. 221-239.

Chew, S. H., Zhao, Z. K., Karunaratne G. P., Tan S. A., Delmas Ph., and Loke K. H. (2000), "Revetment geotextile filter subjected to cyclic wave loading." Advances in Transportation and Geoenvironmental Systems Using Geosynthetics, ASCE Geotechnical Special Publication No.103, pp. 162-175.

Chin, Y. M., Nikraz, H. R., and Press, M. (1994), "Laboratory filtration performance of nonwoven geotextiles." Proceedings of 5th International Conference on Geotextiles, Geomembranes and Related Products, Singapore, Vol. 2, pp. 635-638

Christopher B. R. and Fischer G. R. (1991), "Geotextile filtration principles, practices and problems." 5th GRI Seminar on Geosynthetics in Filtration, Drainage and Erosion Control, Philadelphia, PA, pp. 6-9.

Christopher, B. R. and Fischer, G. R. (1992), "Geotextile filtration principles, practices and problems." Geotextiles and Geomembranes, Vol. 11, pp. 337-353.

Christopher, B. R. and Holtz, R. D. (1985), "Geotextile engineering manual." U.S. Department of Federal Highway Administration, Report FHWA-TS-86/203, National Highway Institute, Washington, D.C., USA.

Chung, W. B. (2007), "Filtration behavior and micro-observation of geotextiles under bi-directional cyclic flow." Master thesis, National Taiwan University, 142 p. (in Chinese).

DGEG, Committee Germany of Soil Mechanic and Foundations Engineering (1986), "Use and examination of civil engineering and hydraulic engineering." Series of publications of the DVWK, N 76, Ed. Verlag Paul Parey, Hamburg (in German).

Fannin, R. J. and Hameiri, A. (1999), "A gradient ratio device for compatibility testing in cyclic flow." Proceedings of Geosynthetics'99, Boston, USA, Vol. 2, pp. 1033-1042.

Fannin, R.J. and Pishé, R. (2001), "Testing and specifications for geotextile filters in cyclic flow applications." Proceedings of Geosynthetics 2001, Portland, Oregon, USA, pp. 423-435.

Farkouh, B. (1994), "Geosynthtics filter performance in the engineering of drainage: laboratory tests and observation in situ." Ph.D dissertation, Joseph Fourier University of Grenoble, France (in French).

Faure, Y. H. (1988), "Structure approach of the filter-draining behavior of the geotextile." Ph.D dissertation, Joseph Fourier University of Grenoble, France (in French).

Faure, Y. H., Elamir, A., Farkouh, B., Gendrin, P., and Reisinger, P. (1992), "Geotextile filter behavior with critical filtration conditions." Proceedings of the 1st International Conference "Geo-filters", Karlsruhe, Germany, pp. 209-216.

Faure, Y.H. and Le Lay, M. (2002), "Behaviour of geotextile filter for bank protection : full scale laboratory experimentation." Proceedings of the 7th International Conference on Geosynthetics, Nice, France, pp. 609-612.

FHWA (1989), "Geotextile design and construction guidelines." US Department of Transportation, Federal Highway Administration, Publication No. FHWA HI-90-001.

FHWA (1990), "Standard Specification for Geotextiles." US Department of Transportation, Federal Highway Administration, AASHTO M288-90, pp. 689-692.

Fischer, G. R., Christopher, B. R. and Holtz, R. D. (1990), "Filter criteria based on pore size distribution." Proceeding of the 4th International Conference on Geotextiles, Geomembranes and related products, Hague, Netherlands, Vol. 1, pp. 289-294.

Francoeur, J. (2001), "Applicability of the gradient ratio test under the conditions of flow alternated for the geotextile-soil systems." Ph.D dissertation, Montreal University, Canada (in French).

Ghosh, C. and Yasuhara, K. (2004), "Clogging and flow characteristics of a geosynthetic drain confined in soils undergoing consolidation." Geosynthetics International, Vol. 11, No. 1, pp. 19-34.

Giroud, J. P. (1982), "Filter criteria for geotextiles." Proceeding of the 2nd International Conference on Geotextiles, Las Vegas, Vol.1, pp. 103-108.

Giroud, J. P. (1996), "Granular filters and geotextile filters." Proceeding of Geofilters'96, Montréal, Canada, pp. 565-680.

Giroud, J. P., Delmas, P., and Artières, O. (1998), "Theoretical basis for the development of a two-layer geotextile filter." Proceedings of the 6th International Conference on Geosynthetics, Atlanta, USA, pp. 1037-1044.

Gourc, J. P. (1982), "Some aspects of the behavior of geotextile in soil mechanics." Ph.D dissertation, Scientific and medical University of Grenoble, France (in French).

Gourc, J.P. and Faure, Y.H. (1990), “Filter criteria for geotextiles.” Proceedings of the 4th International Conference of Geotextiles, The Hague, Netherlands, Vol. 4, pp. 949-971.

Haliburton, T.A. and Wood, P.D. (1982), “Evaluation of the US Army Corps of engineer gradient ratio test for geotextile performance.” Proceedings of the 2nd International Conference on Geotextiles, Las Vegas, Vol. 1, pp. 97-102.

Heerten, G. (1981), “Geotextiles in hydraulic engineering. Examination, application, probation.” Franzius-institute for Hydraulic (FIH), Waterways and Coastal Engineering University, Hanover, Germany, R.F.A., N 52, 261 p. (in German).

Heerten, G. (1982), “Dimensioning the filtration properties of geotextiles considering long-term condition.” Proceedings of the 2nd International Conference on Geotextiles, Las Vegas, Vol. 1, pp. 115-120.

Hoare, D. J. (1984), “Geotextiles as filter.” Ground Engineering, Vol.17, pp. 29-44.

Holtz, R. D., Christopher, B. R., and Berg, R. R. (1998), “Geosynthetic design and construction guidelines.” U.S. Department of Transportation, Federal Highway Administration, Washington, DC, Publication No. FHWA HI-95-038, 459 p.

Hsieh, E. T. (2006), “Soil – geotextile filter system influenced by cyclic flows under changing surcharges and fine contents.” Master thesis, National Taiwan University, 90 p. (in Chinese).

Hsu, C. Y. (2006), “Filtration behavior of geotextile under bi-directional cyclic flow.” Master thesis, National Taiwan University, 113 p. (in Chinese).

Hung, C. C., Shan, H. Y., Jean, G. Y., and Leu, A. L. (1998), “Infiltration tests and seepage analyses for reinforced and unreinforced clay embankment.” Proceedings of the 13th Southeast Asian Geotechnical Conference, Taipei, Taiwan, pp. 321-324.

Ingold, T. S. (1982), “An analystical study of geotextile reinforced embankments.” Proceedings of the 2nd International Conference on Geotextiles, Las Vegas, Vol. 2, pp. 683-688.

Ingold, T. S. (1985), “A theoretical and laboratory investigation of alternating flow criteria for woven structures.” Geotextiles and Geomembranes, Vol. 2, No. 1, pp. 31-45.

John, W. (1994), “Geomembrances and related products.” Proceedings of the 5th International Conference on Geotextiles, Geomembranes, and Related Products, Singapore, pp. 415-418.

Kenney, T. C. and Lau, D. (1986), “Internal stability of granular filters : Reply”, Canadian Geotechnical Journal, Vol. 23, pp. 420-423.

Koerner, R.M. (1998), “Designing with geosynthetics”, Prentice Hall, 816 p.

Koerner, R. M. and Ko, F. K. (1982), “Laboratory studies on long-term drainage capability of geotextiles”, Proceedings of the 2nd International Conference on Geotextiles, Las Vagas, USA, Vol. I, pp. 91-96.

Kohata, Y., Tanaka, M., Sato, O., and Hirai, T. (2006), “Clogging evaluation on cross-plane flow performance of geotextile filter.” Proceedings of the 8th International Conference on Geosynthetics, Yokohama, Japan, pp. 561-564.

Kutay, M.E. and Aydilek, A.H. (2005), “Filtration performance of two-layer geotextile systems.” Geotechnical Testing Journal, ASTM, Vol. 28, No. 1, pp. 1-13.

Lafleur, J., Francoeur, J., and Faure, Y. H. (2002), “Piping, bridging and blinding of geotextiles as evaluated from the gradient ratio test.” Proceedings of the 7th International Conference on Geosynthetics, Nice, France, pp.1069-1074.

Lafleur, J., Mlynarek, J. and Rollin, A.L. (1989), “Filtration of broadly graded cohesionless soils.”, Journal of Geotechnical Engineering, ASCE, Vol. 115, No. 2, pp.1747-1768.

Lawson, C. R. (1982), “Filter criteria for geotextile : relevance and use.” Journal of the Geotechnical Engineering Division, ASCE, Vol. 108, No. GT10, pp. 1300-1317.

Lawson, C. R. (1992), “Geotextile revetment filters.” Journal of Geotextiles and Geomembranes, Vol. 11, No. 4-6, pp. 431-448.

Le Lay, M. (2001), “The behavior of geosynthetic interface under the action of hydrodynamic pressures (wave)”, The student training report, INSA, Rennes and LIRIGM, Grenoble, France, 71 p. (in French).

Loudière, D. and Fayoux, D. (1982), “Filtration and drainage by means of geotextile - tests and specifications.” Proceedings of the 2nd International Conference on Geotextiles, Las Vegas, U.S.A., Vol. I, pp. 61-66.

Luettich, S. M., Giroud, J. P., and Bachus, R. C. (1992), “Geotextile filter design guide.” Journal of Geotextiles and Geomembranes, Vol. 11, No. 4-6, pp. 353-370.

Machizaud, Ch. (1982), “The filtration behavior of geotextile.” Ph. D dissertation, Scientific and Medical University of Grenoble (in French).

Mark, B. D. (1975), “The behavior of aggregate and fabric filter in sub-grad applications.” Ph.D dissertation, Department of Civil Engineering, Tennessee University, Knoxville, USA, 144 p.

Miller, B. and Tyomkin, I., (1983), “Pore size distribution from measurements of liquid uptake and retention.” 11th Technical Symposium, Nonwoven Technology – A steppingstone to growth, Baltimore, USA, pp. 73-82.

Mlynarek, J. (2000), “Geo drains and geo filters – Retrospective and future trends.” Proceedings of Geofilters 2000, Edited by W. Wolski and J. Mlynarek, Warsaw, pp. 27-47.

Mlynark, J. B. L., Andrel, R. and Gilles, B. (1991), “Soil geotextile system interaction.” Geotextiles and Geomembranes, Vol. 10, pp. 161-176.

Ogink, M. J. M. (1975), “Investigations on the hydraulic characteristics of synthetic fabrics.” Delf Hydraulics Laboratory, The Netherlands, publication N.146.

Palmeira, E. M. and Bessa da Luz, D.W. (2005), “Soil-geotextile filter interaction under high stress levels in the gradient ratio test.” Geosynthetics International, Vol. 12, No. 4, pp. 162-175.

Palmeira, E. M., Fannin, R. J. and Vaid, Y. P. (1996), “A study on the behavior of soil-geotextile systems in filtration tests.” Canadian Geotechnical Journal, Vol. 33, pp. 899-912.

Palmeira, E.M. and Fannin, R.J., (2002), “Soil-Geotextile compatibility in filtration.”, Proceedings of the 7th International Conference on Geosynthetics, Keynote Lecture, Vol. 3, pp. 853-869.

Palmeira, E. M. and Gardoni, M. G. (2002), “Drainage and filtration properties of non-woven geotextiles under confinement using different experimental techniques.” Geotextiles and Geomembranes, Vol. 20, No. 2, pp. 97-115.

PIANC (1987), “Guidelines for the design and construction of flexible revetments incorporating geotextiles for inland waterways.” Supplement to Bulletin No.57, Permanent International Association of Navigation Congresses.

Ragutzki, G. (1973), “Contribution for the determination of the filter effectiveness of permeable materials.” Research centre Norderney, Annual report 1973, Vol.15, Nordeney (in German).

Rollin, A. and Lombard, G. (1988), “Mechanisms affecting long-term filtration behavior of geotextiles.” Geotextiles and Geomembranes, Vol. 7, No. 1-2, pp. 119-145.

Scherzinger, Th. (1984), “Erosion behavior of laminated gravel/sandy soil during horizontal flow.” Deep work (unpublished) on Institute for Soil Mechanics and Rock Mechanics of Karlsruhe University (in German).

Schober, W. and Teindl, H. (1979), “Filter criteria for geotextiles.” Proceedings of the 7th Europian Conference on Soil Mechanics and Fundation Engineerings, British Geotechnical Society, Vol. 2, pp. 121-129.

Scott, J. D. (1980), “The filtration – permeability test.” Proceedings of the 1st Canadian Symposium on Geotextiles, Calgary, Alberta, Canada, pp. 175-185.

Shi, Y. C., Fannin, R. J., and Vaid, Y. P. (1994), “Interpretation of gradient ratio test results.” Proceedings of the 5th International Conference on Geotextiles, Geomembranes and Related Products, Singapore, Vol. 2, pp. 673-676.

Tian, H., Chew, S. H., Karunaratne, G. P., Loke, K. H., and Delmas, P. (2002), “Laboratory study of stability of punctured geotextile subjected to cyclic wave, Proceedings of the 7th International Conference on Geosynthetics, September 22-27, Nice, France, pp. 1075-1078.

Tonus, S. (1985), “Analysis criticizes criteria of filtration for geotextile.” Swiss Review Association of the Professionals of Geotextile, Annexes Technical, December.

Toralba, C. (2003), “Stability of the banks – The behavior of the banks protected under the wave action.” The student training report, LIRIGM, Grenoble, France, 36 p. (in French).

Vidal, D., Muñoz, C. S., and Urashima, D. C. (2006), “Rational retention criteria design applied to internal unstable cohesionless soil filtration.” Proceedings of the 8th International Conference on Geosynthetics, Yokohama, Japan, pp. 569-572.

Wan, C. F., and Fell, R. (2002), “Investigation of internal erosion and piping of soils in embankment dams by the Slot Erosion Test and the Hole Erosion Test.” UNICIV Report No.R-412, July, ISBN 85841 379 5, 325 p.

Wan, C. F., and Fell, R. (2004), “Investigation of rate of erosion of soils in embankment dams.” Journal of Geotechnical and Geoenvironmental Engineering, ASCE, Vol. 130, No. 4, April, pp. 373-380.

Wan, C. F., Fell, R., Cyganiewicz, J., and Foster, M. (2003), “Time for development of internal erosion and piping in embankment dams.” Journal of Geotechnical and Geoenvironmental Engineering, ASCE, Vol. 129, No. 4, April, pp. 307-314.

Williams, N. D. and Abouzakhm, M. A. (1989), “Evaluation of geotextile/soil filtration characteristics using the hydraulic conductivity ratio analysis.” Geotextiles and Geomembranes, Vol. 8, No. 1, pp.1-26.

Williams, N. D. and Luettich, S. M., (1990), “Laboratory measurement of geotextile filtration characteristics.” Proceedings of the 4th International Conference on Geotextiles, Geomembranes and Related Products, Hague, Netherlands, Vol. 2, pp. 273-278.

Wittman, L. (1980), “Filtration and transportation phenomena in porous media.” Publications of the Institute for soil mechanics and rRock mechanics of the Karlsruhe University, N86 (in German).

Wu, C.S., Hong, Y. S., Chang, B.S., and Yan, Y. W. (2006), “Soil-nonwoven geotextile filtration behavior under contact with drainage materials.” Geotextiles and Geomembranes, Vol. 24, No. 1, pp. 1-10.

Zhao, Z. K., Chew, S. H., and Karunaratne, G. P. (2000), “Performance of geotextile filters in revetment under cyclic wave loading.” Proceedings of the 2nd Asian Geosynthetics Conference, May, Kuala Lumpur, Malaysia, pp. 143-148.

Zitsher, F. F. (1975) “Recommendation for the useing plastics material in hydraulic engineering.” Civil Engineering, No. 12 (in German).

Appendix I

The variation of displacement of the geotextile bag by reinforced revetment using geotextile test

A. X displacement on the vertical face of the geotextile bag.

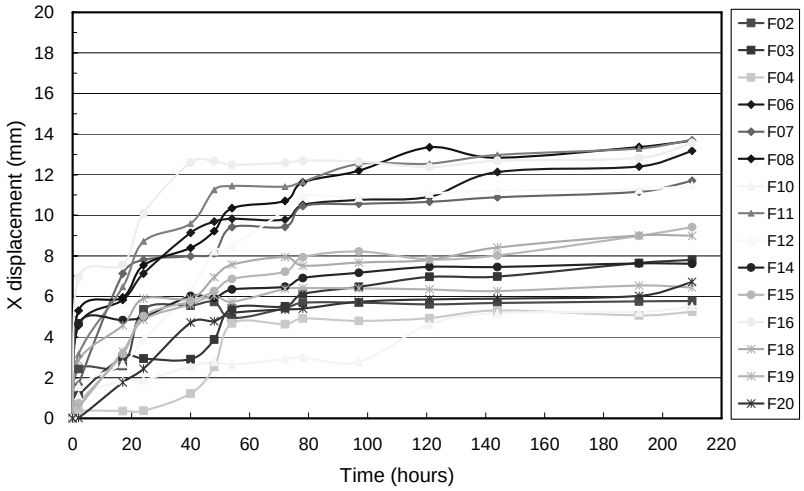

(a) The variation of X displacement by time for each conference point.

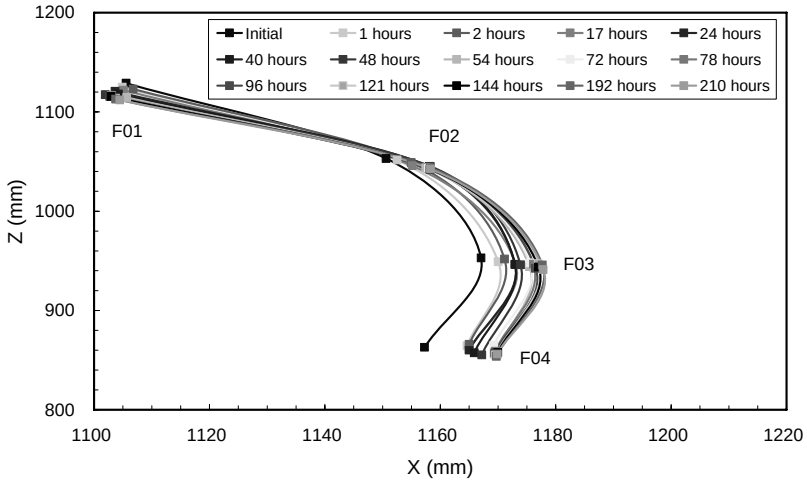

(b) Section A

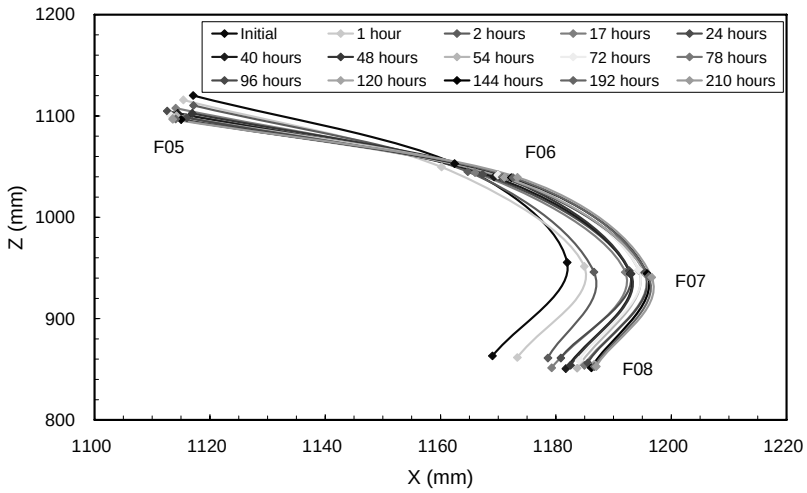

(c) Section B

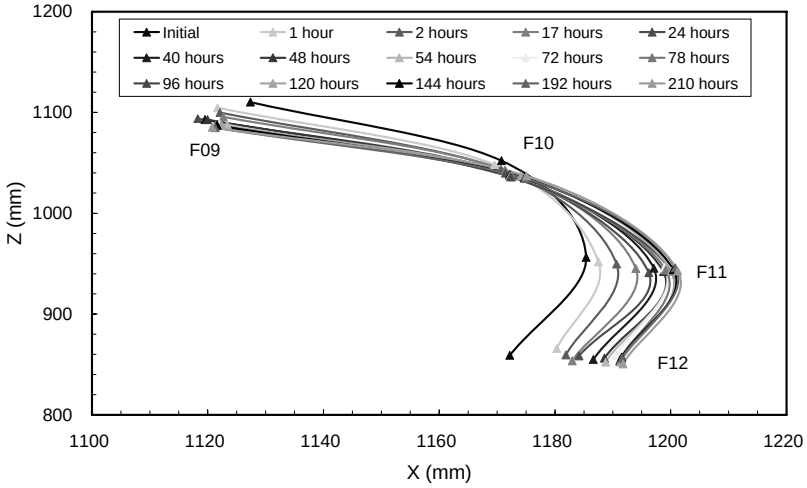

(d) Section C

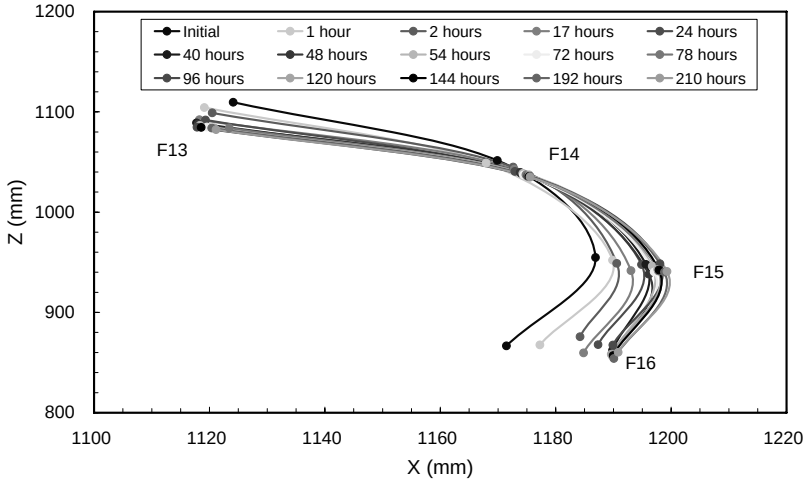

(e) Section D

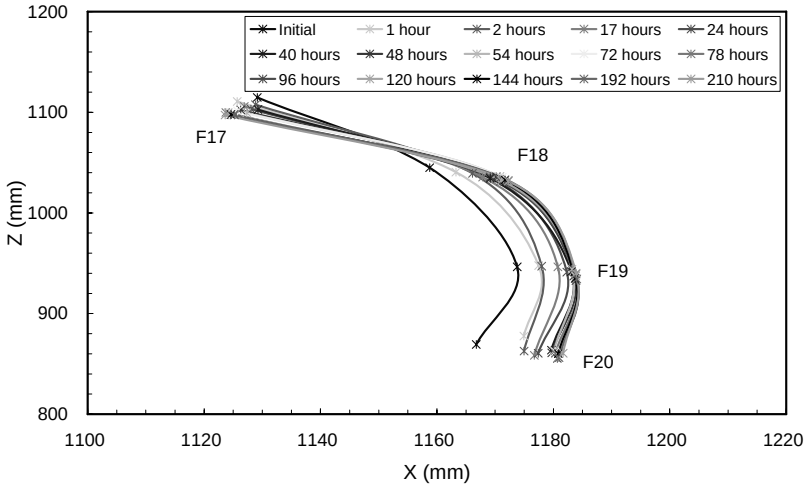

(f) Section E

Figure I.1 The variation of X displacement under E150.

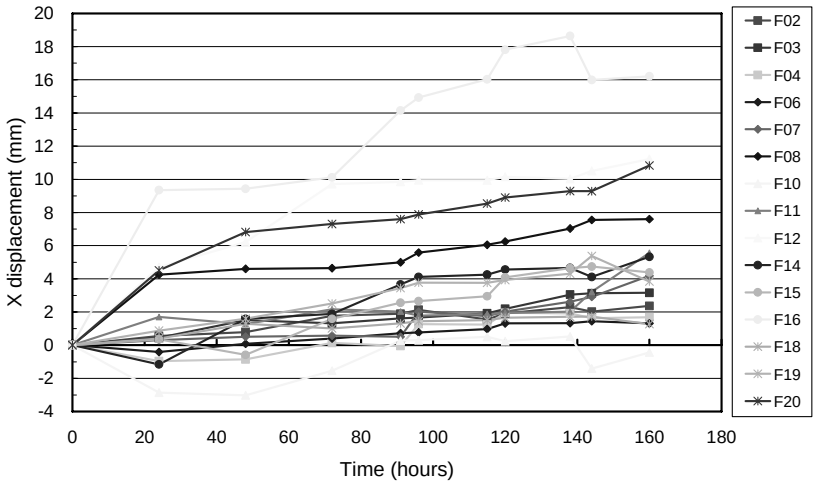

(a) The variation of X displacement by time for each conference point.

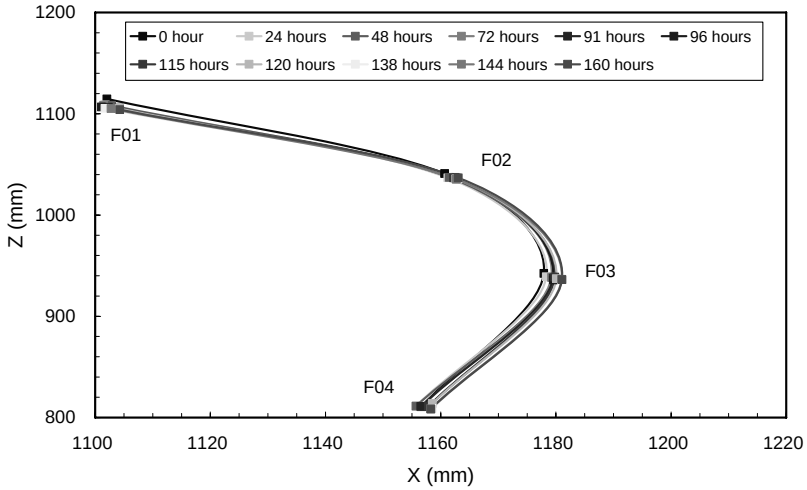

(b) Section A

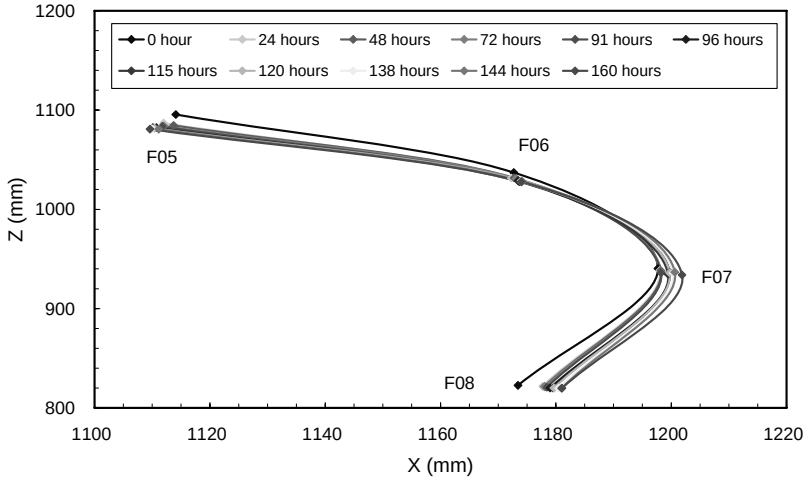

(c) Section B

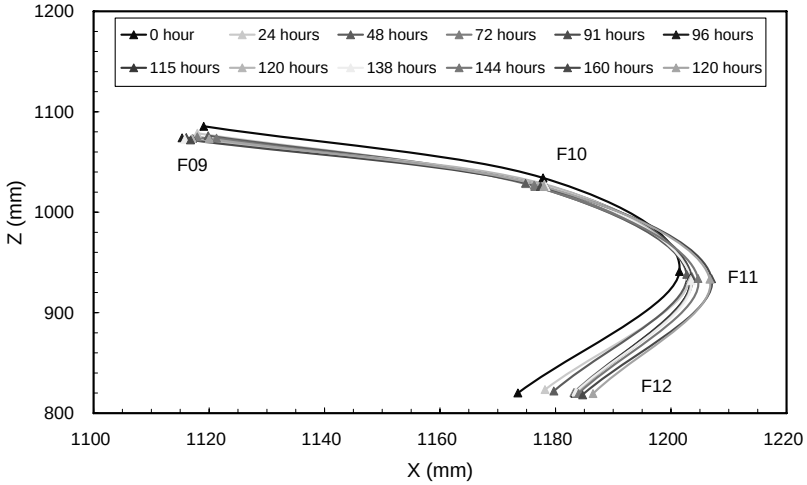

(d) Section C

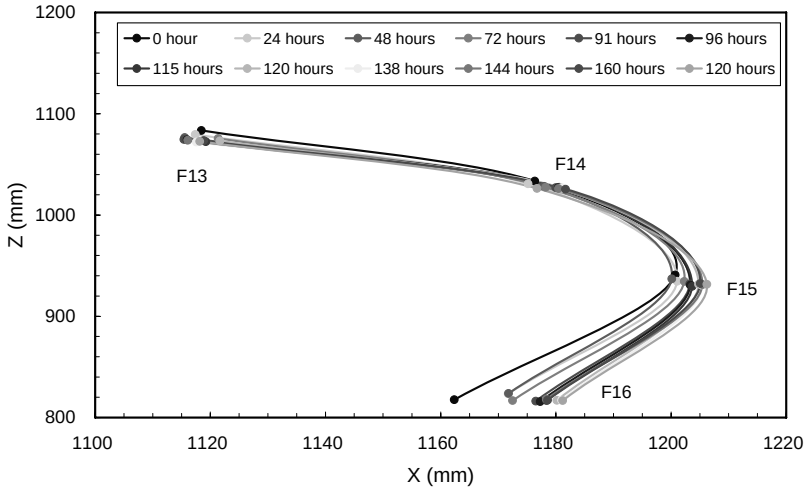

(e) Section D

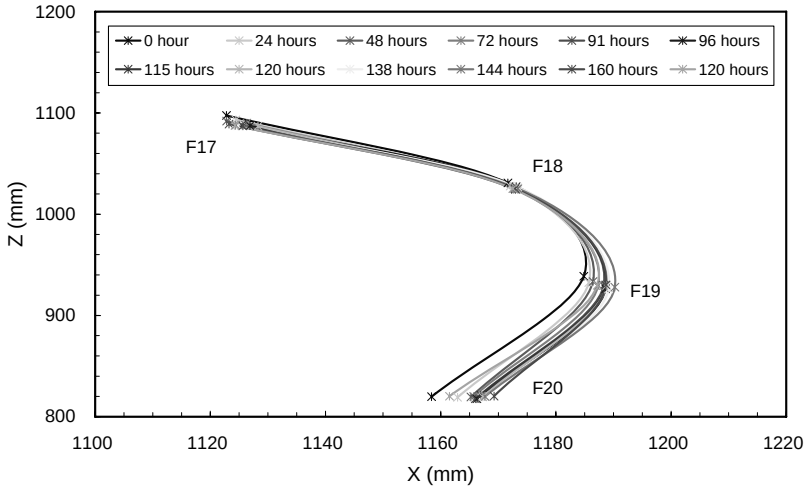

(f) Section E

Figure I.2 The variation of X displacement under E250.

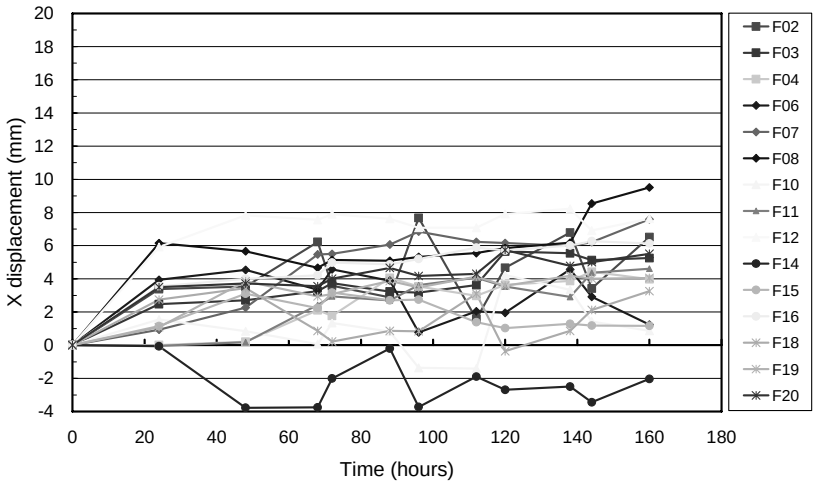

(a) The variation of X displacement by time for each conference point.

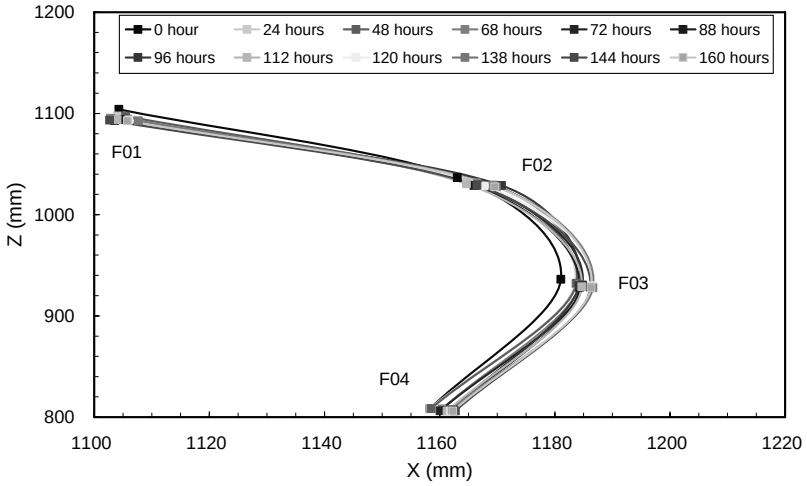

(b) Section A

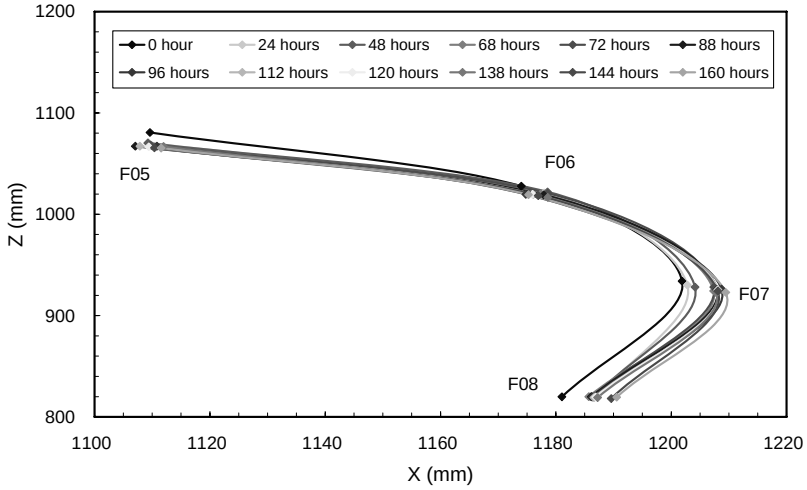

(c) Section B

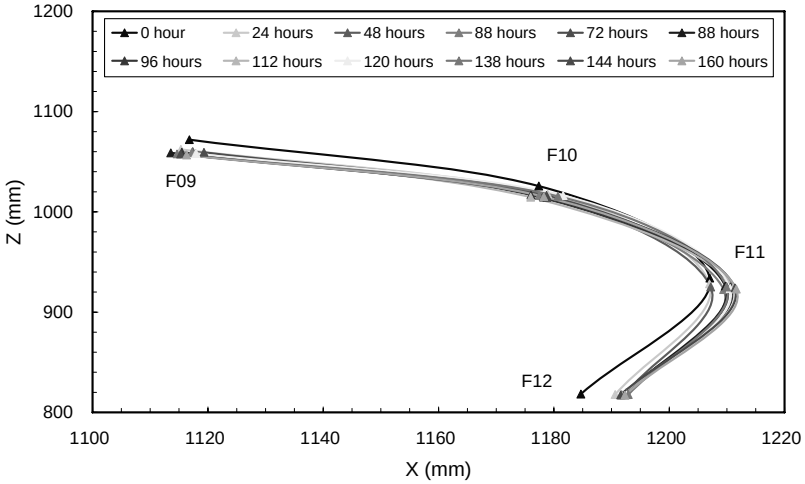

(d) Section C

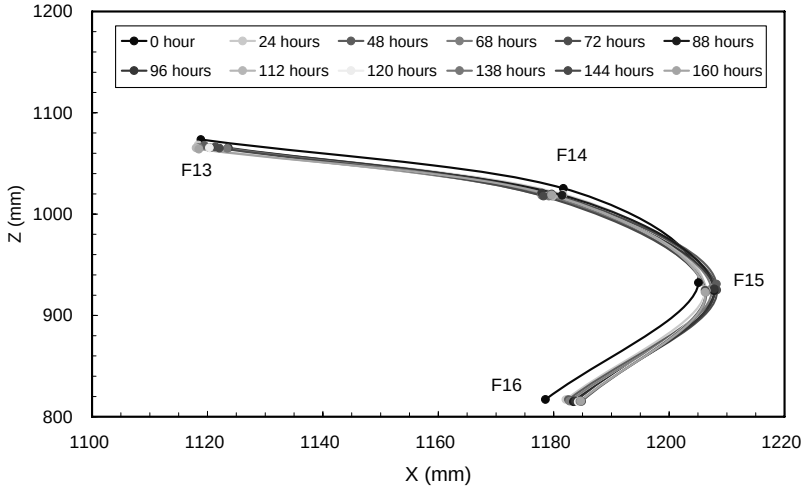

(e) Section D

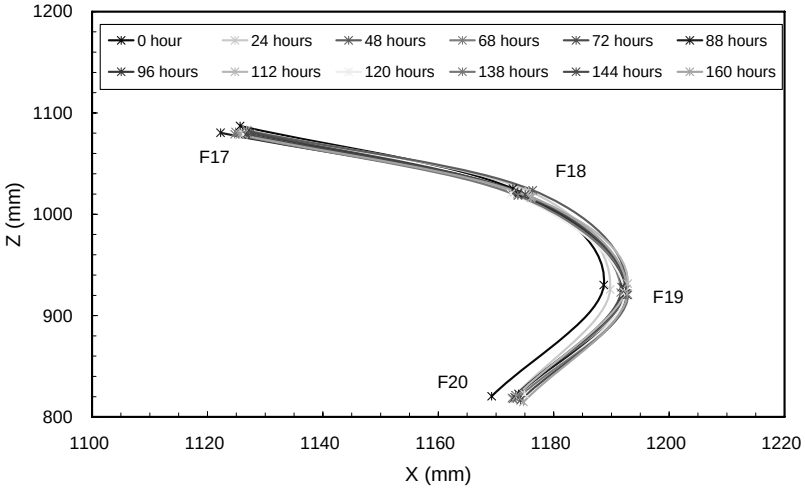

(f) Section E

Figure I.3 The variation of X displacement under E350.

B. Z displacement (Settlement) on the top face of the geotextile bag.

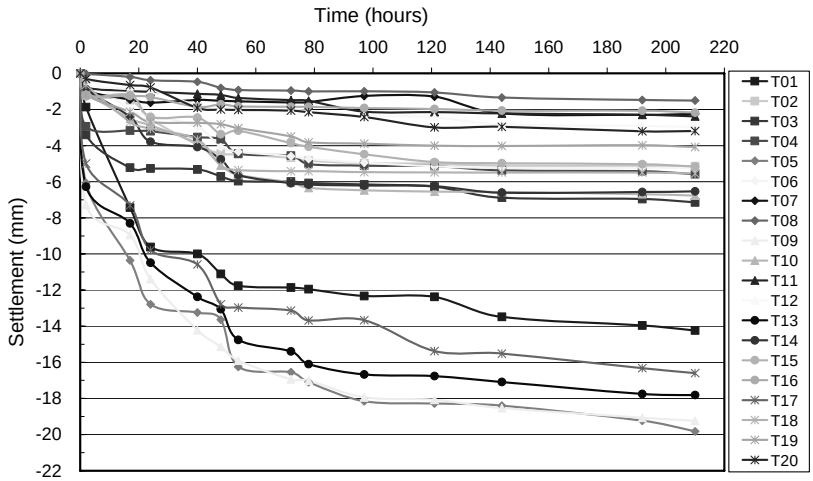

(a) The variation of settlement by time for each conference point.

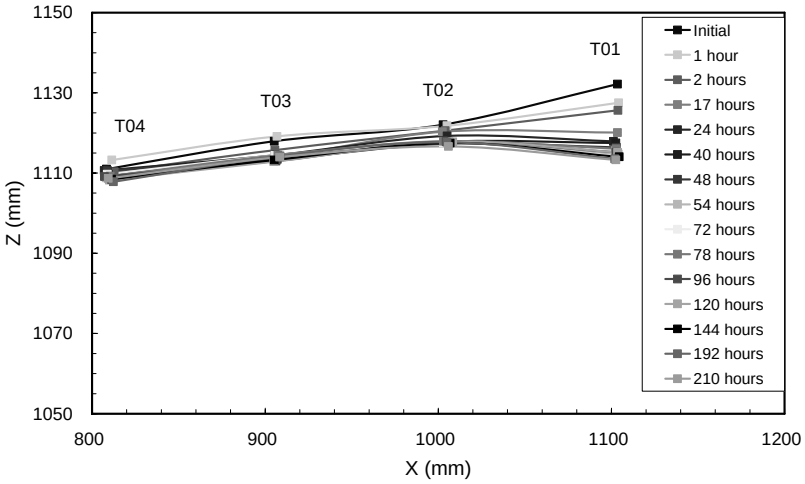

(b) Section A

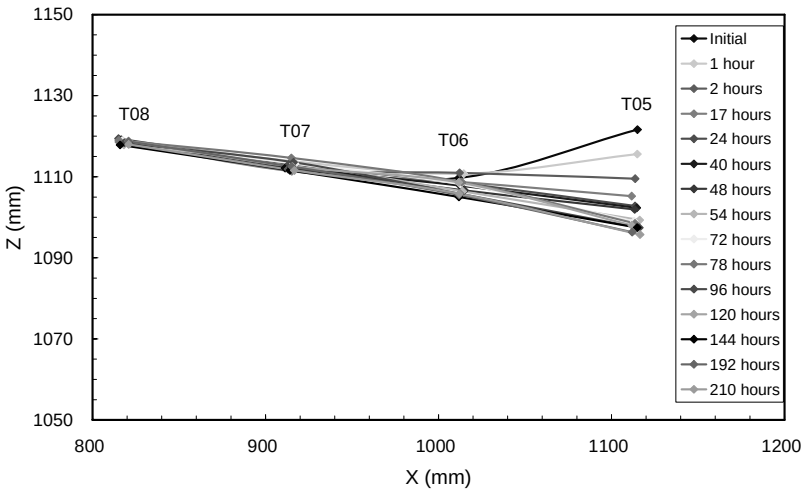

(c) Section B

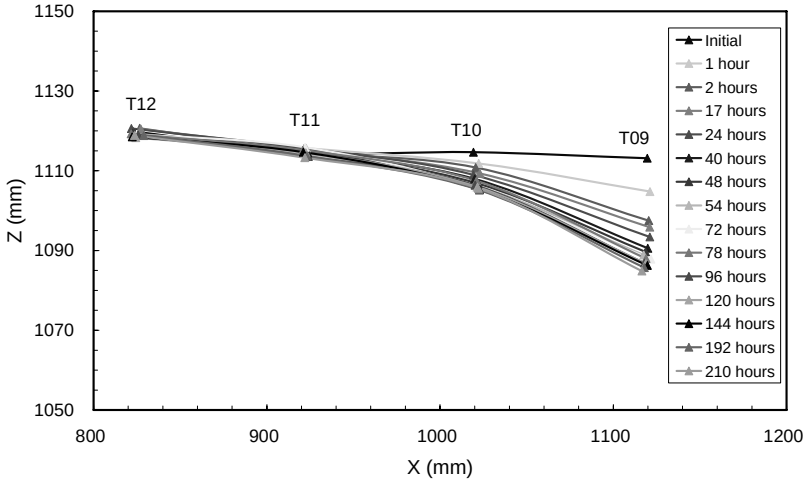

(d) Section C

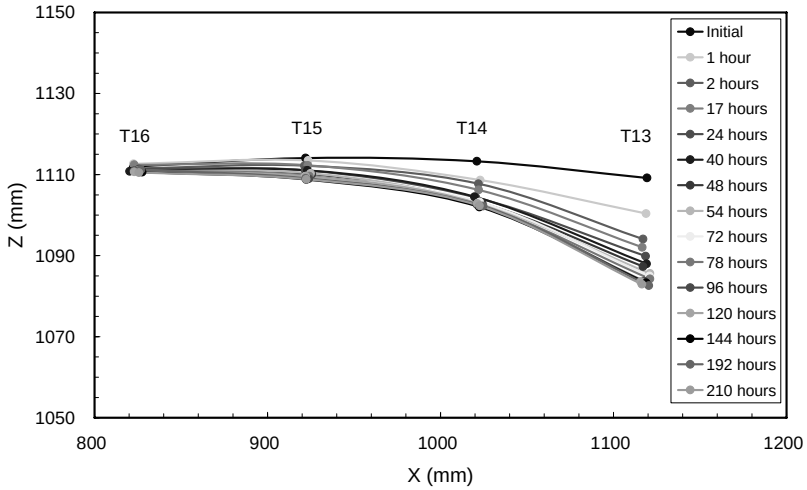

(e) Section D

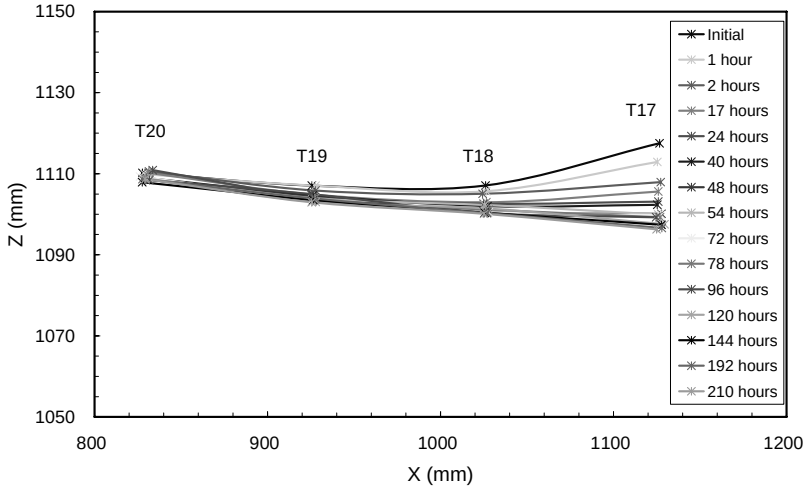

(f) Section E

Figure I.4 The variation of settlement under E150.

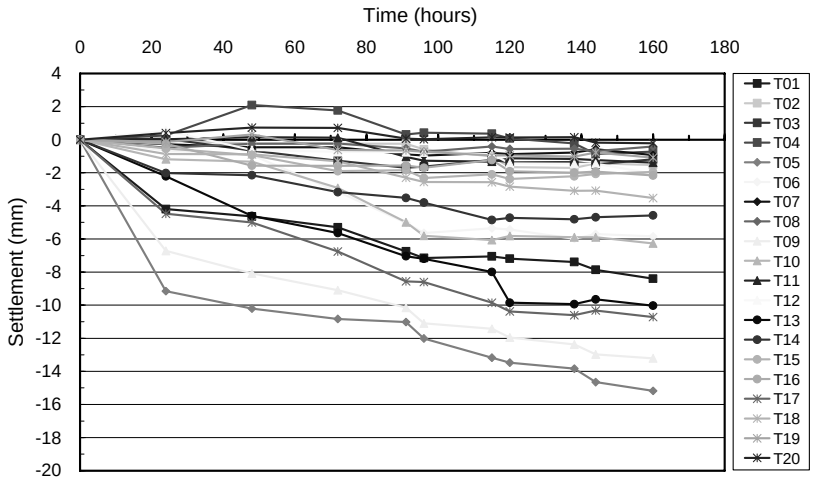

(a) The variation of settlement by time for each conference point.

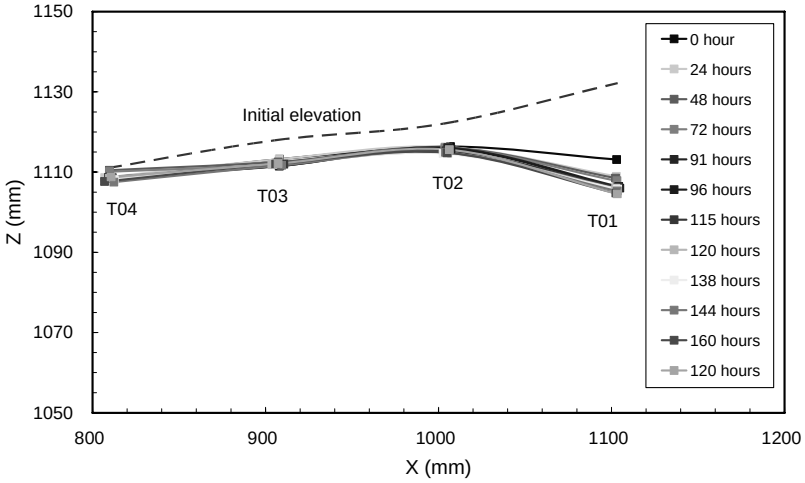

(b) Section A

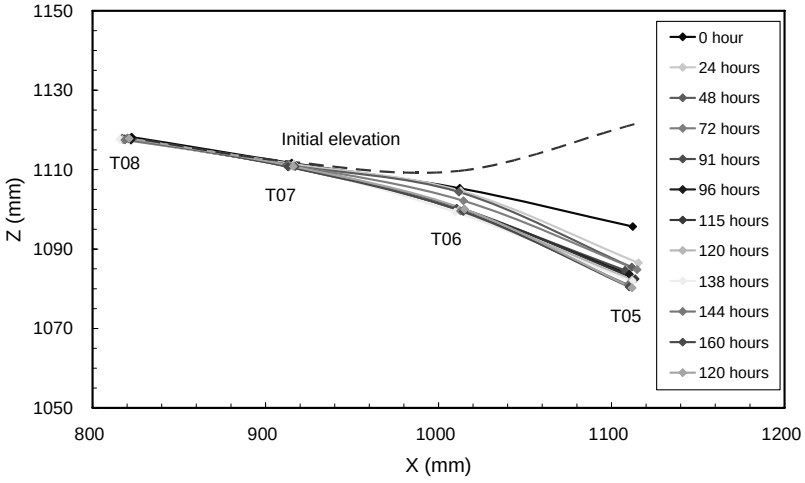

(c) Section B

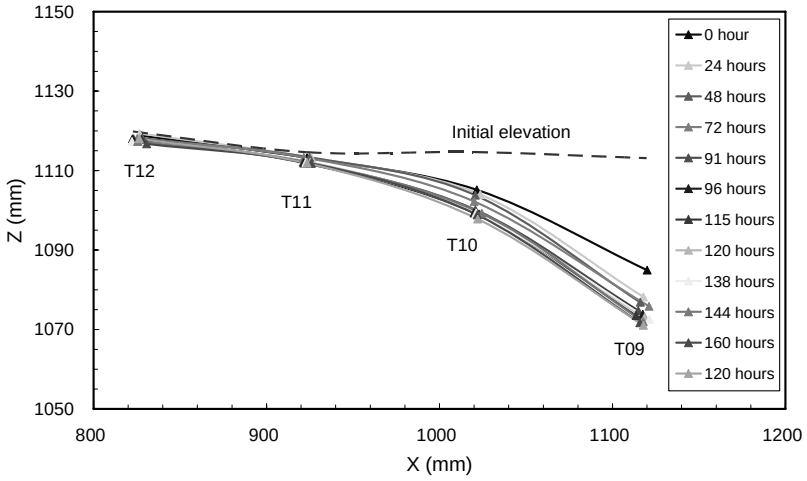

(d) Section C

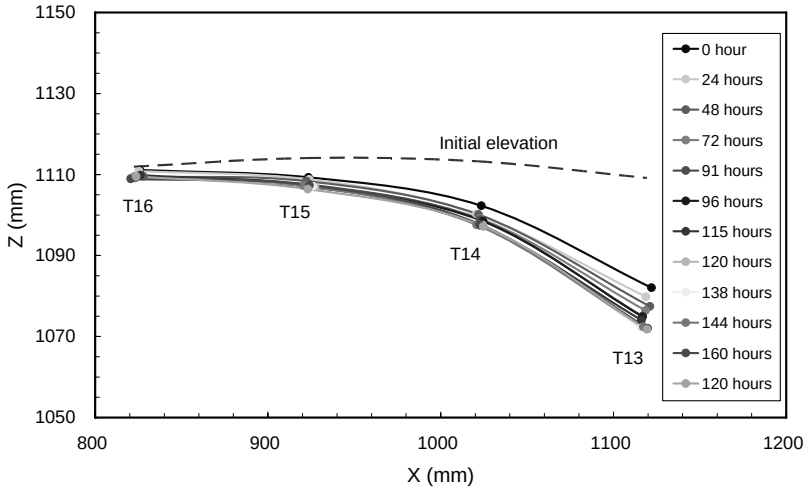

(e) Section D

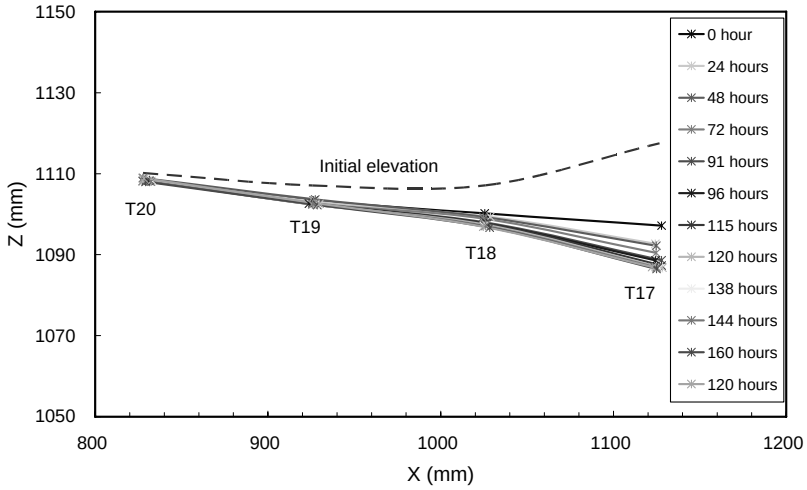

(f) Section E

Figure I.5 The variation of settlement under E250.

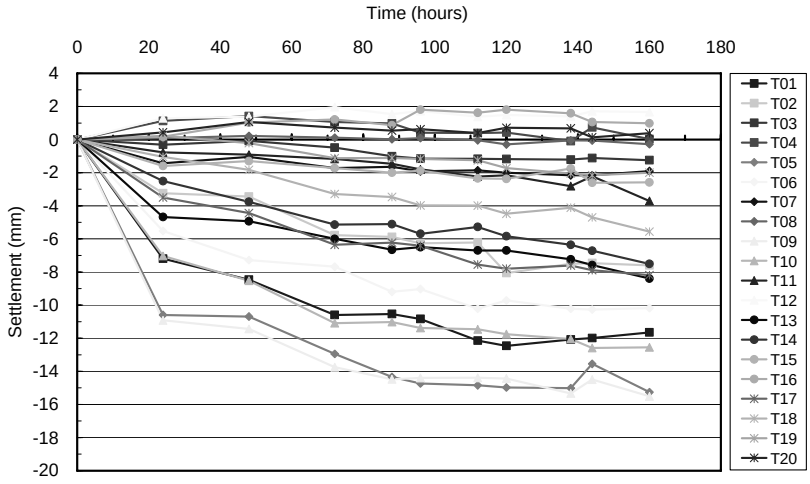

(a) The variation of settlement by time for each conference point.

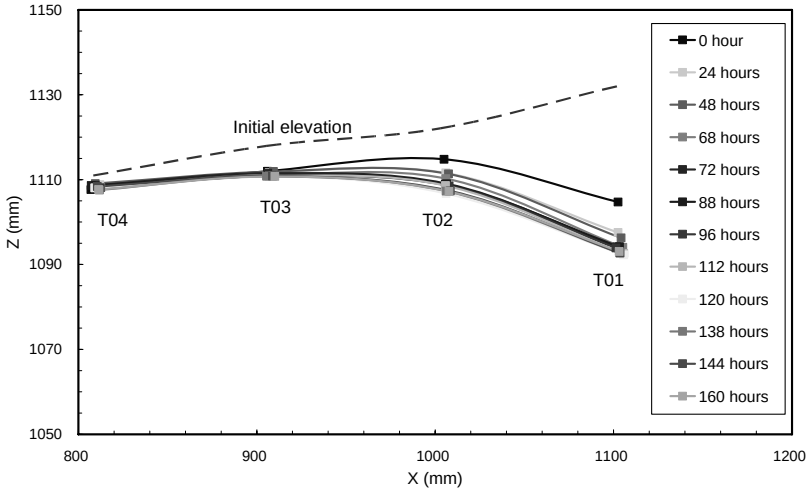

(b) Section A

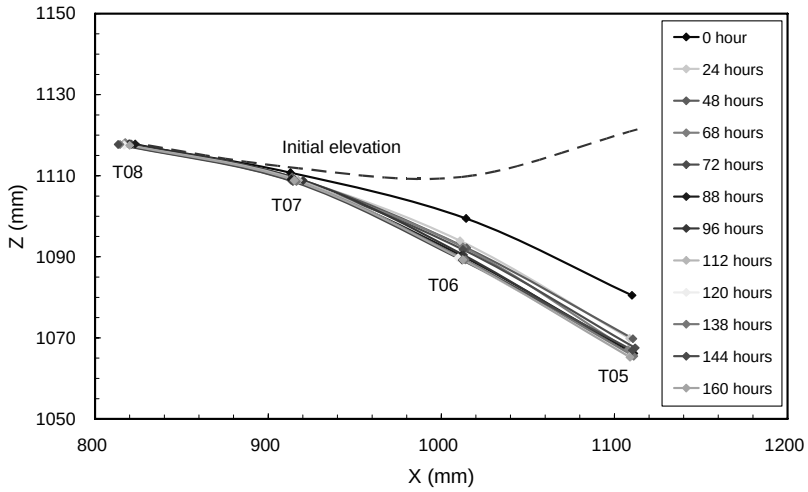

(c) Section B

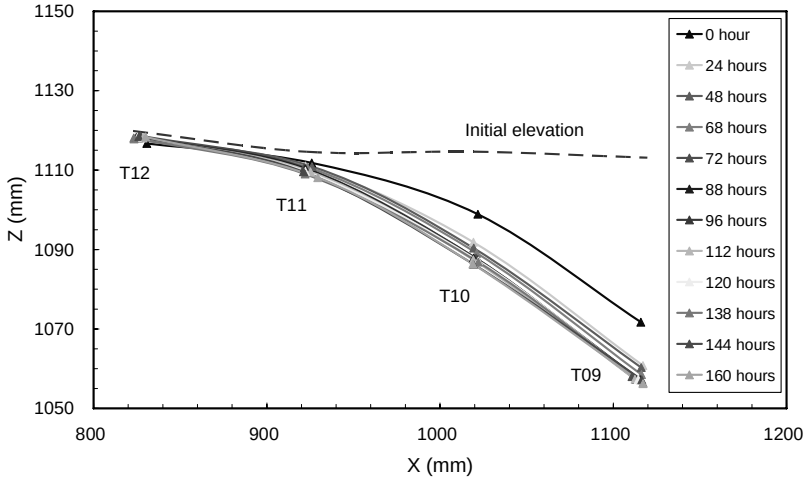

(d) Section C

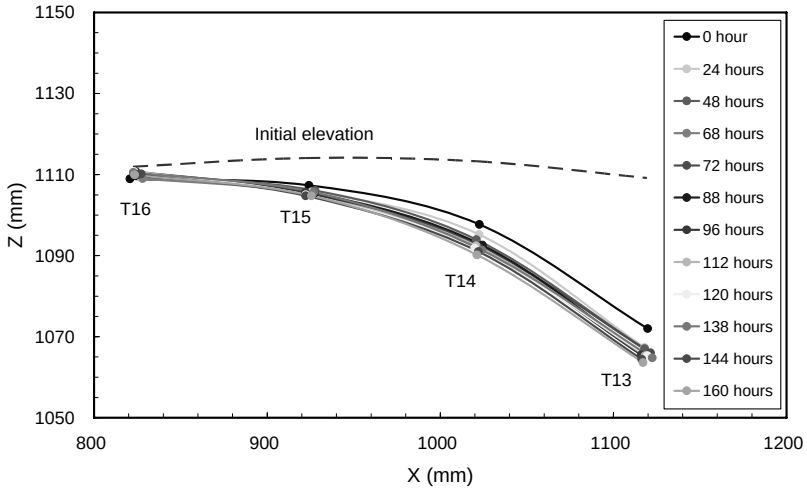

(e) Section D

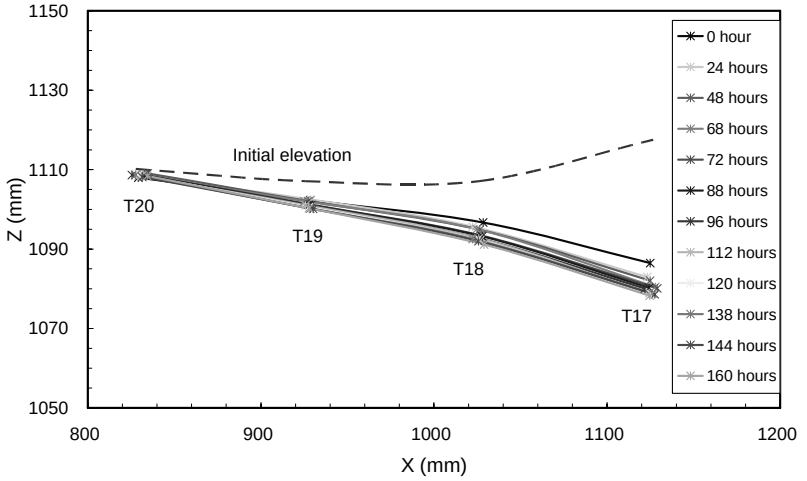

(f) Section E

Figure I.6 The variation of settlement under E350.

Appendix II

The instruction manual

A. Piezometers (KYOWA PGM-05KG)

20 to 100kPa

High-accuracy measurement of low-range pressure

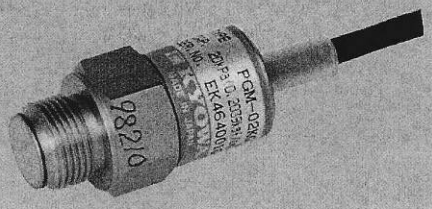

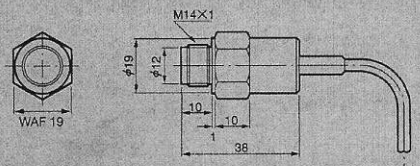

Unit: mm

Low Capacitance Small Pressure Transducers

PGM-G

The back-pressure compensating pipe is built in the cable, thereby permitting ease of handling. High accuracy and high stability measurement of low-range pressures is possible. For back-pressure compensation, contact Kyowa for information.

- ✔ ***Ease of handling***
- ✔ ***Highly accurate and dependable measurement of low-range pressures***

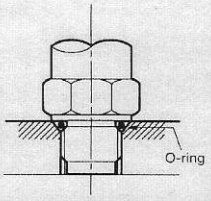

Example installation

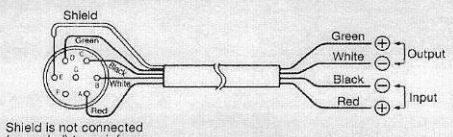

Shield is not connected (grounded) to mainframe.

Connector's input/output wiring

Performance

Model	Rated capacity (Ref. value)	Natural freq. (app.)
PGM-02KG	20kPa (203.9gf/cm²)	2kHz
PGM-05KG	50kPa (509.9gf/cm²)	3kHz
PGM-1KG	100kPa (1.020kgf/cm²)	4kHz

Overall accuracy: ±0.5%RO
Non-linearity: ±0.5%RO
Hysteresis: ±0.3%RO
Rated output: PGM-02KG: 0.75mV/V (1500 x 10^{-6} strain) or higher
PGM-05KG: 1.25mV/V (2500 x 10^{-6} strain) or higher
PGM-1KG: 1.4mV/V (2800 x 10^{-6} strain) or higher

Environmental characteristics
Safe temperature range: –20 to 70°C
Compensated temperature range: –10 to 60°C
Thermal effect on zero: ±0.02%RO/°C
Thermal effect on output: ±0.03%/°C

Electric characteristics
Safe excitation voltage: 5V AC or DC
Recommended excitation voltage: 1 to 3V AC or DC
Input resistance: 350Ω±10%
Output resistance: 350Ω±10%
Cable: 0.08mm², 4-conductor shielded Teflon 3m, ø4.2mm, terminated in connector plug (NDIS)

Mechanical characteristics
Safe overload rating: 150%
Material: Mainframe, SUS metal surface; liquid contacting section, SUS304
Weight: 40g, approx. (including cable)
Mount screw: M14, P=1 male screw
Standard accessory: O-ring JIS B 2401-P14

B. Displacement transducer (KYOWA DT-30F)

IM-T-163g '97.8

DT-F•G Displacement Transducers
INSTRUCTION MANUAL

Thank you for purchasing this KYOWA product. Before using it, read this instruction manual carefully. Also, keep the manual within easy reach so that you can refer to it whenever necessary.

1. Handling precautions

1.1 Do NOT disassemble the displacement transducer.
1.2 Carefully handle the transducer in the same manner as with an ordinary dial gauge.
1.3 Keep the rod always clean.
1.4 Do NOT put the transducer in water, and avoid water on it.
1.5 Do NOT use in areas where the transducer may be exposed to vibrations.
1.6 The transducer is unable to measure a dynamic phenomenon with a rise time faster than 2Hz.
1.7 Do not detach the sensor because it also acts as a stopper. If the transducer is used with the sensor having been detached, a stopper should be provided where the sensor was.

2. Mounting

2.1 Using the accessory mounting bracket, fix the transducer at a steady point. Or, fix it at the ø8 flange section.
2.2 When fixing, give 0.5 to 1mm displacement to the transducer.

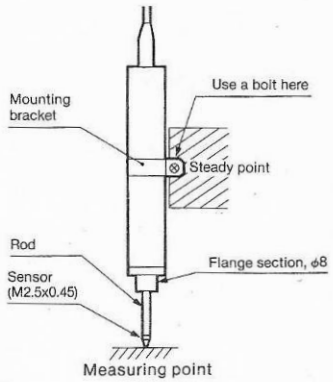

2.3 Same as a dial gauge, the transducer's sensor is made to contact the measuring point by the transducer's reaction. In measuring dynamic displacement, the rod may fail to respond to it. If it occurs, detach the sensor and fix the transducer to the measuring point using an M2.5 screw.
When tightening the screw, take care to avoid a bending and/or turning force on the transducer.
If the measuring point moves in a direction other than the axial direction, the transducer may be damaged by a bending force, etc.

3. Connection

3.1 Connect the displacement transducer to a strain amplifier.
3.2 When using a strain amplifier other than KYOWA, observe the pin assignment of the connector plug illustrated below.

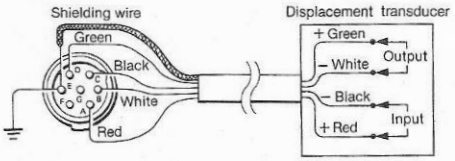

4. Conversion

4.1 To convert readings into displacement values, use the calibration factor stated in the calibration sheet.
4.2 When using a strain amplifier, outputs will read in $\varepsilon \times 10^{-6}$ equivalent strain. The displacement value corresponding to 1 $\times 10^{-6}$ equivalent strain is stated in the calibration sheet. The displacement value is then found through multiplication.

Acceleration= (Strain amplifier's output: $\varepsilon \times 10^{-6}$)
x (Calibration factor: mm/1 $\times 10^{-6}$)

4.3 If an amplifier of other type or a recorder is in use, it is necessary to measure the applied bridge excitation voltage accurately. The calibration sheet states the acceleration value which corresponds to 1µV output caused by a bridge excitation voltage of 1V. The acceleration is then found through multiplication using the following equation.

$$\text{Acceleration} = \frac{\text{Bridge output voltage: } \mu V}{\text{Bridge excitation voltage: V}} \times (\text{Calibration factor: mm/1}\mu V/V)$$

5. Storage precautions and inspection

5.1 Avoid water, oil and dust on the transducer.
5.2 For storage, be sure to apply the accessory protecting pipe to the rod.
5.3 If an initial value and/or output value are found abnormal, measure the bridge resistance and insulation resistance (which should be 100MΩ or higher). If the measured values are found abnormal, the cause may be failure of the transducer element.
CAUTION: In measuring the insulation resistance, do NOT apply a voltage exceeding 50V to the insulation resistance tester.

KYOWA
KYOWA ELECTRONIC INSTRUMENTS CO., LTD.

6. Specifications

Model		Measuring range
DT-10F	DT-10G	0 to 10mm
DT-20F	DT-20G	0 to 20mm
DT-30F	DT-30G	0 to 30mm

Rated output:	5mV/V (10000 x 10^{-6} strain)±10%(DT-F) 5mV/V (10000 x 10^{-6} strain)±0.1%(DT-G)
Non-linearity:	±0.1%RO
Hysteresis:	±0.1%RO
Repeatability	0.1%RO or better
Response freq. range:	DC to app. 2Hz
Measuring reaction force:	App. 200gf
Recommended bridge voltage:	1 to 4V, AC or DC
Safe bridge voltage:	6V, AC or DC
Bridge resistance:	120Ω±2%(DT-F), 350Ω±1%(DT-G)
Compensated temp. range:	0 to 60°C (no dew-condensing)
Safe temp. range:	−10 to 70°C (no dew-condensing)
Thermal effect on zero balance:	±0.01%RO/°C
Thermal effect on output:	±0.01%/°C
Weight (incl. cable):	DT-10F, G, 20F, G Approx.180g DT-30F, G Approx.200g
	0,08mm², 4-conductor shielded chloroprene 2m, ø4mm, terminated in connector plug

■ Accessories:

Calibration sheet	1
Warranty	1
Instruction manufal	1
Mounting bracket	1
Small round screw (M6 x 10)	1
Flat washers (for M6)	2

KYOWA
KYOWA ELECTRONIC INSTRUMENTS CO., LTD.
Overseas Department:
Address: 1-22-14, Toranomon, Minato-ku, Tokyo 105-0001 Phone:03-3502-3553 Fax:03-3502-3678

C. Turbidity meter (LAT N1)

Beam-Turbidity Meter serie LAT N1

Application
- turbidity measurement from 0 up to 5000NTU resp. 0 up to 1250EBC
- filter monitoring
- phase separation of low turbid media

Application Examples
- process control of brewing processes
- fresh water control in the beverage industry
- water- / waste water control e.g. in dairys
- quality control

Hygienic Design / Process Connection
- CIP-/ SIP-cleaning up to 130°C
- fitting completely made of stainless steel, optical block made of PEEK, glass panes made of sapphire glass (FDA-conform)
- further process connections: dairy flange DIN11851; hygienic thread connection DIN11864; TriClamp; DIN flange

Features
- pollution of the glass panes will be compensated
- compact device, no separate evaluation unit necessary
- units NTU and EBC switchable (11 ranges per unit)
- smallest measurement range 0-5NTU resp. 0-1EBC
- highest measurement range 0-5000NTU resp. 0-1250EBC
- 4 externally switchable measurement ranges
- smallest pipe diameter DN40
- colour independent measurement principle (wave length 860nm)
- switching and analog output

Options / Accessories
- electrical connection with M12 plug-in
- cable ex factory for M12 plug-in
- other process connections on request

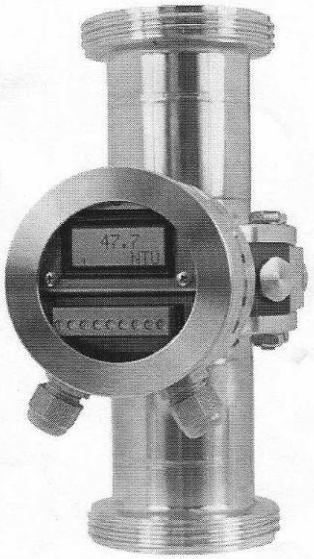

LAT N1

Specification

Process connection	dairy flange DIN 11851	DN 40; 50; 65; 80; 100
	hyg. conn. DIN 11864	DN 40; 50; 65; 80; 100
	DIN-flange	DN 40; 50; 65; 80; 100
	TriClamp	DN 40; 50; 65; 80; 100
Materials	connection head	SS V2A (1.4305), 89mm dia.
	fitting	SS V4A (1:4404)
	optical block	PEEK
	glass panes	sapphire glass
Temperature ranges	ambient	-10...+60°C
	process	0...100°C
	CIP-/ SIP-cleaning	up to 130°C 30 min max
Pressure		6bar max
Protection type		IP69K
Measurement principle	acc. to EN 7027	4-beam-altern. light
Wave length	acc. to EN 7027	860nm ± 60nm
LCD-Indicator	with illumination	2x8-digit
Accuracy		see page 4

Electr. connection	cable entry	2xPG (M16x1,5)
	cable connection	2xM12 plug-in (SS 316)
	supply voltage	18...36V DC 160mA max.
Input	range switching	E1 and E2 (24V DC) DC decoupled
Output short circuit proof	analog	4-20mA DC decoupled
	switching	24V DC 80mA max. respectively to GND of power supply
Measurement ranges	NTU	0-5; 10; 20; 50; 100; 200; 500; 1000; 2000; 4000; 5000
	EBC	0-1; 2; 5; 10; 20; 50; 100; 200; 500; 1000; 1250
Damping time	seconds	0; 1; 2; 4; 8; 16; 32; 64; 128

KOBOLD INSTRUMENTATION
BP 9051
95071 CERGY PONTOISE CEDEX
T : 01 34 21 91 15 F 01 34 21 92 18
Site:www.kobold.com Mail:info.fr@kobold.com

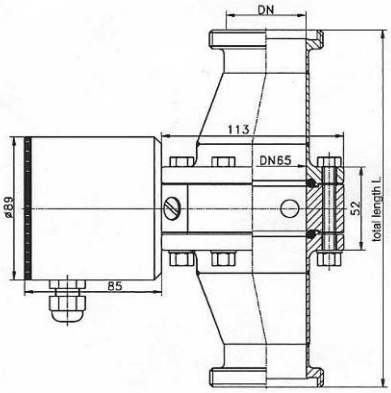

dairy flange / hygienic thread connection

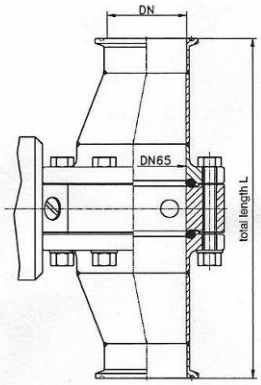

TriClamp

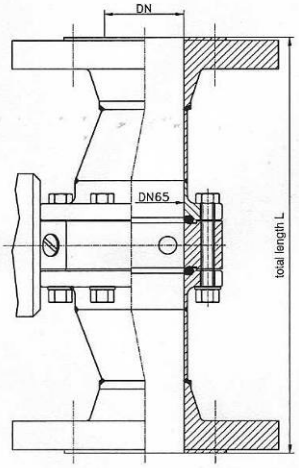

DIN flange

Table total length of the fitting (tol.: ±2mm)

Process-connection / nominal width	dairy flange (-gg) acc. to DIN11851	hygienic screw connection (-hh) acc. to DIN11864	TriClamp (-tc) acc. to DIN32676	DIN flange (-df) acc. to DIN2632/33
DN40	298,0mm	284,0mm	275,0mm	316,0mm
DN50	236,0mm	226,0mm	209,0mm	256,0mm
DN65	250,0mm	236,0mm	256,0mm	290,0mm
DN80	250,0mm	236,0mm	216,4mm	260,4mm
DN100	378,0mm	362,0mm	320,8mm	368,8mm

Accuracy:

Accuracy	at the calibration points (20; 200; 2000NTU)			+-2%
Offset dirft				<+-0,3NTU (+-0,075EBC)
Slope accuracy	Range	0...1000NTU	(0...250EBC)	<3%
	Range	1001...2000NTU	(250...500EBC)	<4%
	Range	2001...5000NTU	(500...1250EBC)	<6%
Reproducibility	Range	0...1000NTU	(0...250EBC)	<2%
	Range	1001...2000NTU	(250...500EBC)	<3%
	Range	2001...5000NTU	(500...1250EBC)	<4%
Resolution	Range	0...100NTU	(0...25EBC)	0,1NTU (0,025EBC)
	Range	100...1000NTU	(25...250EBC)	1NTU (0,25EBC)
	Range	1001...5000NTU	(250...1250EBC)	10NTU (2,5EBC)

To ensure the accuracy data above, we suggest you to send back the turbidity meter every two years for checking it.

Appendix III

The variation of turbidity and velocity with time by parallel erosion test

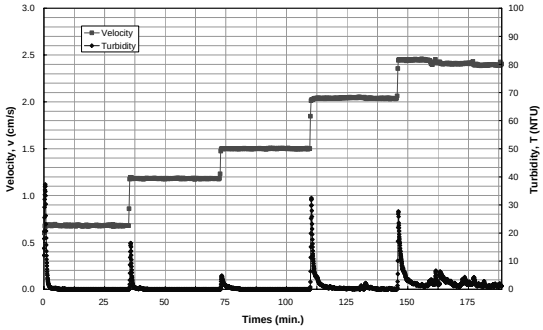

(a) T01

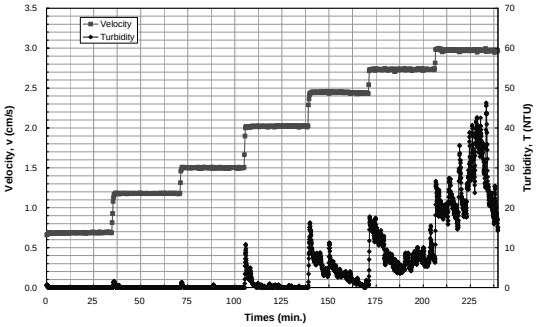

(b) T02

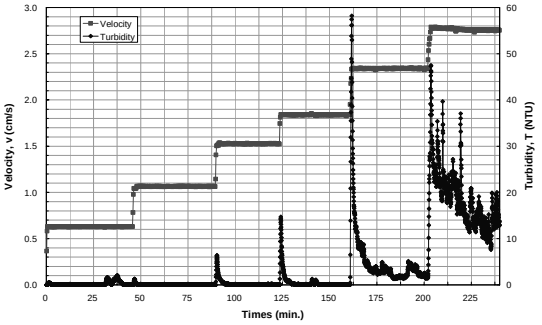

(c) T03

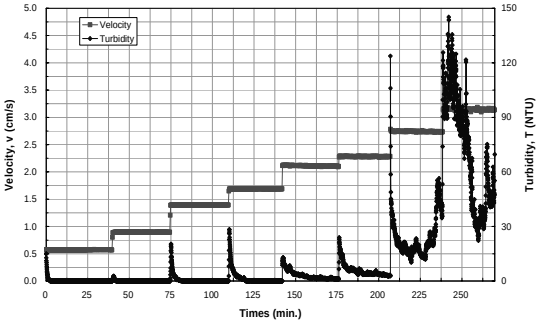

(d) T04

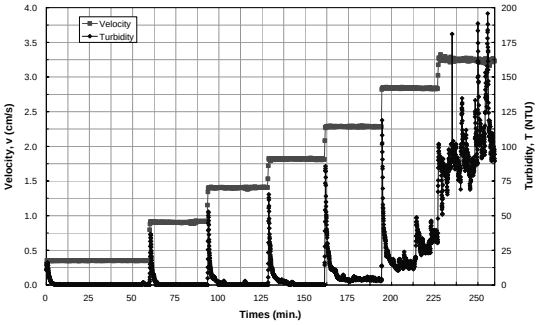

(e) T05

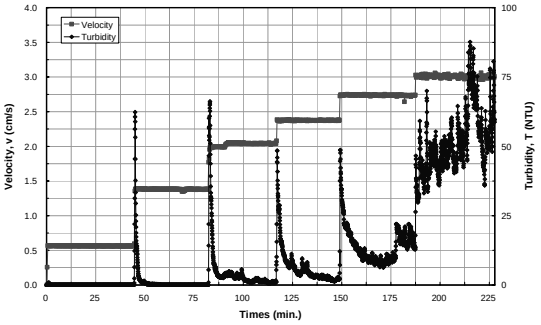

(f) T06

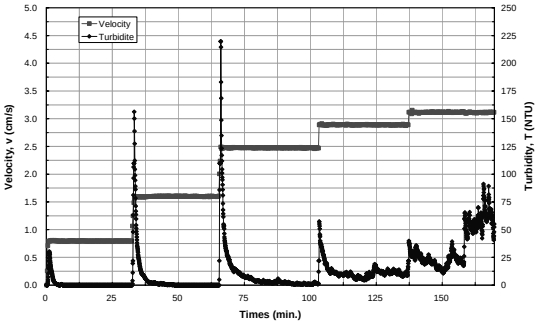

(g) T07

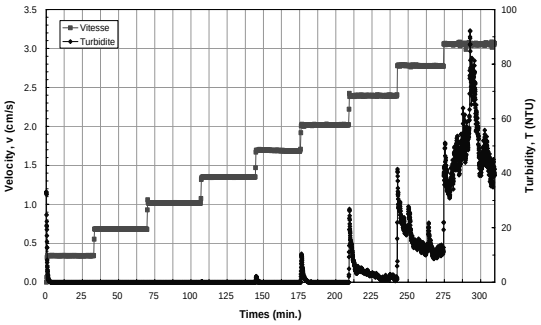

(h) T08

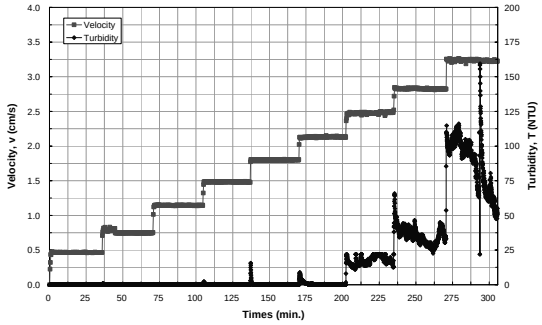

(i) T09

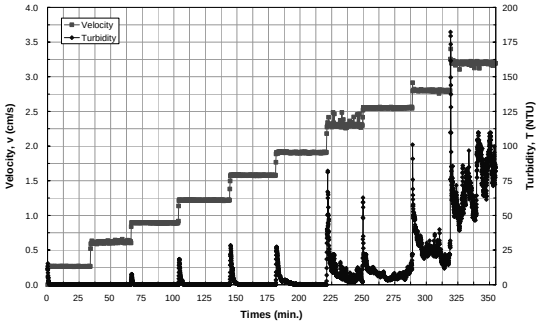

(j) T10

Figure III.1 The variation of turbidity and velocity with time (SET 01)

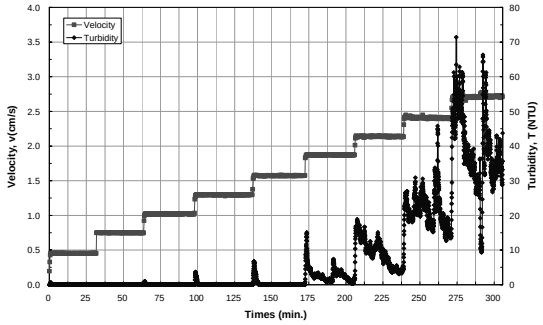

(a) T11

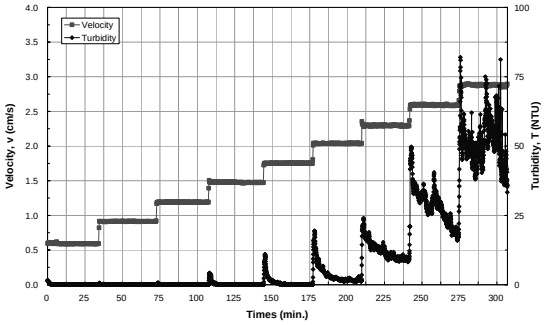

(b) T12

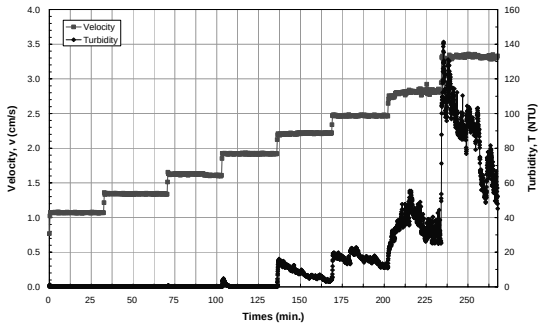

(c) T13

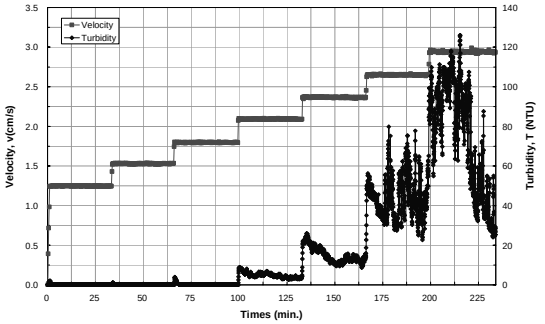

(d) T14

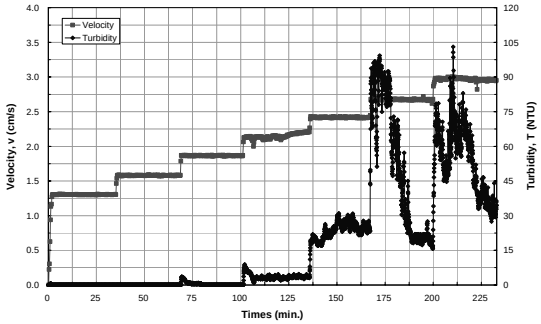

(e) T15

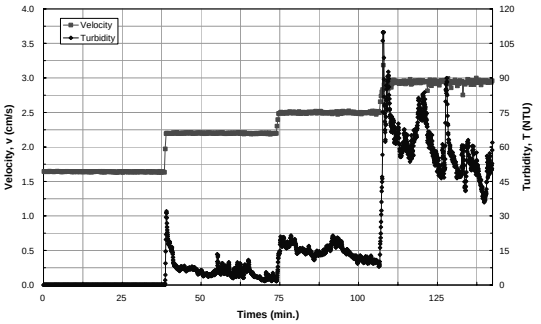

(f) T16

Figure III.2 The variation of turbidity and velocity with time (SET 02)

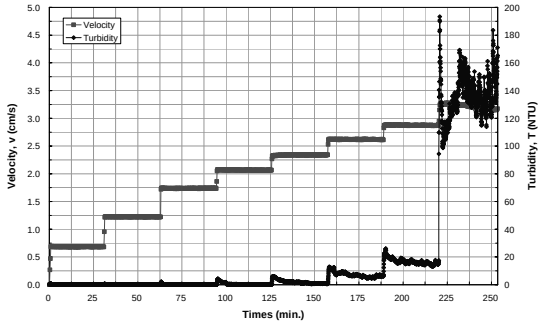

(a) T17

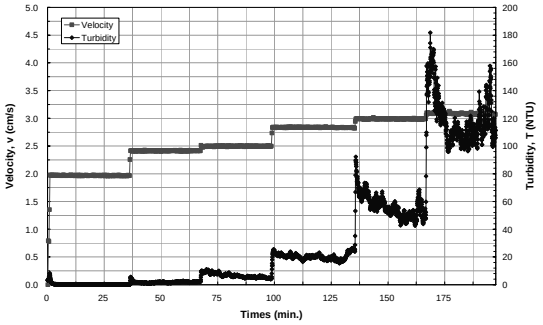

(b) T18

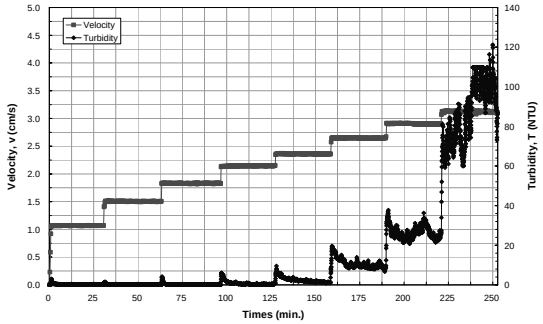

(c) T19

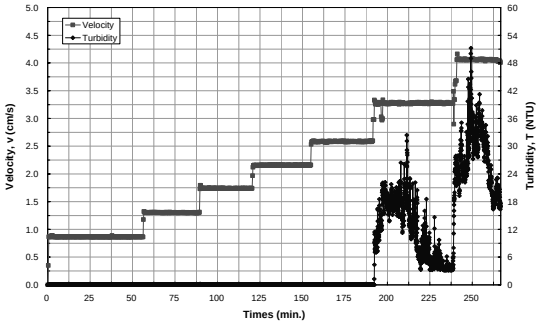

(d) T20

Figure III.3 The variation of turbidity and velocity with time (SET 03)

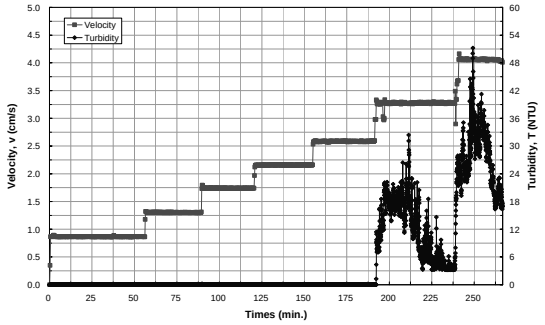

(a) T21

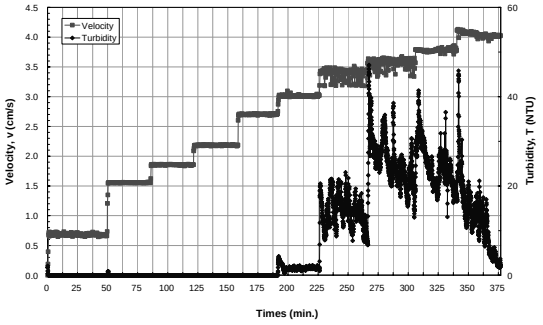

(b) T22

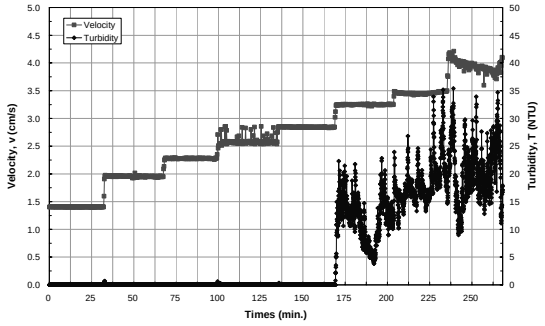

(c) T23

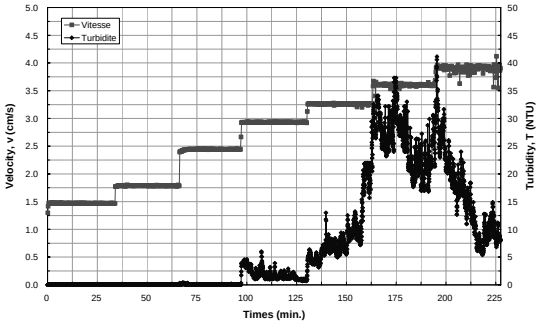

(d) T24

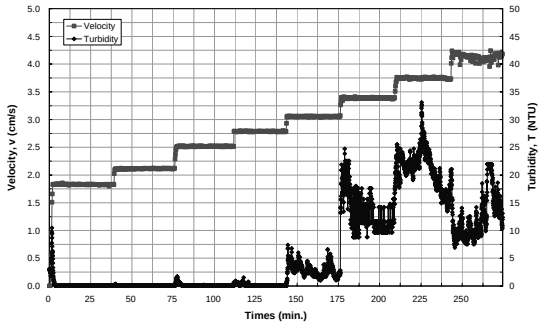

(e) T25

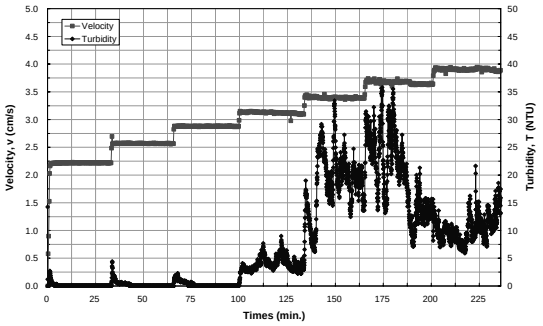

(f) T26

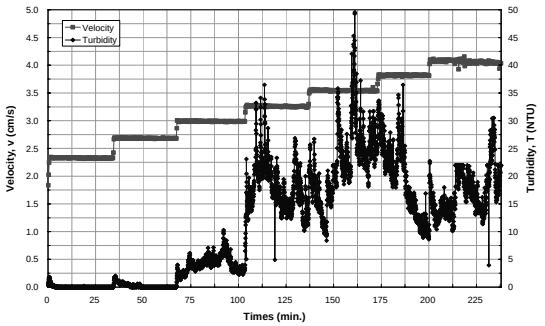

(g) T27

Figure III.4 The variation of turbidity and velocity with time (SET 04)

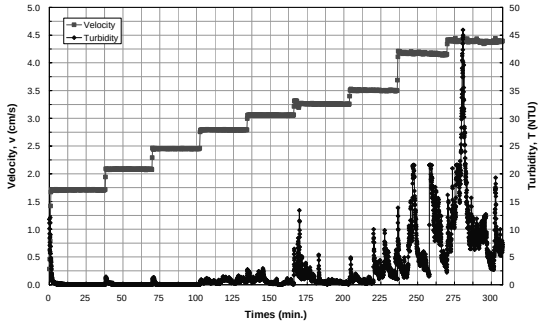

(a) T28

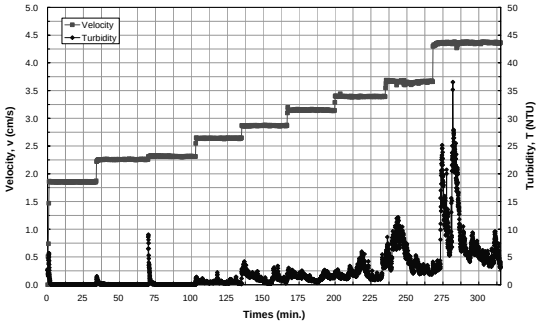

(b) T29

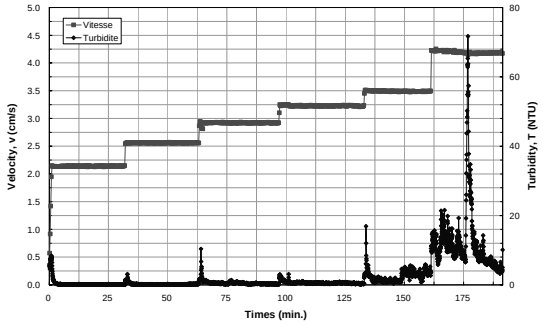

(c) T30

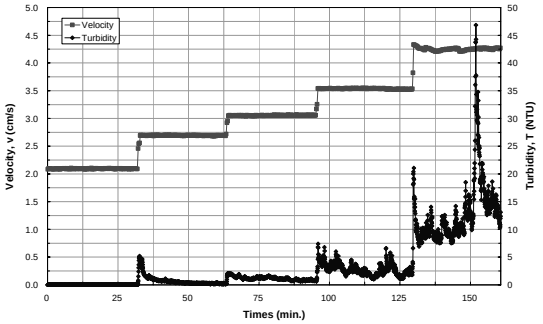

(e) T31

Figure III.5 The variation of turbidity and velocity with time (SET 05)

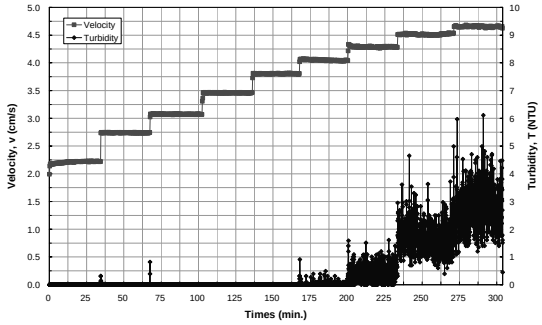

(a) T32

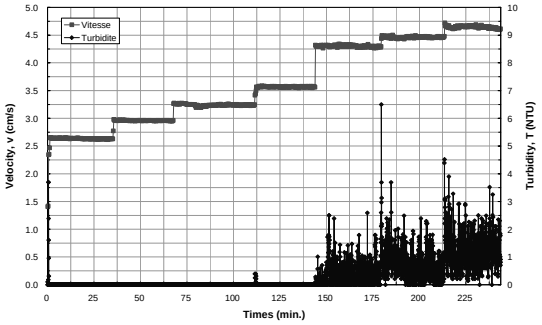

(b) T33

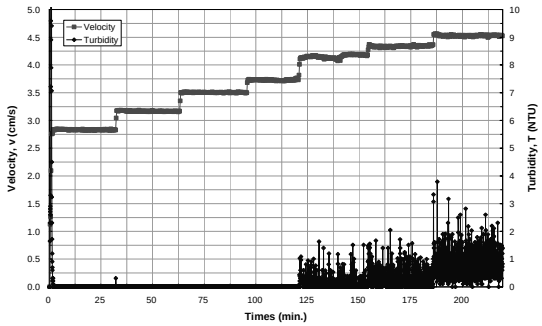

(c) T34

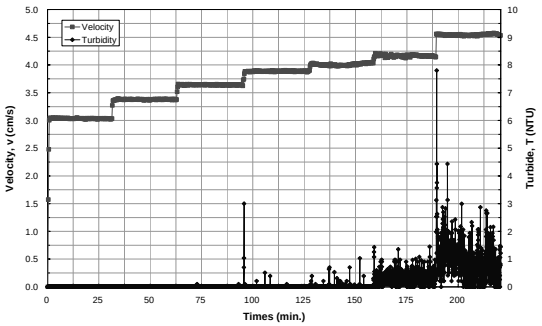

(d) T35

Figure III.6 The variation of turbidity and velocity with time (SET 06)

Appendix IV

The variation of mass of soil erosion with time by parallel erosion test

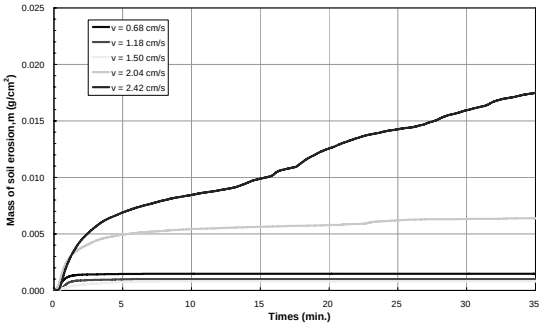

(a) T01

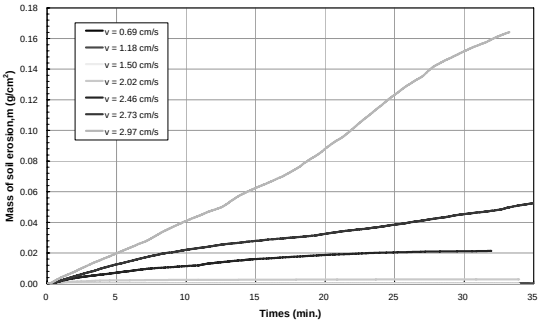

(b) T02

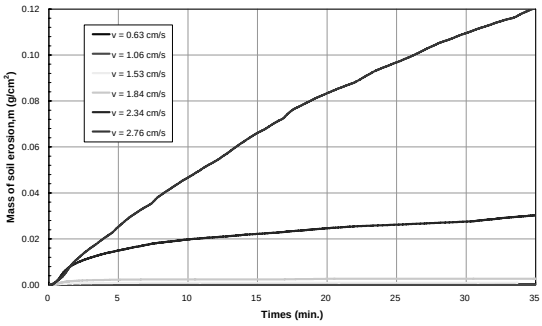

(c) T03

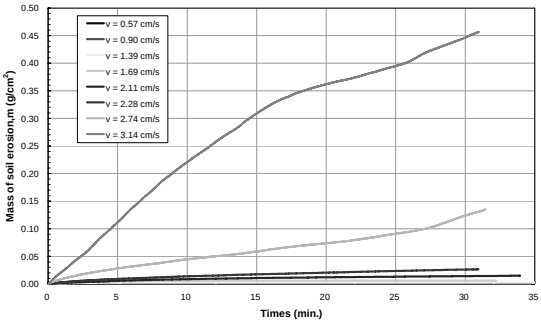

(d) T04

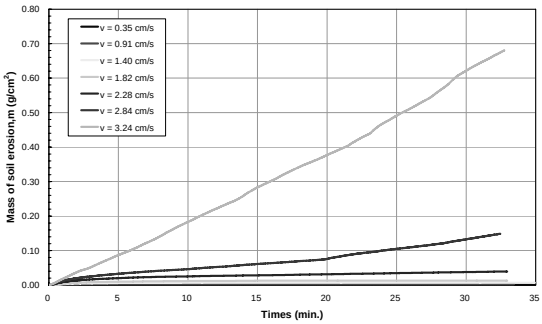

(e) T05

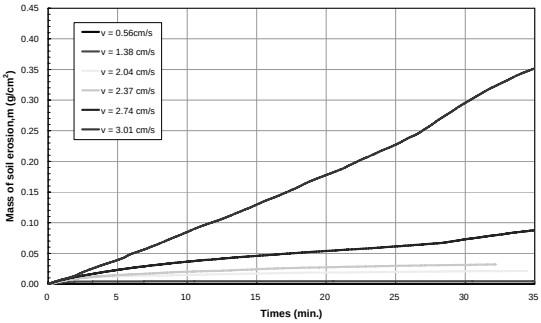

(f) T06

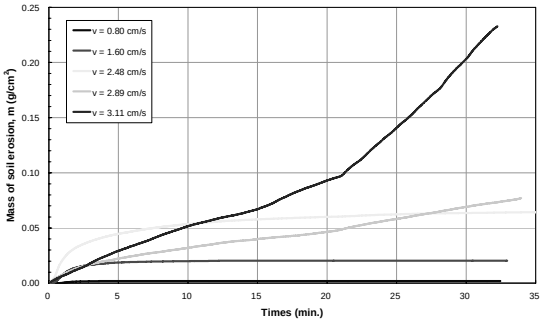

(g) T07

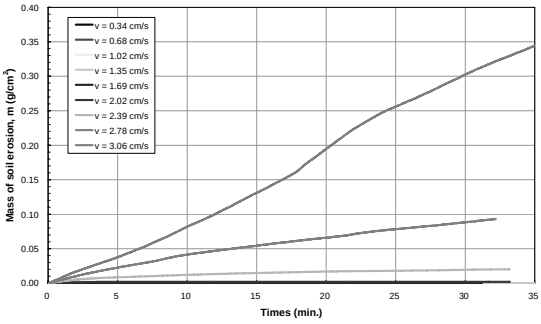

(h) T08

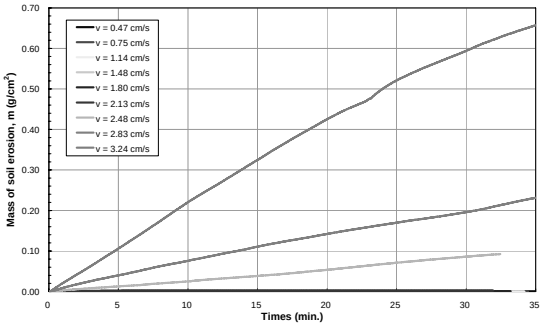

(i) T09

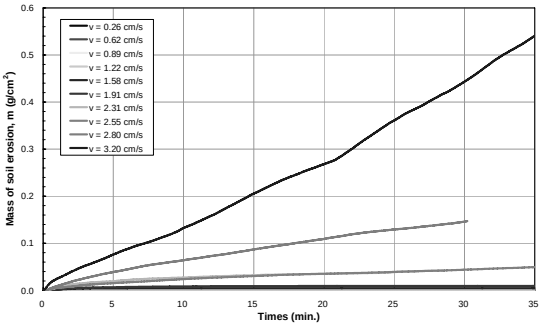

(j) T10

Figure IV.1 The variation of mass of soil erosion with time (SET 01)

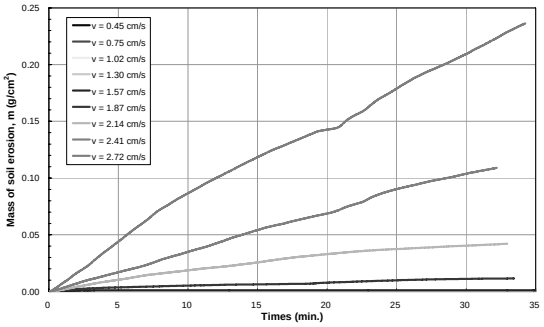

(a) T11

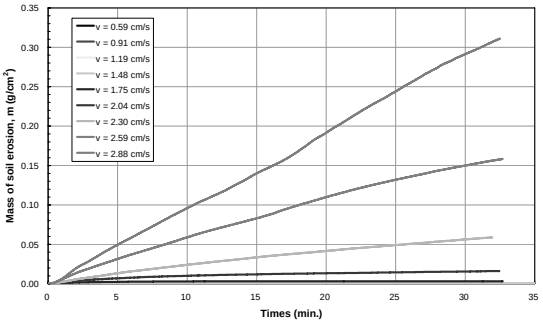

(b) T12

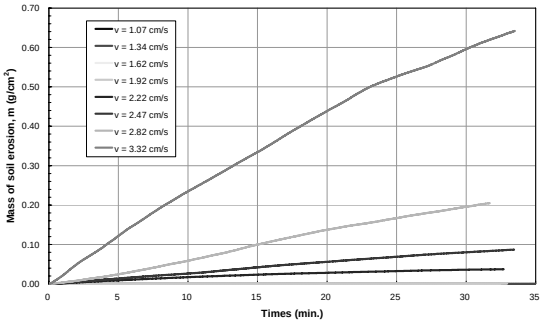

(c) T13

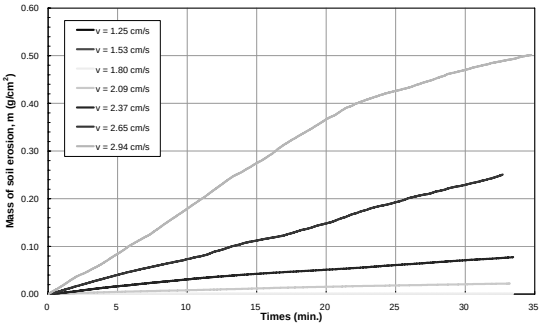

(d) T14

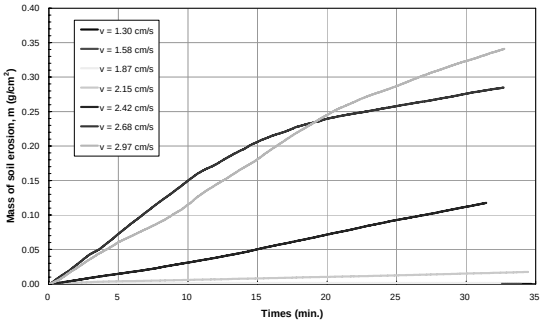

(a) T15

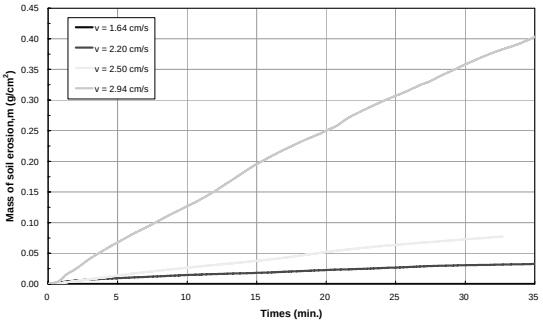

(b) T16

Figure IV.2 The variation of mass of soil erosion with time (SET 02)

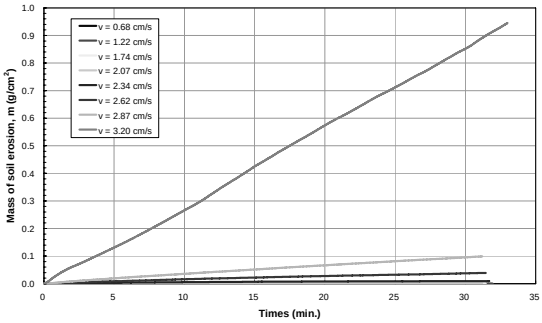

(a) T17

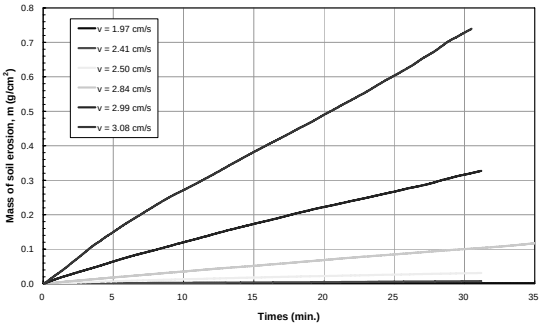

(b) T18

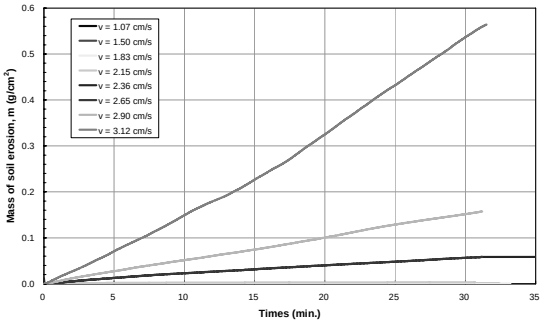

(c) T19

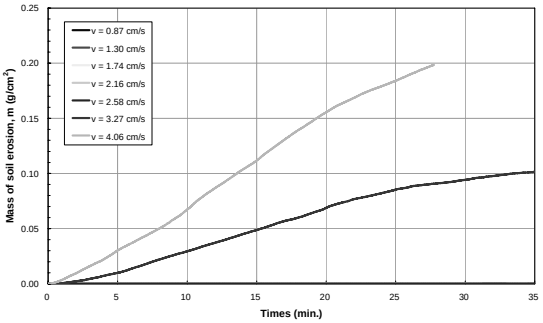

(d) T20

Figure IV.3 The variation of mass of soil erosion with time (SET 03)

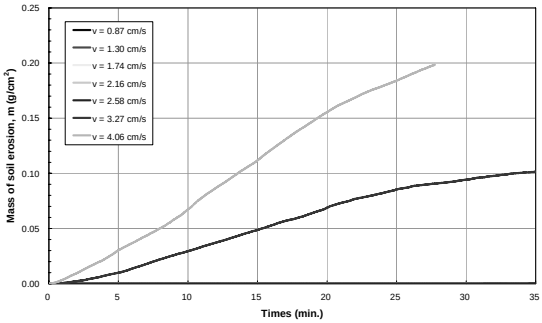

(a) T21

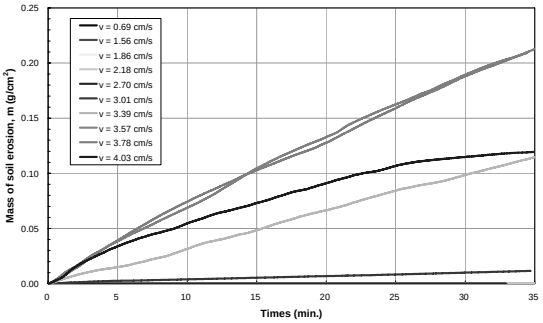

(b) T22

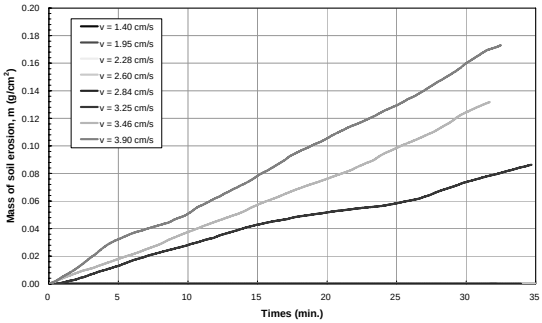

(c) T23

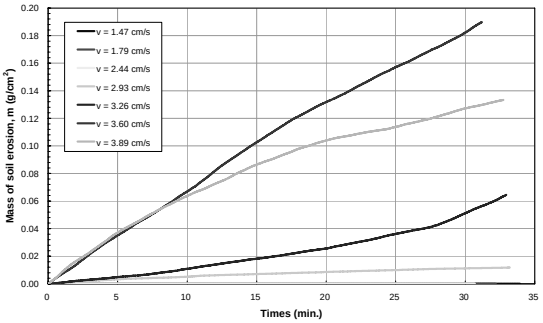

(d) T24

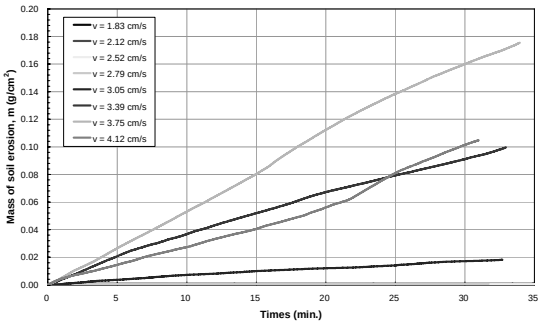

(e) T25

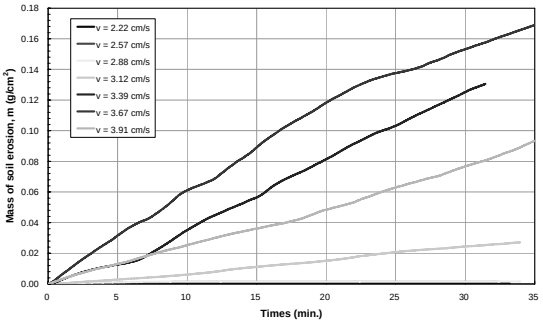

(f) T26

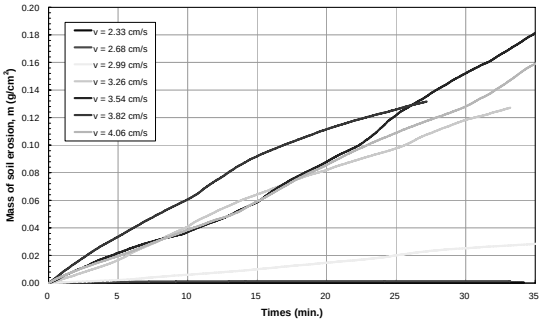

(g) T27

Figure IV.4 The variation of mass of soil erosion with time (SET 04)

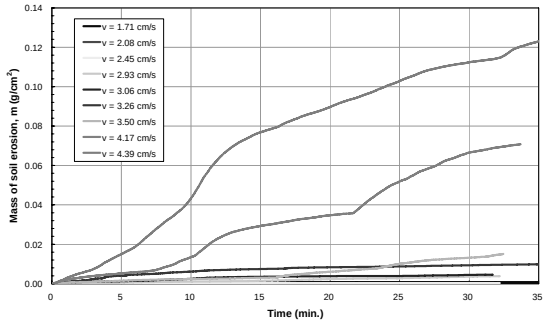

(a) T28

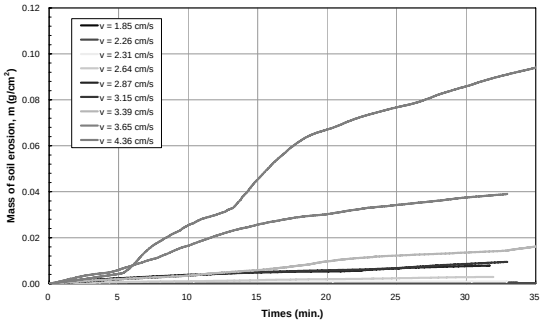

(b) T29

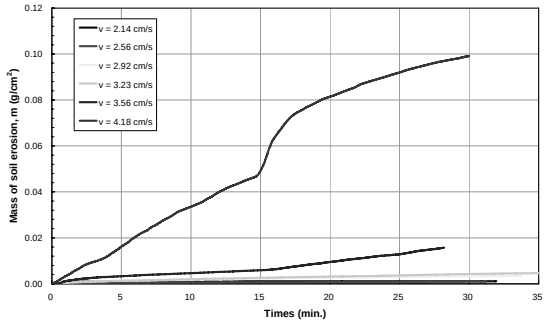

(c) T30

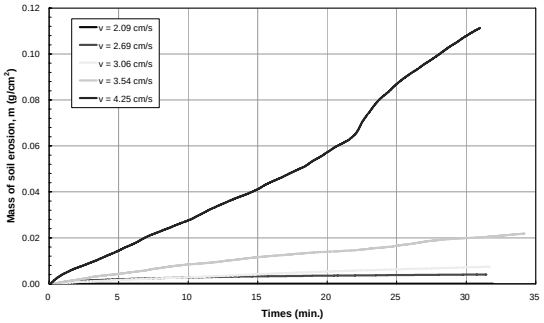

(d) T31

Figure IV.5 The variation of mass of soil erosion with time (SET 05)

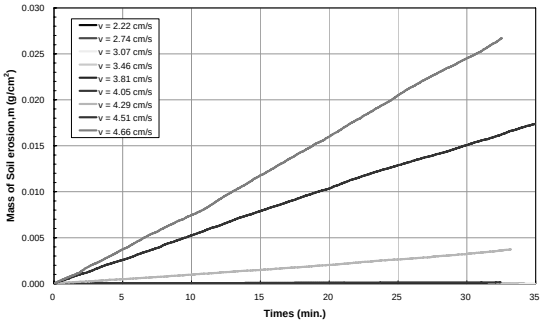

(a) T32

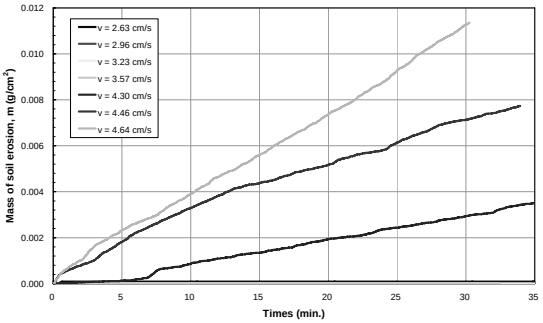

(b) T33

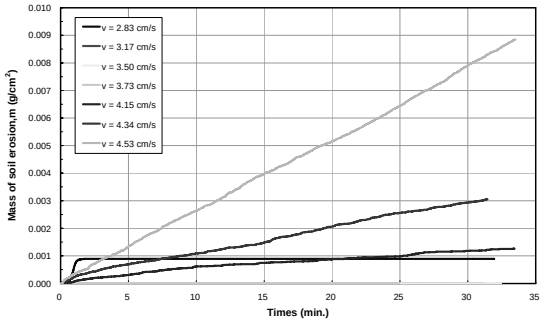

(c) T34

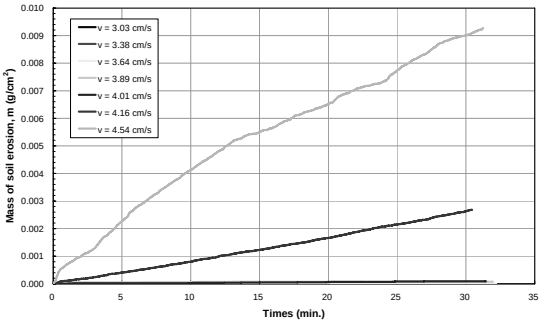

(d) T35

Figure IV.6 The variation of mass of soil erosion with time (SET 06)